



HAL
open science

Application des méthodes du chaos quantique aux oscillations d'étoiles en rotation rapide

Michael Pasek

► **To cite this version:**

Michael Pasek. Application des méthodes du chaos quantique aux oscillations d'étoiles en rotation rapide. Dynamique Chaotique [nlin.CD]. Université Paul Sabatier - Toulouse III, 2012. Français. NNT: . tel-00997861

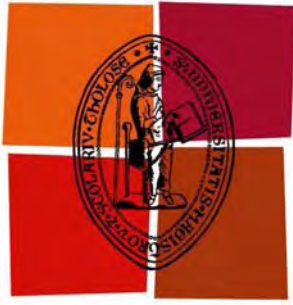
HAL Id: tel-00997861

<https://theses.hal.science/tel-00997861>

Submitted on 29 May 2014

HAL is a multi-disciplinary open access archive for the deposit and dissemination of scientific research documents, whether they are published or not. The documents may come from teaching and research institutions in France or abroad, or from public or private research centers.

L'archive ouverte pluridisciplinaire **HAL**, est destinée au dépôt et à la diffusion de documents scientifiques de niveau recherche, publiés ou non, émanant des établissements d'enseignement et de recherche français ou étrangers, des laboratoires publics ou privés.



Université
de Toulouse

THÈSE

En vue de l'obtention du

DOCTORAT DE L'UNIVERSITÉ DE TOULOUSE

Délivré par l'Université Toulouse III - Paul Sabatier
Discipline ou spécialité : *physique de la matière*

Présentée et soutenue par *Michael PASEK*
Le 20 décembre 2012

Titre :

*Application des méthodes du chaos quantique
aux oscillations d'étoiles en rotation rapide*

Jury

François CHARRU	Examineur
Jørgen CHRISTENSEN-DALSGAARD	Rapporteur
Dominique DELANDE	Rapporteur
Bertrand GEORGEOT	Directeur de thèse
Marie-Jo GOUPIL	Examinatrice
François LIGNIÈRES	Co-directeur de thèse
Michel RIEUTORD	Président du jury
Bart VAN TIGGELEN	Examineur

École doctorale : *Sciences De la Matière*
Unité de recherche : *Laboratoire de Physique Théorique de Toulouse - IRSAMC*
Institut de Recherche en Astrophysique et Planétologie - OMP
Directeurs de Thèse : *Bertrand Georgeot, François Lignièrès*

Remerciements

Je souhaite tout d'abord remercier les membres du jury, Jørgen Christensen-Dalsgaard et Dominique Delande pour avoir accepté d'être les rapporteurs de mon manuscrit, ainsi que François Charru, Marie-Jo Goupil et Bart van Tiggelen d'être venus assister à ma soutenance en tant qu'examineurs. Je remercie aussi Michel Rieutord, pour avoir accepté son mandat de président de jury.

Ces trois années passées au Laboratoire de Physique Théorique et à l'Institut de Recherche en Astrophysique et Planétologie ont été un réel bonheur. C'est donc avec le plus grand plaisir que je remercie les permanents, postdocs, bibliothécaires, doctorants, ingénieurs, secrétaires, stagiaires, plombiers et personnels d'entretien... (et j'en oublie) du LPT et de l'IRAP (et de l'OMP ! et de l'IRSAMC !) pour avoir contribué de différentes façons au bon déroulement de ces trois ans de thèse.

Côté LPT, je remercie particulièrement Clément Sire, *rock*-directeur (et voisin d'en face), pour m'avoir accueilli au labo. Merci aussi à Sandrine Le Magoarou, Malika Bentour et Nicolas Elefantis pour l'aide précieuse qu'ils m'ont apporté à de multiples reprises, mais aussi pour leur sympathie. Merci aux thésards du LPT ou de l'IRSAMC, les "vieux" (Thomas, Ludovic, Clément, Sylvain, David, Wes, Charlotte, Vincent, Yasir ...) pour avoir montré l'exemple, et les "jeunes" (Anil, Xavier, Juan Pablo, Frédéric, Helder, François, Vivek, Thibaut, Philipp, ...) pour avoir pris la relève.

Côté IRAP, je remercie particulièrement les membres de l'équipe PSE et ex-DFA, avec une mention spéciale pour les "locataires du couloir" : Katia, François R., Thierry, Giovanni, Boris, Torsten, Laurène, Jérôme et Frédéric, mais aussi Pascal P, Pascal F., Étienne, Stéphane, Sébastien ... Merci aussi aux doctorants de l'IRAP, trop nombreux pour être cités, en particulier merci à mes colocs de bureau Aurélie, Delphine, Simon, Johann, Jules, Vincent, et Antoine de (ne pas) m'avoir laissé travailler. Merci aussi évidemment aux services informatique et administratifs de l'IRAP, ainsi qu'au personnel de la bibliothèque de l'OMP.

Merci à l'Ecole Doctorale, Cécile Bon et à la Faculté de Pharmacie de m'avoir permis d'enseigner durant les deux dernières années de ma thèse, merci aux étudiants de ne pas avoir mis le feu à la salle de TP, et merci aux "DCCE" d'avoir mis le feu aux soirées.

Merci à tous mes professeurs de physique, du collège à l'université, grâce à qui j'ai, depuis quelques temps, adopté la maxime qu'écrivit William Shakespeare dans Macbeth (Acte 2, Scène 3) : "... we delight in physics ...".

Je remercie très sincèrement Bertrand Georgeot et François Lignièrès, mes directeurs de thèse, pour m'avoir fait confiance au début, pour avoir encadré mes travaux ensuite, pour m'avoir fait partir autour du monde et pour m'avoir accompagné (en garde partagée). Merci aussi pour m'avoir considérablement appris, scientifiquement et humainement.

Un grand merci à mes amis.

Je remercie aussi mon père, pour m'avoir encouragé dans la poursuite de mes études, et pour m'avoir donné l'envie d'apprendre. "Bosse ! Bosse ! ...", je n'oublierais pas.

Enfin, Gabrielle, merci pour ta relecture du manuscrit, ta patience et ton soutien, merci pour tout.

Contents

1	Introduction	1
2	Asteroseismology	5
2.1	Observations of pulsating stars	5
2.1.1	Detection techniques	6
2.1.2	The different classes of pulsating stars	7
2.1.3	Rapidly rotating pulsating stars	10
2.2	The theory of stellar oscillations	12
2.2.1	Equations of stellar oscillations	13
2.2.2	Oscillations of non-rotating stars	17
2.2.3	Oscillations of rotating stars	20
3	Concepts of quantum chaos	25
3.1	Integrability and chaos in classical Hamiltonian systems	26
3.1.1	Classical Hamiltonian systems	26
3.1.2	Integrability and chaos	27
3.1.3	Mixed systems	29
3.2	Integrability and chaos in quantum systems	30
3.2.1	The classical limit and phase space distributions	32
3.2.2	Statistical properties of energy levels and frequencies	34
3.2.3	Quantum integrable systems	38
3.2.4	Quantum chaotic systems	39
3.2.5	Quantum mixed systems	43
4	Signs of wave chaos in rapidly rotating stars	47
4.1	Brief history	47
4.2	Acoustic ray dynamics	48
4.2.1	Rays in a non-rotating stellar model	48
4.2.2	Rays in rapidly-rotating stellar models	49
4.3	Classification of modes from phase space distributions	50
4.4	Frequency statistics and regularities	51
5	Regular modes in rotating stars	55
5.1	Equilibrium stellar models	55
5.2	Short-wavelength pressure wave equation	56
5.3	Derivation of the acoustic ray limit	60
5.4	The parabolic equation method	63
5.5	Numerical implementation of the method	66
5.5.1	Numerical integration of ray equations	66
5.5.2	Computation of periodic trajectories	67
5.5.3	Computation of the monodromy matrix	68
5.5.4	Mode eigenfunctions	70

5.5.5	Accuracy on frequency spacings	71
5.6	Complete two-dimensional numerical computations	73
5.6.1	Numerical method and accuracy	73
5.6.2	Mode following and numerical results	74
5.7	Brief summary of our results	77
5.7.1	Comparisons with two-dimensional complete computations	77
5.7.2	Spectral observables and their evolution with rotation	80
5.8	Publication I	83
5.9	Publication II	89
6	Conclusion and perspectives	103
A	Résumé étendu	107
A.1	Introduction générale	107
A.2	Astérosismologie	108
A.3	Chaos quantique et chaos ondulatoire	109
A.4	Chaos ondulatoire dans les étoiles en rotation rapide	110
A.5	Modes réguliers dans les étoiles en rotation	112
A.6	Conclusion	112

Chapter 1

Introduction

“L’esprit n’use de sa faculté créatrice que quand l’expérience lui en impose la nécessité.”

Henri Poincaré, *La Science et l’Hypothèse*, 1902.

Almost all information that can be collected about astronomical objects comes from light, or more generally electromagnetic radiation, that such objects may have emitted, scattered, occulted or bent (the exceptions to this rule being cosmic rays, neutrinos, and, potentially, gravitational waves). When stars experience some physical changes, these alterations can affect the properties of the light they emit. One manifestation of these changes comes from the surface oscillations of stars that are caused by elastic waves propagating in their interiors. The corresponding periodic variations in the amplitudes of the stellar light curves are most of the time small, but they can be detected by high-precision photometry or spectroscopy. The analysis of these light curves in order to constrain the internal structure of stars is called asteroseismology, by analogy with the study of seismic waves inside the Earth. For the Sun, and many other observed stars that display solar-like oscillations, this technique has led to considerable progresses in our understanding of the structure and evolution of these stars (see e.g. Aerts et al., 2010, and references therein). Also, beyond stellar physics *per se*, asteroseismology has contributed to advances in the standard model of particle physics (cf. the many works dealing with the ‘solar neutrino problem’, e.g. in Christensen-Dalsgaard (2002); Turck-Chièze et al. (2004)), and exoplanetary science, where the asteroseismic study of host stars allows to determine the masses and radii of exoplanets with high accuracy (see e.g. Kjeldsen et al., 2008; Batalha et al., 2011).

In order to constrain the various physical parameters of stellar models from observed oscillation frequencies, it is important to have *a priori* information on the structure of the frequency spectrum. In the asymptotic high-frequency regime of pressure modes, the oscillation frequencies are usually deemed to follow the so-called ‘Tassoul’s asymptotic formula’ (Tassoul, 1980) whose first-order takes the form:

$$\omega_{n,\ell} \simeq \frac{\pi}{\int_0^R \frac{dr}{c_s(r)}} \left(n + \frac{\ell}{2} + \frac{1}{4} + \alpha \right), \quad (1.1)$$

where n, ℓ are the quantum numbers of oscillation modes, $c_s(r)$ the speed of sound inside the star, R the stellar radius, and α a phase term that depends on the assumptions

that one makes about the surface properties of the star. This asymptotic formula, and its associated ‘large frequency separation’ and ‘small frequency separation’ (see Sect. 2.2.2 for definitions) are widely used in the asteroseismology community for the mode identification process, that associate peaks in observed spectra with the appropriate oscillation modes. However, it is assumed in the derivation of Tassoul’s formula that the star is approximately spherically symmetric. This is a judicious assumption for the Sun, as well as for most *slowly* rotating stars, but not all stars rotate slowly.

Indeed, it is known from measurements of projected rotational velocities (see Sect. 2.1.3) that typical non-evolved pulsating stars with masses $M \geq 1.5M_{\odot}$ (where M_{\odot} is the mass of the Sun) rotate rapidly (the surface velocity at the equator is on average 150 km.s^{-1} ; for comparison, the Sun rotates at 2 km.s^{-1} at the equator). For such high rotation rates, the effect of the centrifugal force becomes so strong that stars are significantly flattened, and they typically reach about 30% of their Keplerian limit Ω_K , which is the rotation rate where the centrifugal force $MR_{\text{eq}}\Omega_K^2$ equals the gravitational attraction GM^2/R_{eq}^2 at the equator. Pulsating stars in this mass range are numerous, and extensive high-precision data has been accumulated on these pulsators by the recently launched space missions CoRoT and Kepler (see e.g. Uytterhoeven et al., 2011). Tassoul’s asymptotic formula cannot be used for these stars, and the lack of a proper understanding of the asymptotic structure of their oscillation spectra makes their interiors largely inaccessible to asteroseismic studies. Two-dimensional numerical codes that take fully into account the effects of rotation on oscillations have been developed to fill in this shortcoming, but they are not well adapted to mode identification, and the physical understanding of their results is missing, especially in the rapidly rotating regime.

In order to obtain such an understanding of the frequency spectrum, Lignières and Georgeot (2008, 2009) have studied the short-wavelength limit of pressure waves, that gives a classical Hamiltonian system for the propagation of acoustic rays, in uniformly rotating polytropic stellar models. They showed that the dynamics of acoustic rays in rotating stars is no longer integrable, and that this system undergoes a transition to chaos (of the Kolmogorov-Arnold-Moser type, see Sect. 3.1.3) as the rotation rate increases. At high rotation rates, this leads to a *mixed* classical system, where regular and chaotic regions coexist in phase space. Are there signs of these ray dynamical properties in the frequency spectrum and eigenfunctions of pressure modes? Similar questions have been considered by the quantum chaos community, that has developed several approximate and statistical techniques for the study of quantum systems whose classical limit is chaotic. More broadly, related concepts have also been applied to classical waves, be they electromagnetic or elastic, propagating in disordered media or complex geometries, going from light in asymmetric dielectric cavities (Nöckel and Stone, 1997) and microwaves in chaotic resonators (Stöckmann and Stein, 1990), to seismic waves in the Earth (Larose et al., 2004) and long-range sound propagation in the ocean (Brown et al., 2003). In the stellar pulsation setting, in accordance with standard results of quantum chaos, Lignières and Georgeot (2008, 2009) found that in the high-frequency limit the pressure-mode spectrum can be described by a superposition of independent sub-spectra that are associated with the regular and chaotic phase space zones of the ray system.

In the present thesis, we build on this work to construct an asymptotic theory for the subset of regular modes that should be the easiest to detect and identify in observations. To do so, we adapt the so-called ‘parabolic equation method’ (Babich and Buldyrev, 1991), a semi-classical method that has been successfully used previously, for example in dielectric micro-cavities (Tureci et al., 2002). We show that this asymptotic theory yields semi-analytical ray-based formulas for the frequencies and eigenfunctions of pressure modes localised on stable periodic acoustic rays. The numerical implementation of this method is realised, and we use a two-dimensional complete numerical oscillation code to compare our semi-classical results with high-frequency modes of uniformly rotating

polytropic stellar models. Our results show that the frequencies and eigenfunctions of these regular modes can be accurately described by our asymptotic theory for almost all rotation rates. The phenomenological implications of the predicted regular frequency spacings in the oscillation spectra of rapidly rotating stars is also discussed. These results were published in the articles Pasek et al. (2011, 2012), that are reprinted in Sect. 5.8, Sect. 5.9. An introductory course on the tools of quantum chaos aimed at the asteroseismology community is also in press (Pasek and Georgeot, 2013).

In Chap. 2, we present a brief account of the observational and theoretical status of the field of asteroseismology, in particular concerning its application to rapidly rotating pulsating stars. In Chap. 3, we present a succinct list of some concepts and methods of classical and quantum chaos that are used in the rest of the thesis. The goal of Chap. 4 is then to give the results on the classification of pressure modes in rapidly rotating stars using the tools of quantum chaos. An important subset of regular modes is studied in details in Chap. 5, that is the core of this thesis. Finally, we give our conclusions and perspectives on this work, and on the study of stellar oscillations with the tools of quantum chaos in general (Chap. 6).

Chapter 2

Asteroseismology

“We are all in the gutter, but some of us are looking at the stars.”

Oscar Wilde, *Lady Windermere’s Fan*, Act III (1892).

The simple experience of laying on the grass to stare at a clear summer night sky leads to the observation that stars twinkle rapidly, due to the disturbances caused by the turbulent earth atmosphere. Beyond this effect, it can also be observed that stars can show time variations of their apparent brightness on longer periods. These stars are called *variable stars*. From very simple considerations of information theory, there is more information contained in a varying signal than in a constant one. This has led to the close scrutiny of variable stars, to gain insights on stellar physics and beyond. There are two broad classes of variable stars (Eyer and Mowlavi, 2008). The *extrinsic* variables owe their variability to changes in their geometrical aspect as viewed from the observer’s location. One rather down-to-earth example of such a change is that of a planet passing in front of the star, thus dimming its luminosity; a phenomenon that has led to the transit method for detecting exoplanets. The *intrinsic* variables display variations in their light curves due to their own physical changes. In this category, the *pulsating variables*, also called *pulsating stars*, undergo changes over time from waves propagating in their interiors. Using these waves as a probe, the field of *asteroseismology* aims at inferring the internal properties of pulsating stars from the monitoring and analysis of their variations. In this chapter, we first present a brief account of the observational results on pulsating stars (Sect. 2.1), and on rapidly rotating pulsating stars in particular. Then, we give a non-exhaustive summary of the theory of stellar oscillations (Sect. 2.2), where we present in particular the regular asymptotic structure of the oscillation spectrum in non-rotating stars (Sect. 2.2.2), and for rotating stars, the results of numerical computations that suggested the existence of asymptotic frequency regularities in the rotating case as well (Sect. 2.2.3).

2.1 Observations of pulsating stars

The compression-dilation movement of the stellar gas due to the oscillations induces temperature, and therefore brightness, variations. For periodic or multi-periodic variations, the Fourier transform of the light curve will give an *oscillation spectrum*, that constitutes the rough material of all asteroseismic studies. We begin this chapter by briefly review-

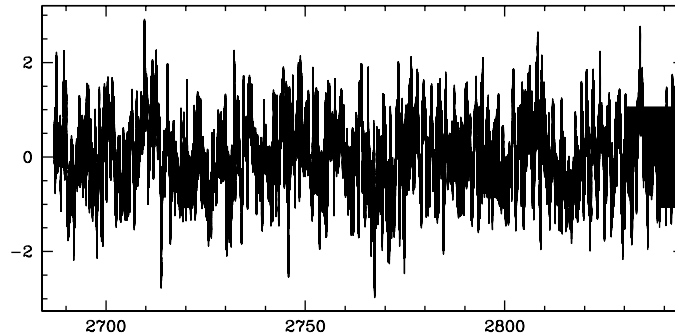


Figure 2.1: CoRoT light curve of the red giant star HR 7349. Top: total CoRoT light curve, bottom: zoom of a portion of the light curve. The units are the millimagnitude (mmag) which corresponds to a one-thousandth variation in the magnitude of the star, and the Heliocentric Julian Date (HJD) which is a measure of time that is convenient for astronomical purposes. The periodicity that can be seen in the bottom panel is of about 8.5 hours ($30 \mu\text{Hz}$) (from Carrier et al., 2010).

ing the different procedures that are used to measure stellar oscillations, as well as the different types of pulsating stars.

2.1.1 Detection techniques

The measurement of stellar oscillations is possible through the techniques of either *spectroscopy*, that monitors the evolution of stellar spectral lines, or *photometry*, that tracks variations in the brightness of the star. We describe both methods in the following.

Photometry

Photometry consists in counting the number of photons a star emits during a certain length of time. Though the detection of stellar oscillations by photometry is perfectly feasible from the ground, the recent space observations by space missions CoRoT (‘CONvection ROTation and planetary Transits’, launched in 2006 by CNES-ESA) and Kepler (launched in 2009 by NASA) have the advantage of allowing uninterrupted observations over long periods of time (up to 5 months for CoRoT and 4 years for Kepler), as well as eliminating the unwanted effects of the terrestrial atmosphere. Five months uninterrupted observations with the CoRoT satellite enable to reach an absolute precision of $0.08 \mu\text{Hz}$ on frequencies. An example of a CoRoT light curve of a red giant star, where the oscillation pattern is clearly visible, can be seen in Fig. 2.1.

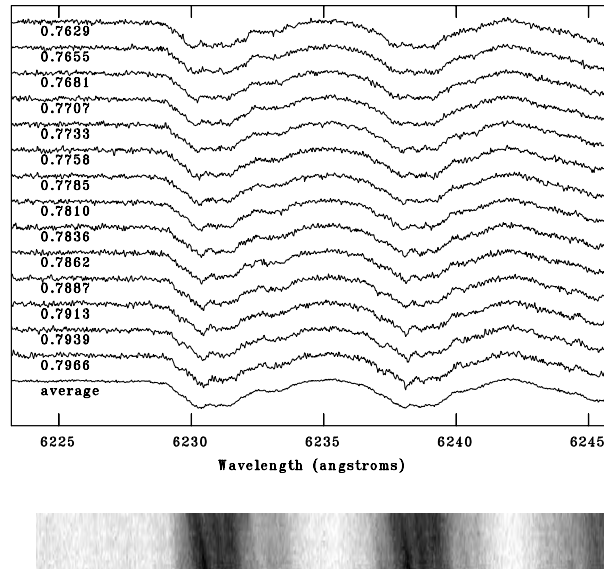


Figure 2.2: Profile variability of the Fe I 6231 Å, and Fe II 6238 Å spectral lines in the spectra of the δ Scuti star HD 21190. In the bottom panel are included all observed spectra, stacked such that time is increasing downwards. The three dark streaks in the bottom panel are signatures of non-radial oscillations (from González et al., 2008).

Spectroscopy

The spectrum of the light emitted by a star presents dark lines at certain wavelengths that are due to photon absorption by chemical species present at the stellar surface. These *absorption lines* are broadened by the Doppler effect if the star is rotating. Since different positions on the stellar surface have different Doppler velocities (velocities projected on the line of sight), the local temperature variations of the oscillations, that result in modifications of the absorption, will induce deformations of the spectral lines profile. By monitoring the time evolution of the spectral lines profile, one can therefore measure the frequencies and surface spatial distributions of oscillations. Such spatial information cannot be obtained from the disk-integrated light measured by photometry. In Fig. 2.2, one can see the profile variations of two iron lines of a δ Scuti star that are due to its pulsations.

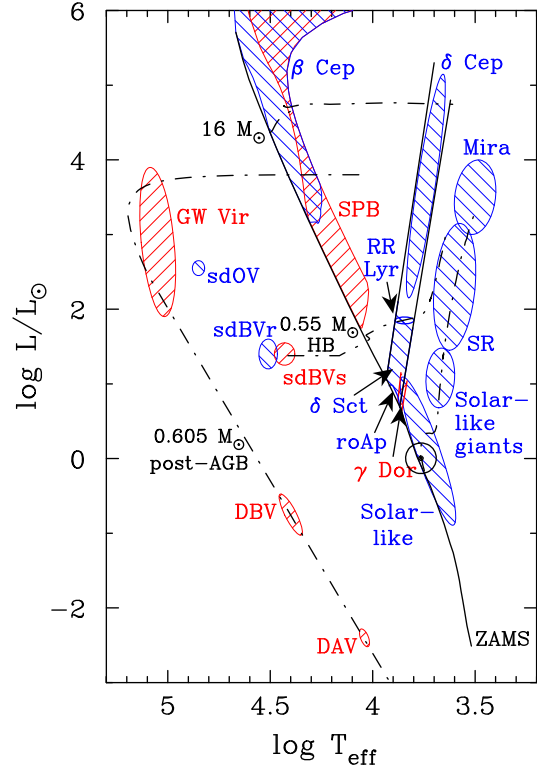
2.1.2 The different classes of pulsating stars

The Hertzsprung-Russell (H-R) diagram is a convenient way to classify stars from their basic physical properties (see e.g. Carroll and Ostlie, 1996). One version of this diagram places stars as a function of their luminosity and effective temperature, as can be seen in Fig. 2.3. Regions of the H-R diagram where stars have been observed to pulsate are highlighted, showing that pulsating stars can be found in a wide range of masses and evolutionary stages. Nevertheless, from the excitation mechanism of their pulsations, pulsating stars can be brought into two categories: *solar-like* and *classical pulsators*.

Solar-like pulsators

Oscillations in the Sun are known to be generated from the stochastic processes occurring in its outer convective zone, where the turbulent motion causes pressure fluctuations. The relative intensity variations in brightness coming from these oscillations were found to

Figure 2.3: Hertzsprung-Russell diagram placing stars as functions of their luminosity versus effective temperature. Locations of the different types of pulsating stars have been highlighted with coloured bands. Absolute luminosities have been normalized by the solar value L_{\odot} . Blue regions: stars showing pressure mode oscillations, red regions: stars showing gravity mode oscillations (cf. Sect. 2.2.2) (from Handler, 2012).



be of a few parts per million, which corresponds to velocity amplitude variations at the surface of a few cm.s^{-1} . They were first observed in the Sun by Leighton et al. (1962). The observed oscillation periods peaked at around five minutes, which corresponds to high-frequency acoustic modes (Christensen-Dalsgaard, 2002). In this regime, it was found that oscillation frequencies are regularly spaced, cf Fig. 2.4. This simple frequency spectrum depends only on two uniform spacings, the so-called *large* and *small frequency separations*. This basic structure can be modelled with an asymptotic theory, which enables to identify the observed frequencies with the correct oscillation modes. The asymptotic theory paved the way for the quantitative analysis of the oscillation spectrum of the Sun that is called *helioseismology*. It has led to a very good knowledge of some of its internal physical characteristics: as can be seen in Fig. 2.5, the sound-speed distribution in most parts of the Sun are known with a few tenth of a percent accuracy. The distribution of the interior rotation rate of the Sun was constrained in a similar way, except close to the centre (Thompson et al., 1996).

Such a success for the Sun has spurred efforts to find similar oscillations in other stars that possess an outer convective zone, that is low mass ($M < 1.5M_{\odot}$, where M_{\odot} is the mass of the Sun) main sequence stars (the *main sequence* is a diagonal strip in the H-R diagram where about 90% of stars lie), and post main-sequence red giant stars. But it is only since the beginning of the twenty-first century that reliable measurements of solar-like oscillations in distant stars have been obtained. The star η Bootis was the first star after the Sun in which solar-like oscillations were clearly measured (Kjeldsen et al., 1995), and since the launches of CoRoT and Kepler, many other stars followed. The asteroseismic study of solar-like oscillating stars, building from previous experience of helioseismology, is expected to advance considerably our understanding of these stars. It must be noted that these studies were possible from the low rotation rates of these stars, making their global structure similar to our (almost) spherical Sun, for which the theoretical tools were well developed. As a conclusion, it can be said that solar-like pulsators have been found to be the perfect playgrounds for asteroseismology, since the simplicity and asymptotic character of their oscillation spectrum allow a systematic identification and interpretation

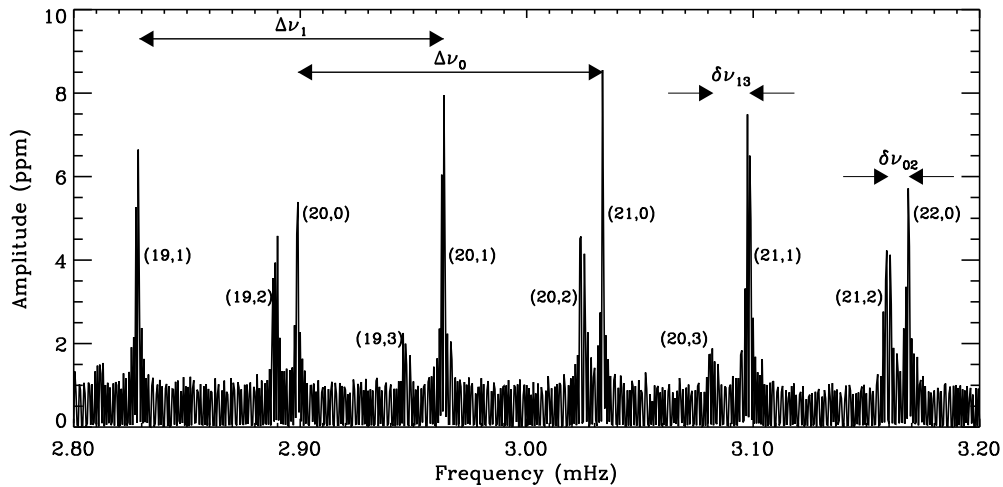


Figure 2.4: Oscillation spectrum of solar oscillations measured by the VIRGO instrument of the space mission SOHO (‘Solar and Heliospheric Observatory’). Amplitudes of oscillation peaks are given in ppm i.e. parts per million. Each mode frequency is identified with its (n, l) quantum numbers. The large and small separations $\Delta\nu$ and $\delta\nu$ (see Sect. 2.2.2) are also indicated (from Bedding and Kjeldsen, 2003).

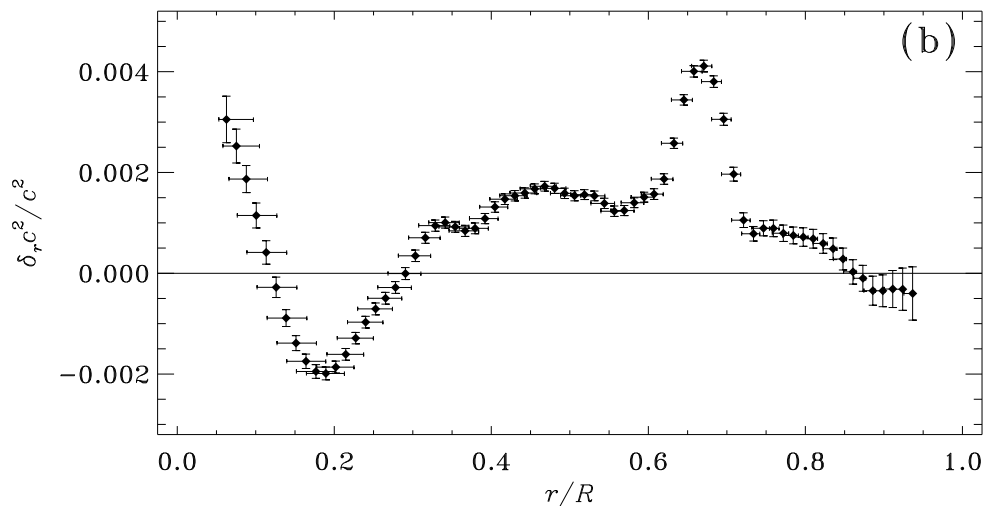


Figure 2.5: Relative difference $\delta_r c^2$ between the squared sound speed c^2 as inferred from sound speed inversion of observed oscillation frequencies, and as inferred from computed frequencies of the standard solar model called ‘Model S’. The relative difference is given as a function of the fractional radius r/R , where R is the solar radius (from Christensen-Dalsgaard, 2002).

of frequencies. For a nice review of the asteroseismology of solar-like pulsators, one can consult Elsworth and Thompson (2004).

Classical pulsators

Contrary to solar-like pulsators, classical pulsators have no significant convective envelope. The process that is thought to be responsible for exciting classical pulsations is known as the opacity (or κ) mechanism. This process can take place in these stars because they have layers where the opacity κ increases with increasing temperature, a feature that is sometimes called the “opacity bump”. These layers are generally regions of partial ionization of chemical elements, e.g. He II for δ Scuti stars. The κ mechanism goes as follows (Kippenhahn and Weigert, 1994). Given a small perturbation that makes the star contract, its temperature increases consequently. As a result, the opacity increases in the partial ionization zone, more radiative energy is stored in the star and the expansion that follows is thus enhanced. The inverse process leading also to an enhanced compression, this vibrational instability keeps growing until non-linear interactions come into effect. The κ mechanism can excite a large number of modes, but the modes with the highest amplitudes are usually at lower frequencies than those of solar-like oscillations.

Oscillations of classical pulsators have been observed far earlier than solar-like pulsators (Goodricke and Bayer, 1786). The Cepheids (δ Cep) and RR Lyrae (RR Lyr) stars may be the most well known classical pulsators since they show large-amplitude *radial* oscillations, and their period-luminosity relation is widely used to measure cosmological distances (see e.g. Carroll and Ostlie, 1996). Therefore, these stars are sometimes called “standard candles” in this context. Classical pulsators showing *non-radial* oscillations are the δ Scuti (δ Sct), β Cephei (β Cep), γ Doradus (γ Dor) and Slowly Pulsating B (SPB) stars (cf. Fig. 2.3), that were classified empirically from the structure of their oscillation spectra. It must be noted that some of these stars can belong to multiple classes, e.g. display δ Sct and γ Dor pulsations at the same time. As a result of the new data coming from space missions CoRoT and Kepler, the observational view on these non-radial classical pulsators is currently evolving (we shall come back to this point in Chap. 6). Nevertheless, until now, mode identification in these intermediate-mass to massive main-sequence pulsators has been found to be possible only in peculiar cases. Consequently, stellar evolution theory cannot be well constrained by a seismic diagnostic in this region of the H-R diagram. This holds in particular for the nuclear reaction rates of the CNO cycle that dominates energy generation in such stars (Kippenhahn and Weigert, 1994), the extra mixing at the outer boundary of the convective core (a phenomenon called *overshooting*) that is known to affect the lifetimes of massive stars (Hansen et al., 2004), or the angular momentum transport in rapidly rotating stars that fixes the internal rotation profile and drives circulation currents (Maeder and Meynet, 2012). The failure to interpret the oscillation spectrum of these stars can be attributed to the incapacity to model two of their physical properties. Firstly, the complex non-linear saturation of modes (from κ mechanism) that determines their amplitudes and thus their intrinsic amplitudes. Secondly, the rotational effects on oscillations that are usually modelled as if they could be treated perturbatively. As we shall see in the next section, this is not correct for typical stars in the $M > 1.5M_{\odot}$ mass range. To our knowledge, the only successful mode identifications in classical non-radial pulsators that have been claimed were for stars that are thought to rotate slowly (see e.g. Aerts et al., 2003; Dupret et al., 2004; Desmet et al., 2009).

2.1.3 Rapidly rotating pulsating stars

At their birth, most stars have a large rotational velocity. Indeed, stars are formed by the gravitational collapse of molecular clouds, that have large angular momenta. Since the angular momentum is conserved during the contraction, newborn stars are usually rapidly

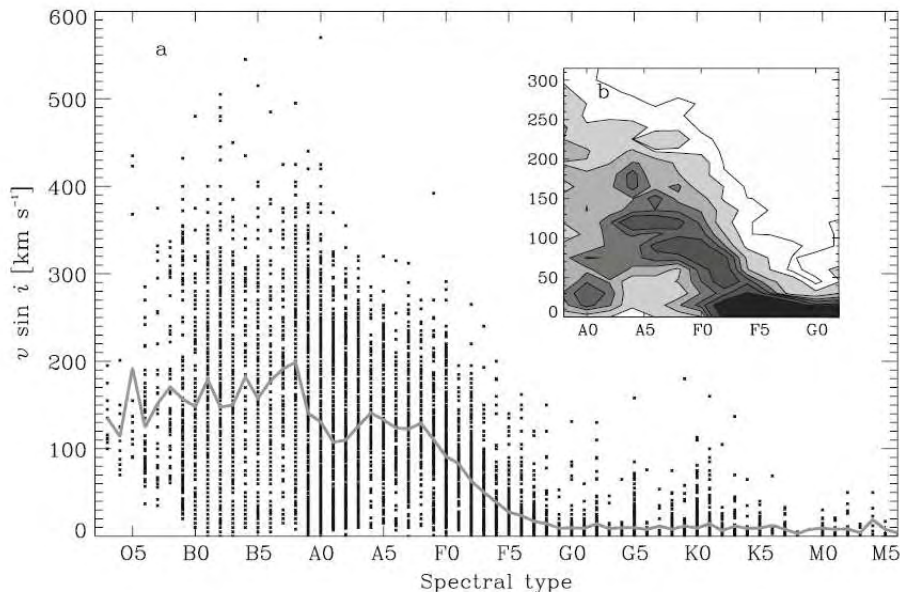


Figure 2.6: Distribution of the measured projected rotational velocities $v \sin i$ of stars (where v is the modulus of the equatorial rotational velocity and i is the inclination angle of the rotation axis of the star with respect to the line of sight) as a function of their spectral types. The average value of $v \sin i$ is indicated by the solid line. The corresponding density of points has been represented in the inset. One can see that most intermediate-mass to massive stars (corresponding to O-, B-, A-, and F-type stars) rotate rapidly (from Royer, 2009). Note that the Sun has the spectral type G2.

rotating, independently of their mass (Rosen et al., 2012). This initial angular momentum is many orders of magnitude above what is observed in most stars, and must therefore be dissipated in some ways during their evolution (Maeder, 2009). Whether a star will dissipate its angular momentum depends on its mass. Low-mass stars have an efficient mechanism to lose angular momentum in the form of magnetic stellar winds (Schatzman, 1962), the magnetic field being generated by a dynamo mechanism in their convective envelope (Hansen et al., 2004). On the other hand, higher-mass stars do not have a convective envelope and thus do not experience magnetic wind breaking. Moreover, low-mass stars live longer than their more massive counterparts, since they burn their nuclear fuel more slowly. Thus, generally on the main sequence, low-mass stars ($M < 1.5M_{\odot}$) rotate slowly and intermediate-mass to massive stars ($M > 1.5M_{\odot}$) rotate rapidly. This is illustrated in Fig. 2.6 where the observed distribution of projected rotational velocities in a large sample of stars is plotted as a function of their spectral types (historically, ‘spectral types’ were assigned to stars depending on the types and strengths of their absorption lines). The projected rotational velocity is measured from the Doppler broadening of the spectral line profile and corresponds to $v \sin i$, where v is the modulus of the equatorial rotational velocity and i is the inclination angle of the rotation axis with respect to the line of sight. The dispersion in the data of Fig. 2.6 is thus partly due to the random distribution of stellar inclination angles.

Typical rotation rates of these non-evolved, intermediate-mass to massive stars should have important effects on their equilibrium structure (Maeder and Meynet, 2012). The *centrifugal flattening* is one of the direct rotational effects on the equilibrium configuration of these stars. This is shown in Fig. 2.7 by the distribution of rotational velocities, from the same set of data as Fig. 2.6, but where the projection effect has been corrected, and

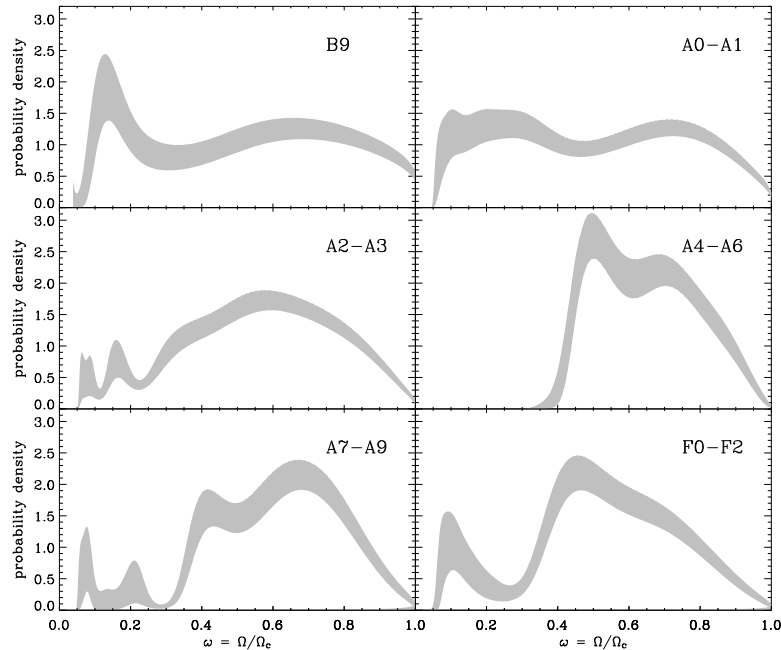


Figure 2.7: Probability densities of stellar rotation rates Ω/Ω_c , where $\Omega_c = \sqrt{GM/R_{\text{eq}}(\Omega_c)^3}$ with R_{eq} the equatorial radius of the star, for different spectral classes of stars. Rotation rates were obtained from the data set of Fig. 2.6 by correcting the projection effect on the rotational velocity and excluding suspected binaries and chemically peculiar stars. The grey strips are the variability bands (from Royer et al., 2007).

suspected binaries and chemically peculiar stars have been excluded. The rotation rate Ω is normalized by the critical velocity Ω_c , where $\Omega_c = \sqrt{GM/R_{\text{eq}}(\Omega_c)^3}$ is the maximum rotation rate allowed for a given mass, R_{eq} being the equatorial radius of the star. We note that an alternative measure of the centrifugal deformation, the Keplerian break-up velocity $\Omega_K = \sqrt{GM/R_{\text{eq}}(\Omega)^3}$, will also be used in the following. In Fig. 2.7 one can see that typical non-evolved intermediate-mass to massive stars rotate rapidly, with a significant centrifugal deformation corresponding to $\Omega/\Omega_c \geq 0.4$. It is also possible to have direct measures of the centrifugal deformation of the closest rapidly rotating stars by the technique of interferometry. In Fig. 2.8, one can see this effect clearly on the rapidly rotating star Altair, located at 16.73 light-years from Earth, from the interferometric imaging of its stellar disk (Monnier et al., 2007).

In conclusion, it is known from observations that most non-evolved stars in the $M > 1.5M_{\odot}$ mass range rotate rapidly, with typical projected rotational velocities of about 150 km.s^{-1} . These high rotation rates cause the centrifugal flattening of such stars that typically reach 50% of their critical velocity. Pulsating stars in this class are numerous, and many of them are being observed by current space missions. We will see in the following that the centrifugal flattening of rapidly rotating stars has important effects on their oscillations.

2.2 The theory of stellar oscillations

The theory of stellar oscillations has been studied by astrophysicists since the work of Eddington in the beginning of the XXth century. Since oscillations correspond to macroscopic changes of the stars, the mixture of ionized gas (mainly hydrogen and helium) and radiation that constitutes stellar matter can be treated as a fluid with continuous prop-

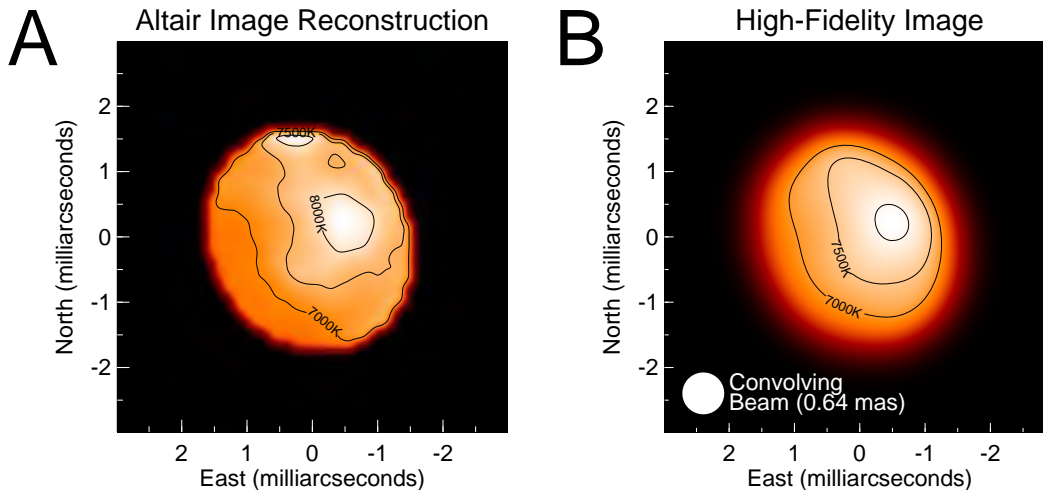


Figure 2.8: Near-infra-red intensity image of the surface of the rapidly rotating star Altair obtained by interferometry (left panel). Right panel: reconstructed image convolved with a Gaussian beam that matches the resolution of the interferometer (from Monnier et al., 2007).

erties. We are here interested in small perturbations around the equilibrium structure, thus oscillations will be treated as linear perturbations. Similarly, we concentrate on the stationary description of oscillations, leaving aside questions related to the mechanisms of excitation and damping that determine the amplitudes of oscillations.

2.2.1 Equations of stellar oscillations

In this section, we derive the general equations governing the dynamics of stellar fluids, following Unno et al. (1989); Gough (1993); Kippenhahn and Weigert (1994); Christensen-Dalsgaard (2003) and Goupil (2009). For a more general treatment of fluid mechanics, one can also consult Landau and Lifshitz (1959).

The state of a fluid in motion can be described by its velocity vector $\mathbf{v}(\mathbf{r}, t)$ and two thermodynamic quantities that are usually chosen to be the pressure $p(\mathbf{r}, t)$ and density $\rho(\mathbf{r}, t)$, which depend on the time t and position \mathbf{r} , where \mathbf{r} corresponds to a fixed point in space. In a star, these five quantities are determined by the equations for mass, momentum and energy conservation, together with the Poisson equation for the gravitational potential and the equation of state of the stellar gas.

The equation for the conservation of mass can be expressed as

$$\frac{\partial \rho}{\partial t} + \nabla \cdot (\rho \mathbf{v}) = 0. \quad (2.1)$$

The equation for the conservation of momentum is

$$\rho \frac{d\mathbf{v}}{dt} = -\nabla p - \rho \nabla \Phi, \quad (2.2)$$

where Φ is the gravitational potential, and we have used the material, also called Lagrangian, time derivative

$$\frac{d}{dt} \equiv \frac{\partial}{\partial t} + \mathbf{v} \cdot \nabla. \quad (2.3)$$

The viscosity has been neglected in Eq. (2.2) since its effects can generally be ignored to study stellar oscillations (Christensen-Dalsgaard, 2003). The equation for the conservation

of energy is derived from the first law of thermodynamics as

$$T \frac{dS}{dt} = \epsilon_N + \frac{1}{\rho} \nabla \cdot \mathbf{F}, \quad (2.4)$$

where S is the specific entropy, T the temperature, ϵ_N the rate of energy generation by nuclear reactions per unit mass, while \mathbf{F} is the energy flux including the transport of energy by radiation, as well as a possible modelling of the transport by turbulent convection. The gravitational potential Φ satisfies the Poisson equation

$$\nabla^2 \Phi = 4\pi G \rho, \quad (2.5)$$

where G is the gravitational constant. Finally, if one considers the stellar gas as a mixture of ideal gases, the equation of state can be expressed as

$$p = \frac{\mathcal{R}}{\mu} \rho T, \quad (2.6)$$

where $\mathcal{R} = 8.31 \times 10^7 \text{ erg.K}^{-1}.\text{g}^{-1}$ is the universal gas constant, and μ the (dimensionless) mean molecular weight, also called mean molecular mass. For a mixture of partially ionized nuclei and free electrons, the mean molecular weight can be written as (Kippenhahn and Weigert, 1994)

$$\mu = \left(\sum_i \frac{X_i}{\mu_i} \right)^{-1} \frac{1}{1 + E}, \quad (2.7)$$

where X_i are the weight fractions of nuclei of type i with molecular weights μ_i , and E is the number of free electrons per atom.

From the small oscillation amplitudes that are observed in the Sun, it is assumed that stellar oscillations can be described by linear perturbations around the equilibrium stellar structure. We will thus express the pressure as

$$p(\mathbf{r}, t) = p_0(\mathbf{r}, t) + p'(\mathbf{r}, t), \quad (2.8)$$

where p' is the small (local) perturbation of the equilibrium pressure p_0 , and the velocity, density and gravitational potential in a similar manner. One then inserts the previous form in the equations for mass (Eq. (2.1)), momentum (Eq. (2.2)) and energy conservation (Eq. (2.4)) as well as in the Poisson equation (Eq. (2.5)). For a static equilibrium stellar model all time derivatives of equilibrium quantities vanish, which yields:

$$\nabla \cdot (\rho_0 \mathbf{v}_0) = 0, \quad (2.9)$$

$$\rho_0 (\mathbf{v}_0 \cdot \nabla) \mathbf{v}_0 = -\nabla p_0 - \rho_0 \nabla \Phi_0, \quad (2.10)$$

$$T_0 (\mathbf{v}_0 \cdot \nabla) S_0 = \epsilon_{N,0} - \frac{1}{\rho_0} \nabla \cdot \mathbf{F}_0, \quad (2.11)$$

$$\nabla^2 \Phi_0 = 4\pi G \rho_0, \quad (2.12)$$

$$p_0 = \frac{\mathcal{R}}{\mu} \rho_0 T_0. \quad (2.13)$$

In Sect. 5.1 we will use a simplified version of these equations in the case of a barotropic equilibrium model, that is a model with a gas density which is a function of pressure only (Kippenhahn and Weigert, 1994).

As concerns the oscillations, we will assume that they are adiabatic. Indeed, the characteristic time scale for radiation and for the generation of energy by nuclear reactions is generally large compared to oscillation periods, consequently it can be assumed in most

parts of the star that $dS/dt = 0$ on the time scale of oscillations (Christensen-Dalsgaard, 2003). Equation (2.4) can also be expressed as

$$T \frac{dS}{dt} = \frac{du}{dt} + p \frac{dV}{dt}, \quad (2.14)$$

where V is the specific volume and u the internal energy per unit mass. Using the fact that $V = 1/\rho$, we obtain

$$T \frac{dS}{dt} = \frac{du}{dt} - \frac{p}{\rho^2} \frac{d\rho}{dt}, \quad (2.15)$$

which can be written as (Kippenhahn and Weigert, 1994)

$$T \frac{dS}{dt} = \frac{1}{\rho(\Gamma_3 - 1)} \left(\frac{dp}{dt} - \frac{\Gamma_1 p}{\rho} \frac{d\rho}{dt} \right), \quad (2.16)$$

where the adiabatic exponents Γ_1 and Γ_3 are defined as

$$\Gamma_1 \equiv \left(\frac{\partial \ln p}{\partial \ln \rho} \right)_{\text{ad}}, \quad \Gamma_3 \equiv \left(\frac{\partial \ln T}{\partial \ln \rho} \right)_{\text{ad}} + 1. \quad (2.17)$$

For adiabatic oscillations, $dS/dt = 0$ and Eq. (2.4) thus transforms into

$$\frac{dp}{dt} = \frac{\Gamma_1 p}{\rho} \frac{d\rho}{dt}. \quad (2.18)$$

Although the adiabatic approximation is known to predict accurately the frequencies of global oscillation modes, it must be noted that it is not adequate close to the surface, since in this part of the star the radiative time scale is low (Christensen-Dalsgaard, 2003).

By keeping only terms that are linear in the perturbations (i.e. primed quantities) one obtains:

$$\frac{\partial \rho'}{\partial t} + \nabla \cdot (\rho' \mathbf{v}_0 + \rho_0 \mathbf{v}') = 0, \quad (2.19)$$

$$\rho_0 \frac{\partial \mathbf{v}'}{\partial t} + \rho_0 \mathbf{v}' \cdot \nabla \mathbf{v}_0 + \rho_0 \mathbf{v}_0 \cdot \nabla \mathbf{v}' + \rho' \mathbf{v}_0 \cdot \nabla \mathbf{v}_0 = -\nabla p' - \rho_0 \nabla \Phi' - \rho' \nabla \Phi_0, \quad (2.20)$$

$$\nabla^2 \Phi' = 4\pi G \rho', \quad (2.21)$$

$$\frac{\partial p'}{\partial t} + \frac{\partial \delta \mathbf{r}}{\partial t} \cdot \nabla p_0 = \frac{\Gamma_{1,0} p_0}{\rho_0} \left(\frac{\partial \rho'}{\partial t} + \frac{\partial \delta \mathbf{r}}{\partial t} \cdot \nabla \rho_0 \right), \quad (2.22)$$

where we have introduced the fluid displacement $\delta \mathbf{r}$, related to the Eulerian velocity perturbation \mathbf{v}' by

$$\mathbf{v}' = \frac{\partial \delta \mathbf{r}}{\partial t} + (\mathbf{v}_0 \cdot \nabla) \delta \mathbf{r} - (\delta \mathbf{r} \cdot \nabla) \mathbf{v}_0. \quad (2.23)$$

To go further in our analysis, we need to make some assumptions on the background configuration of the star. If we assume that our background stellar model is axially symmetric, and uniformly rotating with some rotational velocity $\boldsymbol{\Omega} = \Omega \mathbf{e}_z$, we obtain that Eqs. (2.10)-(2.13) on the equilibrium model turn into (Unno et al., 1989)

$$\boldsymbol{\Omega} \times \boldsymbol{\Omega} \times \mathbf{r} = -\frac{1}{\rho_0} \nabla p_0 - \nabla \Phi_0, \quad (2.24)$$

$$\nabla \mathbf{F}_0 = \rho_0 \epsilon_{N,0}, \quad (2.25)$$

$$\nabla^2 \Phi_0 = 4\pi G \rho_0, \quad (2.26)$$

$$p_0 = \frac{\mathcal{R}}{\mu} \rho_0 T_0, \quad (2.27)$$

and Eqs. (2.19)-(2.22) on the perturbations take the form:

$$\frac{D\rho'}{Dt} + \nabla \cdot (\rho_0 \mathbf{v}') = 0, \quad (2.28)$$

$$\rho_0 \frac{D\mathbf{v}'}{Dt} + 2\rho_0 \boldsymbol{\Omega} \times \mathbf{v}' = -\nabla p' - \rho_0 \nabla \Phi' - \rho' \nabla \left(\Phi_0 - \frac{\Omega^2 d^2}{2} \right), \quad (2.29)$$

$$\nabla^2 \Phi' = 4\pi G \rho', \quad (2.30)$$

$$\frac{Dp'}{Dt} + \mathbf{v}' \cdot \nabla p_0 = \frac{\Gamma_{1,0} p_0}{\rho_0} \left(\frac{D\rho'}{Dt} + \mathbf{v}' \cdot \nabla \rho_0 \right), \quad (2.31)$$

where $d = r \sin \theta$ is the distance to the rotation axis, (r, θ, ϕ) are the spherical coordinates, and we have used the time derivative in the local rotating frame defined as

$$\frac{D}{Dt} \equiv \frac{\partial}{\partial t} + \Omega \frac{\partial}{\partial \phi}. \quad (2.32)$$

We remark that the hypothesis of axial symmetry should be satisfied for non-strongly magnetic isolated stars, but can be broken in the case of close binaries. Without loss of generality, it is possible to express perturbations as the real parts of harmonic complex functions, e.g. the pressure perturbation will be written as

$$p'(\mathbf{r}, t) = \text{Re}[\tilde{p}'(\mathbf{r}) \exp(-i\omega t)]. \quad (2.33)$$

Also, from the axial symmetry of the stellar model with respect to the rotation axis, it is possible to write perturbations as $f(r, \theta) \exp(im\phi)$, where m is an integer. In this way, we end up with the following equations in the meridional plane of the star:

$$-i\omega \rho' + \nabla \cdot (\rho_0 \mathbf{v}') = 0, \quad (2.34)$$

$$-i\omega \rho_0 \mathbf{v}' + 2\rho_0 \boldsymbol{\Omega} \times \mathbf{v}' = -\nabla p' - \rho_0 \nabla \Phi' - \rho' \nabla \left(\Phi_0 - \frac{\Omega^2 d^2}{2} \right), \quad (2.35)$$

$$\nabla^2 \Phi' = 4\pi G \rho', \quad (2.36)$$

$$-i\omega p' + \mathbf{v}' \cdot \nabla p_0 = \frac{\Gamma_{1,0} p_0}{\rho_0} (-i\omega \rho' + \mathbf{v}' \cdot \nabla \rho_0), \quad (2.37)$$

where ω is the mode frequency in the rotating frame, which is such that $\omega = \omega^{(I)} - m\Omega$, where $\omega^{(I)}$ is the mode frequency in the inertial frame (note that, for simplification, we have dropped the tildes on perturbation amplitudes). Usually, the associated boundary conditions are that the Lagrangian pressure perturbation vanishes at the surface ($\delta p = 0$) and the gravity potential goes to zero at infinity. At the centre, due to the singularity of spherical coordinates, the perturbations are regularized appropriately. The full Eqs. (2.34)-(2.37) together with the associated boundary conditions form a two-dimensional eigenvalue problem that can be solved numerically.

These equations take a simple form in the non-rotating limit, as the Coriolis term $2\rho_0 \boldsymbol{\Omega} \times \mathbf{v}'$ can be neglected, and the stellar background model is spherically symmetric. The spherical symmetry simplifies the problem greatly since it allows to use separation of variables as, for example,

$$p'(r, \theta, \phi) = p'(r) f(\theta) g(\phi). \quad (2.38)$$

In the asymptotic regime of high-frequencies, we can also neglect the perturbations of the gravitational potential ($\Phi' = 0$), an approximation due to Cowling (1941). Indeed, the gravitational potential can be expressed as

$$\Phi' = -G \int_V \frac{\rho'(\mathbf{r}', t)}{|\mathbf{r} - \mathbf{r}'|} dV, \quad (2.39)$$

showing that the contributions to this integral from regions with density perturbations of opposite signs will cancel out for rapid spatial variations, that is for modes with small wavelengths.

In Sect. 2.2.2, we shall use these two assumptions to find the physical behaviour and trapping regions of the different types of oscillations, and to derive an asymptotic expression for their mode frequencies.

2.2.2 Oscillations of non-rotating stars

As usual for normal modes of spherically symmetric systems, we start from the separation of radial and angular variables, and find that physical quantities (e.g. the pressure perturbation p') can be expressed using spherical harmonics as

$$p'(r, \theta, \phi, t) = \sqrt{4\pi} p'(r) Y_\ell^m(\theta, \phi) \exp(-i\omega t), \quad (2.40)$$

where Y_ℓ^m is a spherical harmonic defined as

$$Y_\ell^m \equiv (-1)^m C_{\ell m} P_\ell^m(\cos \theta) \exp(im\phi), \quad (2.41)$$

and P_ℓ^m is the Legendre function (and we remind here the reader that there is always the relation $|m| \leq \ell$). Therefore, we obtain that adiabatic oscillations of a non-rotating spherical stellar model, using the Cowling approximation, are described by the following equations:

$$\frac{1}{r^2} \frac{d}{dr} (r^2 \xi_r) + \frac{\nabla_r \Phi_0}{c_s^2} \xi_r + \left(1 - \frac{S_\ell^2}{\omega^2}\right) \frac{p'}{\rho_0 c_s^2} = 0, \quad (2.42)$$

$$\frac{1}{\rho_0} \frac{dp'}{dr} - \frac{\nabla_r \Phi_0}{\rho_0 c_s^2} p' + (N_0^2 - \omega^2) \xi_r = 0. \quad (2.43)$$

In these equations, ξ_r is the radial component of the fluid displacement $\delta \mathbf{r}$, S_ℓ is the characteristic acoustic frequency (also called the Lamb frequency) defined as

$$S_\ell^2 \equiv \frac{\ell(\ell+1)c_s^2}{r^2}, \quad (2.44)$$

N_0 is the buoyancy frequency (also called the Brunt-Väisälä frequency) that is defined as

$$N_0^2 \equiv \nabla \Phi_0 \cdot \left(\frac{\nabla \rho_0}{\rho_0} - \frac{1}{\Gamma_{1,0}} \frac{\nabla p_0}{p_0} \right), \quad (2.45)$$

and c_s is the celerity of sound such that

$$c_s^2 \equiv \frac{\Gamma_{1,0} P_0}{\rho_0}. \quad (2.46)$$

Now, we wish to transform Eqs. (2.42)-(2.43) into a second-order differential equation for p' (Unno et al., 1989). For simplification, we neglect derivatives of equilibrium quantities since they are generally small compared to k_r^2 for oscillations of high radial order (i.e. large number of nodes in the radial direction). We thus obtain that

$$\frac{d^2 \tilde{\Psi}}{dr^2} + k_r^2 \tilde{\Psi} = 0, \quad (2.47)$$

where the change of variable $\tilde{\Psi} \equiv \rho_0^{-1/2} r (|N_0^2 - \omega^2|)^{-1/2} p'$ has been made. The modulus of the radial wavevector k_r is here defined as

$$k_r^2 \equiv \frac{\omega^2}{c_s^2} \left(\frac{N_0^2}{\omega^2} - 1 \right) \left(\frac{S_\ell^2}{\omega^2} - 1 \right). \quad (2.48)$$

From Eqs. (2.47)-(2.48), one can see that there are two different types of oscillation modes corresponding to the two limit cases of high and low frequencies ω .

Gravity modes (g-modes)

At low frequencies, using that $\omega^2 \ll S_\ell^2$, one can approximate the radial wavenumber as

$$k_r^2 \simeq \frac{1}{\omega^2} (N_0^2 - \omega^2) \frac{\ell(\ell+1)}{r^2}. \quad (2.49)$$

This relation is similar to the dispersion relation for gravity waves, where gravity (or buoyancy) is the restoring force, therefore these modes are called gravity modes. Gravity modes have oscillatory solutions in regions of the star where $|\omega| < N_0$ and $|\omega| < S_\ell$, and exponentially decreasing solutions elsewhere.

Pressure modes (p-modes)

At high frequencies, using that $\omega^2 \gg N_0^2$, one can approximate the radial wavenumber as

$$k_r^2 \simeq \frac{\omega^2 - S_\ell^2}{c_s^2}. \quad (2.50)$$

This relation is similar to the dispersion relation for pressure waves, where pressure is the restoring force, therefore these modes are called pressure modes. They propagate within the regions where $|\omega| > N_0$ and $|\omega| > S_\ell$.

Propagation diagram

The computed values of the squared characteristic acoustic frequency S_ℓ^2 for $\ell = 1$ and buoyancy frequency N_0^2 for a pulsating pre-main sequence star are plotted in Fig. 2.9 as a function of the normalised radius. From the form of the S_ℓ^2 and N_0^2 curves, it can be seen that, in the oscillation spectrum, pure gravity modes should be found at lower frequencies, and pressure modes at higher frequencies. Between the dotted lines at $50\mu\text{Hz}$ and $140\mu\text{Hz}$ lies a region where both pressure and gravity waves are evanescent. Since it is small, mode couplings by tunnelling effect are possible. This should lead to the presence of *mixed modes*, i.e. modes with a mixed p and g character, in the oscillation spectrum of this star. In red-giant stars, the analysis of mixed modes has provided important constraint on the interior rotation profile (see e.g. Beck et al., 2012).

The asymptotic p-modes spectrum: WKB method and Tassoul's formula

In this section, we derive the formula giving the frequencies of pressure modes in the asymptotic regime, a formula that was found to be crucial for the interpretation of observed solar-like oscillations. Indeed, this formula relates frequency spacings with physical properties of the star, such as its sound speed distribution. Since the inference of a stellar model from a given oscillation spectrum is an under-constrained inverse problem (i.e. data are not enough to determine all the parameters of the model), any additional information on the spectrum, in particular its asymptotic structure, or on the stellar properties, is beneficial.

The asymptotic formula that describes the p-mode frequencies has been first derived by Vandakurov (1967); Tassoul (1980), and is known as *Tassoul's formula*. For its mathematical derivation we follow Unno et al. (1989); Christensen-Dalsgaard (2003). A very enjoyable introduction to the asymptotic theory of stellar oscillations can also be found in the KITP Blackboard Lunch talk of Richard Townsend (Townsend, 2011).

The WKB method has been developed in the context of quantum mechanics in order to solve one-dimensional problems in the regime of small effective Planck constant $\hbar \rightarrow 0$ (Shankar, 1994). The method can also be applied to any wave system, in the regime where

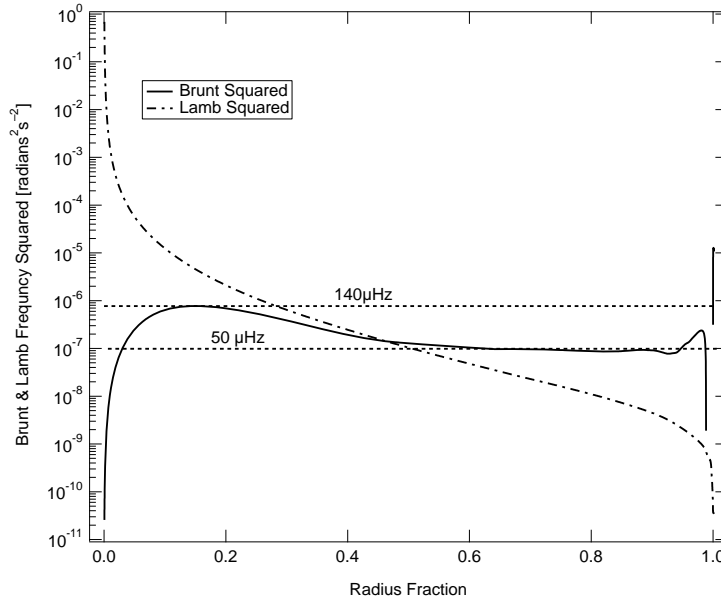


Figure 2.9: Propagation diagram for a stellar model of the pulsating pre-main sequence star V 589 Mon. The square of the Brunt Väisälä N_0^2 (continuous line) and Lamb frequencies S_ℓ^2 for $\ell = 1$ (dashed dotted line) are plotted (in $\text{rad}^2 \cdot \text{s}^{-2}$) as a function of the normalised radial coordinate r/R where R is the stellar radius. Gravity modes propagate in the lower part of the diagram, where $\omega^2 < N_0^2$, $\omega^2 < S_\ell^2$, and pressure modes in the higher part, where $\omega^2 > N_0^2$, $\omega^2 > S_\ell^2$ (from Zwintz et al., 2011).

the phase of the wave varies rapidly compared with the length-scale of the medium. We start by writing the pressure function $\tilde{\Psi}$ in Eq. (2.47) as

$$\tilde{\Psi}(r) = A(r) \exp[i\phi(r)], \quad (2.51)$$

where the phase $\phi(r)$ is assumed to vary rapidly such that $\frac{d\phi(r)}{dr}$ is large compared to $\frac{1}{A} \frac{dA}{dr}$, and $A(r)$ is a slowly varying amplitude. Inserting this form of solution into Eq. (2.47) yields an expression for the variation of the phase as

$$\frac{d\phi}{dr} = |k_r| = \left| \frac{\omega^2}{c_s^2} \left(\frac{N_0^2}{\omega^2} - 1 \right) \left(\frac{S_\ell^2}{\omega^2} - 1 \right) \right|^{1/2}, \quad (2.52)$$

and the amplitude

$$A(r) = |k_r|^{-1/2} = \left| \frac{\omega^2}{c_s^2} \left(\frac{N_0^2}{\omega^2} - 1 \right) \left(\frac{S_\ell^2}{\omega^2} - 1 \right) \right|^{-1/4}, \quad (2.53)$$

where the term smaller than $\frac{d\phi}{dr}$ has been neglected. The WKB method is not valid when $k_r = 0$, i.e. at the *turning points* of the waves, and the correct boundary conditions are imposed by matching functions at each side of the turning points. Along these lines, one can obtain the correct solution to the problem.

We now aim to obtain a formula for the frequencies of pressure modes starting from the approximate solution given by the WKB method. As stated in the previous section, one can use the approximation $k_r^2 \simeq (\omega^2 - S_\ell^2)/c_s^2$ for high-frequency p-modes. From the matching conditions at the turning points, one obtains that (Christensen-Dalsgaard, 2003)

$$\int_{r_t}^R \frac{(\omega^2 - S_\ell^2)^{1/2}}{c_s} dr = (n + \alpha)\pi, \quad (2.54)$$

where r_t is the position of the lower turning point, R the stellar radius, n an integer, and α a phase constant. Since we assumed that the outer turning point is located on the surface, and since the contribution from the inner turning point is known to be $1/4$, α thus depends on surface properties. The relation in Eq. (2.54) can be simplified in the case of low-degree (ℓ quantum number) modes. Indeed, for ℓ small, the pressure wave is reflected close to the centre and we can take $r_t \sim 0$. If one assumes that the celerity of sound is homogeneous in the centre of the star, and using $\sqrt{\ell(\ell+1)} \sim \ell + 1/2$, we obtain the first order (in frequency ω) of Tassoul's asymptotic formula that reads:

$$\omega_{n,\ell} \simeq \Delta\omega \left(n + \frac{\ell}{2} + \frac{1}{4} + \alpha \right), \quad (2.55)$$

where

$$\Delta\omega \equiv 2\pi \left(2 \int_0^R \frac{dr}{c_s(r)} \right)^{-1} \quad (2.56)$$

is the *large frequency separation*. This formula describes correctly the frequencies of high order (n quantum number), low degree (ℓ quantum number) pressure modes, as was confirmed by numerous observations of the Sun's oscillations (Claverie et al., 1979). For a more accurate description of frequencies, it is possible to take into account the variation of c_s in the core of the star. This leads to the relation (Tassoul, 1980; Gough, 1986)

$$\omega_{n,\ell} \simeq \Delta\omega \left(n + \frac{\ell}{2} + \frac{1}{4} + \alpha \right) - (AL^2 - \delta) \frac{\Delta\omega^2}{\omega_{n,\ell}}, \quad (2.57)$$

where $L^2 = \ell(\ell+1)$ and

$$A = \frac{1}{2\pi\Delta\omega} \left(\frac{c_s(r=R)}{R} - \int_0^R \frac{dc_s}{dr} \frac{dr}{r} \right). \quad (2.58)$$

One can obtain from Eq. (2.57) the so-called *small frequency separation* as:

$$\delta\omega_{n,\ell} \equiv \omega_{n,\ell} - \omega_{n-1,\ell+2} \simeq (4\ell+6) \frac{\Delta\omega}{4\pi^2\omega_{n,\ell}} \left[\frac{c_s(R)}{R} - \int_0^R \frac{dc_s}{dr} \frac{dr}{r} \right]. \quad (2.59)$$

Between homologous spherical stellar models, the large separation scales as $\sqrt{GM/R^3}$, and is thus proportional to the square root of the mean density. The small separation, on the other hand, is sensitive to the stellar age since it depends on the speed of sound inside the core, where the chemical stratification with age takes place. In particular, the small frequency separation diminishes with increasing age in hydrogen burning stars (Christensen-Dalsgaard, 1988).

2.2.3 Oscillations of rotating stars

The formalism of Sect. 2.2.2 cannot be applied directly to rotating stars due to their lack of spherical symmetry. As we have seen in the previous section, the small amplitude adiabatic perturbations of a rotating star are governed by Eqs. (2.28)-(2.31), when the background stellar model is assumed to be axially symmetric and uniformly rotating. From the form of these equations, one sees that rotational effects on the oscillation modes come from the Coriolis and centrifugal forces. The two principal approaches that can be used to compute oscillations of rotating stars are the *perturbative approaches* and the *full two-dimensional computations*. Naturally, both approaches have pros and cons, that we list in the following paragraphs. Ray theory, which is a third and complementary approach, will be discussed extensively in Chap. 4 and Chap. 5.

Types of oscillations in rotating stars

In the rotating case we recover the two types of modes that we discussed in the previous section, namely pressure and gravity modes, but with modifications in their structures and frequencies. Indeed, pressure modes are affected by the centrifugal deformation of their resonant cavity inside the star. On the other hand, high-frequency pressure modes are not affected by the Coriolis force because, in this frequency regime, the time scale associated with the Coriolis force is much longer than the mode period. Gravity modes are strongly modified by the Coriolis force leading to so-called ‘gravito-inertial’ modes (see e.g. Rieutord, 2009). The effect of the centrifugal force on g-modes is weaker since these modes are often concentrated close to the centre, where the centrifugal deformation of the stellar structure is weak. Moreover, for rapid rotation rates, the Coriolis force acts as a restoring force by itself, and the modes whose restoring force is the Coriolis force are called *inertial modes*. In the remaining of this thesis, we will study the high-frequency regime where we mostly consider pressure modes.

Perturbative methods

When the stellar rotation rate Ω is assumed to be small, it is possible to treat its effects as a perturbation. The perturbation method allows to simplify the two-dimensional eigenvalue problem of Eqs. (2.34)-(2.37) into a sequence of one-dimensional problems that are less numerically demanding. To that end, one writes the frequencies and amplitudes of the oscillation modes, as well as the equilibrium model, as power series in Ω of the form

$$\omega_{n,\ell,m} = \omega_{0,n,\ell,m} + \sum_{j=1}^k C_{j,n,\ell,m} \Omega^j + \mathcal{O}(\Omega^{k+1}), \quad (2.60)$$

where ω_0 is the mode frequency at zero rotation and $C_{j,n,\ell,m}$ are the perturbative coefficients. First-order perturbation theory was developed by Cowling and Newing (1949); Ledoux (1951). Second-order corrections were introduced by Simon (1969); Smeyers and Denis (1971), and generalized by Saio (1981); Gough and Thompson (1990); Dziembowski and Goode (1992); Suárez et al. (2006). Finally, third-order corrections to the theory were added by Soufi et al. (1998); Karami (2008). From a simple geometrical argument (see e.g. Christensen-Dalsgaard, 2003), one can see that frequencies in the inertial frame form *rotational multiplets* with $2\ell + 1$ components at small rotation rates. From the first-order perturbation theory, one finds that there exists a m -splitting in the rotating frame also, due to the effects of the Coriolis force. For high-frequency p-modes though, the Coriolis force is negligible, and thus we have $C_{1,n,\ell,m} \sim 0$. Higher-order effects on p-mode frequencies come mainly from the distortion of the star by the centrifugal force. The validity domains of perturbation theories can be precisely known only through comparisons with full two-dimensional computations, we present one example of such a comparison in the next section. For more details on perturbative methods, one can consult Goupil (2009).

Complete computations

To take fully into account the effects of rotation on pulsation modes for a given stellar model, the two-dimensional eigenvalue problem Eqs. (2.34)-(2.37) has to be solved numerically. This task is far more numerically demanding than perturbative methods. Recent reviews on complete two-dimensional computations of oscillation modes can be found in Goupil (2009); Reese (2010) and Ballot et al. (2013).

It is acknowledged that the two-dimensional numerical computation of linear oscillations in a rapidly rotating star is a difficult problem (see e.g. Papaloizou and Pringle, 1980; Clement, 1981; Dintrans and Rieutord, 2000). For pressure modes, the first accurate

computations (‘accurate’ in the sense that the reached accuracy was enough to study the asymptotic regime of high frequencies, and to reach the accuracy of current long-term spatial observations) were carried out by Lignières et al. (2006); Reese et al. (2006) with the TOP code, with the limitation that they used polytropic stellar models. Then, Reese et al. (2009) extended their numerical method to more realistic stellar models. At the moment, there are three major codes that are used to compute stellar oscillations in rapidly rotating stellar models without approximation: the TOP (Reese et al., 2006, 2009), ROTORC (Deupree, 1990, 1995, 1998) and ACOR (Ouazzani et al., 2012) codes.

Complete computations can be used to infer the validity domains of perturbative methods. To this aim, the ‘mode following technique’ (explained in Sect. 5.6) has been used by Reese et al. (2006), where oscillation frequencies were computed first for a non-rotating polytropic stellar model, and then followed for increasing rotation rates. The polynomial fits of these frequencies as functions of the rotation rate are then used to derive *ad hoc* perturbative coefficients. The validity domains of perturbative approximations are then obtained by fixing the maximal allowed difference ϵ_ω between the “exact” and perturbative frequencies. It can be seen in Fig. 2.10 that for pressure modes in a polytropic model of a typical A-type star with $M = 1.9M_\odot$ and $R = 2.3R_\odot$, the perturbative approximation fails at around 100 km.s^{-1} ($\sim 0.22 \Omega/\Omega_K$) for low frequencies and 45 km.s^{-1} ($\sim 0.1 \Omega/\Omega_K$) for high frequencies, if ϵ_ω corresponds to the standard accuracy of CoRoT data. The effect of the centrifugal force on oscillation frequencies was thus found to get stronger with increasing frequency. In conclusion, from Fig. 2.6 and Fig. 2.10, one can expect that typical A/F stars should be outside the validity domains of perturbative methods. Therefore, the interpretation of their oscillation spectra should require the use of non-perturbative methods.

Unlike perturbative methods, two-dimensional computations have permitted to numerically observe the strong rotational effects of the centrifugal deformation on p-mode frequencies and amplitude distributions. A first series of study (Lignières et al., 2006; Reese et al., 2006, 2008; Reese, 2006) followed the influence of rotation on low ℓ spherical harmonics, in the asymptotic regime of p-modes. It was found that, starting from zero to high rotation rates, these high-frequency p-modes are subjected to drastic changes in their amplitude distributions, departing strongly from a single spherical harmonic at high rotation, as can be seen in Fig. 2.11. Despite these strong modifications in the amplitude distributions of modes, it was observed that a frequency regularity with the same form as the one predicted by Tassoul’s formula (cf. Sect. 2.2.2) persisted at high rotation rates. Indeed, frequencies of oscillations in polytropic stellar models were shown to follow the empirical relation:

$$\omega_{\tilde{n}, \tilde{\ell}, \tilde{m}} \simeq \delta_{\tilde{n}} \tilde{n} + \delta_{\tilde{\ell}} \tilde{\ell} + \delta_{\tilde{m}} |\tilde{m}| + \tilde{\alpha}, \quad (2.61)$$

with an agreement that got better for higher frequencies. Though Eq. (2.61) is similar to Tassoul’s formula, the quantum numbers ($\tilde{n}, \tilde{\ell}, \tilde{m}$) were found to have a different physical meaning from the quantum numbers at zero rotation (n, ℓ, m) that are associated to spherical harmonics. These new quantum numbers reflected the novel geometry of the pulsation modes at high rotation rates, as they correspond to node numbers of the amplitude distributions (Lignières and Georgeot, 2008; Reese et al., 2008). Although these results were obtained for uniformly rotating polytropic stellar models, they were later confirmed for more realistic stellar models and in presence of differential rotation (Reese et al., 2009). In Chap. 4, we shall present a different approach to the numerical exploration of high-frequency pressure modes in rotating polytropic stellar models, as a more complete spectrum (i.e. not restricted to modes that have low ℓ at zero rotation) is obtained at a fixed rotation rate and analysed with the aid of asymptotic analysis. In Chap. 5, we will use the TOP code to obtain new results for high rotation rates in order to verify the asymptotic formula for regular frequency spacings of high-frequency pressure modes that will be derived in Chap. 5.

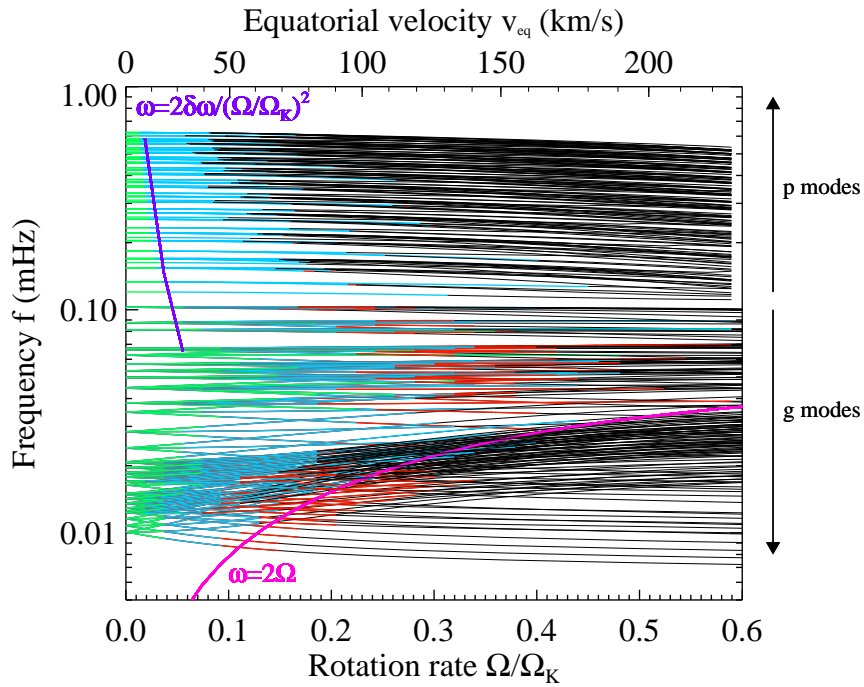


Figure 2.10: Oscillation frequencies in polytropic stellar models obtained from two-dimensional complete numerical computations. Only mode frequencies with quantum numbers $\ell = \{0, 1, 2, 3\}$ have been included. Frequencies are computed in the frame rotating with the star, and plotted as functions of the rotation rate Ω/Ω_K , where $\Omega_K = \sqrt{GM/R_{\text{eq}}^3}$, and equatorial velocity v_{eq} in km/s. The green, cyan, and red curves indicate the validity domains of the 1st, 2nd and 3rd order perturbative approximations, respectively, for a maximal departure ϵ_ω of $0.1\mu\text{Hz}$ from results of full computations. The purple line indicates the limit of first-order perturbative methods for p-modes (from Ballot et al., 2013).

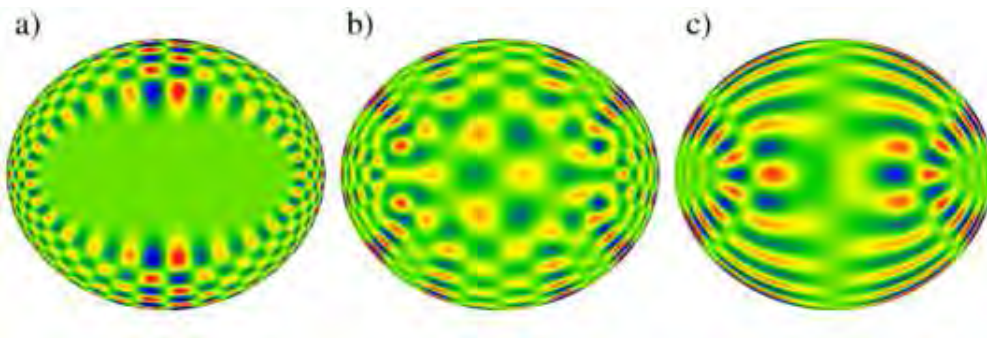


Figure 2.11: Normalised pressure amplitudes $p'/\sqrt{\rho_0}$ (where ρ_0 is the equilibrium density) in the meridional plane of the star, for three typical pressure modes in a polytropic stellar model rotating at $\Omega/\Omega_K = 0.6$. The physical explanation for the amplitude distributions of their eigenfunctions is given in Chap. 4 (from Reese et al., 2006).

Chapter 3

Concepts of quantum chaos

“I tell you: one must still have chaos within oneself, to give birth to a dancing star.”

Nietzsche, Thus Spoke Zarathustra (1885)

In the literature, one may find several definitions of quantum chaos that can be different in their formulation and meaning. Bogomolny (2006) has given a nice definition of quantum chaos, that is reproduced thereafter:

Quantum chaos is a nickname for the investigation of quantum systems which do not permit exact solutions. The absence of explicit formulas means that underlying problems are so complicated that they cannot be expressed in terms of known (\simeq simple) functions. The class of non-soluble systems is very large and practically any model (except a small set of completely integrable systems) belongs to it. An extreme case of quantum non-soluble problems appears naturally when one considers the quantisation of classically chaotic systems which explains the word ‘chaos’ in the title.

In most works of quantum chaos, only the wave-like character of quantum systems is actually relevant, without the need for properties such as quantum entanglement, that are peculiar to quantum systems (Steane, 1998). Therefore, most results of quantum chaos can be applied also to classical wave systems, be they elastic or electromagnetic. Consequently, in this thesis, we will use the words ‘quantum’ and ‘wave’ interchangeably.

As was hinted in the quotation above, one of the ways of defining quantum chaos is through the presence of chaos in the *classical limit* of a quantum system. This classical limit can be obtained in two ways. Firstly, if its physical quantities that have the dimension of an action (cf. Sect. 3.1.2) are much larger than Planck’s constant \hbar . Mathematically, this is equivalent to saying that $\hbar \rightarrow 0$, and in this limit one finds classical Hamiltonian equations of motion. In the language of wave mechanics this corresponds to the short-wavelength limit, which also exists for classical waves (Sect. 3.2.1). Secondly, the transition from a quantum system to a classical system can also be obtained by the process of decoherence (Zurek, 2003). This corresponds to the loss of coherence between states of a quantum superposition through multiple interactions with their environment. In this thesis, the ‘classical’ limit of interest is the one that is also meaningful for classical waves, that is: the short-wavelength limit. Thus, the terms ‘classical’ and

‘short-wavelength’ limit will also be used interchangeably. In order to recall the important concepts of classical Hamiltonian systems, we begin this chapter by a quick review of the field, as well as a discussion of the definitions of classical integrability, chaos, and the mixed regime that possesses elements of both (Sect. 3.1). We then move forward to the quantum realm, where we introduce some tools that serve to define ‘integrability’ and ‘chaos’ in this context, namely the classical limit (Sect. 3.2.1) and the statistical properties of energy levels (Sect. 3.2.2). Then, as was done for classical systems, we detail the cases of integrable (Sect. 3.2.3), chaotic (Sect. 3.2.4), and mixed (Sect. 3.2.5) quantum systems. For additional information on quantum chaos, one can consult the books and reviews on the subject by Eckhardt (1988); Gutzwiller (1990); Giannoni et al. (1991); Ott (2002); Haake (2010), and for a gentle introduction to the field one can read Gutzwiller (1992). A similar discussion about quantum chaos concepts was written for the short review Pasek and Georgeot (2013).

3.1 Integrability and chaos in classical Hamiltonian systems

Before the 20th century, there was probably a belief among scientists that most classical dynamical systems were integrable, the problem in understanding them being to find the corresponding constants of motion and action-angle coordinates (see Sect. 3.1.2). But, from the pioneering works of Poincaré on the three body problem in celestial mechanics (Poincaré, 1890), and the blossoming of computer-assisted simulations in the 20th century, it has been found that many systems in nature display various degrees of chaos. We give in the following a quick review of the basics and tools of classical Hamiltonian systems, and then discuss the subject of integrability and chaos in classical mechanics, which will be useful to understand the quantum case. For more details on Hamiltonian dynamical systems, one can consult Arnol’d (1989); Lichtenberg and Lieberman (1983); Ott (2002).

3.1.1 Classical Hamiltonian systems

Hamiltonian systems are dynamical systems which are defined in a *phase space* formed by N spatial coordinates $\mathbf{q} = q_1, q_2, \dots, q_N$ and N associated momentum coordinates $\mathbf{p} = p_1, p_2, \dots, p_N$, where N is the number of degrees of freedom. These systems are characterized by the existence of a Hamiltonian function $H(\mathbf{p}, \mathbf{q}, t)$ which describes the evolution of the system in the $2N$ -dimensional phase space (\mathbf{p}, \mathbf{q}) through Hamilton’s equations:

$$\frac{\partial H}{\partial p_i} = \dot{q}_i, \quad \frac{\partial H}{\partial q_i} = -\dot{p}_i, \quad (3.1)$$

where $i \in \llbracket 1, N \rrbracket$, and dot denotes time derivative. A simple form for the Hamiltonian function H consists of a kinetic and potential term V with $H = \mathbf{p}^2/2 + V(\mathbf{q})$. From the so-called “symplectic structure” of Eq. (3.1), we have the equality

$$\frac{d}{dt}(\delta\mathbf{p} \cdot \delta\mathbf{q}' - \delta\mathbf{q} \cdot \delta\mathbf{p}') = 0, \quad (3.2)$$

where $(\delta\mathbf{p}, \delta\mathbf{q})$ and $(\delta\mathbf{p}', \delta\mathbf{q}')$ are infinitesimal displacements from the trajectory (\mathbf{p}, \mathbf{q}) . Consequently, any $2N$ -dimensional volume of phase space is conserved through the evolution of Eq. (3.1), thus precluding the existence of attractors in Hamiltonian dynamical systems. Additionally, if H does not depend explicitly on time t , there is a conserved quantity corresponding to the Hamilton function H itself, which is usually the energy of the system.

An important tool of dynamical systems theory is the Poincaré Surface of Section (PSS). Indeed, for systems with two degrees of freedom, the phase space is of dimension four, and therefore hard to visualize. However, if there is a conserved quantity such as

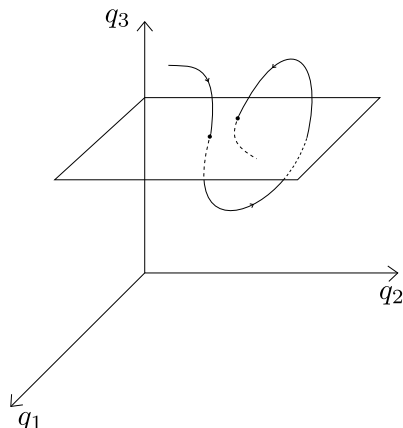


Figure 3.1: Illustration of the construction of a Poincaré Surface of Section (PSS) where, to construct the surface, the coordinate q_3 is set to a constant. The Poincaré map is obtained from the intersections of the Hamiltonian system trajectories with the surface, where only the trajectories that are coming downwards are used.

energy, the motion takes place on a surface of dimension three. If additionally we choose a surface of lower dimension transverse to the flow of trajectories and plot crossings of these trajectories with this surface, the motion becomes discrete (it is sometimes called a “Poincaré map”) and two-dimensional, thus easier to visualize (cf. Fig. 3.1). If the PSS is chosen by setting one of the phase space coordinates p_i, q_i to a constant, the discrete dynamics of the Poincaré map is still Hamiltonian (Lichtenberg and Lieberman, 1983). In the Poincaré map representation, the discrete time corresponds to the number of crossings with the PSS, and does not necessarily reflect time in the continuous system. Indeed, two trajectories of the continuous system may cross the surface of section at different times. Moreover, if one wishes the Poincaré map to be invertible (i.e. given a point on the PSS, the next point on the PSS is uniquely determined), then it is necessary to include only the contribution of trajectories that intersect the PSS in the same direction (see Fig. 3.1). In the following, the PSS will enable us to view the different structures of phase space, and in particular to visually distinguish between integrable and chaotic systems.

3.1.2 Integrability and chaos

Generic Hamiltonian systems fall in-between two extreme classes. The first one corresponds to integrable systems. In some sense, they can be considered as exactly solvable models. Indeed, integrable systems possess as many independent constants of motion as degrees of freedom. In Hamiltonian mechanics, two constants of motion f_1 and f_2 are said to be independent, or in involution, if their Poisson bracket vanishes, where the Poisson bracket is defined as (Arnol’d, 1989)

$$\{f_1, f_2\} = \sum_{i=1}^N \left(\frac{\partial f_1}{\partial q_i} \frac{\partial f_2}{\partial p_i} - \frac{\partial f_1}{\partial p_i} \frac{\partial f_2}{\partial q_i} \right). \quad (3.3)$$

Thus, for an integrable system with a $2N$ -dimensional phase space, N quantities that we will call I_1, \dots, I_N must be conserved (i.e. $\{H, I_i\} = 0$ for all $i \in \llbracket 1, N \rrbracket$) and in involution. For example, for systems with one degree of freedom where the Hamiltonian function H does not depend explicitly on time, the conservation of energy is sufficient to ensure that the system is integrable. In any dimension, if the system is completely separable (i.e. if the Hamiltonian can be expressed as $H = \sum_i H_i(x_i, p_i)$), then it is known that the system is integrable (but the opposite is not true). It can be demonstrated that for an integrable

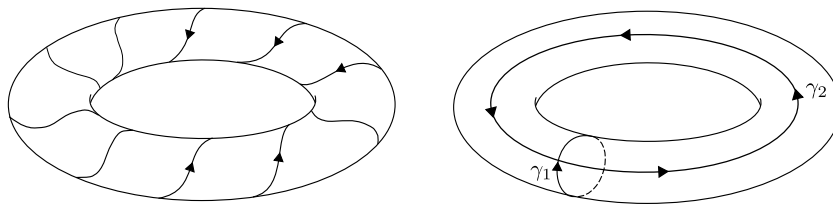


Figure 3.2: One trajectory of an integrable Hamiltonian system winding around a 2-dimensional torus in phase space (left panel). Right panel: A 2-dimensional torus, with its irreducible paths γ_1 and γ_2 (Figure inspired from Ott (2002)).

system, the motion takes place on N -dimensional tori in the $2N$ -dimensional phase space (Arnol'd, 1989), as is illustrated in Fig. 3.2. These tori are the so-called *invariant tori*, in the sense that they are invariant under the dynamics, that foliate the whole phase space of integrable Hamiltonian systems. It must be noted though, that these surfaces are tori in a topological sense only (cf. Fig. 3.2), and may appear very distorted in a given choice of coordinates. When a Hamiltonian system is integrable, it can be shown that there exists a ‘canonical’ change of variables (where ‘canonical’ means that this change of variables preserves the form of the equations of motion Eq. (3.1)) to a specific type of variables, called *action-angle variables* (Arnol'd, 1989). When written in the action-angle variables $(\mathbf{I}, \boldsymbol{\theta})$, the new Hamiltonian depends only on $\mathbf{I} = (I_1, \dots, I_N)$, and Hamilton’s equations of motion Eq. (3.1) become:

$$\dot{I}_i = 0, \quad \dot{\theta}_i = \omega_i, \quad (3.4)$$

where $i \in \llbracket 1, N \rrbracket$, and ω_i are constants. As one can see from Eq. (3.4), the equations of motion become very simple in the action-angle variables, and their integration is straightforward. The action variables I_i are defined, in terms of the ‘old’ coordinates (\mathbf{p}, \mathbf{q}) , as

$$I_i = \oint_{\gamma_i} \mathbf{p} \cdot d\mathbf{q}, \quad (3.5)$$

where γ_i denote paths on the torus that are irreducible to a point when continuously deformed (see Fig. 3.2 for the case of a 2-dimensional torus). Famous examples of classical integrable systems are the harmonic oscillator, the square and circular billiards, and the two-body Kepler problem.

The other extreme class of Hamiltonian systems is the one of *chaotic* systems. Chaotic systems have no constant of motion besides their energy. Thus, for systems with at least two degrees of freedom, the motion in phase space is not restricted to tori, and most trajectories may fill the constant energy surface of dimension $2N - 1$ densely. This chaotic behaviour can be described statistically, leading to the characterization of various degrees of chaos (Lichtenberg and Leiberman, 1983; Gutzwiller, 1990). These degrees of chaos form a so-called “ergodic hierarchy”, since each level of increasing chaos implies the previous one. The first degree, *ergodicity*, implies that for any function on phase space, its spatial mean equals its temporal mean for infinitely long times for almost all initial conditions. Roughly, this signifies that almost all trajectories will come arbitrarily close to any phase space point after sufficiently long times. This property is important, since it forms the basis for the *ergodic hypothesis* of classical statistical mechanics. The *mixing* is satisfied if, given any two regions of phase space A and B , the volume of the time-forward evolution of subset A that ends in B at infinite times is proportional to the volume of B , that is to say the subset A gets spread out homogeneously on phase space (Arnol'd, 1989; Gutzwiller, 1990). Finally, *K-systems* show an exponential divergence of nearby trajectories everywhere in their phase space, which is sometimes called “hard chaos”, implying the widely popularized “butterfly effect”. These systems are mixing systems where the mixing is exponentially

fast. Famous examples of chaotic systems include the Bunimovich (or stadium) billiard, the motion of a particle on a surface of constant negative curvature, and the kicked rotor for large values of the kick parameter (see Sect. 3.1.3).

The PSS can be used as an empirical way of determining whether a system is integrable or chaotic. For simplicity, we take the example of a system with only two degrees of freedom. If the system is integrable, its trajectories will follow 2-dimensional tori. Their intersections with the surface of section will therefore lead to 1-dimensional structures, i.e. the intersections form *lines* on the PSS. If the system is chaotic, trajectories fill the 3-dimensional energy shell, and the intersections of these trajectories with the surface of section will thus form 2-dimensional surfaces, i.e. fill *domains* on the PSS. We will see in the next section that the two extremes presented above are in fact exceptional, and that the majority of Hamiltonian dynamical systems will have both integrable and chaotic structures interwoven in their phase space. Thus, most Hamiltonian systems are between the two extremes of integrability and chaos, and are called *mixed systems* for this reason. One of the possible ways to obtain such phase space structure is given by the Kolmogorov-Arnold-Moser (KAM) theorem, that describes what happens when an integrable system is perturbed, and whose results are sketched thereafter.

3.1.3 Mixed systems

The generic transition to chaotic behaviour for a perturbed integrable system is described by the famous Kolmogorov-Arnold-Moser (KAM) theorem (Arnol'd, 1989; Ott, 2002). This theorem describes the behaviour of an integrable Hamiltonian system $H_0(\mathbf{p}, \mathbf{q})$ that is subjected to a small and sufficiently smooth perturbation of the form

$$H(\mathbf{p}, \mathbf{q}) = H_0(\mathbf{p}, \mathbf{q}) + \epsilon H_1(\mathbf{p}, \mathbf{q}). \quad (3.6)$$

The procedure for finding this perturbative behaviour actually comes across a ‘small denominators problem’ (Arnol'd, 1989). One can define the so-called *resonant tori* of the integrable Hamiltonian by their actions \mathbf{I} satisfying the relation

$$\mathbf{m} \cdot \frac{\partial H_0}{\partial \mathbf{I}} = 0, \quad (3.7)$$

where \mathbf{m} is a vector of integers. Then, the theorem states that resonant tori must be destroyed as soon as $\epsilon > 0$. However, most of the invariant tori of the unperturbed Hamiltonian H_0 , the *non-resonant tori* or *KAM tori*, survive for a sufficiently small perturbation and are only deformed by its effect. In place of the resonant tori, an equal number of alternating *elliptic* and *hyperbolic periodic orbits* can be found (see e.g Lichtenberg and Lieberman, 1983, for a definition). Since the motion close to an elliptic orbit can be put in a form similar to Eq. (3.6), elliptic orbits are encircled by KAM tori, and this pattern repeats itself on smaller and smaller scales, leading to a *fractal* structure (nice illustrations of this structure can be found in Ott (2002)). The phase space of a perturbed integrable Hamiltonian system is thus made of an intricate mixture of *stable islands* encircling elliptic orbits, surrounded by chaotic zones created by the hyperbolic orbits. A ‘typical’ PSS will thus be made of chaotic domains filling the space between integrable lines. For systems with two degrees of freedom, these different phase space regions are dynamically isolated by KAM tori and a trajectory always stays in some definite region of phase space.

As an illustration of a KAM-like transition, we consider the case of the kicked rotor defined by the Hamiltonian (Lichtenberg and Lieberman, 1983)

$$H(p_\theta, \theta, t) = \frac{p_\theta^2}{2} + K \cos \theta \sum_n \delta(t - n), \quad (3.8)$$

where δ is the Dirac delta function, K is the positive *stochasticity parameter*, and the angle θ and angular momentum p_θ are canonically conjugate variables. This system thus

consists in a rotor that is kicked at $t = 1, 2, 3, \dots$, and between these kicks are periods of free motion where p_θ is constant. Though this system has only one degree of freedom, it can nevertheless display chaos since H depends explicitly on time t and energy is not conserved. It is possible, thanks to the periodicity, to transform this dynamical system into a discrete map by considering the mapping between states at times $n - \epsilon$ and $(n + 1) - \epsilon$ where ϵ is small (i.e. just before the n -th and $(n + 1)$ -th kicks). This discretisation yields the so-called *standard map*, that is

$$p_{n+1} = p_n + K \sin \theta_n, \quad (3.9)$$

$$\theta_{n+1} = (\theta_n + p_{n+1}) \bmod 2\pi. \quad (3.10)$$

Given that θ is an angle, the phase space is topologically a cylinder. The map is also 2π -periodic in p_θ , and so we can represent the phase space in terms of variables (\tilde{p}, θ) , where $\tilde{p} = p \bmod 2\pi$. Now, let us analyse the dynamical evolution of Eqs. (3.9)-(3.10) as a function of the parameter K . For $K = 0$, we recover the (friction-less) ordinary rotor since there is no perturbation and only the free motion remains. In this form the system is integrable, since p_θ is conserved throughout the motion and there is just one degree of freedom. Indeed, as one can see on the first panel of Fig. 3.3, the phase space of the standard map for $K = 0$ is foliated by 1-dimensional tori (i.e. circles), where each torus is associated to a value of p_θ . As soon as $K \neq 0$, a KAM-like transition of the dynamics takes place. Tori such that $p_\theta = N/M$ where N and M are coprime integers (i.e. the resonant tori) are instantaneously destroyed by the perturbation, and chains of M integrable islands are formed around elliptic fixed points. Also, as we stated previously, between these integrable islands are hyperbolic fixed points that will lead to the chaotic behaviour of some trajectories. In the second panel of Fig. 3.3, where the iterations of the standard map for $K = 0.1$ are plotted, one can see the appearance of the major resonance ($M = 1$) of the system corresponding to the hyperbolic point $(0, 0)$, and the elliptic point $(\pi, 0)$ whose associated integrable island can be seen. From the results of the KAM theorem, we know that the non-resonant tori survive a small perturbation. For the standard map, it can be demonstrated that all KAM (non-resonant) tori are destroyed for $K > K_c$ where $K_c \approx 0.9716$. As concerns the integrable islands, for increasing values of the parameter K , the elliptic periodic orbits undergo successive *period doubling bifurcations* (Ott, 2002). Consequently, the size of integrable islands tends to zero as K increases. In the regime $K \gg K_c$, one observes numerically signs of strong chaos, and trajectories follow a random walk in the momentum p , which thus follow a diffusion process (Lichtenberg and Lieberman, 1983). For other illustrations of the standard map, and a more detailed treatment of its properties, the reader can consult Reichl (2004). The behaviour as described here is known to be generic among perturbed Hamiltonian maps. Similarly, the PSS of a typical perturbed 2-dimensional Hamiltonian system is expected to show a mixture of integrable islands and chaotic seas.

3.2 Integrability and chaos in quantum systems

The notion of integrability is not as clear-cut in quantum and wave mechanics as it is in classical mechanics (Weigert, 1992; Caux and Mossel, 2011). Similarly, characteristic properties of chaos such as ergodicity on a well-defined phase space and the exponential divergence of nearby trajectories are harder to define in quantum mechanics, due to the uncertainty principle ($\Delta x \Delta p \geq \frac{\hbar}{2}$) and the linearity of Schrödinger's equation, respectively. It was thus necessary to find novel definitions of chaos that apply to quantum systems. In this section, we will focus on two possible signs of chaos in the quantum regime, namely the presence of chaos in the classical limit $\hbar \rightarrow 0$, and the Wigner-Dyson statistics of the energy levels of the system. These two phenomenons are related, in the form of the so-called *Bohigas-Giannoni-Schmit conjecture*, as we will see in Sect. 3.2.2.

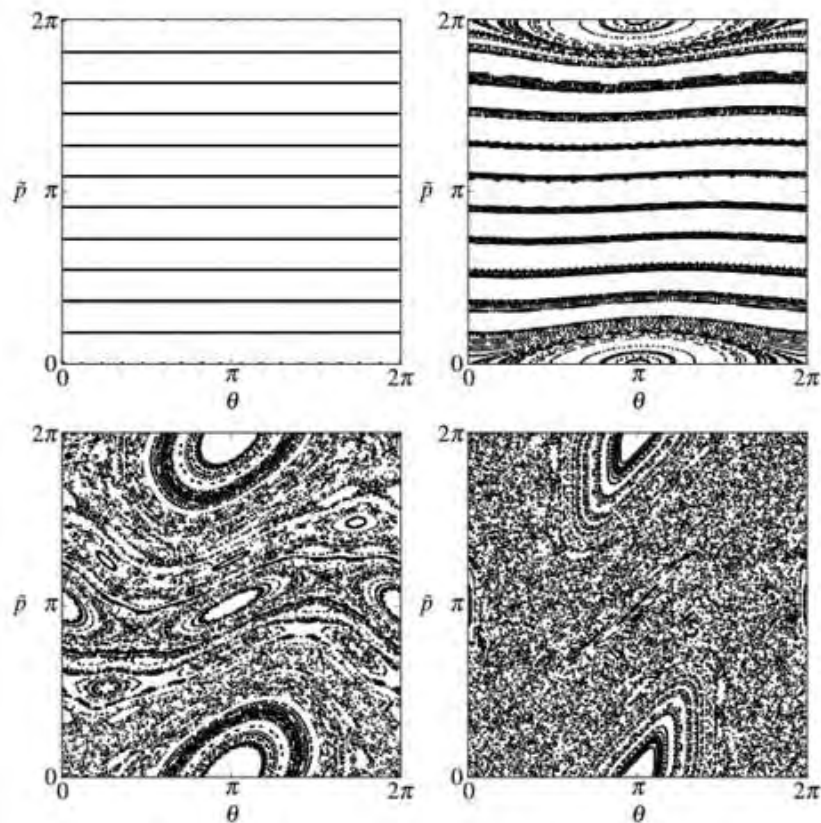


Figure 3.3: Plots of the standard map, defined by Eqs. (3.9)-(3.10), for increasing values of the perturbation parameter $K = 0.0, 0.1$ (upper row), 0.9716 and 2.0 (lower row). Coordinates of the map are the angle θ , and angular momentum $\tilde{p} = p \bmod 2\pi$. In the figure, 187 initial conditions have been used, and the map has been iterated 200 times.

We thus present in the following how to find the classical limit in quantum mechanics (or ‘ray limit’ in wave mechanics), and how one can define an equivalent of phase space for quantum systems (Sect. 3.2.1). Next, we present the relevant tools for the statistical analysis of energy levels and frequencies (Sect. 3.2.2). Once the classical limit of a quantum system is known, it is possible to obtain approximately its energy levels and eigenfunctions by so-called *semi-classical quantisation* techniques. Depending on the integrability or “chaoticity” of the classical limit, different semi-classical techniques must be used. Similarly as in the classical case, we will distinguish integrable (Sect. 3.2.3), chaotic (Sect. 3.2.4) and mixed (Sect. 3.2.5) quantum systems.

3.2.1 The classical limit and phase space distributions

Waves propagating in a spatially inhomogeneous medium must react to the variations of this medium. In cases where these variations occur on a length scale that is much longer than the wavelength of the wave, the medium can be considered as locally homogeneous. For a given medium, one can thus take the *short wavelength limit* of the wave equation to get the propagation equations for a locally plane wave. This propagation can be put in the form of an equation on ‘rays’, or ‘trajectories’ that are always tangent to the direction of propagation of this plane wave. Let us take the example of a sound wave, following Landau and Lifshitz (1959). The wave equation has the form

$$\frac{1}{c_s(\mathbf{x})^2} \frac{\partial^2 \Phi}{\partial t^2} - \nabla^2 \Phi = 0, \quad (3.11)$$

where Φ is the complex pressure amplitude perturbation and $c_s(\mathbf{x})$ the inhomogeneous celerity of sound. It can be noted that the equivalent equation for the propagation of a *scalar* electromagnetic field is obtained by replacing $1/c_s(\mathbf{x})$ by $n(\mathbf{x})/c$ where n is the inhomogeneous optical index of the medium and c the speed of light in vacuum. One writes the amplitude function in the form $\Phi = Ae^{iS}$, and makes the assumption, on the basis of a slowly varying medium, that the amplitude A is also a slowly varying function of time and position and that the phase S varies comparatively quickly. Recalling the case of a plane wave that varies as $\exp(i\mathbf{k} \cdot \mathbf{x} - i\omega t)$, one writes the phase S (also sometimes called the *eikonal*) as

$$S = S_0 + \frac{\partial S}{\partial \mathbf{x}} \cdot \mathbf{x} + \frac{\partial S}{\partial t} t. \quad (3.12)$$

The local wavevector and frequency are thus defined as

$$\mathbf{k} = \frac{\partial S}{\partial \mathbf{x}}, \quad \omega = \frac{\partial S}{\partial t}. \quad (3.13)$$

This leads to

$$\dot{\mathbf{k}} = -\frac{\partial \omega}{\partial \mathbf{x}}, \quad \dot{\mathbf{r}} = \frac{\partial \omega}{\partial \mathbf{k}}, \quad (3.14)$$

where ‘dot’ denotes time derivative. One will undoubtedly recognize in Eq. (3.14) the equations for trajectories of a Hamiltonian system. Depending on the system considered, this limit takes different names. In the case of wave optics, this limit corresponds to geometrical optics. In the case of quantum mechanics, the limit $\hbar \rightarrow 0$ gives the classical limit where the quantum world recovers the classical mechanics of Hamilton (the singular character of this limit, and of all types of short-wavelength limits, is discussed in Berry (1991)). The classical limit can also be obtained through the *stationary phase approximation* of the quantum propagator (Shankar, 1994; Schulman, 2005). One must note that in certain cases it is difficult to obtain a meaningful classical limit of quantum mechanics, e.g. for certain many-body systems.

Knowing the phase space of the classical limit, it is possible to infer some properties of the wavefunctions of the associated quantum system. But a direct comparison is not

possible because phase space is not well-defined in quantum mechanics. Indeed, though classical phase space distributions are functions of both position and momentum variables, in quantum mechanics these variables represent independent bases with respect to which the wavefunction can be written, and momentum and position operators do not commute. To circumvent this problem one can use the phase-space distribution known as *Wigner's distribution* (Wigner, 1932) that is defined as

$$\Psi(p, q) = (2\pi\hbar)^{-n} \int d^n q' \psi(q - q') \psi^*(q + q') \exp\left(\frac{-2ipq'}{\hbar}\right), \quad (3.15)$$

where $\psi(q)$ is the quantum wavefunction in the position representation, and n the number of degrees of freedom. The probability density in position space is obtained from Wigner's function Ψ as

$$\int d^n p \Psi(p, q) = |\psi(q)|^2, \quad (3.16)$$

and similarly for the momentum basis. It might be more convenient to find a quantity comparable to a classical probability distribution in phase space, i.e. a measure of the likelihood of finding a classical particle in some volume $d^n p d^n q$ of phase space. Wigner's distribution is real and of absolute value less than one, but it can be negative. Thus, Wigner's distribution only falls into the class of *quasiprobability distributions*, and it must be modified to be directly comparable to probability distributions. To this aim, one can do the *coarse-graining* of the Wigner function by its convolution in phase space with appropriate quantum states. Indeed, there exist 'minimum-uncertainty' wavepackets in quantum mechanics, i.e. quantum states prepared in such a way as to reach the lower bound of the uncertainty relation $\Delta q \Delta p \geq \frac{\hbar}{2}$. These states are in some sense the most classical states in the quantum world. It can be shown that these states have the form of Gaussian wavepackets, that also correspond to the ground-state solution of the quantum harmonic oscillator (Shankar, 1994). One can thus project the quantum wavefunction on these coherent states of varying widths and positions. Such a coherent states representation is possible since they form an over-complete basis. The phase space distribution that is obtained by projecting quantum wavefunctions onto Gaussian wavepackets is known as the *Husimi distribution* (Chang and Shi, 1986). It can be defined from Wigner's distribution $\Psi(p, q)$ as (see e.g. Gutzwiller, 1990)

$$\Phi(p, q) = (\pi\hbar)^{-1} \int dp' dq' \Psi(p', q') \exp\left(-\frac{(q - q')^2}{\hbar\Delta_q^2} - \Delta_q^2 \frac{(p - p')^2}{\hbar}\right) \quad (3.17)$$

where Δ_q is the width of the Gaussian wavepackets in position space. The coarse-graining procedure implies that one cannot obtain details smaller than a certain scale set by \hbar , according to the uncertainty principle.

Now, we illustrate how Husimi distributions can be used for the analysis of a complex quantum system. We choose the *quantum kicked rotor* as an example, which is the quantisation of the classical system Eqs. (3.9)-(3.10). The Hamiltonian operator for the quantum kicked rotor is obtained by applying the correspondence principle (where classical observables are replaced by corresponding quantum Hermitian operators) to Eq. (3.8). This yields the operator

$$\hat{H}(\hat{p}_\theta, \hat{\theta}, t) = \frac{\hat{p}_\theta^2}{2} + K \cos(\hat{\theta}) \sum_n \delta(t - n), \quad (3.18)$$

where $\hat{p}_\theta = -i\hbar \frac{\partial}{\partial \theta}$ in the position representation. The wavefunction $|\psi(t)\rangle$ of the quantum kicked rotor naturally evolves in time following Schrödinger's equation

$$i\hbar \frac{\partial}{\partial t} |\psi(t)\rangle = \hat{H} |\psi(t)\rangle. \quad (3.19)$$

This time evolution can be cast into the form of a (unitary) propagator $U(t, t_0)$ such that

$$|\psi(t)\rangle = U(t, t_0)|\psi(t_0)\rangle, \quad (3.20)$$

where

$$\hat{U}(t, t_0) = \exp \left[(-i/\hbar) \int_{t_0}^t \hat{H}(t') dt' \right]. \quad (3.21)$$

As in the classical case, we will consider the states that precede the kicks by some infinitely small time ϵ . The evolution between these states is given by the Floquet operator \hat{U}_F which is found to be of the form (Reichl, 2004)

$$\hat{U}_F = \exp \left[-i\hbar \frac{\hat{n}^2}{2} \right] \exp \left[-i \frac{K}{\hbar} \cos 2\pi \hat{\Theta} \right], \quad (3.22)$$

where we have introduced the operators $\hat{n} = \hat{p}_\theta/\hbar$, and $\hat{\Theta} = \hat{\theta}/2\pi$. There are two parameters in Eq. (3.22): \hbar , which determines the strength of quantum effects, and K , that rules the behaviour of the system in the limit $\hbar \rightarrow 0$. To close the phase space in the momentum direction, the periodic boundary condition $\langle p + 2\pi m | \psi \rangle = \langle p | \psi \rangle$ is chosen, where m is the number of cells.

To view in phase space the evolution of the wavefunction, we use Husimi distributions constructed using the coherent states

$$|\phi(p_0, \theta_0)\rangle = A \sum_p \exp \left(\frac{-(p - p_0)^2}{4a^2} - i\theta_0 p \right) |p\rangle, \quad (3.23)$$

where the normalization constant A is set to one, and we choose $a = 1/(\sqrt{N}\sqrt{12})$ such that the relative widths $\Delta p/N$ and $\Delta\theta/2\pi$ of the coherent states are comparable, as suggested in Frahm et al. (2004). In Fig. 3.4, we plot these Husimi representations of the wavefunction after $t = 10^3$ applications of the operator U_F for different values of K and for different initial quantum states. It can be seen in Fig. 3.4 that for $K = 0$, since the system is integrable, the wavefunction stays localised on one invariant torus at constant p_θ in the semi-classical limit. For $K = 2.0$, the system is mixed (see Sect. 3.2.5), and a wavefunction that was initially on a given zone of phase space will stay in this zone during the evolution in the semi-classical limit. The wavefunction that started in the chaotic region spreads ergodically over this region after some time, while the wavefunction that started on a near-integrable torus stays localised on this torus. Finally, for $K = 15.0$, all tori are destroyed and the wavefunction will spread over the whole phase space for any initial conditions. In conclusion, by comparing the Husimi distributions of quantum states with the corresponding classical system phase space, one can therefore identify the dynamical character of the quantum system (integrable, mixed or chaotic), and the comparison with the classical distribution evolution allows to see the correspondence principle in action.

3.2.2 Statistical properties of energy levels and frequencies

A very useful tool to obtain the generic properties of a complex quantum system is the statistical description of its energy levels. This subject can be traced back to the seminal works on the statistical description of nuclear spectra by Wigner (1951), and it has attracted much attention since then, in particular for its use to obtain tell-tale signs of integrability or chaos. Following Bohigas (1991); Guhr et al. (1998) and Mehta (2004), we review here the spectral observables that are used for such a statistical description of spectra. They will be applied to quantum integrable, chaotic and mixed systems in the next sections. Again, we want to stress that the following tools are not bound to be applied to the energy levels of quantum systems, but can also give important information

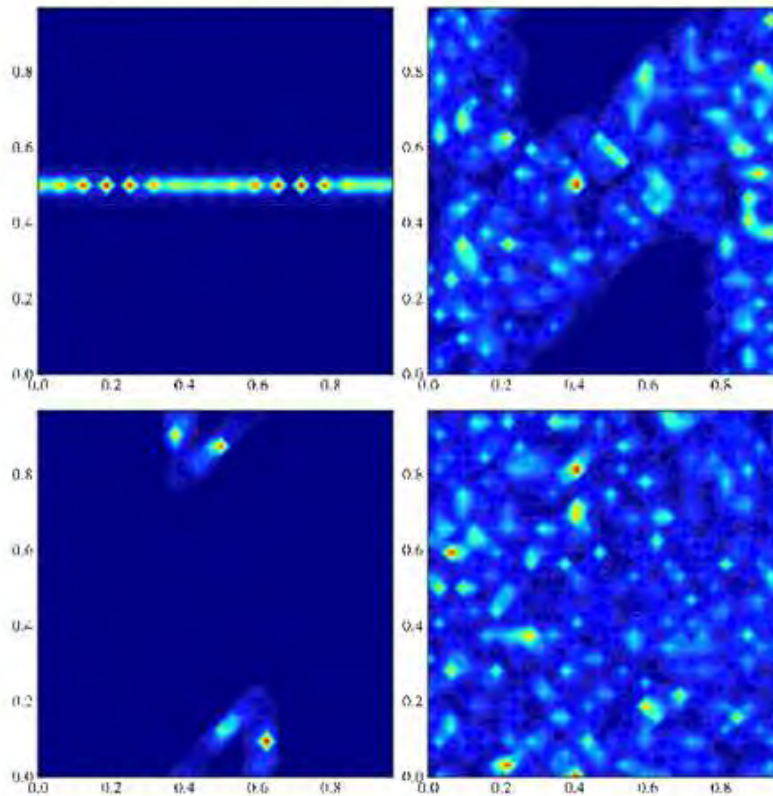


Figure 3.4: Husimi distributions $\Phi(\theta, p)$ of the quantum kicked rotor, θ being on the horizontal axis, at $t = 10^4$ for: $K = 0.0$ with an initial Gaussian wavepacket centred on $(\theta_0, p_0) = (0.6, 0.5)$ (upper row, left figure), $K = 2.0$ with the same state centred on $(0.6, 0.5)$ (upper row, right figure), again $K = 2.0$ but with an initial Gaussian wavepacket centred on $(0.6, 0.0)$ (lower row, left figure), and $K = 15.0$ with the same state centred on $(0.6, 0.0)$ (lower row, right figure). We have set the number of cells to one ($m = 1$), and the number of states in the Hilbert space to $N = 1024$, which corresponds to $\hbar \simeq 6.14 \cdot 10^{-3}$ ($N = \frac{2\pi m}{\hbar}$ being the number of states in the Hilbert space).

on the frequencies of quartz blocks (Ellegaard et al., 1996) or flexural plates vibrations (Legrand et al., 1992), modes of microwave cavities (see e.g. So et al., 1995) or pressure modes of rotating stars (see Chap. 4).

One considers the spectrum $E_1 \leq E_2 \leq \dots \leq E_n \leq \dots$ of some operator \hat{H} . The *counting function* $\eta(E)$, that is defined as

$$\eta(E) = \sum_i \Theta(E - E_i) = \text{Tr} \Theta(E - \hat{H}), \quad (3.24)$$

where Θ is the Heaviside step function, counts the number of eigenvalues that are less than or equal to some eigenvalue E . The derivative of the counting function yields the *density of states*, also called the *spectral function*, that is

$$\rho(E) = \frac{d\eta}{dE} = \sum_i \delta(E - E_i) = \text{Tr} \delta(E - \hat{H}), \quad (3.25)$$

where δ is the Dirac delta function. In order to separate the average (or smooth) spectrum from its fluctuating part, one expresses the counting function as

$$\eta(E) = \bar{\eta}(E) + \eta_{\text{fluct}}(E), \quad (3.26)$$

where $\bar{\eta}$ is the mean counting function and η_{fluct} the fluctuations from the mean. This yields the mean level density $\bar{\rho}(E)$ as

$$\bar{\rho}(E) = \frac{d\bar{\eta}(E)}{dE}. \quad (3.27)$$

One can get a semi-classical estimate of the smoothed number of states from the *Thomas-Fermi distribution* that is expressed as (Gutzwiller, 1990)

$$\bar{\eta}(E) \simeq \frac{1}{(2\pi\hbar)^N} \int d^N p \, d^N q \, \Theta(E - H(p, q)), \quad (3.28)$$

where N is the number of degrees of freedom of the system. It estimates the number of frequencies in some interval ΔE by counting the number of ‘Planck cells’ (portions of phase space with a volume of $(2\pi\hbar)^N$) contained in the phase-space volume $\int d^N p \, d^N q \, \delta(E - H(p, q))$ of the energy surface. When it is applied to the problem of a quantum particle trapped in a plane two-dimensional domain \mathcal{D} with Dirichlet boundary conditions (also known as a *quantum billiard*), one obtains that

$$\bar{\eta}(E) \simeq \frac{1}{4\pi} A E, \quad (3.29)$$

which is the first term of the so-called *Weyl’s expansion*, where A is the area of the domain \mathcal{D} (Weyl, 1912). This is actually the first term of a series expansion in powers of \hbar , the next order terms corresponding to the contributions from the length, curvature and angles of the boundary $\partial\mathcal{D}$, as well as the topology (connectedness) of the domain \mathcal{D} . As we have seen, the mean level density does not depend on the dynamics, i.e. on whether the system is integrable or chaotic. Since our goal is to obtain the generic statistical properties of complex quantum systems, it is required to remove the system-specific average level density. This operation is known as *unfolding the spectrum*, and consists in the mapping

$$x_i = \bar{\eta}(E_i), \quad (3.30)$$

where the set $\{x_i\}$ is the unfolded spectrum. We thus obtain the new form of the counting function as

$$\hat{\eta}(x) = x + \hat{\eta}_{\text{fluct}}(x), \quad (3.31)$$

which gives a mean level density of the unfolded spectrum equals to unity since

$$\frac{d\langle\hat{\eta}\rangle}{dx} = \frac{dx}{dx} = 1, \quad (3.32)$$

as expected.

It is now possible to characterize the universal properties of spectrum fluctuations. To do so, one must first define a number of statistical observables that will be used to probe the properties of the spectrum. The n -point correlation functions $R_n(x_1, \dots, x_n)$ describe all the statistical properties of the unfolded spectrum. They are given by (see e.g. Bohigas, 1991)

$$R_n(x_1, \dots, x_n) = \frac{N!}{(N-n)!} \int dx_{n+1} \cdots dx_N P_N(x_1, \dots, x_N), \quad (3.33)$$

where $P_N(x_1, \dots, x_N)$ is the normalised probability density. One of the simplest statistical observables is the *nearest neighbour spacing distribution* $P(s)$. The probability density $P(s)$ is such that the probability for the spacing between any two neighbouring energy levels $s_i = x_{i+1} - x_i$ to lie between s and $s + ds$ is $P(s)ds$. To avoid binning effects, that can be problematic in cases where the number of energy levels is small, one can use the *integrated* or *cumulative level-spacing distribution* $F(s)$ defined as (Guhr et al., 1998)

$$F(s) = \int_0^s P(s') ds'. \quad (3.34)$$

The nearest neighbour spacing distribution will be used to probe the short-range correlations of the spectrum. For example, the behaviour of $P(s)$ near $s = 0$ measures the degree of *level repulsion* (see Fig. 3.5). On the other hand, there are measures of long range correlations in the form of the *level number variance* $\Sigma^2(L)$ and the related *level compressibility* χ . These are defined as (see e.g. Bogomolny and Giraud, 2011)

$$\Sigma^2(L) = \langle n(L)^2 \rangle - \langle n(L) \rangle^2 \underset{L \rightarrow \infty}{\sim} \chi L, \quad (3.35)$$

where $n(L)$ is the number of ('unfolded') energy levels contained in an interval L , and $\langle n(L) \rangle = L$ from the unfolding procedure. A closely related long-range measure of the spectrum is the *spectral rigidity* $\Delta_3(L)$, which is also called the *Dyson-Mehta least square deviation*. It is defined as (Gutzwiller, 1990)

$$\Delta_3(L) = \frac{1}{L} \min_{A,B} \int_0^L [\hat{\eta}(x) - Ax - B]^2 dx, \quad (3.36)$$

where the coefficients A and B are found from the best linear fit of the counting function $\hat{\eta}$. We note that the above spectral measures can be related to the different *n -level correlation* (given in Eq. (3.33)) and *cluster functions* of the spectrum, that are discussed in Bohigas (1991).

It is known that in cases where the system has some degree of symmetry, the spectrum will be a superposition of independent, uncorrelated, sub-spectra, where each sub-spectrum corresponds to a different symmetry class. In these cases, the total level density is the sum of all the level densities of the different sub-spectra, i.e.

$$\rho(E) = \sum_{\alpha} \rho_{\alpha}(E). \quad (3.37)$$

In this situation, the expression for the total nearest neighbour spacing distribution as a function of those of the sub-spectra is rather complex (Mehta, 2004). However, the level number variance and the spectral rigidity have simple expressions as (Guhr et al., 1998)

$$\Sigma^2(L) = \sum_{\alpha} \Sigma_{\alpha}^2(g_{\alpha}L), \quad (3.38)$$

and

$$\Delta_3(L) = \sum_{\alpha} \Delta_{3,\alpha}(g_{\alpha}L), \quad (3.39)$$

where $g_{\alpha} = \rho_{\alpha}(E)D$, D being the total mean level spacing of the energy interval centred around E . When one wants to use spectral measures to analyse the dynamics of experimental or numerical data, the crucial point to consider is the number of available frequencies in a given symmetry class, and to be able to distinguish which energy levels belong to different symmetry classes. If one has only few frequencies, or a noisy spectrum, the cumulative level-spacing distribution can be used to probe short-range correlations and the spectral rigidity for longer-range correlations, since the latter is robust against spurious and missing energy levels (Delande, 2001).

3.2.3 Quantum integrable systems

Quantum integrable systems are arguably the simplest known quantum systems. Among these systems are the few systems that are exactly solvable, including the free particle, the particle in a spherically symmetric potential, the hydrogen atom and the quantum harmonic oscillator.

Poissonian spectrum

A conjecture from Berry and Tabor (1977) states that the spectrum of generic quantum systems whose classical dynamics is integrable should display *Poissonian statistics*. This conjecture can be understood on semi-classical arguments. In the semi-classical limit, eigenstates of a quantum integrable system concentrate on some invariant tori that foliate phase space. Quantum states associated to different tori do not interact: the total spectrum is thus a superposition of their independent sub-spectra. Since the levels are uncorrelated, they can be described by a Poisson distribution. After unfolding the spectra, the corresponding nearest neighbour spacing distribution is (Guhr et al., 1998)

$$P(s) = \exp(-s). \quad (3.40)$$

The corresponding number variance is

$$\Sigma^2(L) = L, \quad (3.41)$$

and spectral rigidity

$$\Delta_3(L) = \frac{L}{15}. \quad (3.42)$$

There are, however, counter-examples to this conjecture, the simplest one being the quantum harmonic oscillator. There is another class of wave systems that typically displays Poissonian statistics. These are the waves that are exponentially localized in position or momentum space through strong interference effects due to their scattering by a disorder medium. This phenomenon is known as *Anderson localization*, and was first studied in relation with the metal-insulator transition. If the spatial overlap between eigenstates that are close in energy is exponentially small, their energy levels are uncorrelated and follow a Poisson distribution (see e.g. Akkermans and Montambaux, 2007).

Semi-classical limit: Einstein-Brillouin-Keller quantisation

It is known from early results in quantum mechanics that the energy levels of one-dimensional bounded quantum systems can be obtained by the *Bohr-Sommerfeld quantisation rule*, also called WKB quantisation, that takes the form

$$\int_T p \, dq = 2\pi n \hbar, \quad (3.43)$$

where T is the period of the bound motion. This condition comes from the requirement that the wave function be single-valued, and can be trivially generalized to higher-dimensional separable systems (the separation of variables allowing to recover the form of Eq. (3.43) for each of the coordinates). Einstein (1917) was the first to propose a form that can be applied to non-separable quantum systems, as long as the motion is multi-periodic. Including later refinements of Einstein's proposition (see e.g. Keller and Rubinow (1960)), this quantisation condition takes the form

$$\oint_{\gamma_i} \mathbf{p} \cdot d\mathbf{q} = 2\pi \left(n_i + \frac{\alpha_i}{4} \right) \hbar. \quad (3.44)$$

where γ_i is an irreducible path on the invariant torus of phase space. The last term on the RHS is sometimes called the *Maslov phase*, where α_i is the *Maslov index* which is the number of caustics encountered along the irreducible path γ_i (see e.g. Haake, 2010). The reader that did not skip Sect. 3.1.2 should recognize in the LHS of Eq. (3.44) the expression for the action variables I_i , that can be used as labels for the different tori. In some sense, one can see the EBK quantisation as a way of selecting the tori with quantised actions among the continuum of existing tori. Equation (3.43) is nowadays called the *Einstein-Brillouin-Keller quantisation condition* (see e.g. Stone, 2005), and is a good approximation for the energy levels of integrable quantum systems in the semi-classical limit $\hbar \rightarrow 0$.

3.2.4 Quantum chaotic systems

Einstein was the first to realize that the Bohr-Sommerfeld quantisation could be only applied to quantum systems that are integrable (in the sense of their classical limit) (Einstein, 1917). Since then, quantum systems whose classical limit is chaotic have been found to display peculiar behaviours in the statistical distribution of their energy levels. Also, these energy levels cannot be obtained in the semi-classical limit by a simple quantisation formula, and one must use an elaborate infinite sum over periodic orbits to obtain some information on the spectrum.

BGS conjecture and Wigner-Dyson spectrum

In the 1950's, while studying the properties of compound nuclear resonances, Eugene Wigner conjectured that the energy levels of quantum systems with many degrees of freedom would have the same statistical behaviour as the eigenvalues of large Hermitian random matrices possessing the same symmetries as the system, especially with respect to time-reversal. Later, the conjecture of Bohigas, Gianonni and Schmit (BGS) (Bohigas et al., 1984) stated that, in analogy with many-body complex quantum systems, the statistical properties of the energy levels of chaotic quantum systems should follow the predictions of this Random Matrix Theory (RMT) (Bohigas, 1991; Mehta, 2004). The conjecture hinted at the existence of a *universal behaviour* in chaotic quantum systems, since the predictions of RMT depend on no adjustable parameter. The three principal RMT ensembles, sometimes called the 'classical ensembles', were defined by Wigner and Dyson and classified as: the Gaussian Orthogonal Ensemble (GOE), the Gaussian Unitary Ensemble (GUE) and the Gaussian Symplectic Ensemble (GSE) (Bohigas, 1991). If the Hamiltonian of the system is invariant under time-reversal and rotations, the random matrices are chosen real symmetric and thus belong to the *orthogonal group*. If the Hamiltonian is not time-invariant, the matrices are complex Hermitian and belong to the *unitary group*. Finally, if the system has time-reversal invariance, is not invariant under rotations and has a total angular momentum that is a half-odd integer, then the matrices are 'quaternion real' and belong to the *symplectic group*. From the properties of these ensembles, one can compute analytically the forms of the spectral observables defined in the previous section. We give here the forms of the corresponding nearest neighbour

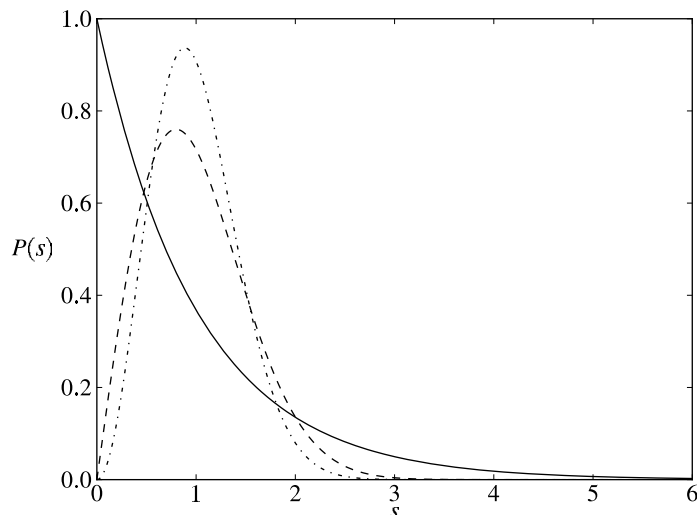


Figure 3.5: Nearest neighbour spacing distribution $P(s)$ corresponding to the Poisson (solid line), GOE (dashed line) and GUE (dash-dotted line) statistics, computed from Eq. (3.40), Eq. (3.45) and Eq. (3.46), respectively.

spacing distributions, and for 2×2 matrices only, since these results are very close to the asymptotic ones for $N \rightarrow \infty$ (Bohigas, 1991). Other analytical predictions of RMT for spectral observables may be found elsewhere (e.g. in Bohigas, 1991; Mehta, 2004). For the Gaussian Orthogonal Ensemble, the nearest neighbour spacing distribution is

$$P_{\text{GOE}}(s) = \frac{\pi s}{2} \exp\left(\frac{-\pi s^2}{4}\right), \quad (3.45)$$

which is also known as the *Wigner's surmise*. For the Gaussian Unitary Ensemble, we have:

$$P_{\text{GUE}}(s) = \frac{32s^2}{\pi^2} \exp\left(\frac{-4s^2}{\pi}\right), \quad (3.46)$$

and for the Gaussian Symplectic Ensemble:

$$P_{\text{GSE}}(s) = \frac{2^{18}s^4}{3^6\pi^3} \exp\left(\frac{-64s^2}{9\pi}\right). \quad (3.47)$$

We have represented in Fig. 3.5, the nearest-neighbour spacing distribution $P(s)$ for the Poisson, GOE and GUE statistics. The ‘hole’ at small s in the nearest neighbour spacing distributions of the GOE and GUE statistics, that can be seen in Fig. 3.5, stems from the effect of level repulsion that characterises quantum chaotic systems. On the other hand, the nearest-neighbour spacing distribution for Poisson statistics shows that the spectrum will present many level quasi-degeneracies. Also, the $P(s)$ distributions for GOE and GUE statistics decrease more rapidly than Poisson statistics at large s . As concerns the long-range properties of the spectrum, the level number variance $\Sigma^2(L)$ for the GOE and GUE cases goes as $\ln(L)$ for large L (see e.g. Bohigas, 1991), which implies that the fluctuations of the number of levels $n(L)$ as function of L are small (logarithmic) in sharp contrast with the linear behaviour of this variance for the Poisson case (see Eq. (3.41)).

Finally, we must say that the BGS conjecture has been verified on countless numerical and experimental systems, be they quantum or classical wave systems (see Guhr et al., 1998, and references therein). Still, one must note that exceptions to this conjecture exist,

such as the classically (extremely) chaotic arithmetical systems whose spectral statistics was found to be close to the Poisson distribution. In this case, infinitely many arithmetical symmetries exist, which was found to yield a Poisson distribution of energy levels (see e.g. Bogomolny, 2006).

Semi-classical limit: Gutzwiller Trace Formula

No simple asymptotic formula for energy levels such as Eq. (3.44) can be constructed for chaotic quantum systems, since there are no invariant tori in phase space that are left to quantise. Nevertheless, starting from an alternative formulation of quantum mechanics known as the *Feynman's path integral*, one can devise a semi-classical quantisation that can be applied to chaotic quantum systems. This formulation is known as the *Gutzwiller Trace Formula* (GTF) and its derivation is sketched in the following (see e.g. Gutzwiller, 1990, 1991; Delande, 2001). The time evolution of a quantum state $\Psi(\mathbf{q}, t)$ can be put in the form of a quantum propagator $K(\mathbf{q}', t'; \mathbf{q}, t)$ such that

$$\Psi(\mathbf{q}', t') = \int d^N \mathbf{q} K(\mathbf{q}', t'; \mathbf{q}, t) \Psi(\mathbf{q}, t). \quad (3.48)$$

The classical approximation to the quantum propagator was derived by Van Vleck in 1928 and is therefore known as *Van Vleck's formula* (Gutzwiller, 1990), which goes as follows:

$$K(\mathbf{q}', t'; \mathbf{q}, t) = \sum_{\text{traj.}} \left(\frac{1}{2i\pi\hbar} \right)^{d/2} \left| \det \left(-\frac{\partial^2 R}{\partial \mathbf{q} \partial \mathbf{q}'} \right) \right|^{1/2} \exp \left[i \frac{R(\mathbf{q}', t'; \mathbf{q}, t)}{\hbar} - i \frac{\pi\nu}{2} \right], \quad (3.49)$$

where d is the number of degrees of freedom, the integer ν a Morse index (see e.g. Gutzwiller, 1990) which counts the number of boundaries or *caustics* encountered by the trajectory, while the *Hamilton's principal function* $R(\mathbf{q}', t'; \mathbf{q}, t)$ is defined as

$$R(\mathbf{q}', t'; \mathbf{q}, t) = \int_t^{t'} d\tau L(\mathbf{q}, \dot{\mathbf{q}}, \tau), \quad (3.50)$$

$L(\mathbf{q}, \dot{\mathbf{q}}, t)$ being the Lagrangian of the system. The sum in Eq. (3.49) is performed over all classical trajectories that go from \mathbf{q} to \mathbf{q}' in a time $\Delta t = t' - t$. We note that R must not to be confused with the action S , R being used for motions that happen during a fixed time interval, while S is defined for motions at a fixed energy.

The Van Vleck propagator can be used to obtain the spectral density of a chaotic quantum system as a function of classical quantities. This is done through expressing the trace of the system's Green's function in terms of classical periodic orbits, which is the aim of the Gutzwiller Trace Formula (GTF). The derivation of the GTF makes extensive use of the *stationary phase method* (Gutzwiller, 1990). This method considers integrals of the form (Schulman, 2005)

$$F(\lambda) = \int_{-\infty}^{+\infty} \exp[i\lambda f(t)] dt. \quad (3.51)$$

If λ is large, we expect the phase of $\exp(i\lambda f(t))$ to vary rapidly when $f'(t) \neq 0$. In these regions, contributions to the integral of Eq. (3.51) should cancel out; the dominant contributions to the integral should thus come from regions close to where $f'(t) = 0$. If $f'(t_0) = 0$, we expand f about t_0 to yield

$$F(\lambda) = \int_{-\infty}^{+\infty} \exp \left[i\lambda f(t_0) + \frac{i}{2} \lambda f''(t_0) + \dots \right] dt. \quad (3.52)$$

Neglecting terms higher than the second-order in f yields a Gaussian integral whose integration is well known; this gives

$$F(\lambda) = \sqrt{\frac{2i\pi}{\lambda f''(t_0)}} \exp[i\lambda f(t_0)]. \quad (3.53)$$

In order to obtain information on the spectral density of energy levels, we need to turn Eq. (3.49) from the time domain to the energy domain. This is done through using the Green's function of the system, which can be defined in the position basis as

$$G(\mathbf{q}', \mathbf{q}, E) = \frac{-i}{\hbar} \int_0^\infty K(\mathbf{q}', \tau; \mathbf{q}, 0) \exp\left(\frac{i}{\hbar} E\tau\right) d\tau. \quad (3.54)$$

We then insert the Van Vleck propagator of Eq. (3.49) into the previous equation and use the stationary phase method to perform the integral over τ . In this manner, one obtains the classical approximation to the Green's function of Eq. (3.54) as

$$G(\mathbf{q}', \mathbf{q}, t) = \frac{2\pi}{(2i\pi\hbar)^{\frac{d+1}{2}}} \sum_{\text{traj.}} \sqrt{(-1)^{d+1} D} \exp\left[\frac{i}{\hbar} S(\mathbf{q}', \mathbf{q}, E) - i\frac{\pi\nu}{2}\right], \quad (3.55)$$

where the action is defined as $S(\mathbf{q}, \mathbf{q}', E) = \int_{\mathbf{q}'}^{\mathbf{q}} \mathbf{p} \cdot d\mathbf{q}$. The determinant D is given by

$$D = \frac{1}{|\dot{q}_\parallel| |\dot{q}'_\parallel|} \left| -\frac{\partial^2 S}{\partial \mathbf{q}_\perp \partial \mathbf{q}'_\perp} \right|, \quad (3.56)$$

where the coordinate q_\parallel is along the trajectory, while q_\perp is transverse to it. Now, the density of states $\rho(E)$ in Eq. (3.25) can be expressed in terms of the Green's function as

$$\rho(E) = -\frac{1}{\pi} \text{Im}[\text{Tr } G(E)] = -\frac{1}{\pi} \text{Im} \int d\mathbf{q} G(\mathbf{q}, \mathbf{q}, E). \quad (3.57)$$

Replacing the classical Green's function of Eq. (3.55) in the previous equation yields a sum over trajectories that start and end at the same point \mathbf{q} i.e. *closed trajectories*. The integral over \mathbf{q} is performed once again using the stationary phase method. The dominant contribution to the integral comes from trajectories for which

$$\left[\frac{\partial S(\mathbf{q}, \mathbf{q}', E)}{\partial \mathbf{q}'} + \frac{\partial S(\mathbf{q}, \mathbf{q}', E)}{\partial \mathbf{q}} \right]_{\mathbf{q}'=\mathbf{q}} = 0, \quad (3.58)$$

that is for trajectories where $\mathbf{p} = \mathbf{p}'$ when $\mathbf{q} = \mathbf{q}'$ i.e. *periodic trajectories*. This yields finally the Gutzwiller Trace Formula that expresses the density of states of the quantum system as a sum over primitive (i.e. non self-retracing) periodic trajectories of the classical system as (written here for a two-dimensional system):

$$\rho(E) = \bar{\rho}(E) + \sum_{\substack{k \text{ primitive p.o.} \\ r \text{ repetitions}}} \frac{T_k \cos\left[r\left(\frac{S_k}{\hbar} - \frac{\pi\nu_k}{2}\right)\right]}{\pi\hbar \sqrt{|\det(1 - M_k^r)|}}, \quad (3.59)$$

where r is the number of repetitions of the primitive periodic trajectories. In this formula, the k -th periodic trajectory is characterized by its period T_k , action S_k , Maslov index ν_k (see Sect. 3.2.3 for its definition), and *monodromy matrix* M_k , also sometimes called the stability matrix, which is the Jacobian matrix of the k -th periodic orbit going from (\mathbf{q}, \mathbf{p}) to $(\mathbf{q}', \mathbf{p}')$, defined as (Haake, 2010)

$$M = \begin{bmatrix} \left(\frac{\partial \mathbf{q}'_\perp}{\partial \mathbf{q}_\perp}\right)_{\mathbf{p}_\perp} & \left(\frac{\partial \mathbf{q}'_\perp}{\partial \mathbf{p}_\perp}\right)_{\mathbf{q}_\perp} \\ \left(\frac{\partial \mathbf{p}'_\perp}{\partial \mathbf{q}_\perp}\right)_{\mathbf{p}_\perp} & \left(\frac{\partial \mathbf{p}'_\perp}{\partial \mathbf{p}_\perp}\right)_{\mathbf{q}_\perp} \end{bmatrix}. \quad (3.60)$$

In summary, the Gutzwiller Trace Formula relates the density of states of a quantum system whose classical limit is chaotic with an infinite sum of contributions from periodic trajectories of the classical system. It yields an infinite sum that is difficult to handle, but simplifications through so-called ‘resummation techniques’ are possible (see e.g. Haake, 2010). The GTF shows in a sense that periodic orbits are the structuring elements of a chaotic system’s phase space (an insight that was already present in the mind of Poincaré), and as such must be the basis of the semi-classical quantisation of these systems. This is natural, since these are the only invariant structures (with the energy surface) that are present in the phase space of chaotic systems.

Wavefunctions of chaotic quantum systems

In contrast with the integrable case where all eigenfunctions are localized on invariant tori, the mode amplitude distributions of chaotic quantum systems are expected to be ergodic on phase space in the semi-classical limit. More precisely, they were conjectured (Berry, 1977) to behave as superpositions of random plane waves such that (Nonnenmacher, 2012)

$$\Psi_{\text{RWM}}(\mathbf{q}) \propto \text{Re} \left[\sum_n a_n \exp(\mathbf{k}_n \cdot \mathbf{q}) \right], \quad (3.61)$$

where the amplitudes a_n and the directions of propagation of the waves are considered as random variables, while keeping $\|\mathbf{k}_n\| = k$ with k constant for all waves. This is the so-called Random Wave Model (RWM) of Berry, where the amplitudes distributions corresponding to the wave superposition above can be shown to be Gaussian distributed. This conjecture has found a rigorous mathematical counterpart in the form of the *quantum ergodicity* theorem (Schnirelman, 1974), which states that for quantum systems whose classical limit is ergodic, the eigenfunctions become uniformly distributed (with respect to an appropriate phase space measure) on the energy shell in the semi-classical limit (see e.g. Nonnenmacher, 2012).

3.2.5 Quantum mixed systems

In the same way as for classical Hamiltonian systems, a typical quantum system will be a *mixed system*, that will display signs of both chaos and integrability, a so-called ‘mixed phase space’, in its classical limit. Though they lack the ‘exact solvability’ property of quantum integrable systems, and the ‘complete stochasticity’ of chaotic quantum systems that lead to the emergence of universal properties, the energy levels and eigenfunctions of quantum mixed systems can nevertheless be predicted.

Berry-Robnik hypothesis

As concerns the energy levels, one can generically apply the Berry-Robnik hypothesis (Percival, 1973; Berry and Robnik, 1984), that tells us that to each phase space region is associated a well-defined, independent sub-spectrum. In particular, one expects the spectrum of mixed systems to be a superposition of as many chaotic sub-spectra (with the adequate Wigner-Dyson statistical properties) as they are disconnected chaotic regions in phase space, with a Poisson spectrum corresponding to integrable regions (a superposition of multiple Poisson distributions yielding only one Poisson distribution). This yields a spectrum that is in-between Poisson and Wigner-Dyson behaviours, with a nearest-level spacing distribution that can be computed on the assumption of uncorrelated sub-spectra (Guhr et al., 1998). One must note, however, that this picture can be modified when partial barriers are present in the chaotic part of phase space (Bohigas et al., 1993). This assumption of uncorrelated sub-spectra should fail at low energies, where the coupling

between regular and chaotic regions due to *dynamical tunnelling* effects should be taken into account (see e.g. Davis and Heller, 1981; Tomsovic, 2001; Bäcker et al., 2008). This effect is thought to be exponentially small, however. Finally, one can obtain a semi-classical estimate of the density of energy levels in each sub-spectrum by using the Thomas-Fermi distribution, that we introduced in Eq. (3.28), integrating over each phase space zone instead of the whole energy shell.

Quantisation methods for the regular and chaotic regions

In mixed quantum systems, semi-classical methods should be applied, in the first approximation (see above), to the regular and chaotic phase space zones separately. In the regular zones of phase space, islands around stable periodic orbits in particular, the EBK quantisation of integrable systems (that we presented in Sect. 3.2.3) can be applied to the invariant tori (Percival, 1973), which has been done in Bohigas et al. (1993). But whereas EBK quantisation applies only to the invariant tori of integrable and near-integrable systems, trace formulas are more general and can be used for integrable (Berry and Tabor, 1976) as well as chaotic systems (see Sect. 3.2.4). In particular, the GTF can be modified to account for the contribution to the density of states of the *stable* periodic orbits that lie inside regular islands, which was done by Miller (1975); Voros (1976). For a stable periodic orbit γ , the determinant in Eq. (3.59) can be written as (Gutzwiller, 1990)

$$\sqrt{|\det(1 - M_\gamma^r)|} = 2 \sin\left(\frac{r\alpha_\gamma}{2}\right), \quad (3.62)$$

where M_γ is the monodromy matrix of the orbit γ , r the number of repetitions of this orbit, and α_γ its stability angle. One can thus write Eq. (3.59) as

$$\rho_{\text{fluct},\gamma}(E) = \sum_{r \text{ repetitions}} \frac{T_\gamma(E)}{\pi\hbar} \frac{\cos\left[r\left(\frac{S_\gamma(E)}{\hbar} - \frac{\pi\nu_\gamma}{2}\right)\right]}{2 \sin\left(\frac{r\alpha_\gamma}{2}\right)}, \quad (3.63)$$

where T_γ is the period of the primitive stable periodic orbit and ν_γ is the number of conjugate points along the orbit. Now, using the fact that

$$\frac{1}{2i \sin\left(\frac{r\alpha_\gamma}{2}\right)} = \sum_{\ell=0}^{\infty} \exp\left[-i\left(\ell + \frac{1}{2}\right)r\alpha_\gamma\right], \quad (3.64)$$

and the Poisson sum formula

$$\sum_{n=-\infty}^{+\infty} \exp(irx) = 2\pi \sum_{n=-\infty}^{+\infty} \delta(x - 2\pi n), \quad (3.65)$$

it was found that the quantisation condition on the phase along the stable orbit can be written as

$$S_\gamma(E) = 2\pi\hbar\left(r + \frac{\nu_\gamma}{4}\right) + \alpha_\gamma\hbar\left(\ell + \frac{1}{2}\right). \quad (3.66)$$

The term $(\ell + 1/2)\hbar$ was interpreted as corresponding to the quantisation of an harmonic oscillator transverse to the periodic orbit. It was shown by Voros (1976) that the preceding formula can be recovered by starting from the EBK quantisation formula and linearising the motion around the stable orbit (i.e. taking the ‘thin-torus’ limit of EBK quantisation (Berry, 2012)). A lesser-known approximation of the EBK quantisation was given by Babich and Buldyrev (1991) in the form of the ‘parabolic equation method’. It yields a quantisation formula for stable periodic orbits similar to Eq. (3.66), but it has the advantage over the GTF formalism to give also approximate eigenfunctions in a simple way. The main steps of its derivation can be found in Sect. 5.4.

The GTF formula for stable periodic orbits that we presented is only valid for *isolated* orbits. However, in mixed quantum systems that possess a control parameter, its variation will induce multiple creations and destructions of periodic trajectories termed *bifurcations*. For bifurcating trajectories, the stability matrix has eigenvalues unity, which makes divergent the terms for individual orbits contributing to the Gutzwiller Trace Formula. The way around this problem was found by using *normal forms* of the classical dynamics, that treat the intricate structure of bifurcating trajectories as a whole (Haake, 2010). The corresponding collective contributions to the Trace Formula are the so-called *uniform approximations* (see e.g. Schomerus and Sieber, 1997). Bifurcations also lead to the enhanced contribution of *ghost orbits*, which are complex-valued trajectories, even for values of the control parameter that are far from the bifurcation (see Kuś et al., 1993).

In the chaotic zones of phase space, one can apply the Gutzwiller Trace Formula to the hyperbolic periodic orbits in a similar way as for completely chaotic systems (see Sect. 3.2.4).

Eigenfunctions of mixed quantum systems

By the so-called “semi-classical eigenfunction hypothesis” (Percival, 1973; Berry, 1977; Voros, 1979), it is known that the phase space distributions of almost all eigenfunctions (Sect. 3.2.1) of mixed quantum systems are localised, in the semi-classical limit, on either the regular or chaotic regions of phase space. In integrable zones, phase space distributions will thus be concentrated on the quantised invariant tori, whereas they will be ergodic over the chaotic zones. As an illustration of this phenomenon, one can refer to the Husimi distributions of the quantum kicked rotor that we showed in Fig. 3.4. Though the semi-classical eigenfunction hypothesis has been confirmed by many numerical and experimental data, it is still studied and debated (see e.g. Bäcker and Schubert, 2002, and references therein).

Chapter 4

Signs of wave chaos in rapidly rotating stars

As we have seen in Sect. 2.2.2, an important ingredient to analyse the oscillation spectrum of a pulsating star resides in the knowledge of its basic asymptotic structure. The only asymptotic formula that provides such an understanding, with numerous successes for solar-like pulsators, is nevertheless restricted to stars that are nearly spherically symmetric. But it is known from observations that many stars rotate rapidly, and that these stars can be significantly flattened. Also, numerical simulations have shown that rotational effects on pulsation frequencies cannot be explained by perturbation theory for already moderate rotation rates (see Sect. 2.2.3). The asymptotic study of stellar oscillation spectra thus needs a more general, or at least different, theory that could be applied to pulsating stars with a large angular momentum.

This kind of situation has already been encountered in the field of quantum chaos; we will take the canonical example of the hydrogen atom in a magnetic field (see e.g. Delande, 1991). From its spherical symmetry, the hydrogen atom is one of the few exactly solvable models. If it is subjected to a very weak static magnetic field, its energy levels can be obtained by first-order perturbation theory. The dominant term in the Hamiltonian, the *paramagnetic term*, which is linear in the magnetic field strength, leads to the m -splitting of energy levels: this is the well-known *Zeeman effect* (see e.g. Cohen-Tannoudji et al., 1973). Now, if one increases the field strength sufficiently, or if the atom is prepared in a highly excited *Rydberg state* so that the electron orbit encloses a large magnetic flux, the *diamagnetic term* (that is quadratic in the field strength) becomes large, and perturbation theory breaks down. As the field strength increases still, this quadratic term leads to the chaotic classical motion of the electron, and accordingly signs of quantum chaos such as the repulsion between energy levels (see Sect. 3.2.2) begin to appear. One can obtain information on such typical quantum chaotic systems however, by using adequate semi-classical quantization techniques, and a statistical description of their energy levels and eigenfunctions. In this chapter, we will see how the techniques from quantum chaos were taken from the microscales of atomic physics to macroscale systems that are more than a million kilometres wide. We thus review previous works on the asymptotic analysis of stellar pressure mode oscillations that were obtained using the tools of quantum chaos; since most of these techniques were exposed in the previous chapter, we only give here a brief account of their results.

4.1 Brief history

The first application of a semi-classical technique to the asymptotic analysis of stellar oscillations dealt with the semi-classical quantization of acoustic rays in slowly rotating

stars by the EBK formula (Gough, 1986, 1993). Around the same time, Perdang (1984, 1986) suggested that the techniques of quantum chaos might provide information on the oscillations of non spherically symmetric stars. Perdang (1988) then analysed the acoustic ray dynamics in ellipsoidal (integrable) and pear-shaped configurations, with a potential application to stellar oscillations of deformed stars in mind. Two decades later, Lignières and Georgeot (2008, 2009) found evidences of quantum chaos in the pressure oscillations of rapidly rotating polytropic stellar models. They obtained that the dynamics of the ray limit of pressure waves in a rotating polytropic stellar model undergoes a transition, as the rotation rate increases, from integrability to chaos. They also found that this chaotic behaviour of the ray limit had important consequences on the oscillation spectrum, which showed frequency repulsion. In what follows, we give a brief account of their findings. At this point, it may be necessary to clarify the distinction between these works and those on the chaotic behaviour of *non-linear* stellar oscillations. Indeed, in articles such as Buchler et al. (1995, 2004), some oscillation modes are found to be irregular in time, due to the presence of non-linear interactions. This occurs between *resonant* modes when the oscillation amplitude is high. On the other hand, quantum chaos is applied to *linear* oscillations, assuming small amplitude perturbations.

4.2 Acoustic ray dynamics

The dynamics of acoustic rays in polytropic stellar models was studied in Lignières and Georgeot (2008), for different values of the rotation rate, by the numerical integration of the two-dimensional conservative Hamiltonian dynamical system (the details of the derivation can be found in Sect. 5.3):

$$\frac{d\mathbf{x}}{dt} = \tilde{\mathbf{k}}_p, \quad (4.1)$$

$$\frac{d\tilde{\mathbf{k}}_p}{dt} = -\nabla V_r(\mathbf{x}), \quad (4.2)$$

where \mathbf{x} is the position of the ray in the meridional plane of the star, and $\tilde{\mathbf{k}}_p = \mathbf{k}_p/\omega$ is the renormalized wavevector projected onto this same plane. The effective potential $V_r(\mathbf{x})$ can be written as

$$V_r(\mathbf{x}) = -\frac{1}{2c_s^2} \left(1 - \frac{\omega_c^2}{\omega^2} - \frac{c_s^2 m^2}{\omega^2 d^2} \right), \quad (4.3)$$

where c_s is the inhomogeneous speed of sound, and ω_c the cut-off frequency of the stellar model. The last term in the potential includes the quantum number m corresponding to the angular momentum along the rotation axis, and the distance d from the ray to this same axis. It should be noted that, though the exact form of ω_c (see Sect. 5.2) depends on the assumption of a polytropic relation between the equilibrium pressure and density of the background stellar model, the form of equations Eqs. (4.1)-(4.2) should be the same for all stellar models.

4.2.1 Rays in a non-rotating stellar model

The numerical integration of Eqs. (4.1)-(4.2) for a non-rotating stellar model yields, as expected, dynamics that are characteristic of an integrable dynamical system. Indeed, one can see in Fig. 4.1 that, for $\Omega = 0$ where Ω is the rotation rate, all ray trajectories are stable. Their intersections with a Poincaré Surface of Section (PSS) (cf. Sect. 3.1) taken at a fixed distance from the stellar surface (see Fig. 4.1) form lines at constant values of k_θ/ω , corresponding to:

$$\tilde{k}_\theta^2 = \tilde{L}^2 - \left(\frac{m}{\omega} \frac{1}{\sin \theta} \right)^2, \quad (4.4)$$

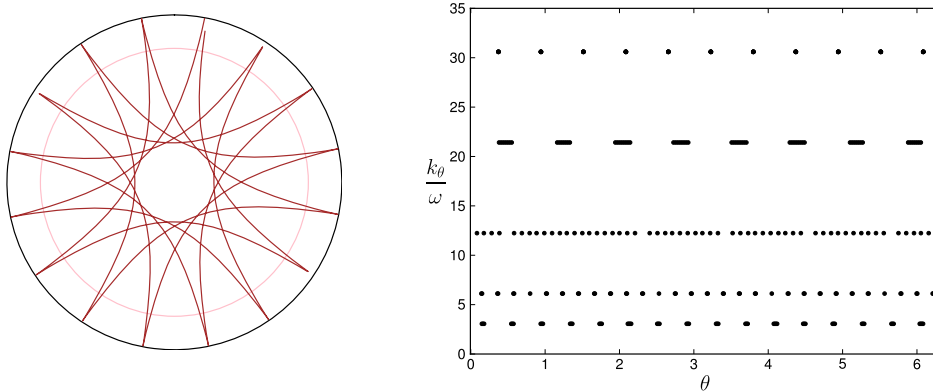


Figure 4.1: Acoustic rays in a non-rotating star for $m = 0$ (left panel), and the associated Poincaré Surface of Section (right panel) taken at a fixed radial distance from the stellar surface corresponding to a radius $r = r_p$ (illustrated by a pink line in the left panel). The coordinates displayed on the surface of section are the scaled wavenumber latitudinal component k_θ/ω , where ω is the mode frequency, and the colatitude θ .

where \tilde{L} is the norm of the angular momentum with respect to the centre of the star. This shows that trajectories stay on invariant two-dimensional tori in the four-dimensional phase space $(\mathbf{x}, \tilde{\mathbf{k}}_p)$. The corresponding constants of motion are easily found to be the mode frequency ω and the angular momentum perpendicular to the rotation axis, which corresponds to the fixed distance between the internal caustic (a caustic is the envelope of rays) and the centre of the star.

4.2.2 Rays in rapidly-rotating stellar models

Integrating Eqs. (4.1)-(4.2) for a polytropic stellar model at increasing values of the rotation rate allowed to observe that the acoustic ray trajectories are profoundly modified by rotation. Indeed, as the perturbation increases, different types of rays with different dynamical behaviours emerge, following a KAM-type transition. In Fig. 4.2, one can see the results of the integration of Eqs. (4.1)-(4.2) for different initial conditions, in a polytropic stellar model of index $N = 3$ (see Sect. 5.1 for a definition) rotating at $\Omega/\Omega_K = 0.59$ (where $\Omega_K = GM/R_{eq}^3$ is the limiting rotation rate for which the centrifugal acceleration equals the gravity at the equator, M being the stellar mass and R_{eq} the equatorial radius). At this rotation rate, two types of rays have emerged. Firstly, one can see that the intersection of some rays with the PSS form lines, which correspond to stable zones (cf. Sect. 3.1.2). Among these stable zones are stable *islands*, that are stable zones centred on a stable periodic orbit. The most visible stable islands on the PSS were found to be the ‘period-2’ and ‘period-6’ islands (islands being labelled according to the number of times their central periodic ray crosses the PSS). It was also found that only the period-2 stable islands survive at higher rotation rates. In this same class of stable zones, there are also ‘whispering gallery’ rays, which follow the outer boundary of the acoustic cavity. In contrast, some ray solutions were found to have a visibly erratic behaviour in position space, the intersections of one such trajectory filling up a whole two-dimensional area in the PSS. This is characteristic of chaotic rays, which are unstable trajectories of the Hamiltonian system. Finally, the dynamical behaviour displayed in Fig. 4.2 was found to be generic for all finite values of the rotation rate and for different quantum number m (see Lignières and Georget (2009) for surfaces of section at different rotation rates).

In conclusion, the dynamics of acoustic rays in rotating polytropic stellar models was

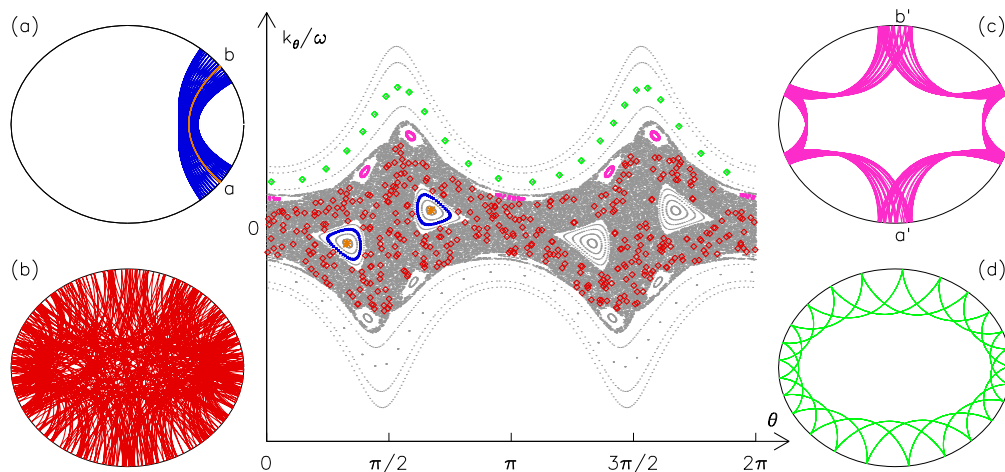


Figure 4.2: Poincaré Surface of Section (central panel) of acoustic rays obtained from Eqs. (4.1)-(4.2), for a PSS at a fixed distance from the stellar surface and $m = 0$. The stellar model is a polytropic model rotating at $\Omega/\Omega_K = 0.59$. The corresponding rays in position space are drawn in panels (a), (b), (c) and (d). One can see in (a): a period-2 island ray (blue) with the central periodic ray shown as the orange line between points a and b; in (b): a chaotic ray (red); in (c): a period-6 island ray (magenta); in (d): a ‘whispering gallery’ ray (green). Intersections of these rays with the PSS can be seen in the central panel, with their corresponding colours. The coordinates of the PSS are the same as Fig. 4.1 (from Lignéres and Georgeot (2009)).

found to undergo a (KAM-like) transition to chaos, and the ray dynamics for large rotation rates was found to have a mixed character (see Sect. 3.1.3), with regular and chaotic regions co-existing in phase space.

4.3 Classification of modes from phase space distributions

The phase space of the ray dynamics was then used to classify the numerically computed high-frequency pressure modes and to infer some of their properties. To associate a given mode with a phase space zone, Lignéres and Georgeot (2009) used the representation of modes by Husimi phase space distributions, which was written as

$$\mathcal{H}(s, \tilde{k}) = \left| \int \Psi'(s') \exp\left(\frac{-(s' - s)^2}{2\Delta_s^2}\right) \exp(i\omega \tilde{k} s') ds' \right|^2, \quad (4.5)$$

where Ψ' is the two-dimensional rescaled mode amplitude, Δ_s the resolution of the distribution in position space, \tilde{k} the scaled wavenumber in the direction tangent to the PSS, and s the curvilinear coordinate along the PSS (that was taken as a surface at a constant distance from the surface of the model). Knowing the coordinates of the PSS, one can then express the Husimi function in terms of $(\tilde{k}_\theta, \theta)$. The results of this representation can be seen in Fig. 4.3, where the Husimi distributions of typical high-frequency p-modes are plotted against the PSS at the same values of m and Ω/Ω_K . Though the association of modes with a given phase space zone is relatively straightforward from the results of Fig. 4.3, it must be noted that, by construction, the Husimi function in Lignéres and Georgeot (2009) differs from the phase space distributions on the PSS since it is symmetric with respect to the scaled momentum \tilde{k}_θ . Also, Husimi distributions of chaotic modes were not found to spread all over the chaotic zone as expected, which was attributed to the relatively low frequencies of modes that were considered (however, one can note that

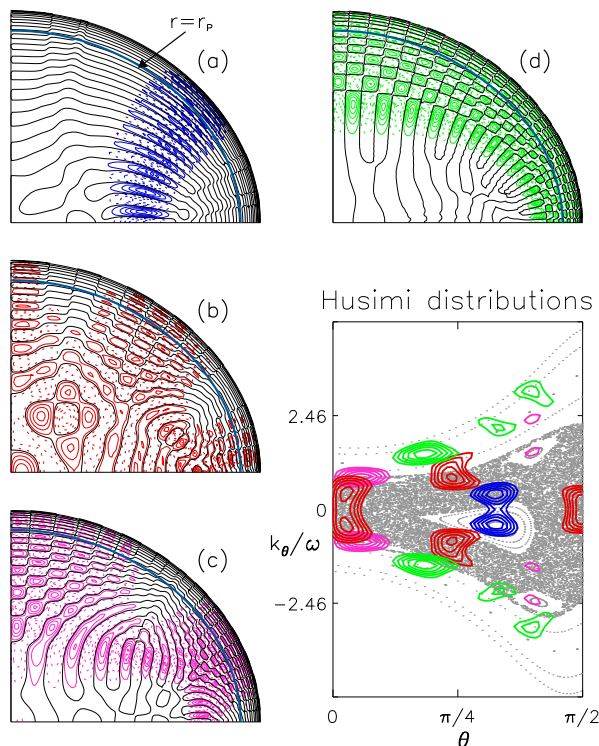


Figure 4.3: Amplitude distributions in position space of four typical high-frequency pressure modes with $m = 0$ in a polytropic stellar model rotating at $\Omega/\Omega_K = 0.589$. Their corresponding Husimi distributions have been plotted on the PSS (taken at a fixed distance $r = r_p$ from the stellar surface) at the same values of m and Ω/Ω_K (lower right panel). The high-frequency pressure modes correspond to (a): a period-2 island mode (blue), (b): a chaotic mode (red), (c): a period-6 island mode (magenta) and (d): a ‘whispering gallery’ mode (green). The coordinates of the PSS are the same as Fig. 4.1 (from Lignières and Georget (2009)).

similar behaviours can be found in ‘scarred’ eigenfunctions (Heller, 1984), due to their partial localisation around unstable periodic orbits). Nevertheless, these findings allowed to check that to each of the four classes of trajectories shown in Fig. 4.2 (period-2 and period-6 islands, ‘whispering gallery’ zones and chaotic zones), one can associate specific modes which are localized in the corresponding phase space regions in the high-frequency limit.

4.4 Frequency statistics and regularities

As expected from the Berry-Robnik conjecture (see Sect. 3.2.5) the different types of high-frequency modes were found to correspond to independent subparts of the oscillation spectrum. Modes localized in near-integrable regions of phase space (stable islands and ‘whispering gallery’ zones) were found to be associated with regular sub-spectra, in the sense that their mode frequencies can be written as $\omega_i = f_i(n_i, \ell_i, m)$, where n_i, ℓ_i, m are integers. In particular, the frequencies of modes localized on period-2 stable islands were asymptotically of the form $\omega_{n,\ell} = n\delta_n + \ell\delta_\ell + \alpha$, where n and ℓ are integers and α is a constant. This is similar to the mode frequencies of a spherical star, although in the rapidly rotating case the spectra should be described by a different function of the quantum numbers. On the other side, modes localized in the chaotic region of phase space were found to produce an irregular sub-spectrum with specific statistical properties (see below). The results of this classification in independent sub-spectra can be seen in Fig. 4.4, where the sub-spectra of the four classes of modes have been split accordingly with the locations in phase space of their Husimi representations.

In order to analyse the statistical distribution of chaotic mode frequencies, Lignières and Georget (2008, 2009) studied the nearest-neighbour frequency spacing $s = x_{i+1} - x_i$, where x_i are the mode frequencies normalized by the mean level spacing in some high-frequency range of the chaotic sub-spectrum. To do so, the chaotic modes have been selected, as explained previously, from the position in phase space of their Husimi distributions. We show in Fig. 4.5 the comparison between the cumulative level distribution

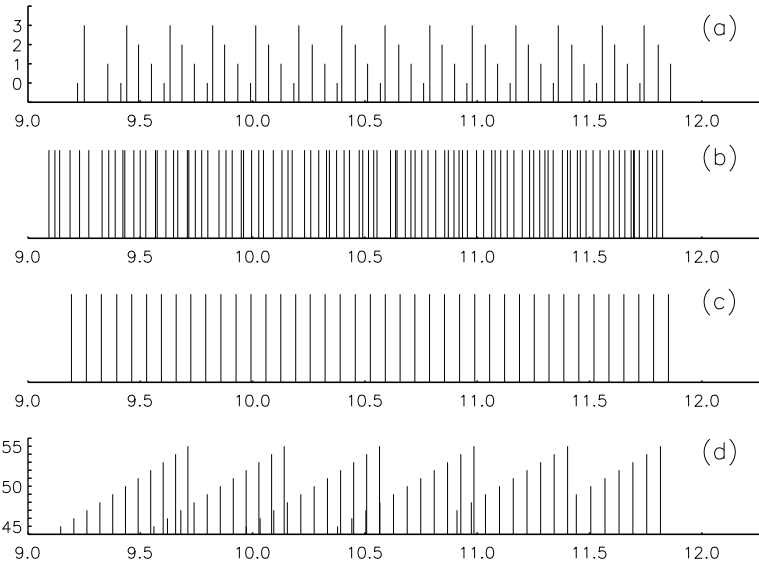


Figure 4.4: Frequency spectra of four classes of axi-symmetric ($m = 0$) high-frequency pressure modes that have been computed in a polytropic stellar model rotating at $\Omega/\Omega_K = 0.59$. Frequencies are given in units of ω_1 , which is the lowest acoustic mode frequency of the stellar model. Displayed sub-spectra are those of (a): period-2 island modes, (b): chaotic modes, (c): period-6 island modes, (d): ‘whispering gallery’ modes. For the two sub-spectra (a) and (d), the heights of the frequency peaks correspond to the quantum number ℓ (from Lignières and Georget (2009)).

$N(\Delta) = \int_0^\Delta P(s)ds$ of computed chaotic modes with predictions from the Poisson distribution $N(\Delta) = 1 - \exp(-\Delta)$ and Random Matrix Theory $N(\Delta) = 1 - \exp(-\pi\Delta^2/4)$ for the Gaussian Orthogonal Ensemble (GOE) (this ensemble has been chosen since the problem is invariant through time-reversal symmetry, see Sect. 3.2.4). To have a larger frequency sample, the spacings were computed within each of the two independent sub-spectra corresponding to the two symmetry classes with respect to the equator, using almost 200 modes. The numerically computed chaotic sub-spectrum of axi-symmetric p-mode oscillations in a polytropic stellar model rotating at $\Omega/\Omega_K = 0.59$ was thus found to be close to the predictions of the GOE of Random Matrix Theory, and far from the result for uncorrelated (Poisson) spectra (we remind here the reader that the Poisson distribution of frequencies is typical of integrable systems, whereas the frequencies of typical chaotic systems follow Wigner-Dyson statistics, cf Sect. 3.2.4). The BGS conjecture (see Sect. 3.2.4) is thus verified by the chaotic subset of the numerical acoustic stellar modes. This good agreement with the predictions of Random Matrix Theory was seen as a strong evidence of the presence of wave chaos in the pressure oscillations of rapidly rotating polytropic models.

Finally, it must be noted that the different dynamical subsets of p-modes that were found in numerical computations are not equally likely to be found in observational data. Indeed, several factors are known to influence the visibility of modes. The question of mode excitation in rapidly rotating stars has not been studied yet, but Lignières and Georget (2009) computed the important effect of the mode visibility, that is the cancellation of mode amplitudes in the disk-integrated light. This disk-integration factor was estimated by integrating the surface temperature perturbation for different oscillation modes in a polytropic stellar model seen from different inclination angles, at a given rotation rate. More modes were found to be visible in the numerical p-mode spectra of rapidly rotating polytropic stellar models than usually found in non-rotating stars (three times more for the rotation considered: $\Omega/\Omega_K = 0.59$). Among the four classes of modes, the period-2

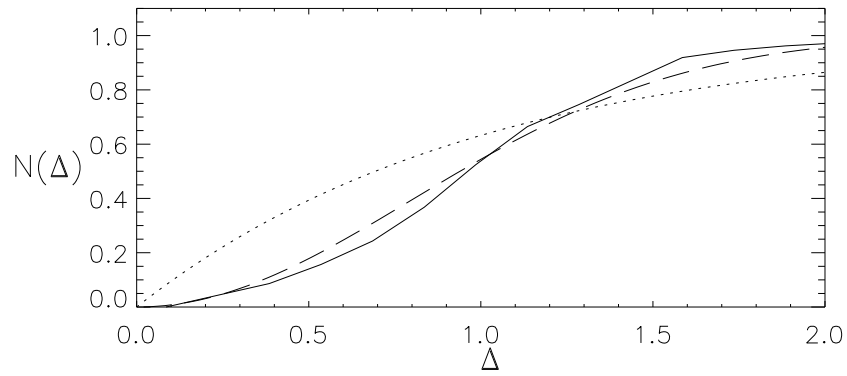


Figure 4.5: Integrated spacing distribution $N(\Delta)$ of chaotic modes for $m = 0$ in a polytropic stellar model rotating at $\Omega/\Omega_K = 0.59$ (full line). The integrated spacing distributions for the Gaussian Orthogonal Ensemble (dashed line), and the Poisson distribution typical of uncorrelated spectra (dotted line) are also plotted for comparison (from Lignières and Georgeot (2008)).

island modes and the chaotic modes were found to have similar visibilities, and to be significantly more visible than the period-6 island modes and ‘whispering gallery’ modes. At high rotation rates, the high-frequency oscillation spectrum is thus expected to be dominated by the period-2 island modes and chaotic modes. It was therefore natural to focus on these two classes for the further asymptotic studies of oscillations in rapidly rotating stars.

Chapter 5

Regular modes in rotating stars

In this chapter we present the results on regular pressure modes in rapidly rotating stars that were obtained in Pasek et al. (2011, 2012). We have seen at the end of Chap. 4 that the regular frequency spacings that were found empirically in numerical computations of stellar oscillations in rapidly rotating polytropic stellar models correspond to modes whose ray limits belong to near-integrable regions of the ray limit's phase space. It was also found that at high rotation rates, the regular modes that are the most visible are the period-2 island modes, which are modes corresponding to the period-2 stable islands of phase space. In this chapter, we use the 'parabolic equation method' to obtain semi-analytical formulae for the amplitude distributions and frequencies of the period-2 island modes. This method uses an approximation of the wave equation in the vicinity of the stable periodic trajectory in the centre of the stable island. This allows to express the pressure wave frequencies in terms of simple dynamical properties of the stable periodic trajectory, that can be obtained by integrating the ray equations. In order to verify the results of the parabolic equation method, we also computed numerical solutions of oscillation modes in polytropic stellar models. We find that the formula and full numerical computations are in good agreement over a large range of rotation rates, and discuss the astrophysical applications of these findings.

We first introduce the polytropic stellar models that have been used for our studies in Sect. 5.1. Then, we derive the equation for pressure waves in rotating stars (Sect. 5.2), and the ray limit of the pressure wave equation (Sect. 5.3). Using the stable periodic solutions of the ray limit, we construct in Sect. 5.4 the regular oscillation modes associated with stable islands using the 'parabolic equation method'. Since this formula allows to derive only semi-analytical formulas, that depend on the properties of numerically computed rays, we give in Sect. 5.5 the numerical implementation of the method. In order to determine the validity of our semi-classical predictions based on rays, we compare these results with those of complete two-dimensional computations, that are described in Sect. 5.6. Finally, in Sect. 5.7, we summarize the results of the articles (included in Sect. 5.8 and Sect. 5.9) where the parabolic equation method has been applied to the high-frequency pressure modes of polytropic stellar models at different rotation rates.

5.1 Equilibrium stellar models

Our stellar model will be a self-gravitating uniformly rotating monoatomic perfect gas with first adiabatic exponent $\Gamma_{1,0} = 5/3$. We assume that our stellar model is axially symmetric, and uniformly rotating with some rotational velocity $\boldsymbol{\Omega} = \Omega \cdot \mathbf{e}_z$, and thus start from Eqs. (2.24)-(2.27). Now, we replace the equation for energy conservation and

the equation of state,

$$\nabla F_0 = \rho_0 \epsilon_{N,0}, \quad (5.1)$$

$$p_0 = \frac{\mathcal{R}}{\mu} \rho_0 T_0. \quad (5.2)$$

that both depend on p_0 , ρ_0 and T_0 , by a *polytropic relation* that relates directly the equilibrium pressure p_0 and density ρ_0 . This relation is such that

$$p_0 = K \rho_0^{1+\frac{1}{N}}, \quad (5.3)$$

where K is the proportionality constant called the *polytropic constant*, and N is the *polytropic index*. One can also define a *polytropic exponent* such that $\gamma_p = 1 + \frac{1}{N}$.

Such an assumption is fully justified when the stellar matter has a simple equation of state of the form $p_0 = K \rho_0^\gamma$, where K is fixed. This happens for a completely degenerate gas (i.e. a gas of fermions where all energy states below the *Fermi energy* are filled), in this case the star is supported by the so-called *degeneracy pressure* that comes from the Pauli exclusion principle. This is the case for *white-dwarf stars*, that are made of completely degenerate *electron* gas, and *neutron stars*, made of completely degenerate *neutron* gas (Kippenhahn and Weigert, 1994). For stars where the gas is non-degenerate, a polytropic relation with a well-chosen index is also a reasonable approximation. First, the entropy is practically uniform in convective regions. Thus, the temperature gradient is close to the adiabatic gradient and the pressure and density are related by $p_0 \sim \rho_0^{\Gamma_{1,0}}$ (Kippenhahn and Weigert, 1994), where the polytropic exponent is the adiabatic exponent, i.e. $\gamma_p = \Gamma_{1,0} = 5/3$ or $N = 3/2$. On the other hand, stellar radiative zones can be rather well approximated by a polytrope with $N \approx 3$. This can be inferred from an envelope model using the simplified Kramers' law for the opacity (Hansen et al., 2004). Or, one can determine empirically a value of the polytropic exponent γ that corresponds to a given realistic stellar model by fitting the values of $\ln p_0$ as a function of $\ln \rho_0$. A star that has both a convective and radiative zone can thus be approximated by a bi-polytropic relation, with the corresponding exponents in each region.

Using the polytropic relation, Eqs. (2.24)-(2.27) collapse to the three equations:

$$0 = -\frac{1}{\rho_0} \nabla p_0 - \nabla \left(\Phi_0 - \frac{1}{2} \Omega^2 d^2 \right), \quad (5.4)$$

$$\nabla^2 \Phi_0 = 4\pi G \rho_0, \quad (5.5)$$

$$p_0 = K \rho_0^{1+\frac{1}{N}}. \quad (5.6)$$

These equations, with the polytropic index set to $N = 3$, were adopted to compute numerically all the stellar models at different rotation rates (see Sect. 5.6) that are used in this thesis.

5.2 Short-wavelength pressure wave equation

We wish to find a short-wavelength approximation of the linear perturbations around the stellar equilibrium. The starting equations, Eqs. (2.28)-(2.31), are reproduced below,

writing time derivatives in the co-rotating frame as $\frac{\partial}{\partial t}$:

$$\frac{\partial \rho'}{\partial t} + \nabla \cdot (\rho_0 \mathbf{v}') = 0, \quad (5.7)$$

$$\rho_0 \frac{\partial \mathbf{v}'}{\partial t} + 2\rho_0 \boldsymbol{\Omega} \times \mathbf{v}' = -\nabla p' - \rho_0 \nabla \Phi' - \rho' \nabla \left(\Phi_0 - \frac{\Omega^2 d^2}{2} \right), \quad (5.8)$$

$$\nabla^2 \Phi' = 4\pi G \rho', \quad (5.9)$$

$$\frac{\partial p'}{\partial t} + \mathbf{v}' \cdot \nabla p_0 = \frac{\Gamma_{1,0} p_0}{\rho_0} \left(\frac{\partial \rho'}{\partial t} + \mathbf{v}' \cdot \nabla \rho_0 \right). \quad (5.10)$$

For high-frequency pressure modes, it is reasonable to neglect the perturbations of the gravitational potential $\Phi' = 0$, an approximation known as the ‘Cowling approximation’ (Cowling, 1941). One can also neglect the Coriolis term $2\rho_0 \boldsymbol{\Omega} \times \mathbf{v}'$, whose effect on pulsation frequencies is known to be weak in the high-frequency regime (Reese et al., 2006, 2008). Using these two approximations we obtain:

$$\frac{\partial \rho}{\partial t} + \nabla \cdot (\rho_0 \mathbf{v}) = 0, \quad (5.11)$$

$$\rho_0 \frac{\partial \mathbf{v}}{\partial t} = -\nabla p + \rho \mathbf{g}_0, \quad (5.12)$$

$$\frac{\partial p}{\partial t} + \mathbf{v} \cdot \nabla p_0 = c_s^2 \left(\frac{\partial \rho}{\partial t} + \mathbf{v} \cdot \nabla \rho_0 \right), \quad (5.13)$$

where we dropped the primes on perturbation quantities. The term $\mathbf{g}_0 = -\nabla \left(\Phi_0 - \frac{\Omega^2 d^2}{2} \right)$ is the effective gravity that results from the gravitational and centrifugal forces, and c_s the sound speed.

As in Gough (1993); Lignières and Georgeot (2009), we now wish to transform Eqs. (5.11)-(5.13) into a form without first-order derivatives, that is expected to yield a better WKB approximation (cf. the appendix of Gough, 1993). To do so, we take the time derivatives of Eq. (5.11) and Eq. (5.13), and use Eq. (5.12) in order to eliminate the perturbation velocity \mathbf{v} . This yields

$$\frac{\partial^2 \rho}{\partial t^2} + \nabla \cdot (\rho \mathbf{g}_0) = \nabla^2 p, \quad (5.14)$$

$$c_s^2 \left(\frac{\partial^2 \rho}{\partial t^2} + N_0^2 \rho \right) = \frac{\partial^2 p}{\partial t^2} + \frac{c_s^2 N_0^2}{g_0^2} \mathbf{g}_0 \cdot \nabla p, \quad (5.15)$$

where N_0 is the Brunt-Väisälä frequency defined as

$$N_0^2 = \mathbf{g}_0 \cdot \left(\frac{\nabla \rho_0}{\rho_0} - \frac{1}{\Gamma_{1,0}} \frac{\nabla p_0}{p_0} \right), \quad (5.16)$$

and $g_0 = \|\mathbf{g}_0\|$. As we are interested in harmonic solutions for the pressure perturbation p , we can write it as $p = \text{Re}[\hat{p} \exp(-i\omega t)]$ where \hat{p} is the complex pressure amplitude and ω the frequency of the perturbation, and similarly for ρ . Putting this form of solutions into Eqs. (5.14)-(5.15) results in the following equations:

$$-\omega^2 \hat{\rho} + \nabla \cdot (\hat{\rho} \mathbf{g}_0) = \nabla^2 \hat{p}, \quad (5.17)$$

$$c_s^2 (-\omega^2 \hat{\rho} + N_0^2 \hat{\rho}) = -\omega^2 \hat{p} + \frac{c_s^2 N_0^2}{g_0^2} \mathbf{g}_0 \cdot \nabla \hat{p}. \quad (5.18)$$

In order to obtain an expression on the pressure amplitude perturbation \hat{p} only, we then insert into Eq. (5.17) the expression for $\hat{\rho}$ in terms of \hat{p} given by Eq. (5.18), to obtain:

$$\begin{aligned} \left[-\omega^4 + \omega^2 c_s^2 \alpha \nabla \cdot \left(\frac{\mathbf{g}_0}{c_s^2 \alpha} \right) \right] \hat{p} + \left[\omega^2 \left(1 + \frac{c_s^2 N_0^2}{g_0^2} \right) - c_s^2 \alpha \nabla \cdot \left(\frac{N_0^2 \mathbf{g}_0}{g_0^2 \alpha} \right) \right] \mathbf{g}_0 \cdot \nabla \hat{p} \\ - \frac{c_s^2 N_0^2}{g_0^2} \mathbf{g}_0 \cdot \nabla (\mathbf{g}_0 \cdot \nabla \hat{p}) - \omega^2 c_s^2 \alpha \nabla^2 \hat{p} = 0. \end{aligned} \quad (5.19)$$

where we have defined the dimensionless quantity α as

$$\alpha = 1 - \frac{N_0^2}{\omega^2}. \quad (5.20)$$

Finally, to cancel the terms in Eq. (5.19) that contain first-order derivatives of \hat{p} , we introduce a new amplitude perturbation $\hat{p} = \lambda \hat{\Psi}$ and insert it into Eq. (5.19). Provided that the function λ verifies

$$\nabla(\ln \lambda) = \frac{\beta}{2c_s^2} \mathbf{g}_0, \quad (5.21)$$

where

$$\beta = 1 + \frac{c_s^2 N_0^2}{g_0^2} - c_s^2 \nabla \cdot \left(\frac{(1-\alpha) \mathbf{g}_0}{\alpha g_0^2} \right), \quad (5.22)$$

we obtain the following equation:

$$\nabla^2 \hat{\Psi} + \frac{\omega^2 - \omega_c^2}{c_s^2} \hat{\Psi} - \frac{N_0^2}{\omega^2} \left[\nabla^2 - \frac{1}{g_0^2} (\mathbf{g}_0 \cdot \nabla)(\mathbf{g}_0 \cdot \nabla) \right] \hat{\Psi} = 0, \quad (5.23)$$

where the so-called *cut-off frequency* ω_c is such that

$$\omega_c^2 = \frac{g_0^2 \beta^2}{4c_s^2} + c_s^2 \alpha \nabla \cdot \left(\frac{\mathbf{g}_0}{c_s^2 \alpha} \right) - \frac{c_s^2}{2} \nabla \cdot \left(\frac{\beta \mathbf{g}_0}{c_s^2} \right) + \frac{1-\alpha}{2} \beta g_0^2 \nabla \cdot \left(\frac{\mathbf{g}_0}{g_0^2} \right). \quad (5.24)$$

Equation (5.23) has a simple physical interpretation since its second and third left hand-side terms correspond to pressure and gravity waves, respectively. In order to study the dynamics of pressure waves only, we restrict our study on the asymptotic high-frequency regime of pressure modes. In this regime, we have $\omega \gg N_0$, and we can neglect the third term on the left hand-side of Eq. (5.23) that corresponds to gravity waves. This yields the equation for the propagation of pressure waves in a stellar model as

$$\nabla^2 \hat{\Psi} + \frac{\omega^2 - \omega_c^2}{c_s^2} \hat{\Psi} = 0. \quad (5.25)$$

where the inhomogeneous sound speed is given by $c_s^2 = \Gamma_{1,0} p_0 / \rho_0$ and the square of the cut-off frequency ω_c by Eq. (5.24). In the high-frequency regime, the dynamics of acoustic waves in a star thus depends on these two quantities only. We plot in Fig. 5.1 a meridional cut of the spatial distribution of the speed of sound in a polytropic stellar model with index $N = 3$ that is uniformly rotating at $\Omega / \Omega_K = 0.707$ (where $\Omega_K = \sqrt{GM/R_{\text{eq}}}$). It can be seen that the speed of sound is greater at the centre, since the gravitational stratification imposes that the temperature is higher in this region. One can also notice that iso-surfaces of the sound speed are nearly spherical in the centre of the star, while they are similar to the surface at higher radii. This is due to the centrifugal force, whose modulus is proportional to the distance from the rotation axis. While the form of ω_c given in Eq. (5.24) is rather general, it can be further simplified for high-frequencies i.e. when $\omega \gg N_0$, while being consistent with the fact that we discarded gravity waves. This limit corresponds to $\alpha \sim 1$, which yields

$$\omega_c^2 = \frac{g_0^2}{4c_s^2} \left(1 + \frac{c_s^2 N_0^2}{g_0^2} \right)^2 + \frac{c_s^2}{2} \nabla \cdot \left[\left(1 - \frac{c_s^2 N_0^2}{g_0^2} \right) \frac{\mathbf{g}_0}{c_s^2} \right]. \quad (5.26)$$

It can also be noted that in this limit, using the polytropic relation $p_0 = K \rho_0^{1+\frac{1}{N}}$, the function λ in Eq. (5.21) is proportional to $\rho_0^{1/2}$ and thus we have $\hat{\Psi} \propto \rho_0^{-1/2} \hat{p}$. Without any further approximation, it is possible to obtain a simpler expression for ω_c by using again the polytropic relation. Consequently, the Brunt-Väisälä frequency N_0 , the effective gravity \mathbf{g}_0 and the speed of sound c_s can be expressed as functions of the specific enthalpy

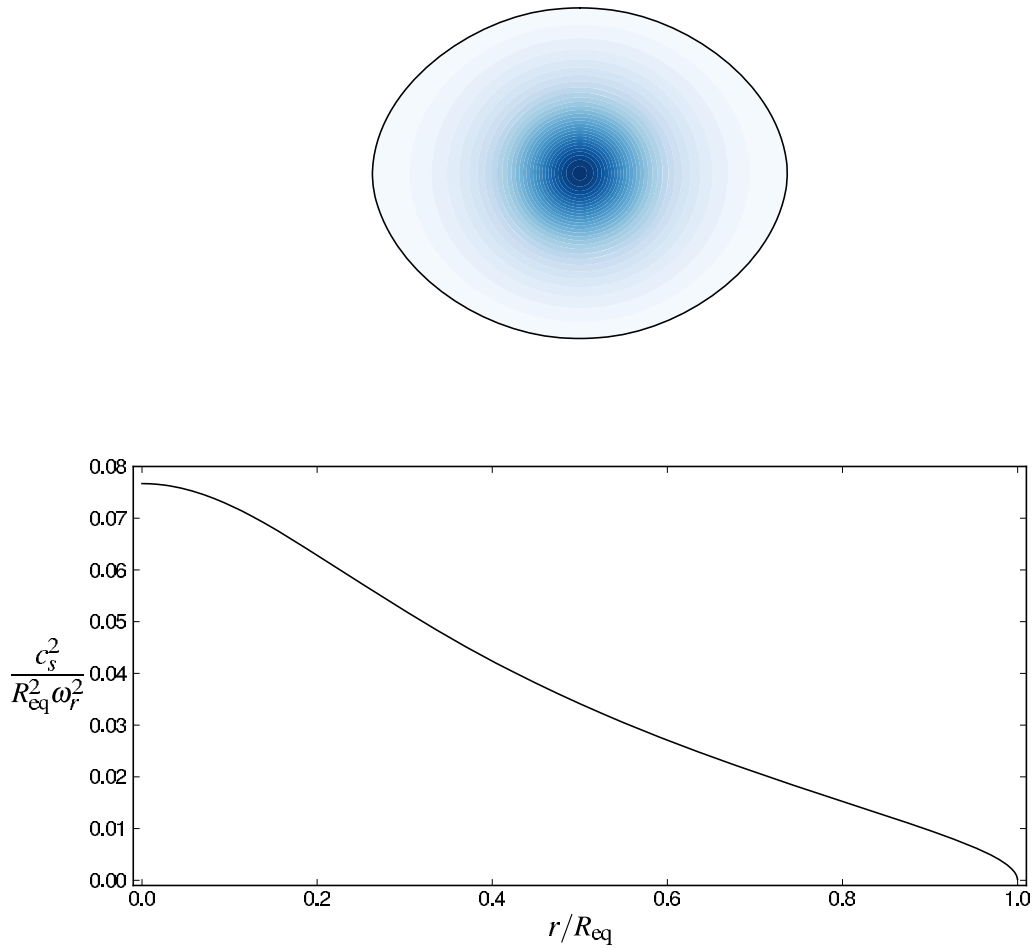


Figure 5.1: Contour plot (upper panel) of the distribution of the squared speed of sound c_s^2 normalized by $R_{\text{eq}}^2 \omega_r^2$, where R_{eq} is the equatorial radius of the stellar model and $\omega_r = (4\pi G \rho_c)^{1/2}$ is a characteristic pulsation frequency, ρ_c being the density at the centre of the model. In the lower panel is plotted a cut along the equator of this same distribution. The model is a polytropic stellar model with index $N = 3$ that is rotating at $\Omega/\Omega_K = 0.707$, where $\Omega_K = \sqrt{GM/R_{\text{eq}}}$.

$h_0 = \int \frac{dp_0}{\rho_0}$, leading to the collapse of the previous expression to our final form for the cut-off frequency as

$$\omega_c^2 = \frac{1}{2} \left[\frac{\Gamma_{1,0} N(N+2)}{2(N+1)} - 2 \right] \frac{g_0^2}{h_0} + \frac{1}{2} \left(2 - \frac{\Gamma_{1,0} N}{N+1} \right) \nabla \cdot \mathbf{g}_0. \quad (5.27)$$

The distribution of ω_c^2 given by Eq. (5.27) is plotted in Fig. 5.2, where it can be seen that ω_c^2 is negligible (compared to pressure wave frequencies) everywhere in the star except close to the surface, where it tends to infinity and provokes the back-reflection of pressure waves. The drastic increase of ω_c^2 in this zone makes it similar to an infinite potential barrier, but it must be noted that this is particular to the polytropic relation that we have chosen. In real stars, ω_c^2 should have a finite value at the surface, thus bounding the frequency of pressure waves that can be reflected.

Using the cylindrical symmetry of the stellar model with respect to the rotation axis, we can obtain a two-dimensional version of Eq. (5.25) by writing that $\hat{\Psi} = \hat{\Psi}_m \exp(im\phi)$, where m is an integer and ϕ is the azimuth angle of spherical coordinates. By inserting this expression into Eq. (5.25) we obtain that

$$\left[\nabla_{r,\theta}^2 + \frac{1}{r} \left(\frac{\partial}{\partial r} + \frac{1}{r \tan \theta} \frac{\partial}{\partial \theta} \right) - \frac{m^2}{(r \sin \theta)^2} \right] \hat{\Psi}_m + \frac{\omega^2 - \omega_c^2}{c_s^2} \hat{\Psi}_m = 0, \quad (5.28)$$

where θ is the colatitude. Again, to put this equation into a ‘normal form’, we write $\hat{\Psi}_m = \beta(r, \theta) \hat{\Phi}_m$ in the previous equation to obtain that $\beta(r, \theta)$ must satisfy

$$\frac{2}{\beta} \frac{\partial \beta}{\partial r} + \frac{1}{r} = 0, \quad (5.29)$$

to cancel out terms in $\frac{\partial \hat{\Phi}_m}{\partial r}$, and

$$\frac{2}{\beta} \frac{\partial \beta}{\partial \theta} + \frac{1}{\tan \theta} = 0, \quad (5.30)$$

to cancel out terms in $\frac{\partial \hat{\Phi}_m}{\partial \theta}$. This leads to

$$\beta(r, \theta) = \frac{B}{\sqrt{r \sin \theta}}, \quad (5.31)$$

and we choose $B = 1$ to yield that $\hat{\Phi}_m = \sqrt{d} \hat{\Psi}_m$ and

$$\nabla^2 \hat{\Phi}_m + \frac{1}{c_s^2} \left[\omega^2 - \omega_c^2 - \frac{c_s^2 (m^2 - \frac{1}{4})}{d^2} \right] \hat{\Phi}_m = 0, \quad (5.32)$$

where $d = r \sin \theta$ is the distance to the rotation axis.

5.3 Derivation of the acoustic ray limit

In order to derive the propagation equation for acoustic rays (called the *geometrical acoustics* limit in Landau and Lifshitz, 1959), we write the complex amplitude perturbation $\hat{\Psi}$ as

$$\hat{\Psi} = A(\mathbf{x}) \exp[i\Phi(\mathbf{x})], \quad (5.33)$$

where $A(\mathbf{x})$ and $\Phi(\mathbf{x})$ are real. It is then assumed that for small wavelengths, $\nabla \Phi(\mathbf{x})$ is large compared to the spatial variations of the amplitude and the typical length-scales of the background model. Inserting Eq. (5.33) into Eq. (5.25), and neglecting $\frac{\nabla^2 A(\mathbf{x})}{A(\mathbf{x})}$ that is

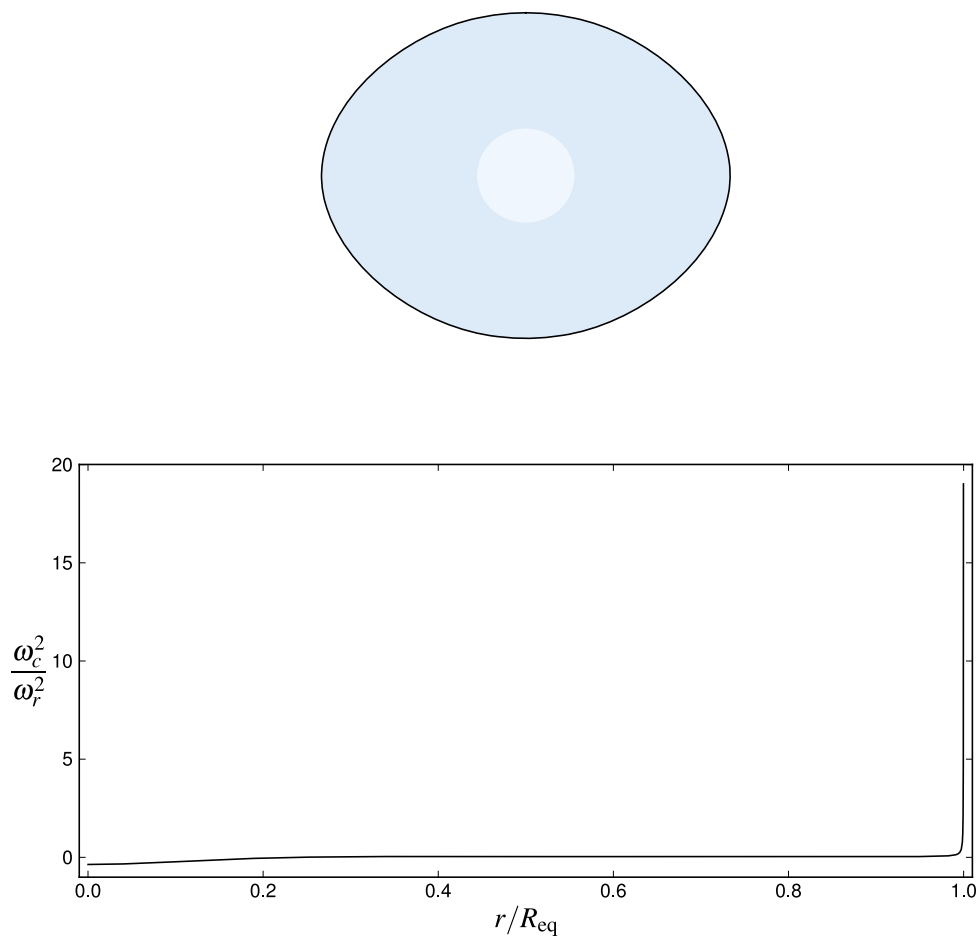


Figure 5.2: Contour plot (upper panel) of the distribution of the cut-off frequency squared ω_c^2 normalized by $\omega_r^2 = 4\pi G\rho_c$, where ρ_c is the density at the centre of the model. The distribution of ω_c^2 is nearly homogeneous everywhere in the stellar model, except close to the surface. This can be seen in the lower panel, where a cut along the equator of the same distribution is plotted. The stellar model is the same as in Fig. 5.1

small compared to $(\nabla\Phi(\mathbf{x}))^2$, we obtain the *eikonal equation* for pressure waves in stars as (Lignières and Georgeot, 2009)

$$\omega^2 = \omega_c^2 + c_s^2 \mathbf{k}^2, \quad (5.34)$$

where the local wavevector \mathbf{k} is defined as $\mathbf{k} = \nabla\Phi(\mathbf{x})$, and Φ is called the *eikonal*. We now wish to write Eq. (5.34) as an Hamiltonian system in the conjugate phase-space coordinates $(\mathbf{x}(t), \mathbf{k}(t))$. Choosing the Hamiltonian H such that

$$H = \frac{\tilde{\mathbf{k}}^2}{2} + V(\mathbf{x}), \quad (5.35)$$

where we have introduced the frequency-scaled wavevector $\tilde{\mathbf{k}} = \mathbf{k}/\omega$ and

$$V(\mathbf{x}) = -\frac{1}{2c_s^2} \left(1 - \frac{\omega_c^2}{\omega^2} \right), \quad (5.36)$$

ensures that the Hamiltonian stays constant along the motion, since we have $H = 0$ according to Eq. (5.34). This yields the corresponding Hamiltonian equations of motion as

$$\frac{d\mathbf{x}}{dt} = \tilde{\mathbf{k}} \quad (5.37)$$

$$\frac{d\tilde{\mathbf{k}}}{dt} = -\nabla V(\mathbf{x}), \quad (5.38)$$

where $dt = c_s ds / \sqrt{1 - \omega_c^2/\omega^2}$ (note that t is *not* homogeneous to a time). Since the potential $V(\mathbf{x})$ is rotationally symmetric with respect to the rotation axis of the star, we know that the angular momentum along the rotation axis L_z is a constant of motion for the ray dynamics. We can thus consider the Hamiltonian system for rays projected onto the meridional plane rotating at the angular velocity $\frac{d\phi}{dt} = \frac{m/\omega}{d^2}$. This yields the two-degree-of-freedom reduced Hamiltonian H_r such that

$$H_r = \frac{\tilde{\mathbf{k}}_p^2}{2} + V_r(\mathbf{x}), \quad (5.39)$$

where $\tilde{\mathbf{k}}_p = \tilde{\mathbf{k}} - (\tilde{\mathbf{k}} \cdot \mathbf{e}_\phi) \mathbf{e}_\phi$ and the reduced potential

$$V_r(\mathbf{x}) = -\frac{1}{2c_s^2} \left(1 - \frac{\omega_c^2}{\omega^2} - \frac{c_s^2 m^2}{\omega^2 d^2} \right). \quad (5.40)$$

This leads to the equations that give the propagation of acoustic rays in polytropic stellar models, when projected onto the meridional plane, as

$$\frac{d\mathbf{x}}{dt} = \tilde{\mathbf{k}}_p \quad (5.41)$$

$$\frac{d\tilde{\mathbf{k}}_p}{dt} = -\nabla V_r(\mathbf{x}). \quad (5.42)$$

The sharp increase of the cut-off frequency ω_c in the outermost layers of the star (see Fig. 5.2) reflects acoustic rays towards the stellar interior, whereas approaching the centre, the increase of c_s (see Fig. 5.1) deflects acoustic rays in the direction of the outer layers.

5.4 The parabolic equation method

In this section, we describe briefly the main steps and assumptions of the parabolic equation method (Babich and Buldyrev, 1991). This method, whose original derivation by V.M. Babich dates back to 1968, aims at giving approximate eigenfunctions and frequencies of modes that are localised, in the short-wavelength limit, around stable periodic orbits. The parabolic equation method, in different forms and sometimes under different names, was successfully applied to various wave and quantum systems (Tureci et al., 2002; Zalipaev et al., 2008; Vagov et al., 2009). We will mention here in particular its use to obtain the resonances (i.e. frequencies of an open wave system) associated to stable periodic orbits of wave-chaotic dielectric micro-cavities (see e.g. Schwefel et al., 2004; Tureci et al., 2005). In this context, some authors have pointed out the similarities that exist between the parabolic equation method and the methods of Gaussian optics (see e.g. Siegman, 1986). When applied to the resonances of asymmetric cavities, it was found that the parabolic equation method could describe simple regular frequency sequences in their otherwise highly irregular spectrum (Tureci et al., 2002). More details on the parabolic equation method can be found in the published papers Pasek et al. (2011, 2012), that are reprinted in Sect. 5.8 and Sect. 5.9.

We start our analysis from the two-dimensional Helmholtz equation (Eq. (5.32)) that describes pressure waves in the meridian plane of the star. This equation can be written as:

$$\nabla^2 \Phi_m + k_m^2 \Phi_m = 0, \quad (5.43)$$

where

$$k_m^2 = \frac{1}{\tilde{c}_s^2} \left[\omega^2 - \omega_c^2 - \frac{c_s^2(m^2 - 1/4)}{d^2} \right] = \frac{\omega^2}{\tilde{c}_s^2}. \quad (5.44)$$

We remind the reader that the associated boundary condition is that the Lagrangian pressure perturbation must vanish at the surface (see Sect. 2.2.1). In the case of a fixed boundary, this would be equivalent to the imposition of Dirichlet boundary conditions on Φ_m . Our goal is now to find the subset of solutions to Eq. (5.43) that are localised around the period-2 stable periodic rays in the short-wavelength limit.

To begin with, we write Eq. (5.43) in the local coordinates (s, ξ) centred on the stable periodic ray, that will be called γ thereafter, where s is the coordinate along γ and ξ the coordinate transverse to γ . Now, the mode amplitude is expressed as

$$\Phi_m(s, \xi) = \exp(i\omega\tau) U_m(s, \xi), \quad (5.45)$$

where τ is the time-scale of the mode variation along the ray γ , and $\tau \sim O(1)$ in the frequency ω . It is thus assumed that $U_m(s, \xi)$ is only left with a slow variation in the s direction, which is similar to the *slowly varying envelope approximation* of wave optics (see e.g. Siegman, 1986). In the short-wavelength limit (i.e. for high frequencies), the transverse envelope of the mode is assumed to decay on a scale proportional to $1/\sqrt{\omega}$, this property being taken into account by assuming that $\xi \sim O(1/\sqrt{\omega})$. Then, an expansion of Eq. (5.43) in ω yields (for the details, see e.g. Vagov et al., 2009) that $d\tau = ds/\tilde{c}_s$ at the dominant order, and at the order ω , a parabolic equation of the form:

$$\frac{\partial^2 V_m}{\partial \nu^2} - K(s) \nu^2 V_m + \frac{2i}{\tilde{c}_s(s)} \frac{\partial V_m}{\partial s} = 0, \quad (5.46)$$

where we have used the scaled coordinate $\nu = \sqrt{\omega}\xi$, the renormalized wavefunction $V_m = U_m/\sqrt{\tilde{c}_s}$, and the function $K(s)$ that is such that

$$K(s) = \frac{1}{\tilde{c}_s(s)^3} \frac{\partial^2 \tilde{c}_s}{\partial \xi^2} \Big|_{\xi=0}. \quad (5.47)$$

As the first two terms of Eq. (5.46) are similar to the equation for a quantum harmonic oscillator (Cohen-Tannoudji et al., 1973), one uses the ansatz

$$V_m^0 = A(s) \exp \left[i \frac{\Gamma(s)}{2} \nu^2 \right], \quad (5.48)$$

where $\Gamma(s)$ is an unknown complex-valued function, which can be viewed as a generalisation of the ground state of the quantum harmonic oscillator $\Psi(x) \propto \exp(-\frac{m\omega}{2\hbar}x^2)$. By inserting Eq. (5.48) into Eq. (5.46), one obtains the equations that must be satisfied by the amplitude $A(s)$ and the width $\Gamma(s)$ of the Gaussian wavepacket in Eq. (5.48) as

$$\frac{1}{\tilde{c}_s} \frac{d\Gamma}{ds} + \Gamma^2 + K(s) = 0, \quad (5.49)$$

$$\frac{1}{A} \frac{dA}{ds} = \frac{-\tilde{c}_s}{2} \Gamma. \quad (5.50)$$

Using the substitution

$$\Gamma(s) = \frac{\frac{1}{\tilde{c}_s(s)} \frac{dz}{ds}}{z(s)}, \quad (5.51)$$

one obtains that $A(s) = \frac{1}{\sqrt{z(s)}}$, and that

$$\frac{1}{\tilde{c}_s(s)} \frac{dz}{ds} = p, \quad (5.52)$$

$$\frac{1}{\tilde{c}_s(s)} \frac{dp}{ds} = -K(s)z. \quad (5.53)$$

At this point, it is important to note that Eqs. (5.52)-(5.53) also describe the motion of a ray nearby the periodic orbit γ , where $z(s)$ is the transverse deviation from γ and $p(s)$ the associated momentum (see e.g. Appendix C of Pasek et al., 2012). Now, Eqs. (5.52)-(5.53) admit two linearly independent complex conjugate solutions, and as these equations are linear equations with periodic coefficients of period L_γ , which is the length of the periodic orbit γ , we can relate its solutions at s and $s + L_\gamma$ by the so-called *monodromy matrix* M such that

$$\begin{bmatrix} z(s + L_\gamma) \\ p(s + L_\gamma) \end{bmatrix} = M \begin{bmatrix} z(s) \\ p(s) \end{bmatrix}. \quad (5.54)$$

For the function V_m^0 in Eq. (5.48) to be uni-valued, it is desirable that V_m^0 be the same after one period up to a global phase, which requires that $\Gamma(s + L_\gamma) = \Gamma(s)$. This condition is fulfilled if we choose the solution $\begin{pmatrix} z \\ p \end{pmatrix}$ of Eqs. (5.52)-(5.53) to be one of the eigenvectors of the monodromy matrix M (see e.g. Tureci et al., 2002). As the periodic trajectory γ is stable, it is known that $\text{Tr}(M) < 2$ and that the eigenvalues of M are complex conjugate and of modulus unity, written $\lambda_{1,2} = \exp(\pm i\alpha)$ where α is called the stability angle, or Floquet phase. It can be expressed in terms of the monodromy matrix as

$$\alpha = \arctan \left(\frac{\sqrt{-\text{Tr}(M)^2 + 4}}{\text{Tr}(M)} \right), \quad (5.55)$$

using that $\det(M) = 1$. The two corresponding eigenvectors are also complex conjugate. One must then choose to use in Eq. (5.48) the eigenvector $\begin{pmatrix} z_{1,2} \\ p_{1,2} \end{pmatrix}$ that satisfies $\text{Im}[\Gamma(s)] > 0$ for all s , which corresponds to a solution V_m^0 exponentially decreasing away from the periodic orbit γ (while the other solution yields an exponentially increasing function), as specified in the hypotheses of the parabolic equation method. In the following, we choose the eigenvalue of the monodromy matrix that corresponds to the localization of V_m^0 to be $\exp(+i\alpha)$.

It is possible to find additional solutions to Eq. (5.46), that corresponds to transverse excitations of the Gaussian wavepacket in Eq. (5.48). The method of construction of these solutions is similar to the algebraic quantisation method for the quantum harmonic oscillator, that uses the creation and annihilation operators \hat{a}^\dagger and \hat{a} , respectively. The expressions and commutation relations of these operators have been given elsewhere (see e.g. Pasek et al., 2012). We will only mention that transverse excitations of Eq. (5.48) are constructed by applying recursively the creation operator \hat{a}^\dagger on Eq. (5.48) as

$$V_m^\ell(s, \nu) = (\hat{a}^\dagger)^\ell V_m^0(s, \nu), \quad (5.56)$$

which yields that

$$V_m^\ell(s, \nu) = \left(\frac{i}{\sqrt{2}}\right)^\ell \left(\frac{\bar{z}}{z}\right)^{\ell/2} H_\ell\left(\sqrt{\text{Im}(\Gamma)}\nu\right) \frac{\exp\left(i\frac{\Gamma}{2}\nu^2\right)}{\sqrt{z}}, \quad (5.57)$$

with H_ℓ the Hermite polynomials of order ℓ . The final form for the eigenfunctions localised on the stable periodic orbit that are solutions to Eq. (5.43) is thus

$$\Phi_m^\ell(s, \nu) = \sqrt{\tilde{c}_s(s)} V_m^\ell(s, \nu) \exp\left(i\omega \int^s \frac{ds'}{\tilde{c}_s(s')}\right). \quad (5.58)$$

Now that the form of the eigenfunctions has been found, it is possible to apply the quantisation condition based on the single-valuedness of Eq. (5.58), which states that the phase accumulated by Φ_m^ℓ after one period must be a multiple of 2π . Knowing that $\Gamma(s + L_\gamma) = \Gamma(s)$, the only contributions to the phase come from the term $\omega \int \frac{ds}{\tilde{c}_s}$ and the phase of $z(s)$ after one round trip. While the monodromy matrix yields that $\begin{bmatrix} z(s+L_\gamma) \\ p(s+L_\gamma) \end{bmatrix} = e^{i\alpha} \begin{bmatrix} z(s) \\ p(s) \end{bmatrix}$, this relation does not give the total phase accumulated by $z(s)$ along the periodic orbit, which is $\alpha + 2\pi N_r$, where N_r is the winding number of the vector $z(s)$ in the complex plane (see Tureci et al., 2002, for a discussion). It can be expressed as

$$N_r = \text{int} \left[\frac{1}{2\pi i} \int_0^{L_\gamma} d(\ln z(s)) \right], \quad (5.59)$$

where $\text{int}[\]$ denotes the integer part, and must be computed from the propagation of $z(s)$ along the periodic ray. As was pointed out previously in Tureci et al. (2002), there should be an associated π phase shift in the solution when N_r is odd, though contrary to these authors we find that this can also affect the transverse mode spacing. This yields that

$$\omega \oint_\gamma \frac{ds}{\tilde{c}_s} - 2(\alpha + 2\pi N_r) \frac{\ell}{2} - (\alpha + 2\pi N_r) \frac{1}{2} = 2\pi n + \pi, \quad (5.60)$$

where n is an integer, and the additional π corresponds to the Maslov phase for the period-2 orbit, that is acquired from the reflection of acoustic waves on the boundary. By re-ordering the terms of the last formula, one obtains an expression for the frequencies of modes associated to period-2 stable orbits in the short-wavelength limit as:

$$\omega_{n,\ell,m} = \frac{1}{\oint_\gamma \frac{ds}{\tilde{c}_s}} \left[2\pi \left(n + \frac{1}{2} \right) + \left(\ell + \frac{1}{2} \right) (2\pi N_r + \alpha) \right]. \quad (5.61)$$

Thus, the frequencies $\omega_{n,\ell,m}$ of the period-2 stable island modes can be described by two constant spacings:

$$\delta_n(m) = \frac{2\pi}{\oint_\gamma \frac{ds}{\tilde{c}_s}} \quad \text{and} \quad \delta_\ell(m) = \frac{2\pi N_r + \alpha}{\oint_\gamma \frac{ds}{\tilde{c}_s}}. \quad (5.62)$$

The frequency spacing δ_n corresponds to the quantization of the oscillation mode in the longitudinal direction of the stable trajectory and depends on the length of the trajectory. On the other hand, δ_ℓ corresponds to the transverse variations of the mode and depends both on the length of the trajectory and on its stability angle.

5.5 Numerical implementation of the method

We describe in this section how the previous ray-based semi-analytical equations for the frequencies (Eq. (5.61)) and amplitude distributions (Eq. (5.58)) of regular island modes are numerically computed.

5.5.1 Numerical integration of ray equations

Equations (5.41)-(5.42) are two coupled first-order differential equations that can be integrated using a Runge-Kutta Method (Press et al., 1992). We thus integrate numerically these equations using the 5-th order numerical implementation of the Runge-Kutta method of Brankin and Gladwell (1994). The ray integration code that we used and extended was initially developed by F. Lignières. This being an initial value problem one needs to specify the initial conditions (r_i, θ_i) as well as $(k_\theta/k_r)_i$ (that is the initial direction of the ray), the fourth initial condition follows from energy conservation. The error control is achieved through specifying a local maximal error. The quantities ω_c and c_s are not known analytically, they are computed numerically and given only at discrete points. Thus, to obtain the values of c_s and ω_c at any point inside the star, as is necessary to integrate the propagation equations, their numerical values are interpolated. These two quantities are obtained from the numerical solutions of the polytropic stellar model, that we computed using a code developed by M. Rieutord (Rieutord et al., 2005). In this code, Eqs. (5.4)-(5.6) are first rewritten by introducing the pseudo-enthalpy h_0 such that

$$h_0 = \int \frac{dp_0}{\rho_0} = (1 + N) \frac{p_0}{\rho_0}, \quad (5.63)$$

this allows to integrate Eq. (5.4), and to express the Poisson equation (Eq. (5.5)) as

$$\nabla^2 \Phi_0 = 4\pi G \rho_c \left(1 - \frac{\Phi_0 - \Phi_c}{h_c} + \frac{\Omega^2 d^2}{2h_c} \right)^N. \quad (5.64)$$

This equation is first discretised using spectral methods (Press et al., 2007) (with Legendre polynomials in the θ direction and Chebyshev polynomials in the radial direction), and then solved by an iterative numerical scheme (described in Bonazzola et al., 1998; Rieutord et al., 2005), using spectral methods. From the aspherical shape of the star, it is necessary to use a coordinate system that adapts to the shape of the star. For this purpose, a spheroidal coordinate system (ζ, θ, ϕ) has been used, which is similar to the one introduced in Bonazzola et al. (1998). The pseudo-radial coordinate ζ is defined as

$$r(\zeta, \theta) = (1 - \epsilon)\zeta + \frac{5\zeta^3 - 3\zeta^5}{2} [R_s(\theta) - 1 + \epsilon] \quad (5.65)$$

in the interior of the star, and in the exterior we have

$$r(\zeta, \theta) = 2\epsilon + (1 - \epsilon)\zeta + (2\zeta^3 - 9\zeta^2 + 12\zeta - 4)[R_s(\theta) - 1 - \epsilon], \quad (5.66)$$

where $\epsilon = 1 - \frac{R_{\text{pol}}}{R_{\text{eq}}}$ and $R_s(\theta)$ corresponds to the radius of the surface, while the co-latitude θ and azimuthal angle ϕ are the same as those of spherical coordinates. This coordinate system is practical since the stellar surface is simply defined by $\zeta = 1$, while $\zeta \propto r$ for small values of ζ , i.e. spheroidal coordinates tend to spherical coordinates in the centre of the model. The pseudo-radial coordinate ζ is decomposed using Chebyshev polynomials, while the angular terms use spherical harmonics.

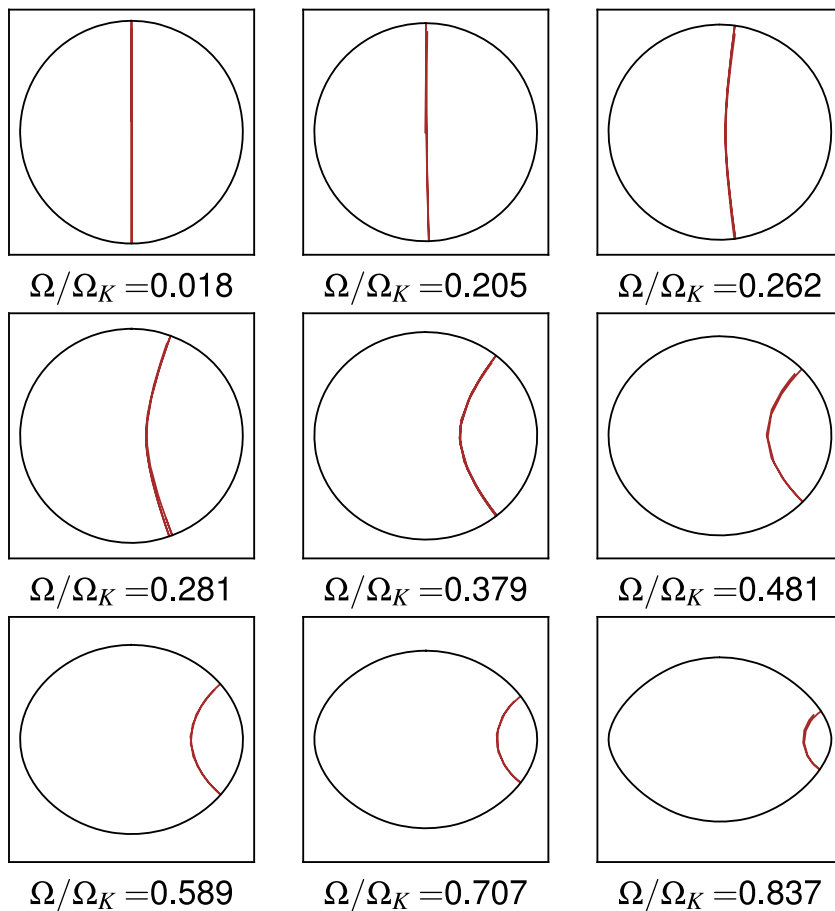


Figure 5.3: Approximate stable period-2 trajectories of the ray system Eqs. (5.41)-(5.42) (in brown) for $\omega = 2.0$ and $m = 0$ in polytropic stellar models with index $N = 3$ at different values of the rotation rate Ω/Ω_K .

5.5.2 Computation of periodic trajectories

Once the spatial distributions of c_s and ω_c are completely determined, only the frequency ω and the quantum number m are left to be specified. We choose $\omega = 2.0$, in units of $\omega_r = \sqrt{4\pi G \rho_c}$ where ρ_c is the density at the centre of the star, to be of the same order as the frequencies of the modes with which we will compare our results. Then, a non-trivial task is to find the initial conditions for the stable period-2 trajectory at a given rotation and quantum number m . Unfortunately, there is no clever way, to our knowledge, to find these orbits. We have chosen to compute a full Poincaré Surface of Section at a given rotation rate by launching rays for a large number of initial conditions, which then allow to find the initial conditions that correspond to the periodic trajectory. It is assumed that the stable periodic orbit does not change drastically if one slightly increases or decreases the rotation rate, which permits to infer gradually the initial conditions of period-2 stable orbits for various rotation rates. In Fig. 5.3, we plot the period-2 stable orbits at $\omega = 2.0$ and $m = 0$ that we found in a polytropic stellar model with $N = 3$, at different values of the rotation rate. Between $\Omega/\Omega_K = 0.205$ and $\Omega/\Omega_K = 0.262$, the stable periodic orbit undergoes a bifurcation, from a stable orbit on the polar axis, to two stable orbits on each

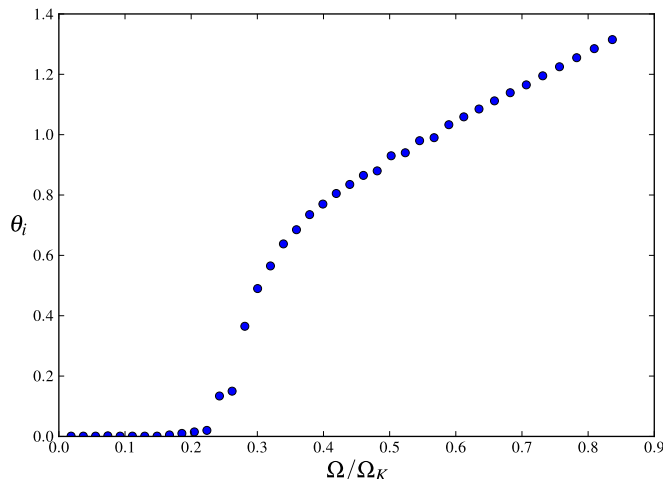


Figure 5.4: Initial conditions of the co-latitude θ_i that lead to period-2 stable trajectories when the initial condition for the radius is set to $r_i = 0.8$, for $\omega = 2.0$ and $m = 0$. The values of θ_i are plotted as functions of the rotation rate Ω/Ω_K .

side of the axis with one unstable orbit in the middle (only the orbit on the right side of the axis is displayed here). This behaviour, called a *bifurcation*, is well-known in dynamical systems theory (see e.g. Lichtenberg and Lieberman, 1983). We illustrate this further by plotting in Fig. 5.4 the initial conditions for θ_i that are required to obtain stable period-2 orbits for different values of the rotation rate, when rays are launched from a constant radius $r_i = 0.8$, for $\omega = 2.0$ and $m = 0$. The typical behaviour of a bifurcation can be recognized, although only the stable branch is depicted here (for a phase space picture of this bifurcation, one can refer to Fig. 2 of Pasek et al. (2011)). From the computed periodic trajectories, one can then compute directly δ_n from the period of these rays (also called ‘acoustic time’ in this context), that is

$$T_\gamma = \oint_\gamma \frac{ds}{\tilde{c}_s}. \quad (5.67)$$

The accuracy of this computation is discussed in Sect. 5.5.5.

5.5.3 Computation of the monodromy matrix

As we have seen, the neighbourhood of stable periodic trajectories has the form of stable islands that take the form of closed curves on a PSS. Near stable periodic trajectories, the linearised motion takes the form of elliptic orbits (Lichtenberg and Lieberman, 1983), whose intersections with a PSS transverse to the periodic ray are ellipses. Since we are interested in studying specifically period-2 stable rays, we choose to take the PSS at fixed angle $\theta = \pi/2$, where θ is the co-latitude which thus corresponds to the equator. Only rays intersecting the PSS while going downwards, i.e. such that $\mathbf{k}_p \cdot \mathbf{e}_z < 0$, are chosen, in order to have a univalued corresponding Poincaré map. As illustrated in Fig. 5.5, we indeed find that the intersections of a given stable orbit with the PSS can be well fitted by an ellipse (see also Fig. 5.7). We also tagged each intersection point in Fig. 5.5 by their intersection order with the PSS, to highlight the regular rotating motion that can be found around a stable periodic acoustic ray.

To determine the monodromy matrix, we first perform a linear least-squares ellipse fitting (based on the paper by Gander et al., 1994) on the data points of the PSS. This method finds the best-fitting ellipse curve by minimizing the algebraic distance with the

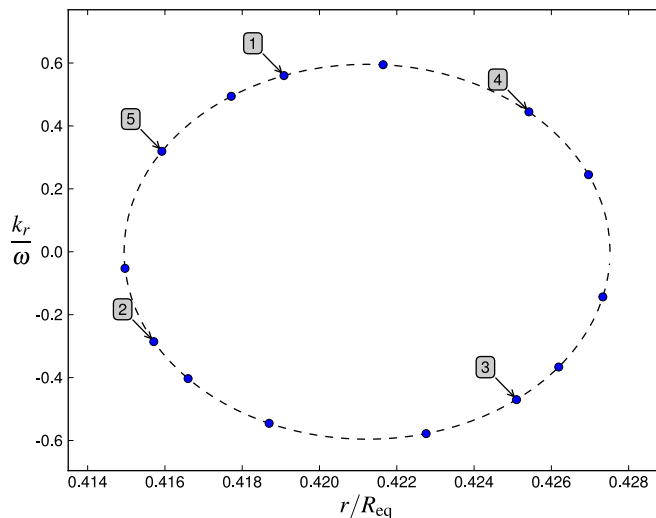


Figure 5.5: Intersections of a stable trajectory with the Poincaré Surface of Section at $\theta = \pi/2$ (which corresponds to the equator), when computed for $\omega = 2.0$ and $m = 0$, in a polytropic stellar model rotating at $\Omega/\Omega_K = 0.481$. Coordinates on the PSS are the normalised position on the equator r/R_{eq} , where R_{eq} is the equatorial radius of the stellar model, and the renormalised modulus of the radial wavevector k_r/ω .

data points. When parametrised by the angle $\theta \in [0, 2\pi[$, this ellipse is given by the equation

$$\begin{bmatrix} r(\theta) \\ \tilde{k}_r(\theta) \end{bmatrix} = \begin{bmatrix} r_c \\ \tilde{k}_{r,c} \end{bmatrix} + Q(\alpha) \begin{bmatrix} a \cdot \cos(\theta) \\ b \cdot \sin(\theta) \end{bmatrix} \quad (5.68)$$

where a, b are constants, $(r_c, \tilde{k}_{r,c})$ is the centre of the ellipse and $Q(\alpha)$ a matrix such that

$$Q(\alpha) = \begin{pmatrix} \cos \alpha & -\sin \alpha \\ \sin \alpha & \cos \alpha \end{pmatrix}. \quad (5.69)$$

This ellipse fitting has several purposes. First, it allows to verify that the chosen trajectory is close enough to the stable periodic trajectory to be described by a linearised (elliptic) motion. The results of the ellipse fitting for a given trajectory can be seen in Fig. 5.5. Then, we use the estimated position of the ellipse centre (x_c, y_c) as the coordinates of the periodic orbit intersection on the PSS. This allows to compute the distance vector on the PSS as

$$\begin{bmatrix} z \\ p \end{bmatrix} = \begin{bmatrix} r_i - r_c \\ \tilde{k}_{r,i} - \tilde{k}_{r,c} \end{bmatrix}. \quad (5.70)$$

The monodromy matrix M for a periodic trajectory is then defined on the PSS as

$$\begin{bmatrix} z \\ p \end{bmatrix}_{\text{final}} = \begin{pmatrix} m_{11} & m_{12} \\ m_{21} & m_{22} \end{pmatrix} \begin{bmatrix} z \\ p \end{bmatrix}_{\text{initial}}. \quad (5.71)$$

We are left with the four unknown entries of the monodromy matrix to determine numerically. This is done by using four intersection points of the stable ray with the PSS. The accuracy of the computation of the monodromy matrix is checked by computing its determinant $\text{Det}(M) = m_{11}m_{22} - m_{12}m_{21}$ that is known to be equal to unity from the symplectic nature of the Hamiltonian equations for rays. Once the monodromy matrix has been computed from the PSS, one can compute its eigenvalues by writing the characteristic polynomial of the 2×2 matrix M as

$$\Lambda^2 - \text{Tr}(M)\Lambda + \text{Det}(M) = 0, \quad (5.72)$$

where the roots of this polynomial $\Lambda_{1,2}$ are the eigenvalues of the matrix. We know that $\det(M) = 1$ and that for a stable ray we have $|\text{Tr}(M)| < 2$. Then, the determinant $\Delta = \text{Tr}(M)^2 - 4\det(M) < 0$, and the eigenvalues $\lambda_{1,2}$ are complex conjugate:

$$\lambda_{1,2} = \frac{\text{Tr}(M)}{2} \pm i \frac{\sqrt{-\Delta}}{2}. \quad (5.73)$$

One now computes the angles $\alpha_{1,2}$ such that $\alpha_{1,2} = \arg(\lambda_{1,2}) \bmod 2\pi$. One can also compute the corresponding eigenvectors $\begin{bmatrix} z_{1,2} \\ p_{1,2} \end{bmatrix}$. But we are actually more interested in the complex quantities $\Gamma_{1,2}$ that will be useful to compute the amplitude distribution of regular modes, as can be seen in Eqs. (5.57)-(5.58). Recalling that $\Gamma_{1,2} = \frac{p_{1,2}}{z_{1,2}}$ we obtain the expressions for $\Gamma_{1,2}$ as, for example,

$$\Gamma_{1,2} = \frac{-m_{11} + m_{22}}{2m_{12}} \pm i \frac{\sqrt{-(m_{11} + m_{22})^2 + 4}}{2m_{12}}, \quad (5.74)$$

using the fact that $\det(M) = 1$. One must then choose between α_1 and α_2 the value which corresponds to a localized wavepacket around the stable trajectory. This is done through checking the sign of the imaginary part of the corresponding $\Gamma_{1,2}$, knowing that the localisation is realized for a negative imaginary part. We call the corresponding angle α and function Γ , and compute the values of δ'_ℓ defined as

$$\delta'_\ell = \delta_n \frac{\alpha}{2\pi}, \quad (5.75)$$

that is, considering that $N_r = 0$. For even values of the quantum number m , only modes that are symmetric with respect to the rotation axis can exist. Now, for slow rotation rates, the stable periodic ray γ at the centre of the stable island coincides with the rotation axis. The value of α being computed for a full island, the corresponding value of δ_ℓ is wrong by a factor of 2, i.e. modes that are anti-symmetric with respect to the rotation axis must be removed. This is what we did for $m = 0$ for the rotation rates that are less than $\Omega/\Omega_K \sim 0.243$. We note that this value is related to the rotation rate at which the bifurcation occurs and thus depends also on ω which is here such that $\omega = 2.0$. To avoid the computation of the winding number N_r , that requires to propagate the complex vector $z(s)$ along the periodic orbit, we simply require that the value of $\alpha + N_r$ varies continuously with the rotation rate. Given the evolution of the angle α as a function of the rotation rate at $m = 0$ and $m = 1$ that can be seen in Fig. 5.6, we obtain that for $m = 1$ we must set $N_r = 1$ for $\Omega/\Omega_K \leq 0.205$ in order to have a continuous variation.

5.5.4 Mode eigenfunctions

For the mode amplitude distributions, we use the position on the equator of the periodic trajectory r_p that is given by the ellipse fitting procedure, and the (complex) value of Γ obtained from the diagonalisation of the monodromy matrix. To obtain the amplitude distribution of the mode as a function of the transverse distance to the ray (Eq. (5.57)), only the value of the quantum number ℓ is then left to be specified. We then use the definition of the coordinate ν as $\nu = \sqrt{\omega}(r - r_p)$, and the form of the Hermite polynomials $H_\ell(x)$ that are given by (Arfken and Weber, 2005):

$$H_0(x) = 1, \quad (5.76)$$

$$H_1(x) = 2x, \quad (5.77)$$

$$H_2(x) = 4x^2 - 2, \quad (5.78)$$

$$H_3(x) = 8x^3 - 12x, \quad (5.79)$$

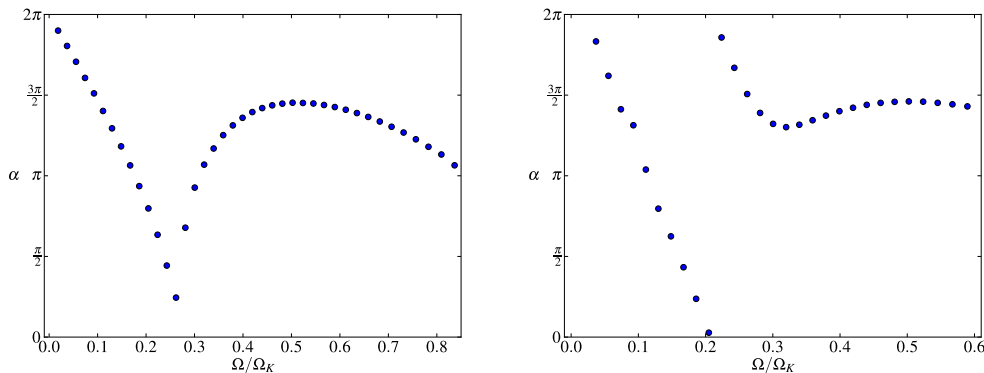


Figure 5.6: Floquet phases α computed from the monodromy matrix of the period-2 stable orbit for $\omega = 2.0$ and $m = 0$ (left panel), $m = 1$ (right panel), as functions of the rotation rate Ω/Ω_K of the stellar model.

and so on, where x is replaced by $\sqrt{\text{Im}(\Gamma)}\nu$. Finally, in order to be comparable with the numerical amplitude distribution, we normalise the equatorial cut of the semi-classical eigenfunctions by $\sqrt{\int dr |\Phi(r)|^2}$. The comparisons of the equatorial cuts of the mode amplitude distributions obtained from the full numerical computations and from the semi-classical formula can be seen in Sect. 5.9.

5.5.5 Accuracy on frequency spacings

The accuracy on the frequency regularities δ_n and δ_ℓ that can be achieved by the ray theory depends on four sources of errors: the resolution of the background stellar model, the method of integration of the ray equations, the determination of the stable periodic orbit, and the computation of the monodromy matrix (that is used only for the determination of δ_ℓ). For the computations of the background stellar model, we have chosen to use a spatial resolution of $n_r = 96$ collocation points in the pseudo-radial direction and a decomposition on 64 spherical harmonics in the angular direction, which according to Reese (2006) provides a high accuracy at different rotation rates. In order to test the dependency of the ray dynamics on this parameter, we changed the radial and angular resolution of the model and observed that this had no significant effect on the positions of the intersection points of the stable rays with the PSS.

The error of the Runge-Kutta integration is controlled by a user-specified maximal relative error, that we tested by computing at each steps the theoretically conserved value of the ray Hamiltonian (see Eq. (5.39)). We also checked that the stable trajectories were not significantly modified when this error tolerance was decreased.

As can be seen in Fig. 5.3, the determination of the *periodic* stable trajectory is not always very accurate. However, we have verified that it has only a very small impact on the computations of the ray period T_γ and stability angle α that are used for the determination of the frequency regularities. The period of the periodic ray T_γ is obtained by computing the time difference between consecutive intersections of the ray with the PSS. Since we do not have a truly periodic ray, we compute the period T_γ by averaging this time difference over multiple consecutive intersections. When this procedure is performed on the stable trajectories whose intersection points with the PSS can be seen in the upper panel of Fig. 5.7, this yields values of δ_n within a standard deviation of 1.10^{-5} , despite the significant deviations from the periodic orbit. This illustrates that the error in the determination of the periodic orbit has no significant effect on the determination of T_γ , and thus δ_n .

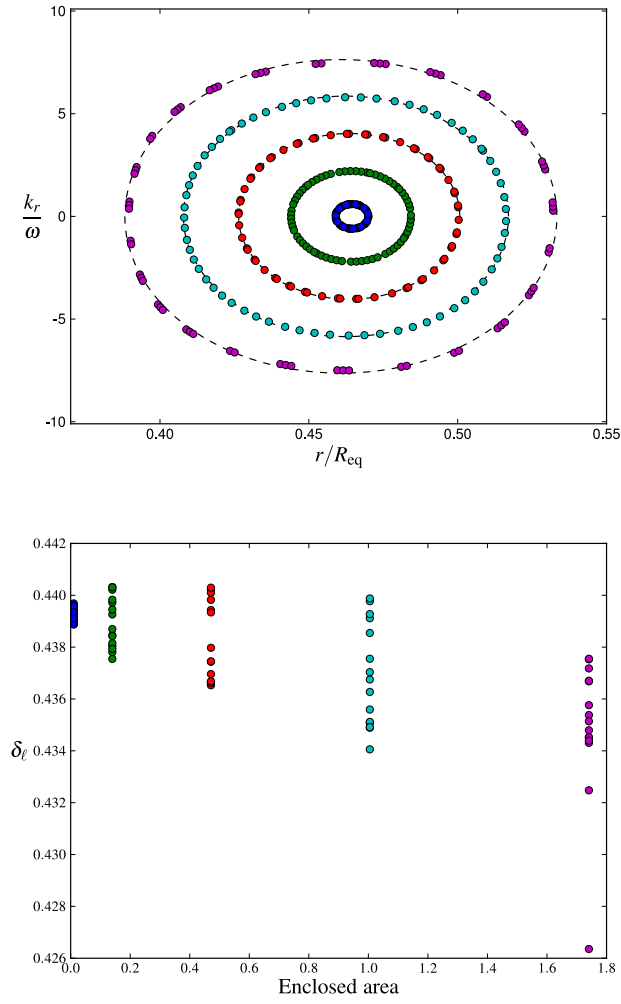


Figure 5.7: Intersections with the PSS at $\theta = \pi/2$ of five different stable acoustic rays in a polytropic stellar model rotating at $\Omega/\Omega_K = 0.524$ for $m = 0$ and $\omega = 2.0$ (upper figure). In the lower figure are displayed the δ_ℓ values, computed from the monodromy matrices corresponding to these rays, as functions of the area on the PSS that are enclosed by these rays (lower figure). The colours are the same for the intersections of rays with the PSS and the corresponding δ_ℓ values.

Now, for the determination of the stability angle α , that is used to compute δ_ℓ , we must compute the monodromy matrix of the stable periodic ray γ using another stable ray nearby γ . The stable periodic orbit then serves as a reference point $(r_0, \tilde{k}_{r,0})$ to compute the deviations $(\delta r, \delta \tilde{k}_r)$ of the nearby ray. Instead, we use the centre of the ellipse, obtained by the ellipse fitting method applied to the nearby stable ray. In the lower panel of Fig. 5.7 can be seen the computed values of δ_ℓ from the intersections with the PSS of the upper panel. Each colour corresponds to a given stable trajectory, while for each trajectory are computed multiple values of α for consecutive groups of four intersections, that are necessary to obtain the entries of the 2×2 monodromy matrix. It can be seen that the dispersion on δ_ℓ for consecutive groups of intersections is kept small, as long as the orbit can be well fitted by an ellipse, i.e. is sufficiently close to the centre of the stable island. It is thus possible by this method to compute both T_γ and α with only one stable trajectory, that we choose to be close to the periodic stable trajectory, while still obtaining accurate values for δ_n and δ_ℓ .

5.6 Complete two-dimensional numerical computations

As we said previously, the computation of stellar oscillation modes in the rapidly rotating regime requires the use of two-dimensional numerical codes to solve the adiabatic perturbation equations (Eqs. (5.7)-(5.10)), while taking fully into account the effects of the Coriolis and centrifugal forces. For this purpose, we used the ‘TOP’ code (Two-dimensional Oscillation Program) of Reese et al. (2006), in a polytropic background stellar model. Some oscillation modes in the high-frequency range ($n \in \llbracket 21, 25 \rrbracket$, $\ell \in \llbracket 0, 3 \rrbracket$ and $m \in \llbracket -3, 3 \rrbracket$, where (n, ℓ, m) is the mode labelling at zero rotation) were already computed by Reese (2006) up to $\Omega/\Omega_K \sim 0.59$. We extended those results by computing these high-frequency oscillation modes for $m = 0$ up to $\Omega/\Omega_K \sim 0.84$. In this section, we give a brief account of the numerical method used by the TOP code (Sect. 5.6.1), and explain how the oscillations modes are computed (the ‘mode following’ technique) in order to compute their frequency spacings (Sect. 5.6.2).

5.6.1 Numerical method and accuracy

The high accuracy of the TOP code is well adapted to study the regime of high-frequency pressure modes. Spectral methods have been chosen, since they are known to allow the resolution of partial differential equations with a high spatial resolution, in comparison with finite difference methods (Press et al., 2007). Spectral methods decompose equilibrium quantities and perturbation solutions on adequately chosen basis functions as truncated expansions of the form

$$\Psi(\mathbf{x}) \simeq \Psi_N(\mathbf{x}) = \sum_{n=0}^N a_n f_n(\mathbf{x}), \quad (5.80)$$

for a scalar function $\Psi(\mathbf{x})$, where the functions f_n are orthogonal. Using spherical harmonics for the angular dependency of functions and Chebyshev polynomials for the pseudo-radial dependency, yields the following decomposition of scalar functions (the decomposition of vector functions can be found in Reese (2006)):

$$\Psi(\zeta, \theta, \phi) = \sum_{\ell=0}^{\infty} \sum_{m=|\ell|}^{\infty} \Psi_m^{\ell}(\zeta) Y_{\ell}^m(\theta, \phi), \quad (5.81)$$

where $Y_{\ell}^m(\theta, \phi)$ are (ℓ, m) -spherical harmonics and

$$\Psi_m^{\ell}(\zeta) = \sum_{j=0}^{\infty} a_j^{\ell, m} T_j(2r - 1), \quad (5.82)$$

where $T_j(2r - 1)$ are Chebyshev polynomials defined on the interval $r \in [0, 1]$. For the numerical procedure of the TOP code, the radial dependency of functions was chosen to be represented in real space, that is functions are represented on collocation points ζ_j that have been chosen from the Gauss-Lobato quadrature (see e.g. Press et al., 2007), and the angular dependency in spectral space, i.e. in the form of the coefficients a_n . After this discretisation, and the projection of all equations on spherical harmonics, one obtains an eigenvalue problem of the form $Ax = \lambda Bx$, where A and B are square full matrices, that is solved using the Arnoldi-Chebyshev method. The Arnoldi’s algorithm was designed to find the solutions to large eigenvalue problems for general matrices (where a simpler version of Arnoldi’s algorithm called the Lanczos’ algorithm applies only to Hermitian matrices). In its variant that was used in the TOP code, the Arnoldi’s method allows to find the eigenvalues that are close to a target value called the ‘shift’. The details of the method can be found in Reese (2006).

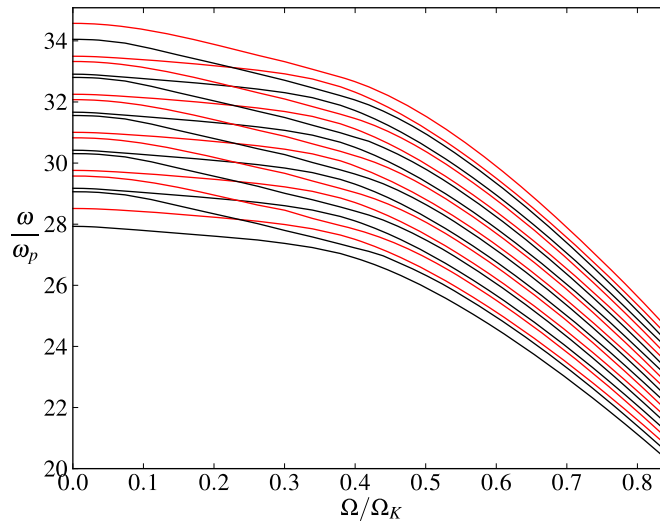


Figure 5.8: Computed mode frequencies normalised by $\omega_p = \sqrt{GM/R_p^3}$, where R_p is the polar radius of the stellar model, as functions of the rotation rate Ω/Ω_K , where $\Omega_K = \sqrt{GM/R_{\text{eq}}}$, R_{eq} being the equatorial radius. The frequencies were computed from the TOP code in polytropic stellar models with $N = 3$. The quantum numbers of the displayed modes are (in terms of quantum numbers at zero rotation, see text): $n \in \llbracket 21, 25 \rrbracket$, $\ell \in \llbracket 0, 3 \rrbracket$ for $m = 0$. The even/odd parity of the modes with respect to the equator is given by the line colours black/red.

The accuracy of the numerical results obtained from the TOP code has been estimated in different ways. By changing the resolution and other numerical parameters, it has been shown that the TOP code reaches, for polytropic models, a relative accuracy on frequencies of the order of 10^{-7} , which is more than current asteroseismology space missions, and clearly good enough to compare with semi-classical approximations.

5.6.2 Mode following and numerical results

The numerical results on high-frequency oscillation modes were obtained by complete computations of Eqs. (5.7)-(5.10) for increasing values of the rotation rate. This ‘mode following’ technique ‘follows’ an oscillation mode obtained at zero rotation up to higher rotation rates, which is adequate to observe the influence of rotation on mode frequencies and eigenfunctions. The technique works as follows. At zero rotation, the modes are labelled with well-defined quantum numbers: the order n of the mode and the (ℓ, m) of spherical harmonics. One then feeds the TOP code with a target eigenvalue that matches the frequency of the (n, ℓ, m) mode at a given rotation rate, and the (n, ℓ, m) mode at the next step in the rotation rate is obtained by selecting the mode with a dominant degree of the spherical harmonics decomposition that is the closest to ℓ . Additionally, the correlation function between modes at successive steps of the rotation rate is required to be close to unity.

The numerical results for the mode frequencies in the $n \in \llbracket 21, 25 \rrbracket$ range, for $\ell \in \llbracket 0, 3 \rrbracket$ and $m = 0$ can be seen in Fig. 5.8 for $0 \leq \Omega/\Omega_K \leq 0.84$. It must be noted that the ‘mode following’ technique is known to fail in the presence of *avoided crossings* (see e.g. Reese, 2006). However, at least in the high-frequency regime, the effects of avoided crossings are small and do not constitute major obstacles to the mode following and the computation of regular mode frequencies. An example of such an avoided crossing in the high-frequency regime between two period-2 island modes can be seen in Fig. 5.9 and Fig. 5.10. The modes

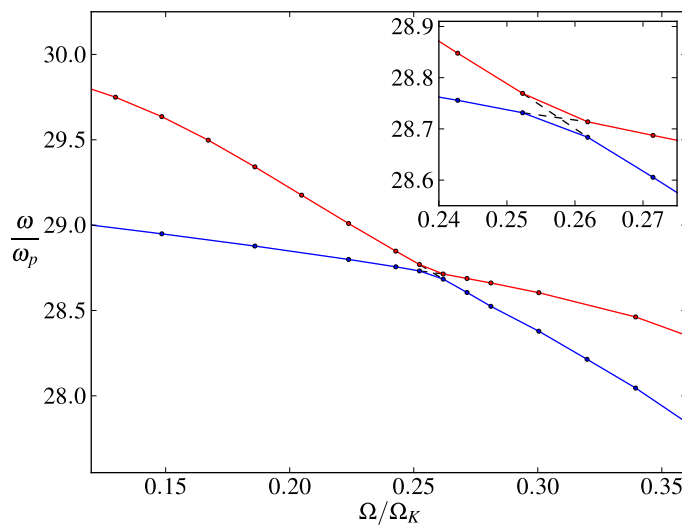


Figure 5.9: Frequencies of the $(n, \ell, m) = (21, 4, 0)$ and $(n, \ell, m) = (22, 0, 0)$ modes during an avoided crossing, as functions of the rotation rate Ω/Ω_K of the stellar model. Mode frequencies have been normalised, and computed from the same oscillation code as in Fig. 5.8, for polytropic stellar models with index $N = 3$. A zoom of the avoided crossing is given in the inset.

that undergo this avoided crossing are the $(n, \ell, m) = (21, 4, 0)$ and $(n = 22, \ell = 0, m = 0)$ modes. These modes are known to be in the same symmetry class since they have the same quantum number $m = 0$ and parity with respect to the equator $p = (\ell + m) \bmod 2 = \text{even}$. It can be seen in Fig. 5.9, that the width of the avoided crossing is $\Delta\omega \sim 0.04$ which is small compared to the values of δ_n and δ_ℓ at the same rotation rate (see e.g. Fig. 3 in Pasek et al., 2011).

Finally, we will mention that instead of the quantum numbers (n, ℓ, m) , at non-zero rotation one can use another set of quantum numbers which have a physical significance in terms of nodal lines of the eigenfunctions. Indeed, these new quantum numbers, that we will call $(\tilde{n}, \tilde{\ell}, \tilde{m})$, correspond to node numbers of the period-2 island modes, such that \tilde{n} is the number of nodes along the period-2 stable orbit (corresponding to the longitudinal quantisation of the island mode), $\tilde{\ell}$ is the number of nodes in the transverse direction of the orbit (associated to transverse excitations of the mode), while \tilde{m} is the number of nodes along the azimuthal direction. They can be related to (n, ℓ, m) quantum numbers following the bijection (Reese et al., 2008):

$$\tilde{n} = 2n + p, \quad (5.83)$$

$$2\tilde{\ell} + p = \ell - |m|, \quad (5.84)$$

$$\tilde{m} = m, \quad (5.85)$$

where $p = (\ell + m) \bmod 2$ corresponds to the parity of modes with respect to the equator, which is equal to zero for even modes, and to one for odd modes. Concerning the physical meaning of Eqs. (5.83)-(5.85), it can be noted that the term $\ell - |m|$ corresponds to the number of nodal lines of spherical harmonics at a constant latitude on the unit sphere, and that the parity p of a given mode is conserved when the rotation rate is changed, at least for the case of uniform rotation, or more generally, for an equatorially symmetric distribution of the rotation rate $\Omega(r, \theta)$.

We have thus obtained the frequency spacings between numerically computed island

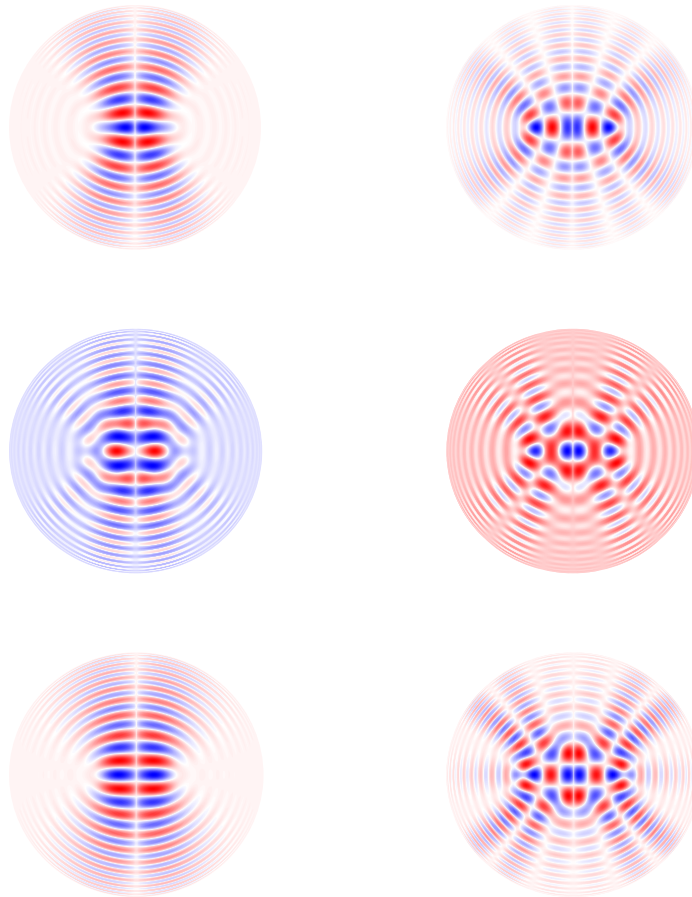


Figure 5.10: Pressure amplitude distributions in the meridian plane $p' \sqrt{d/\rho_0}$, where d is the distance to the rotation axis and ρ_0 the equilibrium density, of the $(n, \ell, m) = (22, 0, 0)$ (left column) and $(n, \ell, m) = (21, 4, 0)$ (right column) modes at $\Omega/\Omega_K = 0.243$ (first row), 0.262 (middle row) and 0.281 (last row). One can see in the middle row the mode coupling effect that results from the avoided crossing shown in Fig. 5.9.

Table 5.1: Mode frequencies that we computed numerically, labelled by the new quantum numbers $(\tilde{n}, \tilde{\ell}, \tilde{m})$.

\tilde{n}	$\tilde{\ell}$	\tilde{m}
42, 44, 46, 48, 50	0	-3, -2, ..., 3
42, 44, 46, 48, 50	1	-1, 0, 1
43, 45, 47, 49, 51	0	-2, -1, ..., 2
43, 45, 47, 49, 51	1	0

modes by calculating the frequency differences

$$\delta_{\tilde{n}}^{\text{num}} = \omega_{\tilde{n}+1, \tilde{\ell}, \tilde{m}}^{\text{num}} - \omega_{\tilde{n}, \tilde{\ell}, \tilde{m}}^{\text{num}}, \quad (5.86)$$

$$\delta_{\tilde{\ell}}^{\text{num}} = \omega_{\tilde{n}, \tilde{\ell}+1, \tilde{m}}^{\text{num}} - \omega_{\tilde{n}, \tilde{\ell}, \tilde{m}}^{\text{num}}, \quad (5.87)$$

$$\delta_{\tilde{m}}^{\text{num}} = \omega_{\tilde{n}, \tilde{\ell}, \tilde{m}+1}^{\text{num}} - \omega_{\tilde{n}, \tilde{\ell}, \tilde{m}}^{\text{num}}, \quad (5.88)$$

for a total of 80 period-2 island modes in the following range of quantum numbers: $n \in \llbracket 21, 25 \rrbracket$, $\ell \in \llbracket 0, 3 \rrbracket$ and $m \in \llbracket -\ell, +\ell \rrbracket$, where the corresponding $(\tilde{n}, \tilde{\ell}, \tilde{m})$ quantum numbers can be found in Table 5.1. If necessary, the frequency differences spacings in Eqs. (5.86)-(5.88) can be written as functions of the n, ℓ, m quantum numbers using Eqs. (5.83)-(5.85) as (Reese et al., 2008)

$$\delta_n = 2\delta_{\tilde{n}}, \quad (5.89)$$

$$\delta_\ell = \frac{\delta_{\tilde{\ell}}}{2}, \quad (5.90)$$

$$\delta_\ell + \delta_m = \delta_{\tilde{m}}. \quad (5.91)$$

For the comparisons of the frequency spacings obtained by the semi-classical theory (as defined in Eq. (5.62)) with those computed from the results of full two-dimensional computations, we have used the numerical frequency spacings $\delta_{\tilde{n}}^{\text{num}}$ and $\delta_{\tilde{\ell}}^{\text{num}}$ (we drop the tildes on quantum numbers $\tilde{n}, \tilde{\ell}, \tilde{m}$ in the following).

5.7 Brief summary of our results

In this section, we summarise the conclusions of our two articles on the application of the parabolic equation method on the period-2 island mode solutions of the pressure wave equation in uniformly rotating polytropic stellar models. Firstly, we make some comments on the results of comparisons with two-dimensional numerical computations of high-frequency adiabatic oscillation modes that take into account the Coriolis and centrifugal forces as well as the perturbations of the gravitational potential. Secondly, we list the main features of the regular frequency spacings' evolution with the rotation rate that we have observed. These numerical observations, though based on polytropic stellar models, should provide a guide for the identification of regular modes in rapidly rotation stars.

5.7.1 Comparisons with two-dimensional complete computations

We compared our semi-classical predictions for the frequencies and eigenfunctions of pressure modes localised on period-2 stable orbits with high-frequency numerically computed modes in uniformly rotating polytropic stellar models. As can be seen in Fig. 5.11, we found a good agreement between the semi-classical estimates for frequency spacings and complete numerical results for $m = 0, \pm 1$ in a large range of rotation rates. For the spacing δ_n , the agreement was found to be good everywhere except at small rotation rates.

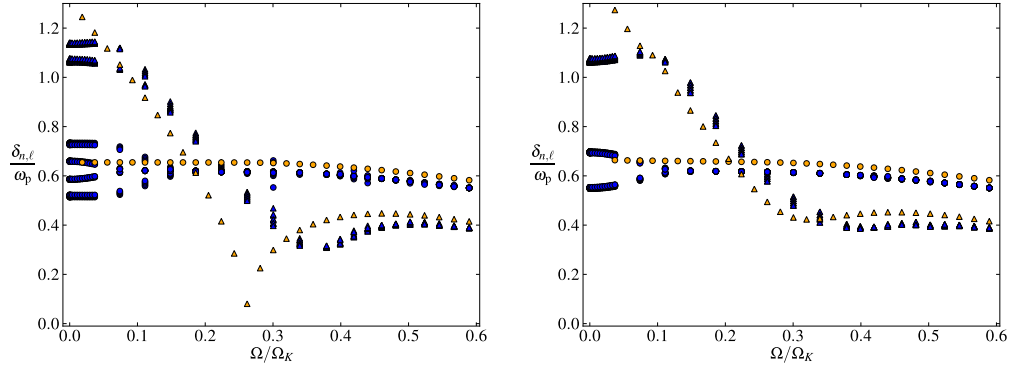


Figure 5.11: Frequency spacings δ_n (circles) and δ_ℓ (triangles) between period-2 regular modes, computed from the semi-classical formulas in Eq. (5.62) (in orange) and from complete numerical computations (in blue), as functions of the rotation rate Ω/Ω_K . Frequency spacings are normalised by $\omega_p = \sqrt{GM/R_p^3}$, where R_p is the polar radius of the stellar model. Frequency spacings in the left panel are for $m = 0$, in the right panel for $m = \pm 1$ (from Pasek et al., 2012).

Discrepancies on the δ_ℓ spacing were found to occur for $m = 0$, in the range of rotation rates where the period-2 stable orbit undergoes a bifurcation ($\Omega/\Omega_K \sim 0.26$ for the considered stellar model). This is understood, since bifurcations are a known limitation of our method, which assumes *isolated* stable periodic orbits. Then, one must note that the numerical frequencies that we considered here are rather low in frequency compared to typical systems that can be studied by semi-classical methods, though they lie in the high-frequency range of observable oscillation modes. Indeed, at low rotation rates, the period-2 stable islands are so small that they are barely ‘seen’ by pressure modes with such large wavelengths. This may explain the small discrepancies of our semi-classical values for both δ_n and δ_ℓ with numerical results at low rotation rates, despite that the theoretical spacing values converge to the first order of Tassoul’s formula. Concerning δ_m , the agreement was found to be bad at low rotation rates, since the numerical results yield a finite value for δ_m (that is equal to half the ‘large separation’ of Tassoul’s theory) while pressure mode frequencies do not depend on the quantum number m in the asymptotic regime (i.e. we expect $\delta_m \sim 0$ for $\omega \rightarrow \infty$). At high rotation rates (for $\Omega/\Omega_K > 0.4$) however, when the numerical values for δ_m are found to be close to zero, we obtained an approximate semi-analytical formula for δ_m that works reasonably well, and in this regime we recover the dependency of δ_m on m/\sqrt{n} that was previously observed in numerical computations (Reese et al., 2009). Details on the derivation of the semi-analytical formula for δ_m , and its comparison with numerical results can be found in the article Pasek et al. (2012) reprinted in Sect. 5.9.

The equatorial cuts of semi-classical eigenfunctions and complete numerical results were found to agree well for many values of the rotation rates and quantum numbers (n, ℓ, m) . Discrepancies were found in cases where edge effects are important, e.g. at low rotation rates when the transverse extent of the mode reaches the rotation axis. As for frequency spacings, the effects on the eigenfunctions of the mode couplings by avoided crossings are not taken into account by our present theory, and thus can lead to discrepancies. We note that even though we did not compare directly the two-dimensional distributions of the eigenfunctions, it should be feasible (as it was done for example in Tureci et al., 2002, for dielectric cavities with uniform index).

In conclusion, the parabolic equation method enables to predict with good accuracy

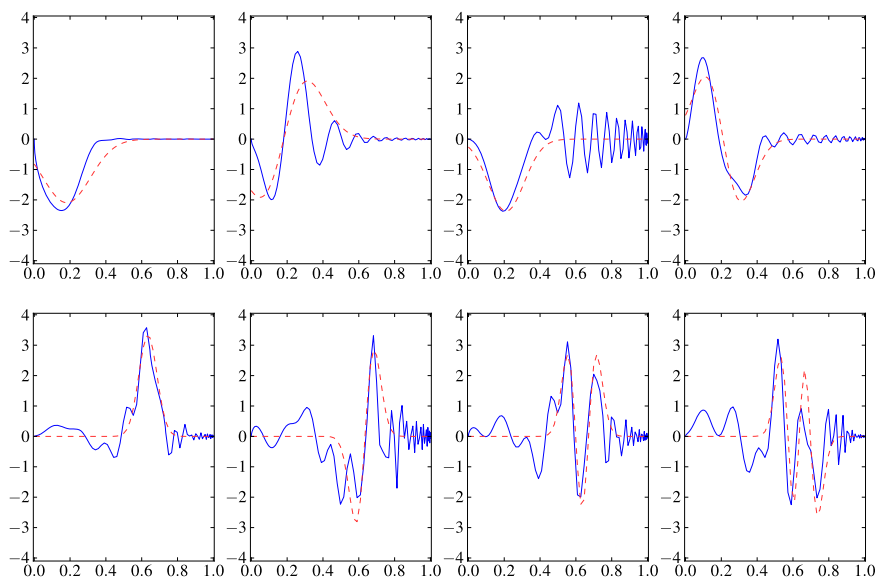


Figure 5.12: Equatorial cuts of the normalised amplitude distributions obtained from the semi-classical formula in Eq. (5.58) (real part of Φ_m^ℓ) (red dashed line), and from numerical computations (blue solid line), as a function of the normalised position on the equator r/R_{eq} , where R_{eq} is the equatorial radius of the stellar model. The displayed modes are the $(n, \ell, m) = (50, 0, 0)$, $(50, 1, 0)$, $(50, 0, 1)$ and $(50, 1, 1)$ at $\Omega/\Omega_K = 0.300$ (upper row) and the $(n, \ell, m) = (50, 0, 0)$, $(50, 1, 0)$, $(50, 2, 0)$ and $(50, 3, 0)$ at $\Omega/\Omega_K = 0.707$ (lower row). The figure is similar to Fig. 7 in Pasek et al. (2012), that can be found in Sect. 5.9.

the frequency spacings and eigenfunctions of the most visible regular subset of pressure modes in polytropic stellar models at almost all rotation rates.

5.7.2 Spectral observables and their evolution with rotation

The observed evolution of regular frequency spacings as functions of the rotation rate, when computed in uniformly rotating polytropic stellar models, is worth describing since this evolution should be at least qualitatively similar in more realistic stellar models. Firstly, we noticed a global decrease of frequency values (normalized by $\omega_p = \sqrt{GM/R_p^3}$, where R_p is the polar radius) for increasing rotation rates, as can be seen in Fig. 5.8. This contraction of the spectrum comes from the increasing volume of the star, which results from the effect of the centrifugal force. Secondly, concerning frequency differences, we observed that the spacing δ_n stays almost constant for all rotation rates, keeping a value close to half the ‘large frequency separation’ of Tassoul’s formula (that we defined in Sect. 2.2.2). The almost-constant value of δ_n can be understood from its only dependency on the acoustic time for a period of the ray $T_\gamma = \oint ds/\tilde{c}_s$. Indeed, the speed of sound c_s is known to be small at the surface (in comparison with its value at the centre), and thus the period T_γ is mostly the time spent by the ray in the region close to the surface. This quantity is simply proportional to the number of reflections of the period-2 stable ray on the surface, that is always equal to two by the definition of this ray. On the other hand, δ_ℓ has a rapid decrease for low rotation rates, while it stays almost constant for $\Omega/\Omega_K \geq 0.45$. This evolution is not easily understandable in terms of ray properties, however. We will only mention that the sudden decrease of δ_ℓ corresponds to an increase of the ‘small frequency separation’ (cf. Sect. 2.2.2), and that this evolution causes the major reorganisation of the spectrum that occurs for increasing rotation rates. These information are enough to describe the evolution of the $m = 0$ regular spectrum, but one expects to observe modes with higher values of the quantum number m . The drift between sub-spectra with different m values can be analysed with the frequency difference $\delta_m = \omega_{n,\ell,m} - \omega_{n,\ell,0}$. In the rotating frame, this spacing goes from $|m|\frac{\Delta\omega}{2}$ (where $\Delta\omega$ is the large separation of Tassoul’s theory) at low rotation to very small values (asymptotically zero) at higher rotations. In the observer’s frame, the evolution of the spectrum at high rotations is thus dominated by the advection term $m\Omega$ (where Ω is the rotation rate), which leads to the reformation of regular multiplets in this regime (for $\Omega/\Omega_K > 0.55$).

We also noticed empirically two major clusterings of mode frequencies that are due to conjunctions between the values of regular frequency spacings and the rotation rate. Indeed, given that the regular sub-spectrum in the observer’s frame can be completely described by four quantities (the spacings δ_n , δ_ℓ , δ_m and the rotation rate Ω), it is expected that the spectrum will become simple when these quantities are commensurate. For the high-frequency oscillation spectrum in polytropic stellar models, we found two such occurrences. The first one happens at $\Omega/\Omega_K \approx 0.25$, when $2\Omega \sim \delta_n$ and $\delta_n \sim \delta_\ell$ simultaneously. This leads to a very simple regular spectrum in the observer’s frame, where only one clear regular spacing is visible. The second conjunction between regularities occurs at $\Omega/\Omega_K \approx 0.56$, when the advection term $m\Omega$ dominates at high rotation rates and $2\Omega \sim 2\delta_n$. This also leads to a simple spectrum, for a rather large range of rotation rates around $\Omega/\Omega_K \approx 0.56$. Though these events may happen at different rotation rates in more realistic stellar model, they should still be taken into account for mode identification.

We have shown that the potential seismic observables δ_n , δ_ℓ and δ_m , are related to internal physical properties of the observed stars. Indeed, the spacing δ_n depends on the acoustic time along the period-2 stable ray, which can be used to infer information about the distribution of the speed of sound along this ray. It has also been shown that δ_n remains approximately proportional to the square root of the mean density of the star at high rotation rates (Reese et al., 2008). The spacing δ_ℓ depends on the dynamical

properties of the ray through the stability angle α of the monodromy matrix, that we linked to the second derivatives of the speed of sound in the transverse direction of the ray. One can thus expect that the δ_ℓ spacing provides information on the chemical stratification inside the stellar core, for rotation rates where the stable ray goes through the central region of the star (i.e. for approximately $\Omega/\Omega_K \leq 0.26$). Finally, at high rotation rates, by detecting the irregularity of rotational multiplets and hence estimating the value of δ_m , one can obtain information on the ratio between the speed of sound and the square of the distance of the ray from the rotation axis (see Eq. (58) in Pasek et al. (2012)).

5.8 Publication I

Regular Modes in Rotating Stars,
M. Pasek, B. Georgeot, F. Lignières, D. R. Reese,
Phys. Rev. Lett. 107, 121101 (2011), arXiv:1105.5586.

Regular Modes in Rotating Stars

Mickaël Pasek,^{1,2,3,4} Bertrand Georgeot,^{2,3} François Lignières,^{1,4} and Daniel R. Reese⁵

¹CNRS; IRAP; 14, avenue Edouard Belin, F-31400 Toulouse, France

²Université de Toulouse; UPS; Laboratoire de Physique Théorique (IRSAMC); F-31062 Toulouse, France

³CNRS; LPT (IRSAMC); F-31062 Toulouse, France

⁴Université de Toulouse; UPS-OMP; IRAP; Toulouse, France

⁵LESIA, CNRS, Université Pierre et Marie Curie, Université Denis Diderot, Observatoire de Paris, 92195 Meudon Cedex, France
(Received 27 May 2011; published 14 September 2011)

Despite more and more observational data, stellar acoustic oscillation modes are not well understood as soon as rotation cannot be treated perturbatively. In a way similar to semiclassical theory in quantum physics, we use acoustic ray dynamics to build an asymptotic theory for the subset of regular modes which are the easiest to observe and identify. Comparisons with 2D numerical simulations of oscillations in polytropic stars show that both the frequency and amplitude distributions of these modes can accurately be described by an asymptotic theory for almost all rotation rates. The spectra are mainly characterized by two quantum numbers; their extraction from observed spectra should enable one to obtain information about stellar interiors.

DOI: 10.1103/PhysRevLett.107.121101

PACS numbers: 97.10.Sj, 05.45.Mt, 97.10.Kc

Stars being far-away objects, the types of information that can be obtained from them are necessarily limited. One of the most important corresponds to luminosity variations, which can reflect the passing of a planet or intrinsic modulations in the light emitted by the star. In particular, the domain of asteroseismology studies stellar oscillation modes, which create periodic variations of the luminosity which can be detected [1]. For the Sun, these modes have been theoretically constructed and successfully compared with observations, leading to detailed information on the Sun's internal structure. However, this theory requires the star to be nearly spherically symmetric, an assumption clearly violated for rapidly rotating stars [2]. With the launch of the recent space missions COROT and Kepler [1], oscillation spectra of rapidly rotating stars are observed with great accuracy. This concerns mainly the stars more massive than the Sun that belong to the main sequence of the Hertzsprung-Russel diagram. In order to access their internal structure through a seismic diagnostic, it is thus essential to understand the oscillation spectra of rapidly rotating stars

Accurate computations of acoustic modes fully taking into account the effects of rotation on stellar oscillations have only recently been performed for rotating stars [3] (an example is shown in Fig. 1). Such stationary patterns of acoustic waves can be described asymptotically through their short-wavelength limit, in the same way as classical trajectories can describe quantum or electromagnetic waves in this limit [4]. These acoustic rays obey Hamiltonian equations of motion. In [5], their dynamics was investigated for a polytropic stellar model, showing that the tools from the fields of classical and quantum chaos enable us to understand the behavior of modes in rapidly rotating stars. Indeed, for increasing rotation rates,

the dynamics undergoes a transition from an integrable to a mixed system, where chaotic and stable zones coexist in phase space. The asymptotic theory built for slowly rotating stars, which does not take these effects into account, cannot thus be applied at high rotation rates. In the latter regime, it was shown that the spectrum of acoustic oscillations can be divided into several subspectra corresponding to regular and chaotic zones in phase space in a way similar to what happens in quantum chaos systems [6].

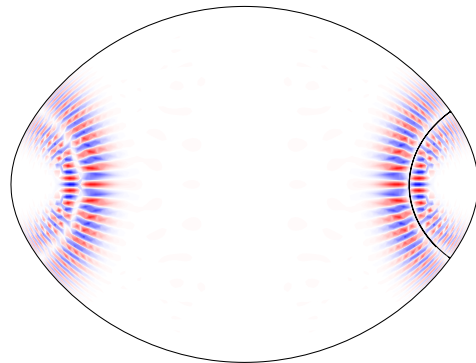


FIG. 1 (color online). Pressure amplitude $P\sqrt{d/\rho_0}$ on a meridian plane for a polytropic model of stars, with d the distance to the rotation axis and ρ_0 the equilibrium density. The mode shown corresponds to $n = 46$, $\ell = 1$ and $m = 0$ at a rotation rate of $\frac{\Omega}{\Omega_K} = 0.783$, with $\Omega_K = (GM/R_{\text{eq}}^3)^{1/2}$ being the limiting rotation rate for which the centrifugal acceleration equals the gravity at the equator, M the stellar mass and R_{eq} the equatorial radius. Colors/grayness denote pressure amplitude, from red/gray (maximum positive value) to blue/black (minimum negative value) through white (zero value). The thick black line on the right is the central periodic orbit γ of the island.

As already demonstrated for the Sun and solar-type stars, a quantitative asymptotic theory is crucial to extract information from the observed spectra as it links the behavior of oscillation modes to physical properties of the star [7]. Furthermore, the complexity of the observed spectra usually requires prior knowledge of an asymptotic theory in order to correctly identify the frequency peaks in the data with specific oscillation modes. In this paper, we present for the first time such a quantitative theory at almost all rotation rates for a specific subset of modes, which should be among the easiest to obtain from observations. Indeed, we focus on a series of modes centered around the largest stable island of the system, and systematically build them using the parabolic equation method [8]. This method was successfully applied to light in dielectric cavities [9], electronic resonators in a magnetic field [10] and quantum chaos systems [11]. The results of the asymptotic theory are then compared with numerical computation of oscillations in a polytropic star, showing that the theory correctly describes the modes even in the bounded frequency range of stellar oscillations.

The study of ray dynamics in [5] showed that for a wide range of rotation rates, three main types of phase space zones with different dynamics can be defined (see Fig. 2): (1) regular structures built around stable periodic orbits (stable islands); (2) whispering gallery rays close to the surface; (3) chaotic zones with ergodic rays in the remaining parts of phase space. Figure 2 shows that for $m = 0$ (axisymmetric modes) the main island undergoes a bifurcation from one island centered on the rotation axis to two islands which move away from the rotation axis as the rotation rate increases. Each phase space region gives rise to a well-defined subspectrum of modes localized inside the region. The whispering gallery modes are essentially unobservable in real stars since the disk-average leads to a very small contribution in observed spectra [5]. Chaotic modes can have visible contributions, but the associated spectra, although they can display well-defined statistical properties, cannot be described by a few quantum numbers. In contrast, the stable island modes give rise to very regular sequences of frequencies described by a few parameters which can be potentially extracted from observed spectra. These modes (an example is shown on Fig. 1) can be characterized on a meridian plane by the number n of nodes along the central periodic orbit γ and the number ℓ of nodes transverse to γ .

To describe asymptotically these island modes, we start from the equation of acoustic waves in stars. We neglect the Coriolis force, which is known to be negligible in the high-frequency regime since the Coriolis force time scale ($1/(2\Omega)$) is much longer than the mode period [3]. We also neglect the perturbations of the gravitational potential, since they are produced by the density fluctuations and tend to cancel out as the number of nodes of the density distribution increases for high-frequency modes, as has

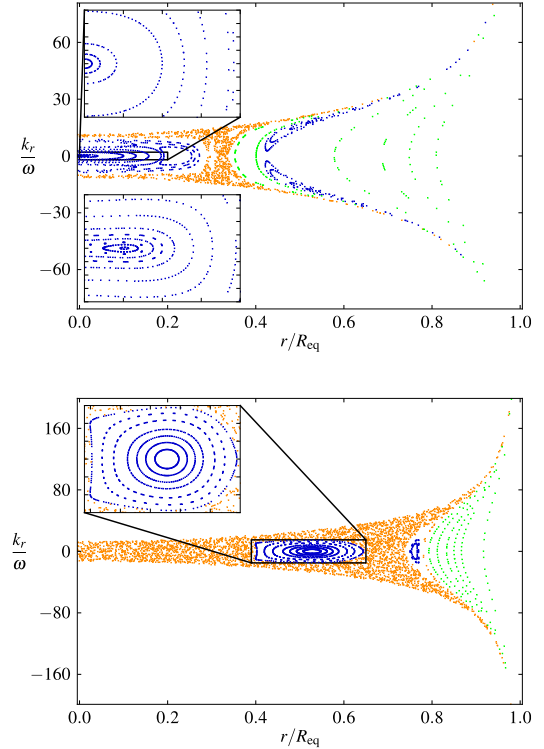


FIG. 2 (color online). Surfaces of section at rotations $\frac{\Omega}{\Omega_k} = 0.224$ (top) and $\frac{\Omega}{\Omega_k} = 0.589$ (bottom) for $m = 0$. Each dot represents the crossing of an acoustic ray with the equatorial half-plane, r being the radial coordinate and k_r the associated momentum. Orange/light gray denote a chaotic ray, green/dark gray a whispering gallery ray, blue/black a stable island ray (see text). Upper insets are close-ups of the main stable island. Lower inset in the top figure shows a close-up of the main island at $\frac{\Omega}{\Omega_k} = 0.262$, just after the bifurcation.

been numerically checked for nonrotating stars [12]. Finally, we use the adiabatic approximation which is known to be a very good approximation to compute frequency modes in nonrotating stars. Indeed, it is accurate enough to interpret the solar acoustic modes despite the fact that these frequencies are determined to high accuracy [7]. In the linear approximation, this gives rise to a Helmholtz-type equation. Using the cylindrical symmetry of the system with respect to the rotation axis, one can rewrite this equation as a two-dimensional problem

$$-c_s^2 \Delta \Phi_m + \left[\omega_c^2 + \frac{c_s^2(m^2 - \frac{1}{4})}{d^2} \right] \Phi_m = \omega^2 \Phi_m. \quad (1)$$

Here Φ_m is the mode amplitude scaled by the square root of the distance d to the rotation axis, c_s is the sound velocity (which depends on the location inside the star), ω is the frequency of the mode, and ω_c is the cutoff frequency whose sharp increase in the outermost layers of the star leads to the reflection of acoustic waves and thus the formation of modes in a bounded frequency range

$\omega \leq (\omega_c)_{\max}$. The integer m is the quantum number corresponding to the quantization of angular momentum along the rotation axis. To construct the island modes centered on the stable periodic orbit γ of length L_γ , we rewrite Eq. (1) in the coordinates (s, ξ) centered on γ , with s the coordinate along γ and ξ the transverse coordinate. The parabolic equation method [8] assumes that the solutions have a longitudinal scaling in $1/\omega$ and a transverse scaling in $1/\sqrt{\omega}$. We introduce the WKB ansatz:

$$\Phi_m(s, \xi) = \exp(i\omega\tau)U_m(s, \xi, \omega), \quad (2)$$

with $d\tau = ds/\tilde{c}_s$, using the renormalized sound velocity defined by $\tilde{c}_s^2 = c_s^2\omega^2/(\omega^2 - \omega_c^2 - \frac{c_s^2(m^2 - \frac{1}{2})}{d^2})$.

An expansion in powers of ω yields a series of equations; keeping terms of order ω and introducing the variable $\nu = \sqrt{\omega}\xi$ and the function $V_m = U_m/\sqrt{\tilde{c}_s(s)}$ give the parabolic equation:

$$\frac{\partial^2 V_m}{\partial \nu^2} + 2i \frac{1}{\tilde{c}_s(s)} \frac{\partial V_m}{\partial s} - K(s)\nu^2 V_m = 0, \quad (3)$$

where $K(s) = \frac{1}{\tilde{c}_s(s)^3} \frac{\partial^2 \tilde{c}_s}{\partial \xi^2} |_{\xi=0}$. The equation in the transverse coordinate ν is similar to the harmonic oscillator in quantum mechanics, with an additional term depending on the longitudinal coordinate. The ground state is of the form $V_m^0 = A(s) \exp[i\frac{\Gamma(s)}{2}\nu^2]$, and obeys the two equations $\frac{1}{\tilde{c}_s(s)} \frac{d\Gamma(s)}{ds} + \Gamma(s)^2 + K(s) = 0$ and $\frac{1}{A(s)} \frac{dA(s)}{ds} = -\frac{\tilde{c}_s(s)}{2}\Gamma(s)$. Defining $z(s)$ through $\Gamma(s) = \frac{1}{z(s)\tilde{c}_s(s)} \frac{dz(s)}{ds}$ implies that $A(s) = 1/\sqrt{z(s)}$ and $z(s)$ should satisfy the following system of equations:

$$\frac{1}{\tilde{c}_s(s)} \frac{dz}{ds} = p, \quad \frac{1}{\tilde{c}_s(s)} \frac{dp}{ds} = -K(s)z. \quad (4)$$

Equations (4) are periodic in the variable s with period L_γ , and according to Floquet theory there exists an operator describing the evolution over one period. To construct it, one uses the fact that system (4) corresponds to the Hamiltonian equations associated with the Hamiltonian $H = \frac{p^2}{2} + \frac{K(s)z^2}{2}$. It can be shown that the same equations (with z and p real) describe the acoustic ray in the vicinity of the central periodic orbit (via a normal form approximation), z being the transverse deviation from γ and p the associated momentum. We linearize the motion around the periodic orbit and construct the monodromy matrix which describes this linearized motion from one point to its image after one period:

$$\begin{bmatrix} z(s + L_\gamma) \\ p(s + L_\gamma) \end{bmatrix} = M \begin{bmatrix} z(s) \\ p(s) \end{bmatrix}. \quad (5)$$

For the mode to be univalued, V_m^0 should be the same after one period up to a global phase and thus z and p should correspond to an eigenvector of M . As γ is stable, the matrix M is conjugate to a rotation matrix and has two

eigenvalues $e^{\pm i\alpha}$, with α in $[0, 2\pi[$. The corresponding eigenvectors are complex conjugate, only one of them giving the physical solution exponentially decreasing at large ν .

The modes of higher frequency can be constructed as for the harmonic oscillator from V_m^0 using standard methods from quantum mechanics; the result, up to a normalization constant, is equivalent to multiplying $V_m^0(s, \nu) = z^{-(1/2)} \exp[i\frac{\Gamma}{2}\nu^2]$ by a function containing the Hermite polynomials of order ℓ noted H_ℓ :

$$V_m^\ell(s, \nu) = \left(\frac{\tilde{z}}{z}\right)^{\ell/2} H_\ell(\sqrt{\text{Im}\Gamma}\nu) z^{-(1/2)} \exp\left[i\frac{\Gamma}{2}\nu^2\right]. \quad (6)$$

Again, for the mode to be univalued, the global phase accumulated after one period should be a multiple of 2π . This phase is $\exp(-i\pi) \exp(-i(2\pi N_r + \alpha)/2) \exp(-i(2\pi N_r + \alpha)\ell) \exp(i\omega \oint_\gamma \frac{ds}{\tilde{c}_s})$. The first two phases correspond to the so-called Maslov indices [4,13] and count the number of caustics encountered in the longitudinal and transverse motions. The number N_r keeps track of the number of times the trajectory solution of Eq. (4) makes a complete rotation around γ in phase space, and can be evaluated from ray simulations. This implies

$$\omega_{n,\ell,m} = \frac{1}{\oint_\gamma \frac{ds}{\tilde{c}_s}} \left[2\pi \left(n + \frac{1}{2} \right) + \left(\ell + \frac{1}{2} \right) (2\pi N_r + \alpha) \right]. \quad (7)$$

The regular subspectrum is thus essentially described by two quantities, $\delta n = \frac{2\pi}{\oint_\gamma \frac{ds}{\tilde{c}_s}}$ and $\delta \ell = \frac{2\pi N_r + \alpha}{\oint_\gamma \frac{ds}{\tilde{c}_s}}$ (which depend on m). This corresponds to the empirical formula found in [3] for $m = 0$ from numerical simulations. The quantities δn and $\delta \ell$ probe the sound velocity along the path of the periodic orbit and its transverse derivatives. Indeed, an explicit expression of α in terms of such transverse derivatives can be derived [13]. Equation (7) is valid asymptotically for n large and $\ell \ll n$. As observable modes in real stars cannot be too high in frequency, we have checked numerically the validity of this formula for moderately high values of n .

In Fig. 3 we plot the numerically computed δn and $\delta \ell$ values vs the theoretical ones for a large range of rotation rates. We restrict ourselves to the case $|m| \leq 1$ which is the most common in observational data. Numerical modes were obtained using a code that computes adiabatic modes of rotating polytropic stars as in [3], and selecting the island modes through their phase space locations. Theoretical values were obtained from the theory explained above, estimating the monodromy matrix entries by following classical trajectories in the vicinity of the periodic orbit, using the fact previously noted that Eq. (4) describes the deviation of a nearby classical trajectory from the central orbit γ . We checked that the results were not sensitive to the choice of the trajectory inside the island. The results of Fig. 3 show that a good agreement

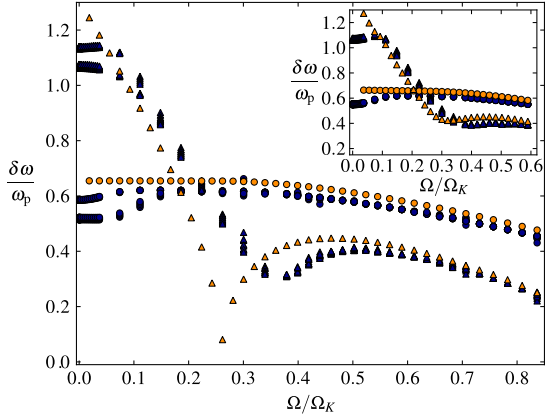


FIG. 3 (color online). Comparison between actual regularities of regular modes and theoretical predictions for $m = 0$ and different values of Ω/Ω_K ($\omega_p = \sqrt{GM/R_p^3}$ with R_p the polar radius). Circles: δn , triangles: $\delta \ell$, orange/light gray: theory, blue/dark gray: numerical results. Numerical results correspond to different sets of values of δn and $\delta \ell$, with n between 42 and 51 and $\ell = 0, 1$. As $m = 0$, only modes symmetric with respect to the rotation axis should be retained, and thus the theoretical value of $\delta \ell$ is multiplied by two below the bifurcation point. Close to $\Omega = 0$, the separation of numerical values in two groups corresponds to the small separation in Tassoul's theory [7]. Inset: Same for $m = 1$.

exists between numerical and theoretical regularities, except close to $\Omega = 0$ where Tassoul's asymptotic theory applies [7]. For δn , the agreement is good over the whole range of rotation. For $\delta \ell$, the agreement is good at large and low rotation, but degrades in the range $[0.25, 0.35]$ for $m = 0$. We attribute this discrepancy to the fact that, as seen in Fig. 2, the periodic orbit of the main stability island undergoes a bifurcation in this range, from one stable central orbit to two stable orbits on each side and a central unstable one. It is known that in such a case, the normal form approximation for the classical motion which is used in the parabolic equation method should be modified by different uniform formulas [14]. Thus in the vicinity of the bifurcation the method is expected not to give accurate results. This picture is confirmed by the inset of Fig. 3, which shows that in the case $m = 1$, where there is no such bifurcation, agreement is good for $\delta \ell$ over the whole range of Ω values. We note that other bifurcations are present in the system which create additional stable and unstable orbits in the vicinity of the central one, but they do not seem to affect the results for the relatively low-frequency modes we consider. We note also that Eq. (7) predicts degeneracies at rational values of α/π . These degeneracies can be avoided crossings or true degeneracies if the modes belong to different symmetry classes. We have checked that it actually enables us to predict such occurrences. We note that while the theory neglects the Coriolis force and perturbations of the gravitational potential, the numerical modes were computed taking into account both effects.

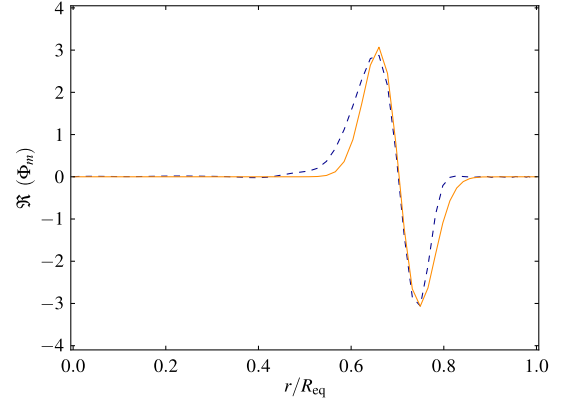


FIG. 4 (color online). Amplitude distributions (real part of Φ_m) on the equator for a theoretical and a numerical mode. Blue dashed line: numerical mode (same as in Fig. 1); orange continuous line: theoretical mode, from Eq. (6).

The good agreement seen in Fig. 3 confirms that these processes can safely be neglected in this regime. We also remark that recent analysis of numerically computed modes in realistic, nonpolytropic, differentially rotating stellar models show the emergence of formulas similar to Eq. (7) for specific subsets of modes [15].

Not only does the parabolic equation method give the frequencies of the modes, but it also yields their amplitude distribution. Indeed, the eigenvector of the monodromy matrix gives $\Gamma(s)$, which enables us to construct an approximation of the mode itself using Eq. (6). Comparisons between theoretical and numerical modes show that the modes are well approximated by the theory (see an example in Fig. 4), although sometimes small oscillations due to interference between different modes are not well reproduced by the theory.

In conclusion, we have shown that the parabolic equation method enables us to build an asymptotic theory for the most visible of the regular acoustic modes of a star rotating at arbitrary rotation rates except for very slow rotation, where Tassoul's theory [7] already applies. Comparisons with numerical computations of oscillations in a stellar model show that the asymptotic theory gives a good description of the frequency differences and amplitude distributions, except for $m = 0$ at a specific rotation rate where a bifurcation takes place and a more refined theory is needed. The spacings δn and $\delta \ell$ which describe the frequency distribution of this type of modes can be expressed in terms of internal characteristics of the star. Our results should enable one to use data from recent space missions such as COROT and Kepler to extract information about the observed stars and use this information to build more accurate stellar models.

We thank J. Ballot for his help at various stages of this work, the ANR project SIROCO for funding and CALMIP and CINES for the use of their supercomputers. D. R. R. acknowledges support from the CNES.

- [1] A. Gautschy and H. Saio, *Annu. Rev. Astron. Astrophys.* **33**, 75 (1995); A. Baglin *et al.*, *ESA SP-1306* (ESA Publications Division, Noordwijk, The Netherlands, 2002), 33; D.G. Koch *et al.*, *Astrophys. J.* **713**, L79 (2010).
- [2] J. D. Monnier *et al.*, *Science* **317**, 342 (2007).
- [3] F. Lignières, M. Rieutord, and D.R. Reese, *Astron. Astrophys.* **455**, 607 (2006); D.R. Reese, F. Lignières, and M. Rieutord, *Astron. Astrophys.* **455**, 621 (2006); *Astron. Astrophys.* **481**, 449 (2008).
- [4] D.O. Gough, in *Les Houches Lectures Session XLVIII*, edited by J.-P. Zahn and J. Zinn-Justin (North-Holland, Amsterdam, 1993), p. 399.
- [5] F. Lignières and B. Georgeot, *Phys. Rev. E* **78**, 016215 (2008); *Astron. Astrophys.* **500**, 1173 (2009).
- [6] I. C. Percival, *J. Phys. B* **6**, L229 (1973); M. V. Berry and M. Robnik, *J. Phys. A* **17**, 2413 (1984).
- [7] M. Tassoul, *Astrophys. J. Suppl. Ser.* **43**, 469 (1980); J. Christensen-Dalsgaard, *Rev. Mod. Phys.* **74**, 1073 (2002).
- [8] V.M. Babich and V.S. Buldyrev *Asymptotic Methods in Short-Wavelength Diffraction Theory* (Alpha Science International, Ltd., Oxford, UK, 2009).
- [9] H.E. Tureci *et al.*, *Opt. Express* **10**, 752 (2002).
- [10] V.V. Zalipaev, F.V. Kusmartsev, and M.M. Popov, *J. Phys. A* **41**, 065101 (2008).
- [11] A. Vagov, H. Schomerus, and V.V. Zalipaev, *Phys. Rev. E* **80**, 056202 (2009).
- [12] J. Christensen-Dalsgaard, *Solar Oscillations and the Physics of the Solar Interior*, Lecture Notes in Physics (Springer, New York, 1991); C. Aerts, J. Christensen-Dalsgaard, and D.W. Kurtz, *Asteroseismology*, (Springer, New York, 2010).
- [13] M.C. Gutzwiller, *Chaos in Classical and Quantum Mechanics* (Springer, New York, 1990).
- [14] H. Schomerus and M. Sieber, *J. Phys. A* **30**, 4537 (1997).
- [15] D.R. Reese *et al.*, *Astron. Astrophys.* **506**, 183 (2009); **506**, 189 (2009).

5.9 Publication II

Regular oscillation sub-spectrum of rapidly rotating stars,
M. Pasek, F. Lignières, B. Georgeot, D. R. Reese,
A&A 546, A11 (2012), arXiv:1205.6689.

Regular oscillation sub-spectrum of rapidly rotating stars

M. Pasek^{1,2,3,4}, F. Lignières^{1,2}, B. Georgeot^{3,4}, and D. R. Reese⁵

¹ CNRS, IRAP, 14 avenue Edouard Belin, 31400 Toulouse, France
 e-mail: pasek@irsamc.ups-tlse.fr

² Université de Toulouse, UPS-OMP, IRAP, Toulouse, France

³ CNRS, LPT (IRSAMC), 31062 Toulouse, France

⁴ Université de Toulouse, UPS, Laboratoire de Physique Théorique (IRSAMC), 31062 Toulouse, France

⁵ Institut d'Astrophysique et Géophysique de l'Université de Liège, Allée du 6 Août 17, 4000 Liège, Belgium

Received 30 May 2012 / Accepted 17 August 2012

ABSTRACT

Aims. We present an asymptotic theory that describes regular frequency spacings of pressure modes in rapidly rotating stars.

Methods. We use an asymptotic method based on an approximate solution of the pressure wave equation constructed from a stable periodic solution of the ray limit. The approximate solution has a Gaussian envelope around the stable ray, and its quantization yields the frequency spectrum.

Results. We construct semi-analytical formulas for regular frequency spacings and mode spatial distributions of a subclass of pressure modes in rapidly rotating stars. The results of these formulas are in good agreement with numerical data for oscillations in polytropic stellar models. The regular frequency spacings depend explicitly on internal properties of the star, and their computation for different rotation rates gives new insights on the evolution of mode frequencies with rotation.

Key words. asteroseismology – chaos – methods: analytical – stars: oscillations – stars: rotation – waves

1. Introduction

The field of asteroseismology has now reached its age of maturity with the exploitation of space missions CoRoT (Baglin et al. 2006) and Kepler (Koch et al. 2010) that are gathering stellar light curves with high accuracy. However, there are still unresolved issues that hinder the successful pairing of light curve frequencies with pulsation modes, which is crucial to obtain detailed information on the inner structure of observed stars. One of these issues is the rapid rotation of a star around its axis, since the exact nature of rotational effects on pulsation modes is not known. In particular, the centrifugal flattening (e.g. Monnier et al. 2007) affects the spectrum of pressure modes (p-modes) in a complex way (Lignières & Georgeot 2009). This difficulty mainly concerns non-evolved massive and intermediate-mass pulsating stars which are typically rapid rotators (Royer 2009). Recently though, hints of regular frequency spacings have been found in the spectrum of rapidly rotating δ Scuti stars observed with CoRoT (García Hernández et al. 2009; Mantegazza et al. 2012), and this could ease future mode identification.

The recent development of accurate numerical models has enabled progress in the comprehension of pulsation modes in rapidly rotating stars. It has been found in particular (Lignières et al. 2006; Reese et al. 2008, 2009) that in the rapidly rotating regime a subset of p-modes shows approximate regular frequency spacings in the form:

$$\omega_{n,\ell,m} \simeq \Delta_n n + \Delta_\ell \ell + \Delta_m |m| + \alpha, \quad (1)$$

where frequencies $\omega_{n,\ell,m}$ are given in the corotating frame. Quantum numbers n , ℓ and m correspond to node numbers of the mode amplitude distributions, Δ_n , Δ_ℓ and Δ_m are frequency regularities, and α is a constant term. The approximate formula in Eq. (1) shows a better agreement with numerical results

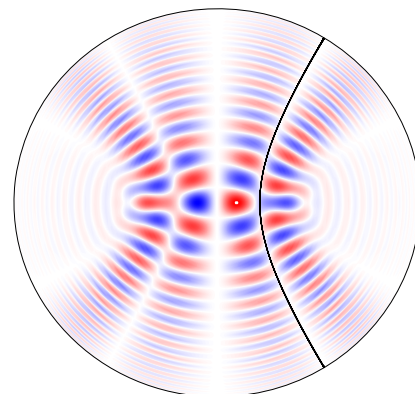


Fig. 1. Pressure amplitude $P \sqrt{d/\rho_0}$ on a meridian plane for a polytropic stellar model, with d the distance to the rotation axis and ρ_0 the equilibrium density. The mode shown corresponds to $n = 50$, $\ell = 1$ and $m = 1$ at a rotation rate of $\Omega/\Omega_K = 0.300$, where $\Omega_K = (GM/R_{\text{eq}}^3)^{1/2}$ is the limiting rotation rate for which the centrifugal acceleration equals the gravity at the equator, M being the stellar mass and R_{eq} the equatorial radius. Colors/grayscale (for respectively the colour/black and white version of the figure) denote pressure amplitude, from red/gray (maximum positive value) to blue/black (minimum negative value) through white (null value). The thick black line is the ray γ located in the center of the main stable island. (This figure is available in color in the electronic form.)

towards high-frequencies, thus suggesting that this relation is of an asymptotic nature. It should also be noted that, from computations of disk-averaging factors, the p-modes following Eq. (1) are expected to be among the most visible ones (Lignières & Georgeot 2009). An example of such a mode can be seen in Fig. 1.

The frequency spacings of Eq. (1) are notably similar to the regularities described by Tassoul's asymptotic formula (Tassoul 1980) for low degree p-modes in non-rotating stars. Tassoul's formula at leading order is

$$\omega_{n,\ell} \simeq \Delta \left(n_s + \frac{\ell_s}{2} + \frac{1}{4} + \alpha_s \right), \quad (2)$$

with the large frequency separation

$$\Delta = 2\pi \left(2 \int_0^R \frac{dr}{c(r)} \right)^{-1}, \quad (3)$$

where $c(r)$ is the radially inhomogeneous sound speed, and R the stellar radius. The integer n_s is the node number of the radial component of the mode, while ℓ_s is the degree of the associated spherical harmonics, and α_s depends on surface properties. Tassoul's theory has proved to be very useful for interpreting solar-like oscillations in slowly rotating stars. Indeed, the formula relates observable quantities, such as the regular frequency spacing Δ , to physical properties of stellar interiors. For rapidly rotating stars, it would be clearly desirable to gain insights on the underlying physics of the potentially observable regular spacings Δ_n , Δ_ℓ and Δ_m by a similar asymptotic analysis. In this paper we derive a formula for these regular frequency spacings in the asymptotic regime.

The generalization of the p-mode asymptotic theory to rapidly rotating stars is not trivial. Tassoul's theory requires separation of variables, which is no longer possible when the star is flattened by rotation. For non-separable wave systems, a well-known technique to obtain eigenmodes is to study the short-wavelength limit of the propagating waves. This limit gives an equation for the propagation of rays that is similar to the geometrical optics limit of electromagnetism, or the classical limit in quantum mechanics. Then, by imposing quantization conditions on the phase of waves propagating on these rays, one obtains the eigenmodes of the wave system. This technique was first developed in the context of quantum physics, and is often called semiclassical quantization.

For spherical stars, the ray limit of pressure waves has been previously used to recover the Tassoul asymptotic formula from the Einstein-Brillouin-Keller (EBK) quantization of ray dynamics (Gough 1993). This analytical approach is possible only when the ray system is integrable. A dynamical system is said to be integrable when it has as many conserved quantities (energy, angular momentum, etc.) as degrees of freedom (Ott 2002). In rapidly rotating stars, there are not enough conserved quantities to ensure integrability of the ray dynamics. Indeed, in Lignières & Georgeot (2008, 2009), it has been found that acoustic rays in rotating stars have a very different dynamical behavior depending on their initial conditions in position-momentum space (the so-called phase space). For a polytropic stellar model, the numerical integration of the equations for acoustic rays displayed various types of solutions. Indeed, one can obtain either stable rays staying on torus-shaped surfaces in phase space which form structures such as stable islands, or chaotic rays that are dense and ergodic on a phase space volume.

A similar behavior has been found in many systems studied in the field of theoretical physics known as quantum chaos or wave chaos (Gutzwiller 1990). This field has among its objectives to analyze quantum (wave) systems whose classical (short-wavelength) limit is partly or fully chaotic. In this framework, one can predict the existence of some eigenfunctions (mode

profiles) and energies (frequencies) of the quantum (wave) system from the different structures that are present in the classical system phase space (Percival 1973; Berry & Robnik 1984). In the stellar pulsation setting, Lignières & Georgeot (2008, 2009) found that the mixed (i.e. regular and chaotic) character of the acoustic ray dynamics in rapidly rotating stars results in a classification of p-modes in two broad families: regular modes either associated with stable islands or whispering gallery zones, and chaotic modes associated with ergodic regions in phase space. For the regular modes associated with stable islands, the so-called island modes, it is known to be possible to obtain approximate analytical solutions by solving the wave equation in the vicinity of a periodic stable ray (Babich & Buldyrev 1991). A simple application of such a method is found in modes of optical resonators, where the periodic stable light ray is a straight line between two reflecting mirrors (Kogelnik & Li 1966). These methods have been previously employed to obtain modes of more complex lasing (Tureci et al. 2002) and electronic (Zalipaev et al. 2008) cavities as well as quantum chaos systems (Vagov et al. 2009). In this paper, we apply this approach to rapidly rotating stars.

In the present analysis, we thus construct an asymptotic formula for regularities in the p-mode spectrum of rapidly rotating stars. Part of the results were already presented in the short communication of Pasek et al. (2011). In the present paper we give a detailed derivation of these results, specify their domain of validity, extend them with a study of rotational splittings, and explore their astrophysical applications.

The paper is organized as follows. In Sect. 2 we present the wave equation for p-modes in rotating stars and its asymptotic limit leading to an equation for acoustic rays. In Sect. 3 we use a stable periodic solution of the ray dynamics to obtain a semi-analytical formula for the associated p-modes, and to derive a formula for the associated regular frequency spacings. We then compare the results obtained from the derived formulas for mode frequencies and spatial distributions with numerical results (Sect. 4). Finally, we suggest directions on how these results could be used for the asteroseismic diagnosis of rapidly rotating stars by discussing the phenomenological implications of the theory in Sect. 5.

2. P-modes in rotating stars and their asymptotic limit

In Sect. 2.1 we introduce the wave equation for p-modes in rotating stars. We then present the asymptotic limit of this equation in order to obtain an equation for the dynamics of acoustic rays (Sect. 2.2).

2.1. Pressure modes in rotating stars

We start with the equation for small adiabatic time-harmonic perturbations of the pressure field in a self-gravitating gas. Since we are interested in obtaining an asymptotic theory for p-modes in the high-frequency regime, we use the Cowling approximation (i.e. we neglect the perturbations of the gravitational potential), an approximation known to be valid for high-frequency perturbations in non-rotating stars (Aerts et al. 2010). We also neglect the Coriolis force. Indeed, in the high-frequency regime, the time scale associated with this force is much longer than the mode period, and thus the influence of the Coriolis force on pulsation frequencies is weak. This has been numerically checked in Lignières et al. (2006), Reese et al. (2006, 2008).

In the asymptotic regime of p-modes, the oscillation frequencies are far greater than the Brunt-Väisälä frequency and thus we can discard the terms corresponding to gravity waves. With these assumptions, the equation for pressure perturbations is a Helmholtz equation such that

$$\Delta\Psi + \frac{\omega^2 - \omega_c^2}{c_s^2}\Psi = 0, \quad (4)$$

where $\Psi = \hat{P}/f$ is the complex amplitude associated with the pressure perturbation $P = \text{Re}[\hat{P}\exp(-i\omega t)]$, f is a function of the background model, ω_c is the cut-off frequency of the model and c_s its inhomogeneous sound velocity (for a detailed derivation of this equation see [Lignières & Georgot 2009](#)). The stellar model is not spherically symmetric due to the centrifugal distortion, but is however cylindrically symmetric with respect to the rotation axis. Therefore, we can write the pressure field as $\Psi = \Psi_m \exp(im\phi)$ where m is an integer and ϕ is the azimuth angle of spherical coordinates. By inserting this expression in Eq. (4) we obtain (cf. Appendix A)

$$\Delta\Phi_m + \frac{1}{c_s^2} \left(\omega^2 - \omega_c^2 - \frac{c_s^2(m^2 - \frac{1}{4})}{d^2} \right) \Phi_m = 0, \quad (5)$$

where d is the distance to the rotation axis. The new mode amplitude Φ_m is such that $\Phi_m = \sqrt{d}\Psi_m$. We introduce a renormalized sound velocity:

$$\tilde{c}_s = \frac{c_s}{\sqrt{1 - \frac{1}{\omega^2} \left(\omega_c^2 + \frac{c_s^2(m^2 - \frac{1}{4})}{d^2} \right)}}. \quad (6)$$

We notice that besides its spatial dependence, \tilde{c}_s also depends on ω and m , and that m is taken as a parameter for the two-dimensional wave equation (Eq. (5)).

2.2. Ray limit of p-modes

In non-rotating stars, the asymptotic theory of high frequency p-modes has first been derived by [Vandakurov \(1967\)](#), and [Tassoul \(1980\)](#). The method was to use the spherical symmetry of the star to reduce the problem to a one-dimensional equation in order to obtain the mode frequencies. This method is not applicable when the centrifugal force breaks the spherical symmetry of the star. In this case though, one can study the short-wavelength limit ($\omega \rightarrow \infty$) of the wave equation (Eq. (4)) (as detailed in [Lignières & Georgot 2009](#)). This provides a Hamiltonian system describing the propagation of acoustic rays. The Hamiltonian has been derived in [Lignières & Georgot \(2009\)](#) as

$$H = -\frac{\tilde{k}_p^2}{2} + \frac{1}{2c_s^2} \left(1 - \frac{\omega_c^2}{\omega^2} - \frac{c_s^2 m^2}{\omega^2 d^2} \right), \quad (7)$$

where the frequency-scaled wavevector \tilde{k}_p is the projection of $\tilde{k} = k/\omega$ onto the meridional plane of the star. We notice that this expression has been derived from the short-wavelength limit of the three dimensional wave equation (Eq. (4)) and then, projected onto the corotating meridian plane. An alternative derivation would be to start from the two-dimensional wave equation (Eq. (5)). In this case, the ray limit yields the same expression with the addition of the 1/4 factor of Eq. (5) that accounts for the impossibility of acoustic rays to go through the rotation axis (i.e. $d = 0$). Throughout the paper we use Eq. (7) as the Hamiltonian for acoustic rays.

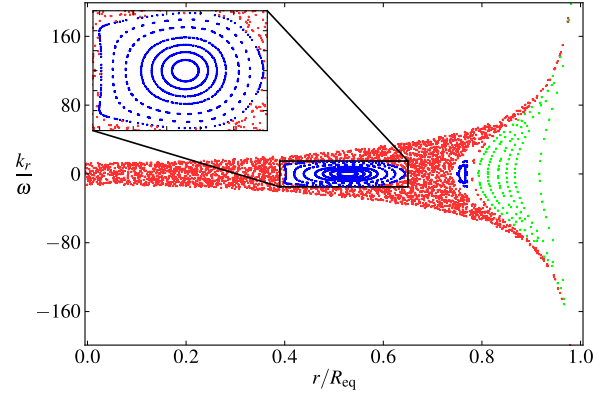


Fig. 2. Poincaré Surface of Section (PSS) at the rotation rate $\Omega/\Omega_K = 0.589$ for quantum number $m = 0$. Each dot corresponds to the crossing of an acoustic ray with the equatorial half-plane in the $(r/R_{\text{eq}}, k_r/\omega)$ phase space, r being the radial coordinate and k_r the associated momentum. R_{eq} is the equatorial radius and ω the mode frequency. Red/dark gray denotes a chaotic ray, green/light gray a whispering gallery ray, blue/black a stable island ray (see text). Upper inset is a close-up of the main stable island. (This figure is available in color in the electronic form.)

To probe the integrability property of a dynamical system, it is convenient to use the Poincaré surface of section (PSS), a standard tool in dynamical systems theory ([Gutzwiller 1990](#); [Ott 2002](#)) to visualize the structures in phase space. A PSS is a lower dimensional slice of phase space. The acoustic ray dynamical system in the meridional plane has two degrees of freedom, which gives a phase space of dimension four (two for positions, and two for momenta). There is one conserved quantity in the form of the acoustic wave frequency, so the dynamics belongs to a three-dimensional manifold in phase space. By fixing an additional position or momentum coordinate, we obtain a two-dimensional PSS which can be easily visualized. An example of such a section for our system is shown in Fig. 2. Different choices of PSS variables are possible, some of which are presented in [Lignières & Georgot \(2009\)](#). We have here chosen to fix the colatitude $\theta = \pi/2$, so that the PSS corresponds to the crossing of rays with the equatorial half-plane. We thus display a section in coordinates $(r/R_{\text{eq}}, k_r/\omega)$ where k_r is the norm of the radial wavevector, ω the mode frequency, and R_{eq} the equatorial radius (that may be greater than the polar radius since the star is flattened by rotation). In such plots, each dot corresponds to the crossing of an acoustic ray with the PSS. Successive dots from a single ray will form lines in integrable zones, or fill surfaces densely in chaotic zones. We see in Fig. 2 that when the rotation rate Ω/Ω_K (where $\Omega_K = (GM/R_{\text{eq}}^3)^{1/2}$ is the limiting rotation rate) is large, different structures coexist in the system phase space: stable islands correspond to concentric circles around a stable ray, whispering gallery rays to lines near the surface, and chaotic zones to densely filled areas (for more details, see [Lignières & Georgot 2009](#)). In this paper, we will focus on the 2-periodic stable island which is the main stable island (shown in the inset of Fig. 2). The rays' dynamics is very sensitive to the rotation rate, so the PSS will be different for each rotational velocity. Indeed, the locus in phase space of the main stable island changes as rotation increases. The major change happens when the central ray of the 2-periodic stable island undergoes a bifurcation at $\Omega/\Omega_K \simeq 0.26$. For slow rotation rates, the central ray of the island is located on the polar axis, and through this bifurcation it transforms into two stable rays surrounding one unstable ray on the polar axis. Then, as rotation

increases, the stable island will coast away from the polar axis. This bifurcation will be of some importance in the following, when we will show that one can construct approximate eigenmodes of the wave system from this 2-periodic stable island. In Fig. 1, one can see an example of an island mode obtained from a full-numerical computation, together with the central ray of the 2-periodic stable island for the same rotation rate and quantum number m .

3. Semi-analytical method for island modes

In this section we construct an asymptotic approximation of a subset of regular p-modes associated with a stable periodic ray. The method is based on the works of Babich and coworkers (see Babich & Buldyrev 1991 and references therein for the general formalism; and e.g. Zalipaev et al. 2008; Vagov et al. 2009, for some applications). It consists in deriving an approximation of the wave equation in the vicinity of the ray (Sect. 3.1), finding Gaussian wavepacket solutions related to the stability properties of the ray (Sect. 3.2), and then deriving the asymptotic formula for the frequencies from a quantization condition (Sect. 3.3).

3.1. Approximate wave equation in the vicinity of a stable ray

For a given rotation rate and quantum number m , we start with the central periodic ray of the main stable island (see Sect. 2). This ray must be computed by numerically evaluating the Hamiltonian equations derived from Eq. (7). In the following we will call this ray γ . The first step is to write the wave equation (Eq. (5)) in the vicinity of γ . For this, we use a local orthonormal coordinate system (s, ξ) defined as $\mathbf{r} = s\mathbf{T} + \xi\mathbf{N}$ where s is the arc length along the ray, \mathbf{T} the unit tangent vector, ξ the transverse coordinate and \mathbf{N} the unit vector normal to \mathbf{T} . The two basis vectors are related by the curvature $\kappa(s)$ of the ray as follows:

$$\kappa(s) = -\frac{d\mathbf{N}}{ds} \cdot \mathbf{T}. \quad (8)$$

In this coordinate system, the wave equation (Eq. (5)) reads

$$\frac{1}{h_s h_\xi} \left(\frac{\partial}{\partial s} \left(\frac{h_\xi}{h_s} \frac{\partial \Phi_m}{\partial s} \right) + \frac{\partial}{\partial \xi} \left(\frac{h_s}{h_\xi} \frac{\partial \Phi_m}{\partial \xi} \right) \right) + \frac{\omega^2}{\tilde{c}_s(s, \xi)^2} \Phi_m = 0, \quad (9)$$

where the scale factors h_s and h_ξ (Arfken & Weber 2005) are

$$h_s^2 = (\mathbf{T} - \xi\kappa(s)\mathbf{T})^2 = (1 - \xi\kappa(s))^2 \quad (10)$$

and

$$h_\xi^2 = \mathbf{N}(s)^2 = 1. \quad (11)$$

This yields

$$\xi \frac{\partial \kappa(s)}{\partial s} \left(\frac{1}{h_s^3} \right) \frac{\partial \Phi_m}{\partial s} + \left(\frac{1}{h_s^2} \right) \frac{\partial^2 \Phi_m}{\partial s^2} - \kappa(s) \left(\frac{1}{h_s} \right) \frac{\partial \Phi_m}{\partial \xi} + \frac{\partial^2 \Phi_m}{\partial \xi^2} + \omega^2 \left(\frac{1}{\tilde{c}_s^2} \right) \Phi_m = 0. \quad (12)$$

In the vicinity of the ray γ , that is for small ξ , the terms of Eq. (9) are simplified using:

$$\frac{1}{(1 - \xi\kappa(s))} \sim 1 + \xi\kappa(s) + \xi^2\kappa(s)^2 + O(\xi^3), \quad (13)$$

$$\frac{1}{(1 - \xi\kappa(s))^2} \sim 1 + 2\xi\kappa(s) + 3\xi^2\kappa(s)^2 + O(\xi^3), \quad (14)$$

$$\frac{1}{(1 - \xi\kappa(s))^3} \sim 1 + 3\xi\kappa(s) + 6\xi^2\kappa(s)^2 + O(\xi^3), \quad (15)$$

and

$$\frac{1}{\tilde{c}_s(s, \xi)^2} = \frac{1}{\tilde{c}_s(s, 0)^2} + \frac{\partial (1/\tilde{c}_s(s, \xi)^2)}{\partial \xi} \Big|_{\xi=0} \xi + \frac{1}{2} \frac{\partial^2 (1/\tilde{c}_s(s, \xi)^2)}{\partial \xi^2} \Big|_{\xi=0} \xi^2 + O(\xi^3). \quad (16)$$

We then express the function $\Phi_m(s, \xi)$ in terms of a Wentzel-Kramers-Brillouin (WKB) ansatz as

$$\Phi_m(s, \xi) = \exp(i\omega\tau) U_m(s, \xi, \omega), \quad (17)$$

where τ is an unknown function of position. The fundamental assumption underlying the theory of Babich is that, as $\omega \rightarrow +\infty$, the mode is localized on the acoustic ray and that its transverse extent scales as $1/\sqrt{\omega}$. Such a solution can be found by assuming that the transverse variable ξ scales as

$$\xi = O(1/\sqrt{\omega}). \quad (18)$$

Then, from an expansion of Eq. (9) in ω , one obtains at the dominant order that the WKB phase in Eq. (17) depends only on s as $d\tau = ds/\tilde{c}_s$. At the next order in ω one finds a parabolic equation for the function V_m :

$$\frac{\partial^2 V_m}{\partial v^2} - K(s)v^2 V_m + \frac{2i}{\tilde{c}_s(s)} \frac{\partial V_m}{\partial s} = 0, \quad (19)$$

with

$$K(s) = \frac{1}{\tilde{c}_s(s)^3} \frac{\partial^2 \tilde{c}_s}{\partial \xi^2} \Big|_{\xi=0}, \quad (20)$$

where we introduced the scaled coordinate $v = \sqrt{\omega} \xi$ and $V_m = U_m/\sqrt{\tilde{c}_s}$.

3.2. Solutions of the parabolic wave equation

To find a solution to Eq. (19), we first find a solution at a fixed arc length s , and then study how this solution must evolve with s . At fixed s , the first two terms of Eq. (19) correspond to the equation for a quantum harmonic oscillator in the direction \mathbf{N} transverse to γ . Thus, as we know from quantum mechanics (Cohen-Tannoudji et al. 1973), a solution of this equation is a Gaussian wavepacket, transverse to the ray, that we write as

$$V_m^0 = A(s) \exp\left(i \frac{\Gamma(s)}{2} v^2\right), \quad (21)$$

with Γ an unknown complex-valued function. To find the variation of this Gaussian wavepacket along the ray γ , we introduce a solution of this form in the parabolic equation (Eq. (19)) and obtain a Riccati equation for Γ

$$\frac{1}{\tilde{c}_s} \frac{d\Gamma}{ds} + \Gamma^2 + K = 0, \quad (22)$$

simple equation for the factor A

$$\frac{1}{A} \frac{dA}{ds} = \frac{-\tilde{c}_s}{2} \Gamma. \quad (23)$$

In the following, we show that the equation for Γ is related to the ray properties in the vicinity of γ and can thus be solved from ray dynamics computations. First, using the variables $(z(s), p(s))$

defined as $\Gamma(s) = \frac{1}{z(s)} \frac{1}{\tilde{c}_s} \frac{dz(s)}{ds}$ and $p(s) = \frac{1}{\tilde{c}_s} \frac{dz(s)}{ds}$, Eq. (22) is transformed into the Hamiltonian system:

$$\frac{dz}{d\tau} = \tilde{c}_s^2 p \quad (24)$$

$$\frac{dp}{d\tau} = -\tilde{c}_s^2 K z, \quad (25)$$

where the (time-dependent) Hamiltonian function is

$$H_0(p, z, \tau) = \tilde{c}_s^2 \frac{p^2}{2} + \tilde{c}_s^2 K \frac{z^2}{2}, \quad (26)$$

τ being the time coordinate. From Eqs. ((24), (25)), one can derive an equation for z only to obtain

$$\frac{1}{\tilde{c}_s^2} \frac{d}{d\tau} \left(\frac{1}{\tilde{c}_s^2} \frac{dz}{d\tau} \right) + K z = 0. \quad (27)$$

Equations ((24), (25)) have two independent solutions (z, p) and (\bar{z}, \bar{p}) that are conjugate to each other. Of these two solutions, only one is physically relevant, i.e. corresponds to a localized wavepacket. According to Eq. (21) this happens if $\text{Im}(\Gamma) > 0$ for all s , and as shown in Appendix B, the sign of $\text{Im}(\Gamma)$ stays constant along γ since

$$\text{Im}(\Gamma) = \frac{1}{2} \frac{1}{|z|^2}. \quad (28)$$

The variation along γ of the Gaussian wavepacket can now be linked to the dynamics of the acoustic rays nearby γ . Indeed, $\text{Im}(\Gamma)$ has a simple expression in terms of the complex variable z , as shown in Eq. (28). This variable, on the other hand, obeys Eq. (27) which can be shown to be the same as the equation describing the deviation from γ of a ray nearby γ (see derivation in Appendix C). The Hamiltonian in Eq. (26) is thus a local integrable approximation, also known as a normal form approximation (Arnol'd 1989), to the full Hamiltonian for acoustic rays written in Eq. (7).

Now, our task is to find the two linearly independent complex conjugate solutions of Eqs. ((24), (25)). The terms in these equations depend only on quantities that are evaluated on the periodic ray γ . Therefore, these equations are periodic in s , or equivalently in τ . Equations ((24), (25)) can thus be written as:

$$\frac{d}{d\tau} \begin{pmatrix} z \\ p \end{pmatrix} = \Sigma(\tau) \begin{pmatrix} z \\ p \end{pmatrix}, \quad (29)$$

where the matrix Σ

$$\Sigma(\tau) = \begin{pmatrix} 0 & \tilde{c}_s^2 \\ -\tilde{c}_s^2 K & 0 \end{pmatrix}, \quad (30)$$

verifies $\Sigma(\tau + T_\gamma) = \Sigma(\tau)$, $T_\gamma = \oint_\gamma \frac{ds}{\tilde{c}_s}$ being the acoustic travel time along γ . Then if $(z(\tau), p(\tau))$ is a solution of Eq. (29), so is $(z(\tau + T_\gamma), p(\tau + T_\gamma))$ and the two solutions are related by the following linear map

$$\begin{bmatrix} z(\tau + T_\gamma) \\ p(\tau + T_\gamma) \end{bmatrix} = M \begin{bmatrix} z(\tau) \\ p(\tau) \end{bmatrix}, \quad (31)$$

where M is called the monodromy matrix (Cvitanović et al. 2010, and references therein). As (z, p) describe ray deviations from γ , the matrix M characterizes the stability of γ . As γ is stable, we know that $|\text{Tr}(M)| < 2$ and that the eigenvalues are of modulus one and complex conjugates of each other i.e. $\Lambda^\pm = \exp(\pm i\alpha)$ with $\alpha \in]0, \pi[$ (cf. Appendix D), where α is

called a Floquet phase or stability angle. Hence the two linearly independent solutions of Eq. (29) can be written in the form:

$$(z(\tau), p(\tau))^\pm = \exp\left(\pm i \frac{\alpha}{T_\gamma} \tau\right) u_\pm(\tau) v^\pm, \quad (32)$$

where the functions $u_\pm(\tau)$ are periodic with period T_γ and v^\pm are independent eigenvectors of the monodromy matrix M .

An expression of the monodromy matrix in terms of second derivatives of the action function S can be derived (Bogomolny 2006). The action function S is defined by a trajectory from the position q_i to q_f for a given energy or frequency ω (Gutzwiller 1990). For our purposes, the action is written as

$$S(q_i, q_f, \omega) = \int_{q_i}^{q_f} \frac{1}{\tilde{c}_s} d\sigma, \quad (33)$$

where σ is the arclength along a ray nearby γ . If we write the monodromy matrix as

$$\begin{pmatrix} z_f \\ p_f \end{pmatrix} = \begin{pmatrix} M_{11} & M_{12} \\ M_{21} & M_{22} \end{pmatrix} \begin{pmatrix} z_i \\ p_i \end{pmatrix}, \quad (34)$$

we can express its components from the second derivatives of the action function S with the following formulas

$$\frac{\partial^2 S}{\partial z_i \partial z_f} = -\frac{1}{M_{12}}, \quad \frac{\partial^2 S}{\partial z_i^2} = \frac{M_{11}}{M_{12}}, \quad \frac{\partial^2 S}{\partial z_f^2} = \frac{M_{22}}{M_{12}}, \quad (35)$$

where the positions q_i and q_f are written as (s_i, z_i) and (s_f, z_f) , z_i and z_f being respectively the initial and final transverse positions of the neighboring ray after one period, and the derivatives are evaluated on the periodic ray. From these expressions, and the simple formula giving the roots of a second degree polynomial (cf. Appendix D), we can obtain an expression for the stability angle α as

$$\alpha = \arctan\left(\frac{\sqrt{-\text{Tr}(M)^2 + 4}}{\text{Tr}(M)}\right), \quad (36)$$

where

$$\text{Tr}(M) = -\left(\frac{\partial^2 S}{\partial z_i \partial z_f}\right)^{-1} \left(\frac{\partial^2 S}{\partial z_i^2} + \frac{\partial^2 S}{\partial z_f^2}\right). \quad (37)$$

We thus have obtained a solution of the approximate wave equation Eq. (19) in the form of a Gaussian wavepacket (Eq. (21)), whose evolution along the ray γ is given by Eqs. ((29), (30)). It is possible to find other solutions of Eq. (19) that have a finite number of nodes in the direction transverse to γ . As for the quantum harmonic oscillator (Cohen-Tannoudji et al. 1973), these solutions can be obtained from Eq. (21) using the annihilation \hat{a} and creation operator \hat{a}^\dagger that are defined as (Babich & Buldyrev 1991)

$$\hat{a} = -iz \frac{\partial}{\partial v} - p v \quad \text{and} \quad \hat{a}^\dagger = -i\bar{z} \frac{\partial}{\partial \bar{v}} - \bar{p} v. \quad (38)$$

These operators have the commutation rule $[\hat{a}, \hat{a}^\dagger] = 1$, where the commutator is defined as $[\hat{A}, \hat{B}] = \hat{A}\hat{B} - \hat{B}\hat{A}$. Indeed, from the commutation relation of \hat{a}^\dagger with the operator of Eq. (19), the functions

$$V_m^\ell = (\hat{a}^\dagger)^\ell V_m^0, \quad (39)$$

are also solutions of Eq. (19) (Babich & Buldyrev 1991). The calculation of these higher- ℓ solutions then leads to

$$V_m^\ell(s, \nu) = \left(\frac{i}{\sqrt{2}} \right)^\ell \left(\frac{\bar{z}}{z} \right)^{\ell/2} H_\ell \left(\sqrt{\text{Im}(\Gamma)} \nu \right) \frac{\exp\left(i\frac{\Gamma}{2}\nu^2\right)}{\sqrt{z}}, \quad (40)$$

with H_ℓ the Hermite polynomials of order ℓ . Finally, we can write the solutions of Eq. (5) as

$$\Phi_m^\ell(s, \nu) = \sqrt{\tilde{c}_s} V_m^\ell(s, \nu) \exp\left(i\omega \int \frac{ds}{\tilde{c}_s}\right). \quad (41)$$

3.3. Quantization condition and regular frequency spacings

The quantization condition is based on the single-valuedness of the solution presented in Eq. (41), and thus asserts that the phase accumulated by the function Φ_m^ℓ over one period must be a multiple of 2π . In the following, we assume without loss of generality that the eigenvalue which corresponds to the wavepacket localization is $\exp(+i\alpha)$. The contribution of function V_m^ℓ to the dynamical phase of Φ_m^ℓ is obtained from Eqs. (32) and (40). We obtain that the phase accumulated over one period is

$$\omega_{n,\ell,m} \oint_\gamma \frac{1}{\tilde{c}_s} ds - \frac{\alpha + 2\pi N_r}{2} - (\alpha + 2\pi N_r)\ell = 2\pi n + \pi, \quad (42)$$

where α is the Floquet phase that is defined modulo 2π . For our purposes, we must also take into account the number N_r of multiples of 2π acquired by the phase. N_r can be computed by following the evolution of the eigenvector ν over one period, and we verified numerically that, alternatively, N_r is also the winding number around γ of a ray nearby γ during one period. The last term in Eq. (42) is the Maslov phase (Gutzwiller 1990) that comes from the reflection of the wave on the boundaries. The formula for the frequencies, $\omega_{n,\ell,m}$, of island modes is thus

$$\omega_{n,\ell,m} = \frac{1}{\oint_\gamma \frac{ds}{\tilde{c}_s}} \left[2\pi \left(n + \frac{1}{2} \right) + \left(\ell + \frac{1}{2} \right) (2\pi N_r + \alpha) \right] \quad (43)$$

or, in a form that makes the regularities more visible,

$$\omega_{n,\ell,m} = \delta_n(m)n + \delta_\ell(m)\ell + \beta(m), \quad (44)$$

with the frequency regularities

$$\delta_n = \frac{2\pi}{\oint_\gamma \frac{ds}{\tilde{c}_s}} \quad \text{and} \quad \delta_\ell = \frac{2\pi N_r + \alpha}{\oint_\gamma \frac{ds}{\tilde{c}_s}} \quad (45)$$

and the constant term

$$\beta = \frac{\delta_n + \delta_\ell}{2}. \quad (46)$$

The quantum numbers n and ℓ correspond to node numbers of the p-mode, respectively in the longitudinal and transverse directions of the central ray γ as illustrated in Fig. 3. This is to be contrasted with the case of a spherical mode where the most natural labeling are the quantum numbers of spherical harmonics. Equation (43) is a semi-analytical formula since the quantities T_γ , N_r and α must be computed numerically from the Runge-Kutta integration of the Hamiltonian equations for acoustic rays. The acoustic time, T_γ , is directly computed from γ itself. From the intersections of a ray nearby γ with the PSS (as can be seen in Fig. 2), we compute the monodromy matrix M that maps one intersection with the PSS to the next one. Then, by diagonalizing this matrix one obtains the Floquet phase α from its eigenvalues,

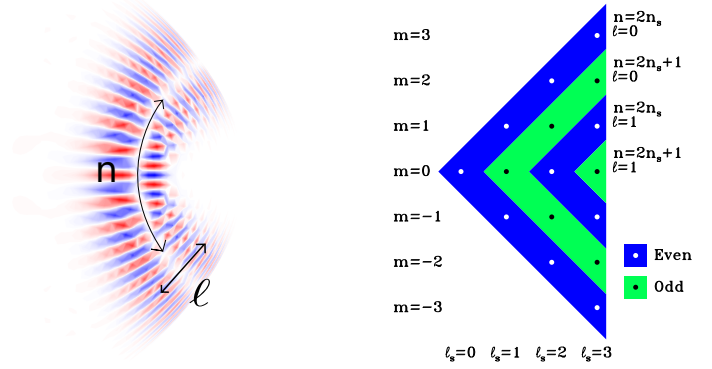


Fig. 3. *Left:* schematic representation of the mode labeling/quantum numbers used for island modes. *Right:* illustration of the relation between the quantum numbers of spherical and island modes. The quantum number n is the number of nodes in the longitudinal direction of the island mode (along the ray γ), ℓ is the number of nodes in the transverse direction of the mode (transverse to γ) and m is the number of azimuthal nodes. n_s , ℓ_s and m_s are the quantum numbers of spherical modes. In the *right* figure, the multiplets of island modes correspond to diagonal colored bands, whereas the multiplets of spherical modes would have the form of vertical bands. The plotted mode on the left corresponds to $n = 46$, $\ell = 1$ and $m = 0$. (This figure is available in color in the electronic form.)

and the functions z and Γ from its eigenvectors. It is important to note that for m even, only modes symmetric with respect to the rotation axis exist. Since the preceding theory does not take this phenomenon into account, the theoretical value of δ_ℓ is multiplied by two when the ray γ coincides with the rotation axis, i.e. for rotation rates less than the bifurcation point. Finally, it can be noted that a formula similar to Eq. (43) can also be obtained through the formalism of the Gutzwiller trace formula following the method of Miller (1975).

4. Comparison with numerical results

As the present asymptotic theory relies on various assumptions, its relevance for stellar seismology is not guaranteed and needs to be assessed through a comparison with exact calculations of realistic stellar models. In this section, the comparison is done with numerically computed modes in uniformly rotating polytropic models of stars. The hypotheses of the asymptotic theory are the following: first, it is valid in the asymptotic regime, that is, for high enough frequencies. Second, the island modes are constructed from a stable island of acoustic ray phase space. At null rotation such a structure does not exist, so we expect that the theory fails to describe spherical mode amplitudes and frequencies. A stable island immediately appears at non-zero rotation, but its phase space volume must be high enough for an island mode to exist. This volume increases with frequency and rotation (see Lignières & Georgeot 2008, 2009, for details). Thus, for a given frequency range, the number of island modes starts from zero at small rotation rates and progressively increases as the rotation and thus the phase space volume of the stable island grows. Actually, low degree spherical modes become progressively island modes as rotation increases. Another assumption used in finding a solution to the wave equation is that the mode decays as $\propto 1/\sqrt{\omega}$ in the direction transverse to the periodic ray. Finally, the theory also neglects the Coriolis force and the perturbations of the gravitational potential.

In the following, the asymptotic theory is compared with highly accurate computations of high frequency adiabatic modes

Table 1. Island mode quantum numbers n , ℓ , m of numerically computed modes, corresponding to $n_s \in [21, 25]$, $\ell_s \in \{0, 1, 2, 3\}$, $m_s \in [-\ell_s, \ell_s]$ in terms of spherical mode quantum numbers.

n	ℓ	m
42, 44, 46, 48, 50	0	-3, -2, ..., 3
42, 44, 46, 48, 50	1	-1, 0, 1
43, 45, 47, 49, 51	0	-2, -1, ..., 2
43, 45, 47, 49, 51	1	0

in uniformly rotating polytropic stellar models with index $N = 3$, the Coriolis effect and perturbations of the gravitational potential being taken into account. The accuracy of these calculations, described in detail in Reese et al. (2006), is very high (the relative precision on the frequencies is 10^{-7}) and thus does not interfere with the present comparison. A large number of modes were followed from $\Omega/\Omega_K = 0$ to $\Omega/\Omega_K = 0.896$. At zero rotation these modes are low degree $\ell_s \in \{0, 1, 2, 3\}$, high order $n_s \in [21, 25]$ modes. At higher rotation rates, they become island modes and can thus be labeled with n and ℓ , the number of nodes along and transverse to γ , respectively, as illustrated in Fig. 3. The relation between the quantum numbers at zero and high rotation rates is (Reese 2008):

$$n = 2n_s + [(\ell_s + m_s) \bmod 2], \quad (47)$$

$$\ell = \frac{\ell_s - |m_s| - [(\ell_s + m_s) \bmod 2]}{2}, \quad (48)$$

$$m = m_s. \quad (49)$$

We remind the reader that rotational multiplets are defined, in the non-rotating case, as a set of frequencies with identical n_s , ℓ_s quantum numbers but different values of m_s for $m_s \in [-\ell_s, \ell_s]$. For rotating stars, we can define multiplets as frequencies with identical n and ℓ but different $m \in \mathbb{Z}$, i.e. without any limiting value for m . The relation between the two sets of quantum numbers and the two types of multiplets is illustrated in Fig. 3. In this figure the multiplets of island modes correspond to diagonal colored bands, whereas the multiplets at zero rotation would have the form of vertical bands. We restricted ourselves to numerical modes with $\ell_s^{\max} = 3$ so, in terms of island mode quantum numbers, the range of numerically computed modes is the one given in Table 1. The associated numerical frequency spacings are defined as:

$$\delta_n^{\text{num}} = \omega_{n+1, \ell, m}^{\text{num}} - \omega_{n, \ell, m}^{\text{num}}, \quad (50)$$

and

$$\delta_\ell^{\text{num}} = \omega_{n, \ell+1, m}^{\text{num}} - \omega_{n, \ell, m}^{\text{num}}. \quad (51)$$

The semi-analytical asymptotic theory also requires determining the α term in Eq. (45) numerically. To test the robustness of this calculation, we checked that the frequency spacing δ_ℓ only weakly depends on the choice of the ray nearby γ that is used to compute α . Also, the spacings δ_n and δ_ℓ neither depend on the resolution of the background model nor on the integration parameters of the Runge-Kutta method.

4.1. Regular frequency spacings

According to Eq. (44), the structure of the spectrum is characterized by the two spacings $\delta_n(m)$ and $\delta_\ell(m)$. In Fig. 4, their semi-analytical and numerical values computed for $m = 0$ and $|m| = 1$ are compared as a function of the rotation rate. One can see that the semi-analytical regularities δ_n , δ_ℓ , and the full computations

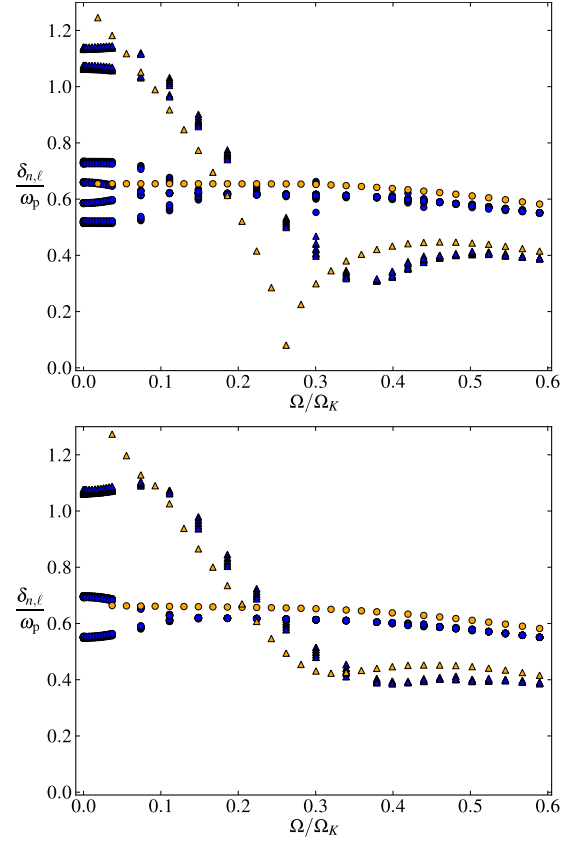


Fig. 4. Comparison of frequency spacings $\delta_{n,\ell}$ between island modes, computed from numerical simulations and semi-analytical formulas for different values of Ω/Ω_K (the frequency spacings are normalized by $\omega_p = \sqrt{GM/R_p^3}$ with R_p the polar radius). Circles: δ_n , triangles: δ_ℓ , orange/gray: semi-analytical results, blue/black: numerical results. Numerical results correspond to different sets of δ_n^{num} and δ_ℓ^{num} values, with $n \in [42, 51]$, $\ell \in \{0, 1\}$ for $m = 0$; and $n \in [42, 51]$, $\ell = 0$, $n \in [42, 44, 46, 48, 50]$, $\ell = 1$ for $m \in \{-1, 1\}$. Upper panel: $m = 0$. Lower panel: $m = \pm 1$. (This figure is available in color in the electronic form.)

of high-frequency p-modes are in good agreement for almost all rotation rates. For $m = 0$, around $\Omega/\Omega_K \approx 0.26$, the agreement degrades significantly. In this rotation range, the ray γ in the center of the main stable island undergoes a bifurcation from one stable ray on the polar axis to two stable rays surrounding one unstable ray. When such a bifurcation occurs, the eigenvalues of the monodromy matrix become $\Lambda^\pm = 1$, corresponding to a Floquet phase $\alpha = 0 \bmod 2\pi$ (see e.g. Brack 2001). This is indeed what happens at $\Omega/\Omega_K \approx 0.26$, as $\delta_\ell \propto \alpha$ goes to zero. Such a behavior conveys the non-validity of the present normal form approximation for rays undergoing a bifurcation. One possibility would be to use other local approximations of the ray dynamics called uniform approximations (Schomerus & Sieber 1997). The discrepancy coming from the bifurcation is not to be found for $m \neq 0$, since the stable ray stays away from the polar axis and does not undergo a bifurcation as rotation increases.

Although, as mentioned before, the theoretical and numerical frequency spacings are not expected to match for slow rotation rates, the discrepancies remain small in this rotation range. This is due to the fact that, as Ω/Ω_K approaches zero, the stable ray is along the polar axis and, according to the expression of δ_n , this implies that $\delta_n = \Delta/2$, i.e. half the large separation defined in Eq. (3). Now, using the first order of Tassoul's formula and the

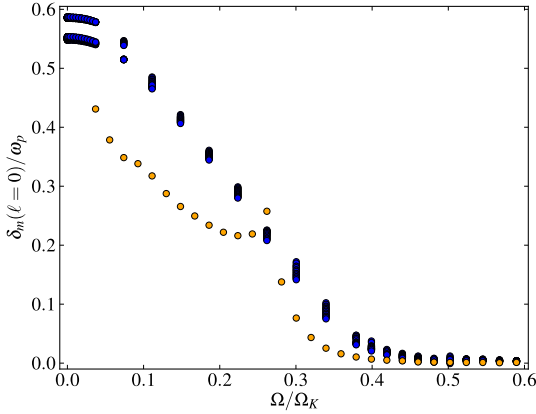


Fig. 5. Comparison of frequency spacing δ_m between island modes, computed from numerical simulations and semi-analytical formula Eq. (53) for different values of Ω/Ω_K (the frequency spacings are normalized by $\omega_p = \sqrt{GM/R_p^3}$ with R_p the polar radius). Orange/gray: semi-analytical results of Eq. (53) for $n = 42$ and $m = 1$, blue/black: numerical results. The numerical results correspond to different sets of δ_m for $n \in [42, 51]$, $\ell = 0$ and $m \in \{-1, 1\}$. (This figure is available in color in the electronic form.)

quantum numbers conversion rules Eqs. ((47)–(49)), it is easy to see that, at zero rotation, $\delta_n^{\text{num}} = \omega_{n+1, \ell, m}^{\text{num}} - \omega_{n, \ell, m}^{\text{num}}$ is expected to be close to half the large separation. Note also that the doubling of the numerical values observed in Fig. 4 at small rotation rates is due to the small separation that appears at the next order of Tassoul’s theory. Concerning δ_ℓ , the semi-analytical calculations indicates that δ_ℓ goes to $2\delta_n$, that is Δ , for slow rotation rates. Again, Tassoul’s formula applied to the n, ℓ quantum numbers shows that δ_ℓ^{num} is close to Δ . For these reasons, the frequency spacings δ_n and δ_ℓ converge to the results of the first order of Tassoul’s formula, though their derivation is formally not possible for non-rotating stars.

In order to investigate the drift between the spectra of different m as rotation increases, we consider the frequency spacing:

$$\delta_m = \omega_{n, \ell, m} - \omega_{n, \ell, 0}. \quad (52)$$

Figure 5 displays a comparison between the numerical and semi-analytical values of δ_m for $\ell = 0$ and $|m| = 1$. As expected, the agreement is not good at small rotation rates. Using the first order of Tassoul’s formula to approximate the numerical results at zero rotation, $\delta_m^{\text{num}} = \omega_{n, \ell, m}^{\text{num}} - \omega_{n, \ell, 0}^{\text{num}}$ is found to be close to $|m|\Delta/2$ when $\Omega/\Omega_K = 0$. This is not compatible with the asymptotic theory of the island mode since it predicts that δ_m goes to zero when ω goes to infinity. Indeed, $\delta_n(m)$ depends on m/ω because \tilde{c}_s and the ray path γ , given by the Hamiltonian Eq. (7), both depend on m/ω . An alternative explanation is to consider the spatial distribution of island modes of fixed m and ℓ : one finds that increasing ω produces both larger derivatives along the stable ray associated with a higher node number n , and larger transverse derivatives because the transverse extent scales as $1/\sqrt{\omega}$. Thus, the contribution of the azimuthal derivatives becomes negligible in the wave equation (Eq. (4)). We also verified that δ_m displayed in Fig. 5 diminishes when n is increased. Thus, for rotation rates such that the numerical modes are not fully island modes, they behave more like spherical modes and δ_m^{num} shows clear discrepancies with the asymptotic results. By contrast, at high rotation rates, an approximate analytical formula for δ_m is derived in the following and shown to closely reproduce the numerical results.

Starting from

$$\delta_m(\ell = 0) = [\delta_n(m) - \delta_n(0)]n + [\beta(m) - \beta(0)], \quad (53)$$

we first assume that n is large enough to neglect $\beta(m) - \beta(0)$. From Eq. (45), $\delta_n(m)$ is equal to $2\pi/T_\gamma(m)$ where

$$T_\gamma(m) = \oint_\gamma \frac{ds}{c_s} \sqrt{1 - \frac{1}{\omega^2} \left[\omega_c^2 + \frac{c_s^2 (m^2 - 1/4)}{d^2} \right]}. \quad (54)$$

The dependence of T_γ on m is explicit in the integrand but is implicit in the integration path γ . In the following, the variation of the location of γ with m/ω is assumed to be negligible. Then, an expansion in $1/\omega$ of the integrand in Eq. (54) leads to:

$$T_\gamma(m) \simeq \oint_\gamma \frac{ds}{c_s} - \frac{1}{2\omega^2} \left[\oint_\gamma \omega_c^2 \frac{ds}{c_s} + \oint_\gamma \frac{c_s (m^2 - 1/4)}{d^2} ds \right]. \quad (55)$$

Hence we obtain an approximate expression for $\delta_n(m)$ of the form:

$$\delta_n(m) \simeq \frac{2\pi}{\oint_\gamma \frac{ds}{c_s}} + \frac{\pi}{\omega^2} \frac{\oint_\gamma \frac{\omega_c^2}{c_s} ds + \oint_\gamma \frac{c_s (m^2 - 1/4)}{d^2} ds}{\left(\oint_\gamma \frac{ds}{c_s} \right)^2}. \quad (56)$$

If we insert the previous expression for $\delta_n(m)$ in Eq. (53) and neglect $\beta(m) - \beta(0)$, we have

$$\delta_m(\ell = 0) \simeq \left[\frac{m^2}{\omega^2} \pi \frac{\oint_\gamma \frac{c_s}{d^2} ds}{\left(\oint_\gamma \frac{ds}{c_s} \right)^2} \right] n. \quad (57)$$

Finally, normalizing by $\omega_p = \sqrt{GM/R_p^3}$ and replacing ω by $n\frac{\omega}{n}$ yields

$$\begin{aligned} \frac{\delta_m(\ell = 0)}{\omega_p} &\simeq \left(\frac{m}{\sqrt{n}} \right)^2 \pi \frac{\oint_\gamma \frac{c_s}{d^2} ds}{\left(\oint_\gamma \frac{ds}{c_s} \right)^2} \left(\frac{n}{\omega/\omega_p} \right)^2 \frac{1}{\omega_p^3} \\ &\simeq \left(\frac{m}{\sqrt{n}} \right)^2 \frac{1}{4\pi\omega_p} \oint_\gamma \frac{c_s}{d^2} ds, \end{aligned} \quad (58)$$

where we have used the fact that $\frac{n}{\omega/\omega_p}$ stays constant in the frequency range considered here, and is known to be close to $\omega_p \oint_\gamma \frac{ds}{c_s} / 2\pi$. The previous expression will be made more precise by renormalizing the value of c_s by $\sqrt{1 - \omega_c^2/\omega^2}$ to take into account that ω_c is not negligible, and indeed is of the order of ω , close to the stellar surface. In Fig. 6, the numerical values of $\delta_m(\ell = 0)$ as well as results for the last term in Eq. (58) are plotted as a function of m/\sqrt{n} for $\Omega/\Omega_K = 0.419$, showing a good agreement. This behavior is valid for rotation rates higher than $\Omega/\Omega_K \approx 0.4$. It must also be noted that in the numerical calculations by Reese et al. (2009), using more realistic stellar models, the asymptotic $\frac{m}{\sqrt{n}}$ dependency was also found empirically.

4.2. Pressure amplitudes of island modes

In this section, we compare the results obtained from the semi-analytical formula for mode spatial distributions Eq. (41) with results from full numerical computations. Equatorial cuts of the semi-analytical modes can be expressed as a function

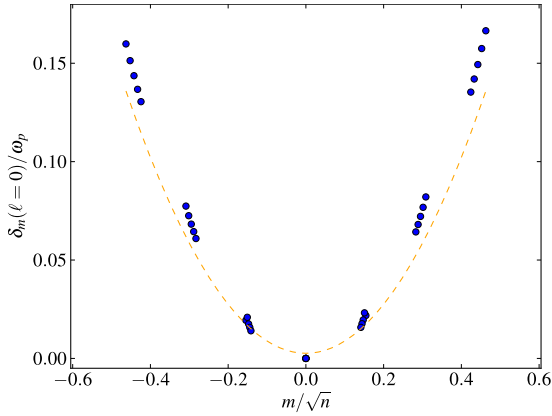


Fig. 6. Frequency spacings $\delta_m(\ell=0) = \omega_{n,\ell=0,m} - \omega_{n,\ell=0,m=0}$, normalized by ω_p , as a function of m/\sqrt{n} . The integers n , ℓ and m are the quantum numbers of island modes. The rotation rate is $\Omega/\Omega_K = 0.419$. Blue/black dots: numerical results. Orange/gray dashed line: semi-analytical results for the last term in Eq. (58). Numerical modes included are for quantum numbers $n \in \{42, 44, 46, 48, 50\}$, $\ell = 0$ and $m \in [-3, 3]$. (This figure is available in color in the electronic form.)

of $v = \sqrt{\omega}(r - r_0)$, where r_0 is the radial position of the ray γ , while the value of Γ is obtained from the eigenvectors of the monodromy matrix M . In Fig. 7, the equatorial cuts of semi-analytical and numerical modes are plotted for different rotational velocities and quantum numbers ℓ and m . The chosen modes are representative of the different behaviors observed. Discrepancies between semi-analytical and numerical results are mainly due to edge effects. This occurs when the transverse extent of the mode (which scales as $1/\sqrt{\omega}$) reaches either the polar axis for small rotations, or the surface near the equator for high rotations. Finally, avoided crossings can also contravene an accurate prediction for mode amplitudes since the amplitudes of crossing modes will be linear combinations of all the modes contributing to the crossing. Hence, modes undergoing an avoided crossing can differ significantly from Eq. (41) (cf. third panel in Fig. 7). Overall, there is nevertheless a good agreement between the semi-analytical and numerical results for mode spatial distributions, showing the validity of Eq. (41).

5. Phenomenology and observables for asteroseismology

In this section, we show that the asymptotic theory provides a simple understanding of the evolution of the island mode spectrum with rotation. Then, the physical content of the potentially observable frequency spacings δ_n , δ_ℓ and δ_m is discussed.

Figure 8 displays the global evolution of all the numerical frequencies considered in the observer's frame, whose island mode quantum numbers can be found in Table 1 (or equivalently $n_s \in [21, 25]$, $\ell_s \in [0, 3]$, $m_s \in [-\ell_s, \ell_s]$ in spherical modes quantum numbers). The first phenomenon that can be noticed is a global decrease of frequencies with rotation. This effect is simply due to the increasing volume of the star when it is spinning rapidly. Besides this global effect, the evolution of the spectrum's organization can be inferred from the evolution of frequency spacings δ_n , δ_ℓ and δ_m . The spacing δ_n stays almost constant from null up to high rotations, its value remaining close to half the large frequency separation of the spherical model. If a large number of island modes are detected in an observed spectrum, δ_n should be easily extracted from the data. By contrast, the rapid evolution of δ_ℓ with rotation will strongly modify

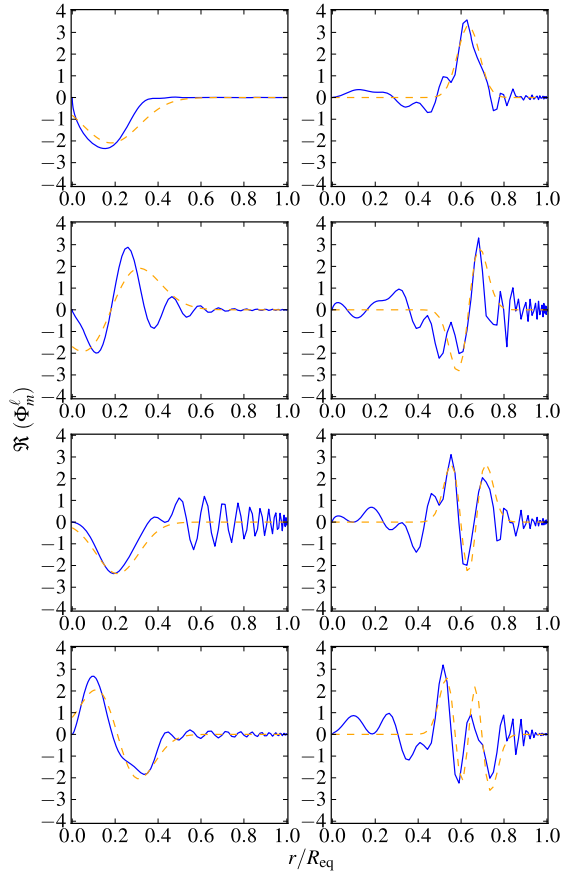


Fig. 7. Examples of normalized amplitudes distributions (real part of Φ_m^ℓ) on the equator as a function of position r/R_{eq} (where R_{eq} is the equatorial radius of the stellar model) for semi-analytical and numerical modes. Modes displayed are for $\Omega/\Omega_K = 0.300$ (left column), and $\Omega/\Omega_K = 0.707$ (right column). Quantum numbers (n, ℓ, m) are as follows. Left column $(50, 0, 0)$, $(50, 1, 0)$, $(50, 0, 1)$, $(50, 1, 1)$. Right column $(50, 0, 0)$, $(50, 1, 0)$, $(50, 2, 0)$, $(50, 3, 0)$. Blue/black continuous line: numerical results; orange/gray dashed line: semi-analytical results. (This figure is available in color in the electronic form.)

the spectrum's organization. This is shown in Fig. 9 where for clarity only a few $m = 0$ modes have been displayed: the $\ell = 0$, $n \in [43, 46]$ and $\ell = 1$, $n \in [42, 44]$ modes (or equivalently the $(n_s, \ell_s) \in \{(21, 1), (21, 2), (21, 3), (22, 0), (22, 1), (22, 2), (23, 0)\}$ modes). Starting from the usual structure at zero rotation involving the large and small separations of Tassoul's theory, the spectrum reorganization induced by the decrease of δ_ℓ can also be viewed as an increase of the small separation δ . Then, above $\Omega/\Omega_K \approx 0.45$, the structure of the $m = 0$ spectrum remains practically unchanged.

Now, to illustrate the evolution of the spectra of different m , Fig. 10 displays the $n = 44$, $\ell = 0$, $m \in \{-2, -1, 1, 2\}$ mode frequencies as a function of the rotation rate together with the $n \in [43, 46]$, $\ell = 0$, $m = 0$ frequencies. The main feature of this evolution is the decrease of δ_m from $\approx \frac{\Delta}{2}|m|$ at zero rotation to very small values at high rotations. When multiplets of island modes are defined as in Sect. 4 and Fig. 3, they show no regularity at small rotation rates. Note, however, that the splitting $\omega_m - \omega_{-m}$ is always very close to $-2m\Omega$ because the effects of the Coriolis force are negligible. By contrast, at high rotation rates, as δ_m vanishes above $\Omega/\Omega_K \approx 0.45$, the $m \in \{-2, -1, 0, 1, 2\}$ modes clearly form a regular multiplet, as can be seen in Fig. 10, where deviations from strict Ω spacings are due to the $(m/\sqrt{n})^2$ term. Since for such rotation rates the structure of the $m = 0$ spectrum

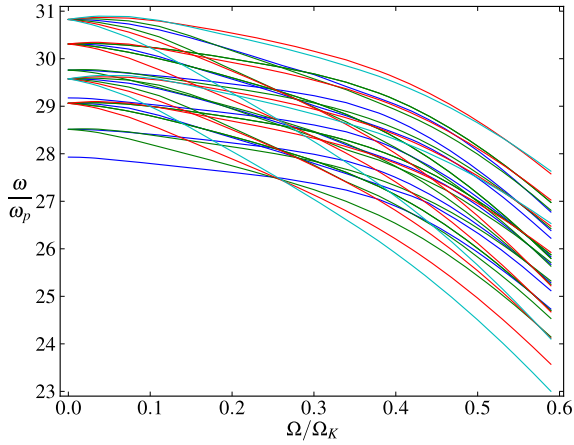


Fig. 8. Normalized frequencies ω/ω_p as a function of normalized rotation velocity Ω/Ω_K in the observer's frame. Different colors correspond to different values of $|m|$. Blue: $m = 0$, green: $|m| = 1$, red: $|m| = 2$, cyan: $|m| = 3$. Modes included are for the quantum numbers $n_s \in [21, 23]$, $\ell_s \in [0, 3]$, $m_s \in [-\ell_s, \ell_s]$ (see Table 1). (This figure is available in color in the electronic form.)

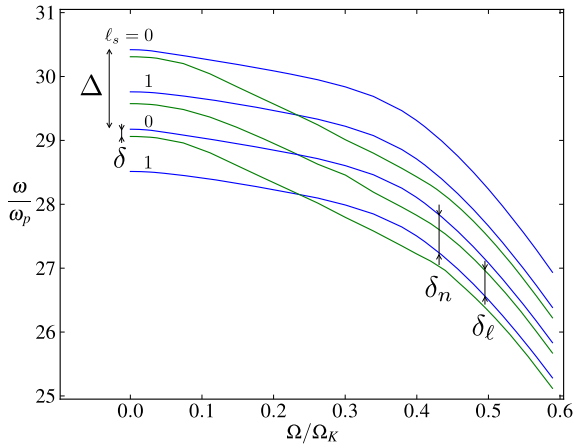


Fig. 9. Normalized frequencies ω/ω_p as a function of normalized rotation velocity Ω/Ω_K . The quantum numbers of the displayed modes are: $\ell = 0$, $n \in [43, 46]$ and $\ell = 1$, $n \in [42, 44]$ with $m = 0$. Blue: $\ell = 0$, green: $\ell = 1$. For clarity, the corresponding degrees of the spherical harmonics are also written. We have outlined the large frequency separation Δ , the small frequency separation $\delta = \omega_{n_s, \ell_s} - \omega_{n_s-1, \ell_s+2}$ and the δ_n , δ_ℓ spacings with arrows. (This figure is available in color in the electronic form.)

remains unchanged, the evolution of the whole spectrum in the observer's frame is dominated by the advection term $m\Omega$.

The global evolution of mode frequencies in the observer's frame shown in Fig. 8 also presents some particular events: a first clustering of mode frequencies occurs around $\Omega/\Omega_K \simeq 0.25$ and then a second one around $\Omega/\Omega_K \simeq 0.56$. Both phenomena can be understood from the asymptotic theory. According to the asymptotic formulas Eqs. ((43)–(46)), crossings of mode frequencies will happen when δ_ℓ/δ_n , or equivalently α/π , has a rational value. Though the asymptotic theory predicts true eigenvalue crossings, it is known that these crossings will be avoided if the two modes are of the same symmetry class (Landau & Lifshitz 1977). As can be seen in Fig. 4, δ_ℓ becomes equal to δ_n at some rotation rate around $\Omega/\Omega_K \simeq 0.25$ where the spectrum for a given m simplifies to $\omega_{n,m} = \delta_n(m)n + \beta$. The degeneracy occurs between modes of a different symmetry class, and the rotation rate at which it occurs depends only weakly on

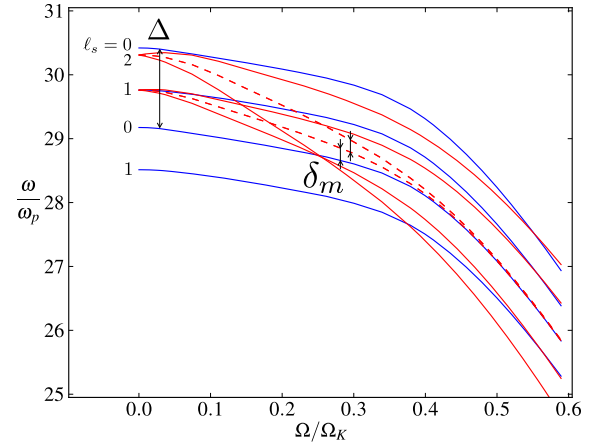


Fig. 10. Normalized frequencies ω/ω_p as a function of normalized rotation velocity Ω/Ω_K . The quantum numbers of the displayed modes are: $n = 44$, $\ell = 0$, $m \in \{-2, -1, 1, 2\}$ with the $n \in [43, 46]$, $\ell = 0$, $m = 0$ modes. Blue: $m = 0$, red: $|m| \in \{1, 2\}$. For clarity, the corresponding degrees of the spherical harmonics are also written. Continuous line: frequencies in the observer frame, dashed line: in the rotating frame. We have outlined the large frequency separation Δ and the δ_m spacing with arrows. (This figure is available in color in the electronic form.)

the m values of the modes, if m is small. This property translates itself into a clustering of the full spectrum in the observer's frame because it turns out that this rotation rate is close to $\delta_n/2$; and δ_m , that decreases from an initial value of $m\delta_n$ to zero at high rotation, is around $m\delta_n/2$ at this intermediate rotation. The second frequency clustering close to $\Omega/\Omega_K \simeq 0.56$ is related to the fact that δ_m vanishes at high rotation. In this regime, the different m spectra are expected to collapse onto a single spectrum in the rotating frame but not in the observer's frame. However, when Ω is equal to δ_n , the near degeneracy of the m spectra produces the frequency clustering observed at $\Omega/\Omega_K \simeq 0.56$.

One of the interests of asymptotic theories in asteroseismology is to gain physical insights into seismic observables such as δ_n , δ_l , and δ_m . In the following, we briefly discuss this point with emphasis on the differences and similarities with the physical content of the large and small separation from Tassoul's theory. The spacing δ_n depends only on the acoustic travel time $T_\gamma = \oint_\gamma \frac{ds}{c_s}$ along the acoustic ray γ . We expect T_γ to be dominated by the time spent in the sub-surface region where the sound speed is much smaller than in the interior. While the path of the ray varies with rotation, δ_n remains approximately proportional to the mean density as shown by Reese et al. (2008). On the other hand, the δ_ℓ spacing depends also on the second derivatives of the sound speed transverse to the ray γ , an information integrated all along the ray. As long as the path of the stable ray goes through the central region of the star, the island mode frequencies should be sensitive to the chemical stratification and thus the age of the star. However, after the bifurcation at $\Omega/\Omega_K \simeq 0.26$, the ray path progressively avoids the central region and the island modes do not contain this information anymore. Another interesting property of δ_ℓ (or δ_ℓ/δ_n) is that it is very sensitive to rotation as long as $\Omega/\Omega_K \leq 0.35$. Finally, for high rotation rates ($\Omega/\Omega_K \geq 0.40$), the value of δ_m , that can be detected through the irregularity of multiplets, also gives an information on rotation since it is proportional to $\oint_\gamma \frac{c_s}{d^2} ds$ (Eq. (58)) where the distance of the ray to the rotation axis d strongly depends on the rotation rate.

6. Conclusions

In this paper, we derived an asymptotic formula for frequencies that predicts and describes regular spacings in the p-mode spectrum of rapidly rotating stars. The derivation relied on finding a stable periodic solution of the acoustic ray dynamics, and obtaining an expression for the modes that are localized around this ray, the so-called island modes. The method thus provides a formula for the island modes frequencies, as well as a formula for the mode spatial distributions. We compared these semi-analytical formulas with results from numerical computations of high-frequency oscillations in rotating polytropic stellar models. The frequency spectrum is characterized by the three spacings δ_n , δ_ℓ and δ_m . The agreement was shown to be good for δ_n and δ_ℓ at almost all rotation rates, while δ_m shows significant discrepancies at low rotation rates. The spacing δ_n stays almost constant at all rotation rates with a value that is close to half the large frequency separation of the non-rotating model. On the other hand, the rapid decrease of δ_ℓ strongly modifies the spectrum's organization up to $\Omega/\Omega_K \simeq 0.4$, while above that rotation rate, δ_ℓ remains approximately constant. For such high rotation rates, the spacing δ_m nearly vanishes, thus in the observer's frame the evolution of the whole spectrum is dominated by the advection term $m\Omega$. We have also seen that the combined evolution of these frequency spacings with rotation leads to particular events such as true or near degeneracies, that can significantly simplify the spectrum. In addition to these new insights on the evolution of the island mode spectrum with rotation, the asymptotic theory provides semi-analytical formulas for the regular spacings, in particular simple formulas for δ_n and δ_ℓ .

The present asymptotic theory should be useful for different aspects of stellar seismology in the presence of rapid stellar rotation. The regular frequency spacings are potentially observable and our results provide guidance to look for them in data. While investigations dedicated to the search for regularities are necessary (e.g. Lignières et al. 2010), we expect that the easiest quantities to detect in an island mode spectrum are δ_n at any rotation rate, $2m\Omega$ at small rotation rates, and Ω at high rotation. For modeling pulsations, the asymptotic theory provides a new approach, complementary to numerical computations. One of its advantages is to give a quick estimate of frequency spacings for a given stellar model, which in turn can be used to search for patterns in numerically computed spectra. In the same spirit, the semi-analytical amplitude distributions might provide a useful approximation for calculating mode visibilities and spectral signatures.

The asymptotic theory in itself can be improved and extended in various ways. We have already mentioned that the method needs to be refined at the rotation rate where the bifurcation of the stable ray occurs, using uniform approximations of the ray dynamics. It would also be interesting to predict analytically the rotation rate of the bifurcation for a given sequence of stellar models. The present method also assumes that the modes are governed by local dynamics around the stable ray. This assumption can be tested with a numerical EBK method applied to the tori of the stable island (Bohigas et al. 1993), although this method is complicated to implement in practice. In this paper, we left aside the determination of the actual number of modes that are described by the asymptotic theory. An estimate of such a number can be obtained by computing systematically the phase space volume of stable islands for different rotations (e.g. Lignières & Georgot 2009). Then, knowing the value of δ_ℓ that gives the mean distance between island mode frequencies, or the mean density of these modes, one could

compute the ℓ^{\max} of the modes that satisfy our formulas. Another aspect that we have not modeled is avoided crossing in spite of the fact that it will induce important deviations, especially at low frequencies. Strong gradients of the sound speed will also produce deviations from the asymptotic theory. A technique called ray-splitting, that has already been used successfully in quantum chaos (Blümel et al. 1996), could account for this effect. Finally, a similar technique could be applied to asymptotic gravity modes, that were shown recently to have connections with ray theory (Ballot et al. 2011).

Acknowledgements. We thank J. Ballot for his help at various stages of this work. We also thank the ANR project SIROCO for funding and CALMIP ("CALcul en Midi-Pyrénées") for the use of their supercomputer. M.P., F.L. and D.R.R. acknowledge the KITP staff of UCSB for their warm hospitality during the research program "Astroseismology in the Space Age". This research was supported in part by the National Science Foundation under Grant No. PHY11-25915. D.R.R. acknowledges financial support through a postdoctoral fellowship from the "Subside fédéral pour la recherche 2011", University of Liège.

Appendix A: Wave equation in the meridional plane

In this section, we derive the two-dimensional wave equation in the meridional plane of the star. We start from the three-dimensional wave equation (Eq. (4)) in spherical coordinates (r, θ, ϕ) , and from the expression of the mode amplitude as $\Psi = \Psi_m \exp(im\phi)$ we obtain the following wave equation:

$$\left[\Delta_{r,\theta} + \frac{1}{r} \left(\frac{\partial}{\partial r} + \frac{1}{r \tan \theta} \frac{\partial}{\partial \theta} \right) - \frac{m^2}{(r \sin \theta)^2} \right] \Psi_m + \frac{\omega^2 - \omega_c^2}{c_s^2} \Psi_m = 0, \quad (\text{A.1})$$

where θ is the colatitude. We want to cancel out of this equation the terms multiplied by first order derivatives of Ψ_m in order to obtain a two-dimensional Helmholtz-like equation. We thus introduce the ansatz $\Psi_m(r, \theta) = \beta(r, \theta) \Phi_m(r, \theta)$ in Eq. (A.1) to obtain that $\beta(r, \theta)$ must satisfy

$$\frac{2}{\beta} \frac{\partial \beta}{\partial r} + \frac{1}{r} = 0 \quad (\text{A.2})$$

to cancel out terms in $\frac{\partial \Phi_m}{\partial r}$, and

$$\frac{2}{\beta} \frac{\partial \beta}{\partial \theta} + \frac{1}{\tan \theta} = 0 \quad (\text{A.3})$$

to cancel out terms in $\frac{\partial \Phi_m}{\partial \theta}$. This leads to the solution

$$\beta(r, \theta) = \frac{B}{\sqrt{r \sin \theta}}, \quad (\text{A.4})$$

and we choose $B = 1$ to yield Eq. (5).

Appendix B: Expression of the imaginary part of Γ

In this section, we derive the expression for the imaginary part of Γ using the Wronskian of Eq. (27). First, we write Eq. (27) as

$$\frac{1}{\tilde{c}_s} \frac{d}{ds} \left(\frac{1}{\tilde{c}_s} \frac{dz}{ds} \right) + Kz = 0. \quad (\text{B.1})$$

Then, we shall use the Abel's differential equation identity that says that for an equation of the following type

$$\frac{d^2 y}{dx^2} + P(x) \frac{dy}{dx} + Q(x)y = 0, \quad (\text{B.2})$$

with the Wronskian defined as

$$\mathcal{W}(x) = y_1 \frac{dy_2}{dx} - \frac{dy_1}{dx} y_2, \quad (\text{B.3})$$

and y_1, y_2 the two independent solutions of Eq. (B.2), there is the identity

$$\mathcal{W}(x) = \mathcal{W}_0 \exp\left(-\int^x P(x') dx'\right). \quad (\text{B.4})$$

With the change of variable $du = \tilde{c}_s ds$ we can transform Eq. (B.1) into a form similar to Eq. (B.2) with $P(u) = 0$. It follows that the Wronskian $\mathcal{W}(u)$ stays constant for all u :

$$\mathcal{W}(u) = \mathcal{W}_0, \quad (\text{B.5})$$

and then, coming back to the s variable, we obtain that

$$W(s) = z(s) \frac{1}{\tilde{c}_s(s)} \frac{d\bar{z}(s)}{ds} - \frac{1}{\tilde{c}_s(s)} \frac{dz(s)}{ds} \bar{z}(s), \quad (\text{B.6})$$

or equivalently

$$W(s) = z(s)\bar{p}(s) - p(s)\bar{z}(s), \quad (\text{B.7})$$

stays constant for all s such that $W(s) = \mathcal{W}(u) = \mathcal{W}_0$. From Eqs. (B.6), (B.5) and the fact that $\Gamma = p/z$ we thus obtain that

$$\bar{\Gamma} - \Gamma = \frac{\mathcal{W}_0}{z\bar{z}}, \quad (\text{B.8})$$

yielding

$$\text{Im}[\Gamma] = \frac{i}{2} \left[\frac{\mathcal{W}_0}{z\bar{z}} \right], \quad (\text{B.9})$$

and therefore

$$\text{Im}[\Gamma] = \frac{i}{2} \left[\frac{\mathcal{W}_0}{|z|^2} \right]. \quad (\text{B.10})$$

Hence this shows that $\text{Im}[\Gamma]$ keeps a constant sign along the ray when s varies. Thus if Γ is chosen such that it localizes the function at s_0 , then the function will stay localized around the ray for all s . Since the localization is obtained for $\text{Im}[\Gamma] > 0$ or equivalently $i\mathcal{W}_0 > 0$, we choose the Wronskian such that

$$W(s) = -i. \quad (\text{B.11})$$

Appendix C: Analogy between the function z and the deviation of nearby rays

In this section, we show that the equation satisfied by the function z , Eq. (27), is the same as the equation describing the deviation of two nearby rays. It will thus be possible to compute the evolution of z from the ray dynamics. To be an acoustic ray of the system, the ray γ must correspond to an extremum of the action S defined as

$$S(q_i, q_f, \omega) = \int_{q_i}^{q_f} \mathbf{p} \cdot d\mathbf{q} = \int_{q_i}^{q_f} \frac{1}{\tilde{c}_s} d\sigma. \quad (\text{C.1})$$

The length element $d\sigma$ can be expressed in the coordinate system centered on the ray γ defined in Sect. 3.1 as

$$d\sigma^2 = (1 - \xi\kappa(s))^2 ds^2 + d\xi^2, \quad (\text{C.2})$$

yielding

$$d\sigma^2 = \left[(1 - \xi\kappa(s))^2 + \left(\frac{d\xi}{ds} \right)^2 \right] ds^2. \quad (\text{C.3})$$

The action function S can therefore be expressed in this coordinate system as

$$S = \int \frac{1}{\tilde{c}_s(s, \xi)} \sqrt{\left[(1 - \xi\kappa(s))^2 + \left(\frac{d\xi}{ds} \right)^2 \right]} ds, \quad (\text{C.4})$$

with the corresponding Lagrangian

$$L(s, \xi, d\xi/ds) = \frac{1}{\tilde{c}_s(s, \xi)} \sqrt{\left[(1 - \xi\kappa(s))^2 + \left(\frac{d\xi}{ds} \right)^2 \right]}. \quad (\text{C.5})$$

The Lagrangian L becomes for ξ small:

$$\begin{aligned} L(s, \xi, \dot{\xi}) = \frac{1}{\tilde{c}_s(s)} & \left[1 - \xi\kappa(s) + \frac{1}{2} \dot{\xi}^2 - \frac{1}{\tilde{c}_s(s)} \frac{\partial \tilde{c}_s}{\partial \xi} \xi \right. \\ & + \frac{\kappa(s)}{\tilde{c}_s(s)} \frac{\partial \tilde{c}_s}{\partial \xi} \xi^2 - \frac{1}{2\tilde{c}_s(s)} \frac{\partial^2 \tilde{c}_s}{\partial \xi^2} \xi^2 \\ & \left. + \frac{1}{\tilde{c}_s(s)^2} \left(\frac{\partial \tilde{c}_s}{\partial \xi} \right)^2 \xi^2 \right] + O(\xi^3), \end{aligned} \quad (\text{C.6})$$

where $\dot{\xi} \equiv d\xi/ds$ and derivatives in ξ are evaluated at $\xi = 0$. As is known from classical mechanics, for the action to be extremum, the associated Lagrangian must satisfy the Euler-Lagrange equation

$$\frac{d}{ds} \left(\frac{\partial L}{\partial \dot{\xi}} \right) - \frac{\partial L}{\partial \xi} = 0. \quad (\text{C.7})$$

Keeping only quadratic terms in ξ from this equation yields

$$\begin{aligned} \ddot{\xi} - \frac{1}{\tilde{c}_s(s)} \frac{d\tilde{c}_s(s)}{ds} \dot{\xi} - 2 \left[\frac{1}{\tilde{c}_s(s)^2} \left(\frac{\partial \tilde{c}_s}{\partial \xi} \right)^2 + \frac{\kappa(s)}{\tilde{c}_s(s)} \frac{\partial \tilde{c}_s}{\partial \xi} \right. \\ \left. - \frac{1}{2\tilde{c}_s(s)} \frac{\partial^2 \tilde{c}_s}{\partial \xi^2} \right] \xi + \left[\kappa(s) + \frac{1}{\tilde{c}_s(s)} \frac{\partial \tilde{c}_s}{\partial \xi} \right] + O(\xi^3) = 0. \end{aligned} \quad (\text{C.8})$$

This equality must be valid for all ξ so we can deduce that:

$$\kappa(s) = -\frac{1}{\tilde{c}_s(s)} \frac{\partial \tilde{c}_s}{\partial \xi}, \quad (\text{C.9})$$

and

$$\begin{aligned} \frac{1}{\tilde{c}_s(s)} \frac{d}{ds} \left(\frac{1}{\tilde{c}_s(s)} \frac{d\xi}{ds} \right) - \frac{2}{\tilde{c}_s(s)^2} \left[\frac{1}{\tilde{c}_s(s)^2} \left(\frac{\partial \tilde{c}_s}{\partial \xi} \right)^2 + \frac{\kappa(s)}{\tilde{c}_s(s)} \frac{\partial \tilde{c}_s}{\partial \xi} \right. \\ \left. - \frac{1}{2\tilde{c}_s(s)} \frac{\partial^2 \tilde{c}_s}{\partial \xi^2} \right] \xi = 0. \end{aligned} \quad (\text{C.10})$$

We thus obtain the equation for the deviation between nearby rays as

$$\frac{1}{\tilde{c}_s(s)} \frac{d}{ds} \left(\frac{1}{\tilde{c}_s(s)} \frac{d\xi}{ds} \right) + K(s)\xi = 0, \quad (\text{C.11})$$

and this equation is the same as Eqs. ((27), (B.1)) that are satisfied by the function z .

Appendix D: Eigenvectors and eigenvalues of the monodromy matrix M

In this section, we derive the necessary formulas to express the stability angle α and the function Γ in terms of the elements of the monodromy matrix M . The characteristic polynomial of a 2×2 matrix M is

$$\Lambda^2 - \text{Tr}(M)\Lambda + \det(M) = 0. \quad (\text{D.1})$$

Then, it is known that a monodromy matrix is a symplectic matrix, which implies that $\det(M) = 1$. For a stable ray, we have $|\text{Tr}(M)| < 2$, and thus the roots of this polynomial become

$$\Lambda_{1,2} = \frac{\text{Tr}(M)}{2} \pm i \frac{\sqrt{-\text{Tr}(M)^2 + 4}}{2}. \quad (\text{D.2})$$

We thus obtain the expression for the stability angle α as

$$\exp(\pm i\alpha) = \frac{1}{2} \left[\text{Tr}(M) \pm i \sqrt{-\text{Tr}(M)^2 + 4} \right], \quad (\text{D.3})$$

and we obtain Eq. (36).

The eigenvector v_1 will then be given by the following equation:

$$\begin{pmatrix} M_{11} - \Lambda_1 & M_{12} \\ M_{21} & M_{22} - \Lambda_1 \end{pmatrix} \begin{pmatrix} z_1 \\ p_1 \end{pmatrix} = 0, \quad (\text{D.4})$$

which corresponds to

$$(M_{11} - \Lambda_1)z_1 + M_{12}p_1 = 0 \quad (\text{D.5})$$

$$M_{21}z_1 + (M_{22} - \Lambda_1)p_1 = 0. \quad (\text{D.6})$$

Recalling that $\Gamma(s) = p(s)/z(s)$ we write

$$\Gamma_1 = \frac{p_1}{z_1}, \quad (\text{D.7})$$

and thus we obtain that

$$\Gamma_1 = -\frac{(M_{11} - \Lambda_1)}{M_{12}} = -\frac{M_{21}}{(M_{22} - \Lambda_1)}. \quad (\text{D.8})$$

This yields

$$\Gamma_1 = \frac{-M_{11} + M_{22}}{2M_{12}} + i \frac{\sqrt{-\text{Tr}(M)^2 + 4}}{2M_{12}}, \quad (\text{D.9})$$

and with the same procedure we obtain the expression of Γ_2 :

$$\Gamma_2 = \frac{-M_{11} + M_{22}}{2M_{12}} - i \frac{\sqrt{-\text{Tr}(M)^2 + 4}}{2M_{12}}. \quad (\text{D.10})$$

References

- Aerts, C., Christensen-Dalsgaard, J., & Kurtz, D. 2010, *Asteroseismology*, Astronomy and Astrophysics Library (Springer)
- Arfken, G., & Weber, H. 2005, *Mathematical Methods For Physicists* (Elsevier)
- Arnol'd, V. 1989, *Mathematical methods of classical mechanics*, Graduate texts in mathematics (Springer-Verlag)
- Babich, V., & Buldyrev, V. 1991, *Short-wavelength diffraction theory: asymptotic methods*, Springer series on wave phenomena (Springer-Verlag)
- Baglin, A., Auvergne, M., Barge, P., et al. 2006, in *ESA Spec. Publ. 1306*, eds. M. Fridlund, A. Baglin, J. Lochard, & L. Conroy, 33
- Ballot, J., Lignières, F., Prat, V., Reese, D. R., & Rieutord, M. 2011 [arXiv:1109.6856]
- Berry, M. V., & Robnik, M. 1984, *J. Phys. A Math. Gen.*, 17, 2413
- Blümel, R., Antonsen, Jr., T. M., Georgeot, B., Ott, E., & Prange, R. E. 1996, *Phys. Rev. Lett.*, 76, 2476
- Bogomolny, E. 2006, in *Frontiers in Number Theory, Physics, and Geometry I*, eds. P. Cartier, B. Julia, P. Moussa, & P. Vanhove (Springer Berlin Heidelberg), 3
- Bohigas, O., Tomsovic, S., & Ullmo, D. 1993, *Phys. Rep.*, 223, 43
- Brack, M. 2001, in *Atomic Clusters and Nanoparticles*, eds. C. Guet, P. Hobza, & F. Spiegelman, 161
- Cohen-Tannoudji, C., Diu, B., & Laloë, F. 1973, *Mécanique quantique I*, Collection enseignement des sciences (Hermann)
- Cvitanović, P., Artuso, R., Mainieri, R., Tanner, G., & Vattay, G. 2010, *Chaos: Classical and Quantum* (Copenhagen: Niels Bohr Institute)
- García Hernández, A., Moya, A., Michel, E., et al. 2009, *A&A*, 506, 79
- Gough, D. O. 1993, in *Astrophysical Fluid Dynamics – Les Houches 1987*, eds. J.-P. Zahn, & J. Zinn-Justin, 399
- Gutzwiller, M. 1990, *Chaos in classical and quantum mechanics*, Interdisciplinary applied mathematics (Springer-Verlag)
- Koch, D. G., Borucki, W. J., Basri, G., et al. 2010, *ApJ*, 713, L79
- Kogelnik, H., & Li, T. 1966, *Appl. Opt.*, 5, 1550
- Landau, L., & Lifshitz, E. 1977, *Quantum mechanics: non-relativistic theory* (Butterworth-Heinemann)
- Lignières, F., & Georgeot, B. 2008, *Phys. Rev. E*, 78, 016215
- Lignières, F., & Georgeot, B. 2009, *A&A*, 500, 1173
- Lignières, F., Rieutord, M., & Reese, D. 2006, *A&A*, 455, 607
- Lignières, F., Georgeot, B., & Ballot, J. 2010, *Astron. Nachr.*, 331, 1053
- Mantegazza, L., Poretti, E., Michel, E., et al. 2012, *A&A*, 542, A24
- Miller, W. H. 1975, *J. Chem. Phys.*, 63, 996
- Monnier, J. D., Zhao, M., Pedretti, E., et al. 2007, *Science*, 317, 342
- Ott, E. 2002, *Chaos in Dynamical Systems* (Cambridge University Press)
- Pasek, M., Georgeot, B., Lignières, F., & Reese, D. R. 2011, *Phys. Rev. Lett.*, 107, 121101
- Percival, I. C. 1973, *J. Phys. B At. Mol. Phys.*, 6, L229
- Reese, D. 2008, *J. Phys. Conf. Ser.*, 118, 012023
- Reese, D., Lignières, F., & Rieutord, M. 2006, *A&A*, 455, 621
- Reese, D., Lignières, F., & Rieutord, M. 2008, *A&A*, 481, 449
- Reese, D. R., MacGregor, K. B., Jackson, S., Skumanich, A., & Metcalfe, T. S. 2009, *A&A*, 506, 189
- Royer, F. 2009, in *Lecture Notes in Physics The Rotation of Sun and Stars* (Berlin Springer Verlag), 765, 207
- Schomerus, H., & Sieber, M. 1997, *J. Phys. A Math. Gen.*, 30, 4537
- Tassoul, M. 1980, *ApJS*, 43, 469
- Tureci, H. E., Schwefel, H. G. L., Stone, A. D., & Narimanov, E. E. 2002, *Opt. Exp.*, 10, 752
- Vagov, A., Schomerus, H., & Zalipaev, V. V. 2009, *Phys. Rev. E*, 80, 056202
- Vandakurov, Y. V. 1967, *AZh*, 44, 786
- Zalipaev, V. V., Kusmartsev, F. V., & Popov, M. M. 2008, *J. Phys. A Math. Gen.*, 41, 065101

Chapter 6

Conclusion and perspectives

In this thesis, we have studied a subset of regular pressure modes in rapidly rotating stars, that should be the easiest to detect and identify in observed oscillation spectra. For this regular subset, we have constructed an asymptotic theory based on rays using the ‘parabolic equation method’. This asymptotic theory gives semi-analytical formula for the frequencies and eigenfunctions of these regular modes, that depend on the properties of periodic stable acoustic rays. We found a good agreement between these semi-classical predictions and two-dimensional complete numerical computations in uniformly rotating polytropic stellar models. The obtained semi-analytical formula for frequency spacings should be important for asteroseismology, as it relates the regular frequency spacings to physical properties of the star, which can provide a guide for identification methods.

Nevertheless, the present form of our asymptotic theory can be improved in different ways. Firstly, the theory can be applied to other periodic stable rays, such as the period-6 rays, though as we have seen the corresponding modes are less likely to be observable due to the cancellation effect of the disk-integrated light. As concerns directly the results that were presented in this thesis, although the semi-classical theory allows to predict the values of frequency spacings δ_n and δ_ℓ for almost all rotation rates, the physical reasons for the rapid decrease of the δ_ℓ spacing in the range $0.0 < \Omega/\Omega_K < 0.4$ is not entirely clear, and deserves to be explained.

Also, in the range of rotation rates where the bifurcation of the period-2 stable ray occurs, the phase space dynamics around the ray cannot be approximated by a simple stable island, and the stable periodic ray is no longer isolated. In such situations, it is necessary to treat the contributions of all the periodic orbits in the vicinity of the 2-period ray collectively, by using uniform approximations (given in Schomerus and Sieber, 1997) to obtain the corresponding frequency density and frequency spacings. Incidentally, the rotation rate at which this bifurcation takes place would be interesting to predict analytically, at least in order to know *a priori* the rotation rate where a more refined method than the one described in this thesis is needed. A related problem concerns our predictions for regular spacings at small rotation rates. Indeed, at these small rotation rates the ray system is ‘near-integrable’, where the phase space is structured around chains of regular islands, and the contributions from the periodic orbits of all these islands to the frequency density should also be treated collectively by uniform approximations (Ullmo et al., 1996).

Besides the short-wavelength approximation, the parabolic equation method assumes that the motion around the stable periodic orbit can be described in a linear approximation (‘thin torus’ limit of EBK quantization). The validity of this approximation can be checked by comparing the results of the parabolic equation method with a numerical implementation of the full EBK quantization of tori in the period-2 stable island, in ways similar to Bohigas et al. (1993). But this method, that computes the actions of all invariant tori in phase space in order to determine those that are quantized and thus obtaining the

corresponding mode frequencies of the system is demanding numerically, and not practical to implement in our system that does not have a ‘scaling’ in energy, as was the case in the study cited above.

In addition, we have shown in this thesis that the parabolic equation method predicts accurately the frequencies of several regular island modes, but we have left aside the determination of the total number of regular island modes that should be present in the spectrum at the different rotation rates. These numbers can be obtained by computing systematically the phase space volume, by e.g. a Monte-Carlo method, of the period-2 stable islands for different rotation rates as was done, for a single value of the rotation, in Lignières and Georgeot (2009). It can be noted that such technique yields also, knowing the value of δ_ℓ , the maximum value of the quantum number ℓ of island modes.

We also note that when the rotation rate of the star is used as a control parameter of our system, the parabolic equation method predicts many frequency crossings when the ratio of the stability angle α over 2π has a rational value. But it is known, from the von Neumann–Wigner theorem (see e.g. Haake, 2010), that crossings between modes of the same symmetry class will actually be *avoided*. Though, as we said previously, avoided crossings do not seem to lead to significant deviations of regular frequency spacings in the high-frequency regime, such avoided crossings can induce important deviations in the low-frequency part of the spectrum, where they can be resolved in observations, and potentially hinder mode identification. Thus, it would be interesting to predict the widths of these avoided crossings, in particular when they couple two regular island modes, or one island mode with a chaotic mode. In the latter case, the coupling with a chaotic mode would potentially provide supplementary information on the stellar interior.

As concerns the comparison of our results with observational data, it would require some further steps in our work, like its comparisons with oscillation modes in more realistic stellar models. It can be noted that some recent numerical computations of oscillation modes in rapidly rotating realistic stellar models have already found frequency spacings and mode eigenfunctions similar to those that were studied in this thesis (Reese et al., 2009), at least for reasonable differential rotation. Our ray tracing code can be adapted to these more realistic stellar models in order to provide estimates of the asymptotic frequency spacings, which can be used to search for such regular patterns in the computed oscillation spectra. In more realistic stellar models, in particular for evolved stars, it is expected that strong gradients of the sound speed should be present in the interior. These strong gradients correspond to discontinuities that are known to affect oscillation mode frequencies and eigenfunctions, but they cannot be taken into account with our present ray theory. However, it has been shown that solutions to the Schrödinger (or Helmholtz) equation in the presence of a finite step potential discontinuity could be obtained using the *ray splitting* technique (Blümel et al., 1996), that incorporates in the semi-classical theory the effects of reflection and refraction of rays at interfaces. This method should be applicable to our problem in a straightforward manner. Also, rapidly rotating classical pulsators do not typically oscillate in the asymptotic regime of pressure modes, so it is necessary to study in details the validity of our asymptotic theory in the low frequency part of the spectrum, knowing that it has been shown previously that regular frequency spacings are also present in this frequency range (Lignières et al., 2006; Reese et al., 2008).

The observational view on rapidly rotating pulsators, δ Scuti stars in particular, is currently evolving thanks to the wealth of available data coming from space missions CoRoT and Kepler. The most interesting study in the light of the results presented here are those that report the detection of regular frequency spacings in δ Scuti stars, such as the works of García Hernández et al. (2009); Zwintz et al. (2011); Mantegazza et al. (2012). These are only preliminary results however, and the analysis of CoRoT and Kepler data is still ongoing. The work presented in this thesis obviously incites to search for regularities in the observed spectra of rapidly rotating pulsators. Adapted techniques

can be developed from the asymptotic theory, and tested on “realistic” synthetic spectra, along the lines of Lignières et al. (2010). But it must be noted that such analyses are not straightforward, since mode intrinsic amplitudes and the necessary stellar characteristics (such as the position of the star in the H-R diagram) are not generally known *a priori*.

Solar-like pulsators that have relatively high rotation rates are also found in observations. These stars would certainly be the more interesting ones for our study since their frequencies should be in the asymptotic regime, where the discrepancies where the asymptotic theory are small. F-type stars, for example, are known to rotate rapidly in comparison with other solar-like pulsators ($\Omega/\Omega_K \sim 0.1 - 0.2$). However, the mode lifetime in these stars is small, and so is the precision on oscillation frequencies. On the other hand, red giant stars are generally slowly rotating, since their expansion phase decreases their rotational velocities by the conservation law of angular momentum. Nevertheless, some rapid rotators among red giant stars (i.e. giant stars with rotational velocities of 10 km.s^{-1} or higher, see e.g. Carlberg et al. (2011)) have been detected. Different ‘spin-up’ mechanisms have been proposed, including the accretion of giant Jupiter-mass planets (see e.g. Carlberg et al., 2009). Three observed red giant stars are particularly interesting since one can obtain an estimate of their centrifugal flattening by computing the values of Ω/Ω_K from the measured large frequency separations and rotation periods, to obtain $\Omega/\Omega_K \sim 0.2 - 0.38$ (R. A. García, private communication). We have already developed and tested a bi-polytropic version of the two-dimensional oscillation code to model red giant stars by accounting for the high density core.

The methods that we developed in this thesis could also be used for planetary seismology. Indeed, the giant planets of our solar system, Jupiter in particular, are known to rotate rapidly and to be significantly flattened by the centrifugal force (see e.g. Guillot, 2004), resulting in a surface oblateness of 6.5% in the case of Jupiter (Mosser, 1990). Recently, pressure mode oscillations have been detected at the surface of Jupiter by Gaulme et al. (2011). From its rapid rotation, one would expect strong rotational effects on the pressure mode spectrum of Jupiter. Indeed, such effects have been studied before, but by perturbation theory only (Vorontsov, 1981; Mosser, 1990). We are thus planning to apply the asymptotic formula for regular frequencies derived here on a reasonably realistic model of Jupiter.

Although the present thesis only deals with the regular subset of pressure modes in rapidly rotating stars, it was obtained in Lignières and Georgeot (2009) that chaotic modes should also be visible in observations, and in large numbers. Though no simple asymptotic formula can be found for the frequencies of chaotic modes, it is possible to extract information on the (unstable) periodic orbits through a “backward” application (Delande, 2001) of the Gutzwiller trace formula on the chaotic spectrum (see Sect. 3.2.4). This could yield information for example on the action correlations between periodic orbits, that depend on the speed of sound distribution in the star. Finding a way to retrieve some information from the chaotic mode frequencies could be very useful for seismology purposes for two reasons: firstly, chaotic modes are the only modes that go through the stellar core at high rotation rates, and this is where the information on the chemical stratification, and thus the age, of the star is contained. Secondly, the eigenfunctions of chaotic modes are known to be highly sensitive to small perturbations (see e.g. Schack and Caves, 1993; Benenti et al., 2002), i.e. changes in the stellar model in our case, thus enhancing the diagnostic potential of inversion techniques.

Finally, it was shown recently (Ballot et al., 2011) that some gravity modes of rapidly rotating polytropic stellar models could be qualitatively described in the asymptotic regime by a ray theory with a mixed phase space. This would provide another potential application of the present asymptotic method, although this should not be straightforwardly applicable since the gravity wave equation in a rotating star cannot be reduced to a Helmholtz-type equation.

Appendix A

Résumé étendu

Le but de cette annexe est de donner un résumé étendu en langue française de ce travail de thèse. Aucune information supplémentaire au corps du texte n'a été ajoutée, et les figures de cette annexe sont des reproductions à l'identique de figures déjà présentes dans le corps du texte.

A.1 Introduction générale

L'astérosismologie a pour but de déduire les propriétés internes des étoiles à partir de la mesure de leurs fréquences d'oscillation. L'analyse du spectre d'oscillation peut-être facilitée par une information a priori sur la structure de celui-ci obtenue grâce à une formule asymptotique. Jusqu'à maintenant, la seule formule asymptotique disponible était limitée aux étoiles à symétrie sphérique. Or, pour une étoile en rotation rapide, la force centrifuge a un effet d'applatissage sur l'étoile, et la formule asymptotique ne peut donc pas être appliquée. Pourtant, les étoiles pulsantes en rotation rapide sont communes dans notre galaxie, en particulier parmi les étoiles massives et de masses intermédiaires, et sont donc présentes en nombre dans les données des missions spatiales dédiées à l'astérosismologie que sont CoRoT et Kepler.

Dans le domaine du chaos quantique, des outils ont été développés pour trouver des expressions approchées ou statistiques des niveaux d'énergie et fonctions d'onde de système quantiques complexes. Un exemple typique d'un tel système est un système quantique dont la limite classique est chaotique. Les concepts du chaos quantique reposent en fait sur la nature ondulatoire des systèmes quantiques auxquels il s'applique. Ceci a permis d'utiliser ces concepts pour d'autres types d'ondes tels que les ondes élastiques ou électromagnétiques se propageant dans des milieux désordonnés ou à géométrie complexe.

Le but de cette thèse est donc d'utiliser les techniques du chaos quantique pour obtenir des informations sur les modes de pression des étoiles en rotation rapide. La limite des petites longueurs d'onde des ondes de pression, aussi appelée limite des rayons acoustiques, peut-être décrite par un système dynamique Hamiltonien. Ce système passe, lorsque l'on augmente la vitesse de rotation d'un modèle d'étoile, d'un système intégrable à un système mixte, où des régions stables et chaotiques co-existent dans l'espace des phases. Il est connu en chaos quantique qu'à chaque région de l'espace des phases peut être associé un sous-spectre défini, ainsi que des fonctions d'onde asymptotiquement localisées dans cette région. Les modes dont la limite des rayons appartient à une zone stable de l'espace des phases possèdent typiquement des fréquences espacées régulièrement. Dans cette thèse, nous montrons comment obtenir des expressions semi-analytiques de ces espacements de fréquences dans le cas des modes de pression d'étoiles en rotation. Nous avons adapté à ce système la méthode de l'équation parabolique, qui a été appliqué précédemment à des systèmes d'ondes électromagnétiques dans des cavités diélectriques, ou des résonateurs électroniques sous champ magnétique. Les formules semi-analytiques obtenues dépendent

des propriétés dynamiques des rayons périodiques stables, que l'on calcule en intégrant numériquement les équations de la dynamique des rayons. Pour vérifier les résultats de ces formules, nous avons effectué des simulations numériques complètes et précises de modes d'oscillations dans des modèles polytropiques d'étoile : un bon accord avec la théorie a été obtenu pour une large gamme de vitesses de rotation. Comme notre théorie relie les espacements réguliers de fréquences d'oscillations aux quantités physique internes des étoiles, ce travail devrait fournir un nouveau type d'outil théorique pour l'interprétation des spectres d'oscillations d'étoiles en rotation rapide.

A.2 Astérosismologie

Les étoiles pulsantes montrent des variations de vitesse à leur surface dues à des modes d'oscillations globaux. Ces modes d'oscillation proviennent des interférences constructives entre ondes élastiques se propageant dans leur intérieurs. Les variations de vitesse à la surface de l'étoile entraînent des variations de température du gaz stellaire, ce qui fait varier la luminosité de ces étoiles pulsantes, qui sont donc des *étoiles variables*. Il est ensuite possible d'obtenir les fréquences correspondantes aux modes d'oscillations de l'étoile en réalisant la transformée de Fourier de sa courbe de lumière. L'astérosismologie a enfin comme but de contraindre la structure interne des étoiles pulsantes à partir de l'analyse de leurs spectres d'oscillation. Pour le Soleil, ainsi que pour de nombreuses autres étoiles pulsantes appartenant à la classe des pulsateurs de type solaires (voir la Sect. 2.1 pour une définition), cette technique a permis de faire des progrès considérables dans notre compréhension de l'évolution et de la structure interne de ces étoiles.

Le 'problème inverse' qui consiste à contraindre les nombreux paramètres physiques intervenant dans le calcul des modèles d'étoiles à partir des fréquences d'oscillation observées peut-être facilité grandement par la connaissance *a priori* d'informations sur la structure du spectre. De telles informations permettent en effet de simplifier le processus d'identification de modes, qui consiste à associer à chaque pic de fréquence du spectre observé le mode d'oscillation de l'étoile correspondant. Pour une étoile à symétrie sphérique, une information sur la structure de base du spectre d'oscillation peut être obtenue dans le cadre d'une 'théorie asymptotique'. En effet, il peut être montré que, dans le régime asymptotique des modes de pression correspondant au régime des hautes-fréquences, les fréquences d'oscillation de l'étoile sont au premier ordre données par la 'formule asymptotique de Tassoul' de la forme:

$$\omega_{n,\ell} \simeq \frac{\pi}{\int_0^R \frac{dr}{c_s(r)}} \left(n + \frac{\ell}{2} + \frac{1}{4} + \alpha \right), \quad (\text{A.1})$$

où n et ℓ sont des entiers appelés "nombres quantiques", c_s est la vitesse du son dans l'étoile, R le rayon de l'étoile, et α est un terme de phase qui dépend des conditions aux limites à la surface de l'étoile. La formule précédente n'étant valable que pour les étoiles proche de la symétrie sphérique, elle ne peut donc s'appliquer aux étoiles en rotation rapide, dont la structure est aplatie par l'effet de la force centrifuge.

D'après les données observationnelles sur les mesures de vitesses de rotation des étoiles, on sait que les étoiles non-évoluées de masse intermédiaire et massives, dont la masse est supérieure à 1.5 fois la masse du Soleil, tournent rapidement en moyenne (leur vitesse équatoriale étant en moyenne de 150 km.s^{-1} , alors que le Soleil tourne à seulement 2 km.s^{-1} à l'équateur). À de telles rotations, les étoiles peuvent être significativement aplaties par la force centrifuge, et les étoiles en rotation rapide atteignent typiquement 30% de leur limite Keplerienne Ω_K , qui correspond au taux de rotation pour lequel la force centrifuge $MR_{\text{eq}}\Omega_K^2$ égale l'attraction gravitationnelle GM^2/R_{eq}^2 à l'équateur. Comme la formule asymptotique de Tassoul ne peut être utilisée pour obtenir la structure asymptotique du

spectre des étoiles déformées, la physique interne des étoiles de masse $M > 1.5M_{\odot}$ ne peut donc être contrainte par le biais de l'astérosismologie. Il a cependant été montré qu'un comportement asymptotique régulier devrait être observé dans les fréquences d'oscillations d'étoiles en rotation rapide. En effet, en se basant sur les résultats de codes d'oscillation numériques bi-dimensionnels, Reese et coll. ont montré empiriquement que les fréquences numériques des modes de pression d'étoiles en rotation rapide suivent asymptotiquement la relation:

$$\omega_{n,\ell,m} \simeq \delta_n n + \delta_{\ell} \ell + \delta_m |m| + \alpha, \quad (\text{A.2})$$

où n , ℓ et m sont des entiers; δ_n , δ_{ℓ} et δ_m étant des différences de fréquences évaluées numériquement dont l'expression n'était pas connue alors. Cette observation empirique a motivé la recherche d'une théorie asymptotique pouvant décrire les fréquences d'oscillations des étoiles en rotation rapide, dans le but d'obtenir une expression analytique de la formule précédente. Une telle expression permettrait de connaître *a priori* la structure asymptotique du spectre d'oscillations des étoiles en rotation rapide et ainsi faciliter le processus d'identification des modes. Aussi elle devrait permettre, comme c'est le cas pour la formule de Tassoul dans le cas sphérique, de relier les espacements de fréquences d'oscillations aux propriétés physiques internes des étoiles en rotation rapide et ainsi, permettre de faire du diagnostic sismique et de l'inversion.

Dans le deuxième chapitre de cette thèse, nous présentons tout d'abord brièvement quelques aspects observationnels liés aux étoiles pulsantes (Sect. 2.1), et nous nous intéressons plus particulièrement aux étoiles pulsantes en rotation rapide. Ensuite, nous faisons un résumé non-exhaustif de la théorie des oscillations stellaires décrivant le comportement de ces étoiles pulsantes (Sect. 2.2). Nous mettons l'accent dans cette partie sur la description de la théorie asymptotique des oscillations stellaires. Dans le cas sans rotation, cette théorie asymptotique décrit le comportement régulier du spectre des modes de pression dans le régime des hautes-fréquences (Sect. 2.2.2). Nous présentons ensuite comment, pour les étoiles en rotation rapide, les résultats des codes d'oscillations numériques bi-dimensionnels ont permis de conjecturer qu'un comportement asymptotique régulier subsiste pour les grandes rotations (Sect. 2.2.3).

A.3 Chaos quantique et chaos ondulatoire

Le domaine du chaos quantique concerne l'étude des systèmes quantiques dont la limite classique est chaotique. Les concepts du chaos quantique peuvent également être appliqués aux systèmes ondulatoires classiques, tels que les ondes élastiques ou électro-magnétiques, ce pourquoi on utilise parfois le terme, plus général, de 'chaos ondulatoire'. La limite classique d'un système quantique, qui est obtenue en faisant tendre \hbar vers zéro, correspond au régime dans lequel le système peut être décrit par les équations de la mécanique classique Hamiltonienne. Pour une onde classique, la limite correspondante est la limite des rayons, qui est obtenue en faisant tendre la longueur d'onde λ vers zéro; cette limite peut aussi être décrite par des équations Hamiltoniennes. Il est connu en mécanique Hamiltonienne qu'il existe deux comportements extrêmes de la dynamique: les régimes intégrable et chaotique. Un système intégrable a autant de constantes du mouvement que de degrés de liberté, ce qui permet en général d'obtenir les différentes quantités caractérisant la dynamique sous forme exacte. Les systèmes chaotiques quant à eux n'ont génériquement que leur énergie de conservée, et leur dynamique est plus complexe. Le comportement de ces systèmes peut cependant être décrit statistiquement; cela permet de définir plusieurs degrés de chaos qui forment ce qui est parfois appelé la 'hiérarchie du chaos'. La plupart des systèmes Hamiltoniens sont en réalité caractérisés par la co-existence dans leur espace des phases de zones quasi-intégrables et chaotiques, et leur dynamique est dite 'mixte'. À partir des différentes propriétés dynamiques de la limite des rayons, il est ainsi possible d'obtenir des

informations sur les fréquences et fonctions propres du système ondulatoire correspondant. Cependant, les notions d'intégrabilité et de chaos sont difficiles à transposer dans le cadre de la mécanique quantique ou ondulatoire. Par exemple, des propriétés caractéristiques des systèmes chaotiques que sont l'ergodicité sur un espace des phases bien défini, ou la divergence exponentielle de trajectoires proches ne sont pas directement transposables à la mécanique quantique à cause du principe d'incertitude de Heisenberg et de la linéarité de l'équation de Schrödinger, respectivement. Il a donc été nécessaire de trouver une nouvelle définition du chaos pouvant être appliquée aux systèmes quantiques. Les applications du chaos quantique sont variées et couvrent une très large gamme d'échelles de longueur, des ondes de matière aux ondes sonores dans l'océan, en passant par les cavités laser.

Dans le troisième chapitre de cette thèse, nous revoyons tout d'abord quelques notions de mécanique classique Hamiltonienne telles que les propriétés des systèmes intégrables, chaotiques et mixtes (Sect. 3.1). En ce qui concerne les systèmes quantiques, nous montrons comment obtenir la limite classique, ou limite des rayons, ainsi que comment définir un espace semblable à l'espace des phases en utilisant les distributions de Wigner et Husimi (Sect. 3.2.1). Nous présentons ensuite quelques outils servant à l'analyse statistique des niveaux d'énergie des systèmes quantiques, en particulier dans le cadre de la théorie des matrices aléatoires (Sect. 3.2.2). Une fois que la limite classique est connue, il est possible d'obtenir les niveaux d'énergie et fonctions propres par la quantification semi-classique de la dynamique. Différentes techniques semi-classiques doivent être utilisées pour les systèmes dont la limite classique est intégrable, mixte, ou chaotique; nous distinguerons donc, d'une façon similaire à ce que nous avons fait pour les systèmes classiques, les systèmes quantiques intégrables (Sect. 3.2.3), chaotiques (Sect. 3.2.4), et mixtes (Sect. 3.2.5).

A.4 Chaos ondulatoire dans les étoiles en rotation rapide

Comme nous avons expliqué dans le chapitre premier, la connaissance de la structure asymptotique de base du spectre d'oscillation d'une étoile pulsante facilite grandement son analyse, en particulier pour le processus d'identification des modes. La seule formule asymptotique connue jusqu'alors pouvant fournir une telle information n'est applicable qu'aux étoiles proches de la symétrie sphérique. Dans le but d'étudier le spectre d'oscillations des modes de pression dans les étoiles en rotation rapide, qui sont déformées par la force centrifuge, Lignières et Georgeot (2008, 2009) ont étudié la limite des rayons des ondes de pression dans des modèles d'étoile polytropiques en rotation uniforme. Ils ont montré que la dynamique des rayons acoustiques dans une étoile en rotation rapide n'est pas intégrable, contrairement au cas d'une étoile sans rotation (voir Fig. A.1). En effet, il a été montré que la dynamique des rayons subit une transition vers le chaos de type Kolmogorov-Arnold-Moser lorsque l'on augmente le taux de rotation du modèle d'étoile. Pour les grandes rotations, la dynamique des rayons acoustiques est donc mixte, certaines conditions initiales conduisant à des rayons au comportement régulier et d'autres à un comportement chaotique (voir la Fig. A.2). En accord avec le caractère mixte de la dynamique des rayons, Lignières et Georgeot (2008, 2009) ont montré que dans le régime asymptotique des hautes-fréquences, le spectre d'oscillation des modes de pression peut être décrit comme une superposition de sous-spectres indépendants, chaque sous-spectre pouvant être associé à une zone bien définie de l'espace des phases de la limite des rayons.

Dans ce quatrième chapitre, nous passons en revue les différents résultats obtenus par Lignières et Georgeot sur l'analyse asymptotique des modes de pression dans les étoiles en rotation rapide. En particulier, nous rappelons les résultats obtenus sur la dynamique des rayons acoustiques dans les modèles d'étoile polytropiques en rotation, la classification des modes à partir de leurs distributions de Husimi dans l'espace des phases, et l'analyse statistique des fréquences d'oscillations issues d'un code d'oscillation numérique complet.

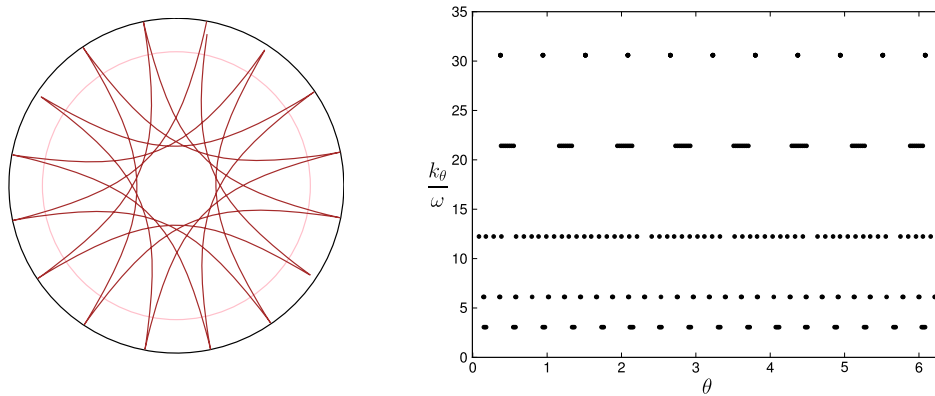


Figure A.1: Rayons acoustiques dans une étoile sans rotation pour $m = 0$ (panneau de gauche). Section de Poincaré associée (panneau de droite) correspondant à la surface à une distance radiale fixe $r = r_p$ de la surface de l'étoile (illustrée par une ligne rose dans le panneau de gauche). Les coordonnées sur la section de Poincaré sont la composante latitudinale du nombre d'onde k_θ normalisée par la fréquence de l'onde ω , ainsi que la colatitude θ .

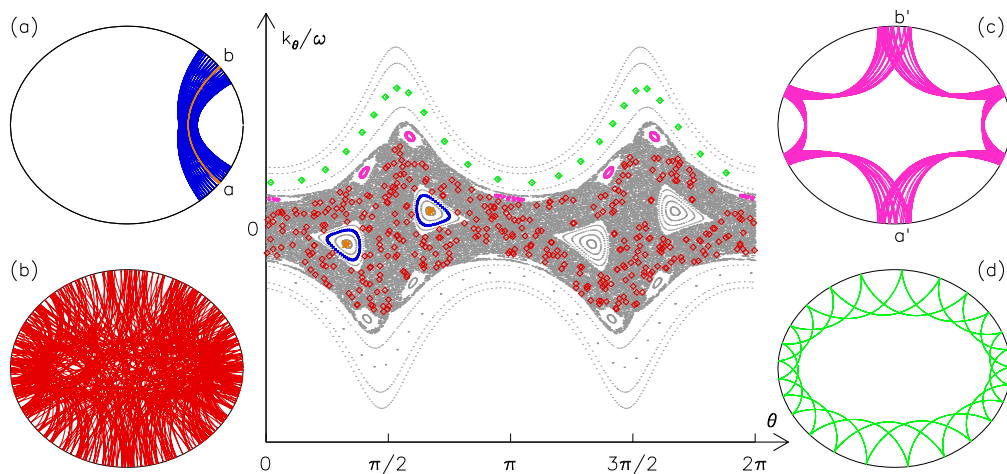


Figure A.2: Section de Poincaré de la dynamique des rayons acoustiques dans un modèle polytropique d'étoile en rotation (panneau central), lorsque la section est choisie comme étant une surface à une distance fixe de la surface de l'étoile et pour un nombre quantique azimuthal $m = 0$. Le modèle d'étoile correspondant est un modèle polytropique avec un taux de rotation de $\Omega/\Omega_K = 0.59$ (où $\Omega_K = \sqrt{GM/R_{\text{eq}}^3}$, R_{eq} étant le rayon équatorial de l'étoile). Les rayons acoustiques correspondants dans l'espace des positions sont tracés dans les panneaux (a), (b), (c) et (d). On peut voir dans ces panneaux: (a) un rayon appartenant à l'îlot stable de période 2 (en bleu) où le rayon périodique central à l'îlot est tracé (en orange); (b): un rayon chaotique (en rouge); (c): un rayon appartenant à l'îlot stable de période 6 (en magenta); (d): un rayon de *whispering gallery* (en vert). Les intersections de ces rayons acoustiques avec la section de Poincaré du panneau central sont également tracées (même couleurs). Les coordonnées sur la section de Poincaré sont les mêmes que celles de la Fig. A.1.

A.5 Modes réguliers dans les étoiles en rotation

Le but de ce cinquième chapitre est de présenter les résultats obtenus pendant ma thèse sur la construction d’une théorie asymptotique pour le sous-spectre des modes réguliers d’étoiles en rotation rapide. Ce sous-spectre, qui peut être associé aux îlots stables de la dynamique des rayons, est particulièrement intéressant pour les observations sismiques car il devrait être le plus simple à détecter et identifier dans les spectres d’étoiles observés. Pour construire cette théorie asymptotique, nous avons adapté la méthode de “l’équation parabolique” (Babich et Buldyrev, 1991), une méthode semi-classique qui a été utilisée précédemment par exemple pour obtenir les résonances de micro-cavités diélectriques de géométrie complexe. La théorie asymptotique développée permet d’obtenir des formules semi-analytiques, évaluées à partir de la dynamique des rayons, donnant les fréquences d’oscillation et fonctions propres des modes de pression localisés autour des rayons acoustiques périodiques stables. L’implémentation numérique de la méthode à partir d’un code de tracé de rayon a été réalisée. Nous avons également utilisé un code d’oscillation numérique bi-dimensionnel complet dans le but de comparer nos résultats semi-classiques avec les fréquences d’oscillations numériques de modèles d’étoiles polytropiques en rotation uniforme dans le régime des hautes-fréquences.

Comme on peut le voir sur la Fig. A.3, nous avons obtenu un bon accord entre les résultats semi-classiques pour les espacements de fréquences et les résultats numériques du code d’oscillation complet pour $m = 0, \pm 1$, et ce pour une large gamme de taux de rotation. Pour la régularité δ_n , l’accord est bon pour tous les taux de rotation à l’exception des rotations faibles. Une différence notable des valeurs de la régularité δ_ℓ existe pour $m = 0$, dans la gamme de rotation pour laquelle le rayon périodique stable au centre de l’îlot bifurque ($\Omega/\Omega_K \sim 0.26$ pour le modèle d’étoile considéré). Cette effet est compréhensible car la bifurcation du rayon central est une limitation connue de notre méthode, qui suppose des rayons périodiques stables isolés, ce qui n’est pas le cas proche d’une bifurcation. Pour $m = 1$, on peut remarquer que le rayon périodique central ne subit pas de bifurcation à ces rotations, et qu’en conséquence l’accord reste bon autour de $\Omega/\Omega_K \sim 0.26$. Aussi, il doit être noté que les fréquences numériques considérées ici sont relativement faibles en comparaison du régime pour lequel les méthodes semi-classiques sont prévues. Ceci peut expliquer la faible différence entre nos valeurs semi-classiques et les valeurs numériques pour δ_n et δ_ℓ que l’on peut trouver à basse rotation, bien que les valeurs semi-classiques tendent vers les résultats du premier ordre de la formule asymptotique de Tassoul.

Comme on peut le voir sur la Fig. A.4, nous avons également obtenu un bon accord entre les coupes équatoriales de distributions d’amplitude de modes obtenues à partir de notre méthode semi-classique et les résultats numériques complets pour de nombreuses valeurs du taux de rotation et des nombres quantiques n , ℓ , et m . Certaines différences sont présentes dans les cas où les effets de bord sur le mode sont importants, par exemple à basse rotation quand l’étendue transverse du mode intersecte l’axe de rotation de l’étoile. Aussi, les effets sur les fonctions propres des couplages de modes lors de croisements évités ne sont pas pris en compte par notre théorie, et ainsi peuvent conduire à des différences dans les distributions d’amplitude des modes.

A.6 Conclusion

Dans cette thèse, nous avons donc étudié un sous-ensemble des modes de pression réguliers des étoiles en rotation rapide, dont les fréquences correspondantes devraient être les plus faciles à détecter et identifier dans les spectres d’oscillation observés. Pour décrire ce spectre nous avons construit une théorie asymptotique en utilisant la méthode de l’équation parabolique, qui utilise la dynamique des rayons. Cette théorie asymptotique permet

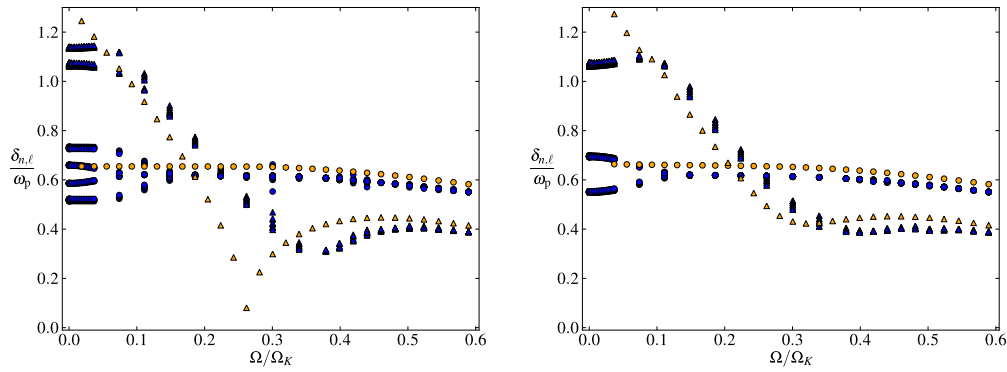


Figure A.3: Espacements de fréquences δ_n (cercles) et δ_ℓ (triangles) séparant les modes réguliers associés aux îlots stables de période 2, calculés à partir des formules semi-classiques Eq. (5.62) (en orange) et à partir du code numérique complet (en bleu), en fonction du taux de rotation Ω/Ω_K . Les espacements de fréquences sont normalisés par $\omega_p = \sqrt{GM/R_p^3}$, où R_p est le rayon polaire du modèle d'étoile. Les espacements de fréquences du panneau de gauche sont pour un nombre quantique azimuthal $m = 0$, et $m = \pm 1$ pour le panneau de droite (d'après Pasek et al., 2012).

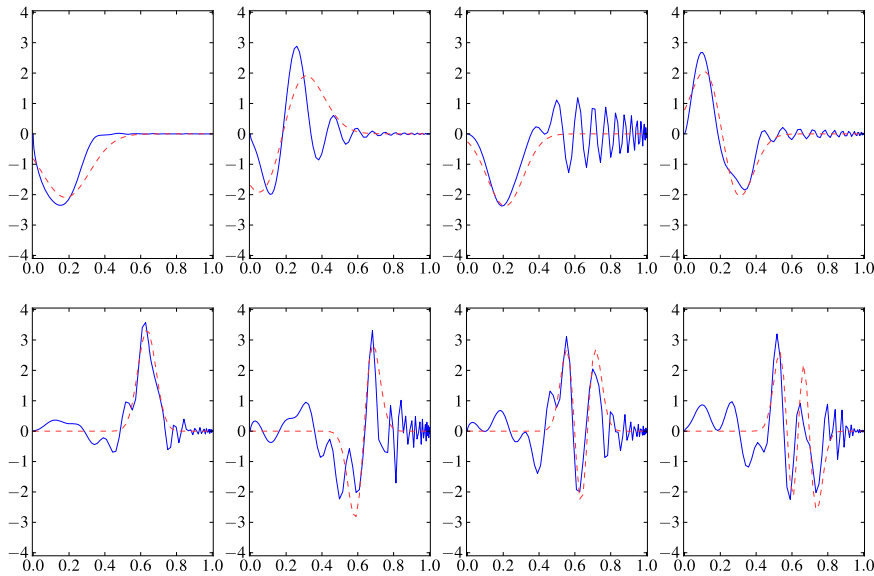


Figure A.4: Coupes équatoriales des distributions d'amplitude normalisées de modes d'oscillation obtenues à partir de la formule semi-classique Eq. (5.58) (partie réelle de Φ_m^ℓ) (ligne rouge en pointillés), et à partir du code d'oscillation numérique (ligne bleue continue), en fonction de la position à l'équateur normalisée r/R_{eq} , où R_{eq} est le rayon équatorial du modèle d'étoile. Les modes d'oscillation correspondant sont $(n, \ell, m) = (50, 0, 0)$, $(50, 1, 0)$, $(50, 0, 1)$ et $(50, 1, 1)$ pour un taux de rotation $\Omega/\Omega_K = 0.300$ (rangée supérieure) et $(n, \ell, m) = (50, 0, 0)$, $(50, 1, 0)$, $(50, 2, 0)$ et $(50, 3, 0)$ pour un taux de rotation $\Omega/\Omega_K = 0.707$ (rangée inférieure) (d'après Pasek et al., 2012).

d'obtenir des expressions semi-analytiques pour les régularités de fréquences et fonctions propres de certains mode de pression. Nous avons obtenu un bon accord entre les valeurs prédites par cette méthode semi-classique et les résultats d'un code d'oscillation numérique bi-dimensionnel complet pour des modèles d'étoile polytropiques en rotation uniforme. Les formules semi-analytiques pour les espacements réguliers de fréquences que nous avons obtenu devraient être utiles pour l'analyse sismique des étoiles en rotation rapide car celles-ci relient des espacements de fréquences observables à des propriétés physiques internes à l'étoile, ce qui devrait servir de guide aux méthodes d'identification de modes.

Bibliography

- C. Aerts, A. Thoul, J. Daszyńska, R. Scuflaire, C. Waelkens, M. A. Dupret, E. Niemczura, and A. Noels. Asteroseismology of HD 129929: Core Overshooting and Nonrigid Rotation. *Science*, 300:1926–1928, June 2003. doi: 10.1126/science.1084993.
- C. Aerts, J. Christensen-Dalsgaard, and D. W. Kurtz. *Asteroseismology*. Astronomy and Astrophysics Library. Springer, 2010. ISBN 9781402051784.
- E. Akkermans and G. Montambaux. *Mesoscopic Physics of Electrons and Photons*. Cambridge University Press, 2007. ISBN 9780521855129.
- G. B. Arfken and H. J. Weber. *Mathematical Methods For Physicists*. Elsevier, 2005. ISBN 9780120598762.
- V. I. Arnol'd. *Mathematical methods of classical mechanics*. Graduate texts in mathematics. Springer-Verlag, 1989. ISBN 9780387968902.
- V. M. Babich and V. S. Buldyrev. *Short-wavelength diffraction theory: asymptotic methods*. Springer series on wave phenomena. Springer-Verlag, 1991. ISBN 9780387191898.
- A. Bäcker and R. Schubert. Amplitude distribution of eigenfunctions in mixed systems. *Journal of Physics A: Mathematical and General*, 35(3):527, 2002.
- A. Bäcker, R. Ketzmerick, S. Löck, M. Robnik, G. Vidmar, R. Höhmann, U. Kuhl, and H.-J. Stöckmann. Dynamical tunneling in mushroom billiards. *Phys. Rev. Lett.*, 100:174103, May 2008. doi: 10.1103/PhysRevLett.100.174103.
- J. Ballot, F. Lignières, V. Prat, D. R. Reese, and M. Rieutord. 2D computations of g modes. *ArXiv e-print 1109.6856*, September 2011.
- J. Ballot, F. Lignières, and D. R. Reese. Numerical exploration of oscillation modes in rapidly rotating stars. In *Studying Stellar Rotation and Convection*, volume 865 of *Lecture Notes in Physics*, Berlin Springer Verlag, 2013.
- N. M. Batalha, W. J. Borucki, S. T. Bryson, L. A. Buchhave, D. A. Caldwell, J. Christensen-Dalsgaard, D. Ciardi, E. W. Dunham, F. Fressin, T. N. Gautier III, R. L. Gilliland, M. R. Haas, S. B. Howell, J. M. Jenkins, H. Kjeldsen, D. G. Koch, D. W. Latham, J. J. Lissauer, G. W. Marcy, J. F. Rowe, D. D. Sasselov, S. Seager, J. H. Steffen, G. Torres, G. S. Basri, T. M. Brown, D. Charbonneau, J. Christiansen, B. Clarke, W. D. Cochran, A. Dupree, D. C. Fabrycky, D. Fischer, E. B. Ford, J. Fortney, F. R. Girouard, M. J. Holman, J. Johnson, H. Isaacson, T. C. Klaus, P. Machalek, A. V. Moorehead, R. C. Morehead, D. Ragozzine, P. Tenenbaum, J. Twicken, S. Quinn, J. VanCleve, L. M. Walkowicz, W. F. Welsh, E. Devore, and A. Gould. Kepler's First Rocky Planet: Kepler-10b. *The Astrophysical Journal*, 729(1):27, 2011.
- P. G. Beck, J. Montalbán, T. Kallinger, J. De Ridder, C. Aerts, R. A. García, S. Hekker, M.-A. Dupret, B. Mosser, P. Eggenberger, D. Stello, Y. Elsworth, S. Frandsen, F. Carrier, M. Hillen, M. Gruberbauer, J. Christensen-Dalsgaard, A. Miglio, M. Valentini,

- T. R. Bedding, H. Kjeldsen, F. R. Girouard, J. R. Hall, and K. A. Ibrahim. Fast core rotation in red-giant stars as revealed by gravity-dominated mixed modes. *Nature*, 481: 55–57, January 2012. doi: 10.1038/nature10612.
- T. R. Bedding and H. Kjeldsen. Solar-like Oscillations. *PASA*, 20:203–212, 2003. doi: 10.1071/AS03025.
- G. Benenti, G. Casati, S. Montangero, and D.L. Shepelyansky. Eigenstates of an operating quantum computer: hypersensitivity to static imperfections. *The European Physical Journal D - Atomic, Molecular, Optical and Plasma Physics*, 20:293–296, 2002. ISSN 1434-6060. doi: 10.1140/epjd/e2002-00127-x.
- M. V. Berry. Regular and irregular semiclassical wavefunctions. *Journal of Physics A Mathematical General*, 10:2083–2091, December 1977. doi: 10.1088/0305-4470/10/12/016.
- M. V. Berry. Some quantum-to-classical asymptotics. In M.-J. Giannoni, A. Voros & J. Zinn-Justin, editor, *Chaos and Quantum Physics - Les Houches Lectures Session LIII*, pages 251–303, 1991.
- M. V. Berry. Martin Gutzwiller and his periodic orbits. In *The legacy of Martin Gutzwiller*, volume 37 of *Commun. Swiss Phys. Soc.*, pages 23–30. 2012.
- M. V. Berry and M. Robnik. Semiclassical level spacings when regular and chaotic orbits coexist. *Journal of Physics A Mathematical General*, 17:2413–2421, August 1984. doi: 10.1088/0305-4470/17/12/013.
- M. V. Berry and M. Tabor. Closed orbits and the regular bound spectrum. *Proceedings of the Royal Society of London. A. Mathematical and Physical Sciences*, 349(1656): 101–123, 1976. doi: 10.1098/rspa.1976.0062.
- M. V. Berry and M. Tabor. Level Clustering in the Regular Spectrum. *Royal Society of London Proceedings Series A*, 356:375–394, September 1977. doi: 10.1098/rspa.1977.0140.
- R. Blümel, T. M. Antonsen, Jr., B. Georgeot, E. Ott, and R. E. Prange. Ray splitting and quantum chaos. *Phys. Rev. Lett.*, 76:2476–2479, Apr 1996. doi: 10.1103/PhysRevLett.76.2476.
- E. Bogomolny. Quantum and arithmetical chaos. In Pierre Cartier, Bernard Julia, Pierre Moussa, and Pierre Vanhove, editors, *Frontiers in Number Theory, Physics, and Geometry I*, pages 3–106. Springer Berlin Heidelberg, 2006. ISBN 978-3-540-31347-2.
- E. Bogomolny and O. Giraud. Eigenfunction entropy and spectral compressibility for critical random matrix ensembles. *Phys. Rev. Lett.*, 106:044101, Jan 2011. doi: 10.1103/PhysRevLett.106.044101.
- O. Bohigas. Random matrix theories and chaotic dynamics. In M.-J. Giannoni, A. Voros & J. Zinn-Justin, editor, *Chaos and Quantum Physics - Les Houches Lectures Session LIII*, pages 87–199, 1991.
- O. Bohigas, M.-J. Giannoni, and C. Schmit. Characterization of Chaotic Quantum Spectra and Universality of Level Fluctuation Laws. *Physical Review Letters*, 52:1–4, January 1984. doi: 10.1103/PhysRevLett.52.1.
- O. Bohigas, S. Tomsovic, and D. Ullmo. Manifestations of classical phase space structures in quantum mechanics. *Physics Reports*, 223(2):43 – 133, 1993. ISSN 0370-1573. doi: 10.1016/0370-1573(93)90109-Q.

- S. Bonazzola, E. Gourgoulhon, and J.-A. Marck. Numerical approach for high precision 3D relativistic star models. *Phys. Rev. D*, 58(10):104020, November 1998. doi: 10.1103/PhysRevD.58.104020.
- R. W. Brankin and I. Gladwell. A Fortran 90 version of RKSUITE: an ODE initial value solver. *Ann. Numer. Math.*, 1(1-4):363–375, 1994. ISSN 1021-2655.
- M. G. Brown, J. A. Colosi, S. Tomsovic, A. L. Virovlyansky, M. A. Wolfson, and G. M. Zaslavsky. Ray dynamics in long-range deep ocean sound propagation. *The Journal of the Acoustical Society of America*, 113(5):2533–2547, 2003. doi: 10.1121/1.1563670.
- J. R. Buchler, T. Serre, Z. Kolláth, and J. Mattei. A Chaotic Pulsating Star: The Case of R Scuti. *Phys. Rev. Lett.*, 74:842–845, Feb 1995. doi: 10.1103/PhysRevLett.74.842.
- J. R. Buchler, Z. Kolláth, and R. R. Cadmus Jr. Evidence for low-dimensional chaos in semiregular variable stars. *The Astrophysical Journal*, 613(1):532, 2004.
- J. K. Carlberg, S. R. Majewski, and P. Arras. The Role of Planet Accretion in Creating the Next Generation of Red Giant Rapid Rotators. *ApJ*, 700:832–843, July 2009. doi: 10.1088/0004-637X/700/1/832.
- J. K. Carlberg, S. R. Majewski, R. J. Patterson, D. Bizyaev, V. V. Smith, and K. Cunha. The Frequency of Rapid Rotation Among K Giant Stars. *The Astrophysical Journal*, 732(1):39, 2011.
- F. Carrier, J. De Ridder, F. Baudin, C. Barban, A. P. Hatzes, S. Hekker, T. Kallinger, A. Miglio, J. Montalbán, T. Morel, W. W. Weiss, M. Auvergne, A. Baglin, C. Catala, E. Michel, and R. Samadi. Non-radial oscillations in the red giant HR 7349 measured by CoRoT. *A&A*, 509:A73, January 2010. doi: 10.1051/0004-6361/200912749.
- B. W. Carroll and D. A. Ostlie. *An Introduction to Modern Astrophysics*. Addison-Wesley, 1996.
- J.-S. Caux and J. Mossel. Remarks on the notion of quantum integrability. *Journal of Statistical Mechanics: Theory and Experiment*, 2011(02):P02023, 2011.
- S.-J. Chang and K.-J. Shi. Evolution and exact eigenstates of a resonant quantum system. *Phys. Rev. A*, 34:7–22, Jul 1986. doi: 10.1103/PhysRevA.34.7.
- J. Christensen-Dalsgaard. A Hertzsprung-Russell Diagram for Stellar Oscillations. In J. Christensen-Dalsgaard and S. Frandsen, editors, *Advances in Helio- and Asteroseismology*, volume 123 of *IAU Symposium*, page 295, 1988.
- J. Christensen-Dalsgaard. Helioseismology. *Rev. Mod. Phys.*, 74:1073–1129, November 2002. doi: 10.1103/RevModPhys.74.1073.
- J. Christensen-Dalsgaard. *Lecture Notes on Stellar Oscillations*. 2003.
- A. Claverie, G. R. Isaak, C. P. McLeod, H. B. van der Raay, and T. R. Cortes. Solar structure from global studies of the 5-minute oscillation. *Nature*, 282:591–594, December 1979. doi: 10.1038/282591a0.
- M. J. Clement. Normal modes of oscillation for rotating stars. I - The effect of rigid rotation on four low-order pulsations. *ApJ*, 249:746–760, October 1981. doi: 10.1086/159335.
- C. Cohen-Tannoudji, B. Diu, and F. Laloë. *Mécanique quantique I*. Collection enseignement des sciences. Hermann, 1973.

- T. G. Cowling. The non-radial oscillations of polytropic stars. *MNRAS*, 101:367, 1941.
- T. G. Cowling and R. A. Newing. The Oscillations of a Rotating Star. *ApJ*, 109:149, January 1949. doi: 10.1086/145114.
- M. J. Davis and E. J. Heller. Quantum dynamical tunneling in bound states. *The Journal of Chemical Physics*, 75(1):246–254, 1981. doi: 10.1063/1.441832.
- D. Delande. Chaos in atomic and molecular physics. In M.-J. Giannoni, A. Voros & J. Zinn-Justin, editor, *Chaos and Quantum Physics - Les Houches Lectures Session LIII*, pages 665–726, 1991.
- D. Delande. Quantum chaos in atomic physics. In R. Kaiser, C. Westbrook, and F. David, editors, *Coherent atomic matter waves*, volume 72 of *Les Houches*, pages 415–479. Springer Berlin / Heidelberg, 2001. ISBN 978-3-540-41047-8.
- M. Desmet, M. Briquet, A. Thoul, W. Zima, P. De Cat, G. Handler, I. Ilyin, E. Kambe, J. Krzesinski, H. Lehmann, S. Masuda, P. Mathias, D. E. Mkrtychian, J. Teltig, K. Uytterhoeven, S. L. S. Yang, and C. Aerts. An asteroseismic study of the β Cephei star 12 Lacertae: multisite spectroscopic observations, mode identification and seismic modelling. *MNRAS*, 396:1460–1472, July 2009. doi: 10.1111/j.1365-2966.2009.14790.x.
- R. G. Deupree. Stellar evolution with arbitrary rotation laws. I - Mathematical techniques and test cases. *ApJ*, 357:175–187, July 1990. doi: 10.1086/168903.
- R. G. Deupree. Stellar evolution with arbitrary rotation laws. II - Massive star evolution to core hydrogen exhaustion. *ApJ*, 439:357–364, January 1995. doi: 10.1086/175179.
- R. G. Deupree. Stellar Evolution with Arbitrary Rotation Laws. III. Convective Core Overshoot and Angular Momentum Distribution. *ApJ*, 499:340, May 1998. doi: 10.1086/305605.
- B. Dintrans and M. Rieutord. Oscillations of a rotating star: a non-perturbative theory. *A&A*, 354:86–98, February 2000.
- M.-A. Dupret, A. Thoul, R. Scuflaire, J. Daszyńska-Daszkiewicz, C. Aerts, P.-O. Bourge, C. Waelkens, and A. Noels. Asteroseismology of the β Cep star HD 129929. II. Seismic constraints on core overshooting, internal rotation and stellar parameters. *A&A*, 415: 251–257, February 2004. doi: 10.1051/0004-6361:20034143.
- W. A. Dziembowski and P. R. Goode. Effects of differential rotation on stellar oscillations - A second-order theory. *ApJ*, 394:670–687, August 1992. doi: 10.1086/171621.
- B. Eckhardt. Quantum mechanics of classically non-integrable systems. *Physics Reports*, 163(4):205 – 297, 1988. ISSN 0370-1573. doi: 10.1016/0370-1573(88)90130-5.
- A. Einstein. *Zum Quantensatz von Sommerfeld und Epstein*. Verhandlungen der Deutschen Physikalischen Gesellschaft. Friedr. Vieweg & Sohn, 1917.
- C. Ellegaard, T. Guhr, K. Lindemann, J. Nygård, and M. Oxborrow. Symmetry breaking and spectral statistics of acoustic resonances in quartz blocks. *Phys. Rev. Lett.*, 77: 4918–4921, Dec 1996. doi: 10.1103/PhysRevLett.77.4918.
- Y. P. Elsworth and M. J. Thompson. Asteroseismology: Asteroseismology of Sun-like stars. *Astronomy and Geophysics*, 45(5):050000–5, October 2004. doi: 10.1046/j.1468-4004.2003.45514.x.

- L. Eyer and N. Mowlavi. Variable stars across the observational HR diagram. *Journal of Physics Conference Series*, 118(1):012010, October 2008. doi: 10.1088/1742-6596/118/1/012010.
- K. M. Frahm, R. Fleckinger, and D. L. Shepelyansky. Quantum chaos and random matrix theory for fidelity decay in quantum computations with static imperfections. *The European Physical Journal D - Atomic, Molecular, Optical and Plasma Physics*, 29:139–155, 2004. ISSN 1434-6060. 10.1140/epjd/e2004-00038-x.
- W. Gander, G. H. Golub, and R. Strebler. Least-squares fitting of circles and ellipses. *BIT Numerical Mathematics*, 34:558–578, 1994. ISSN 0006-3835. 10.1007/BF01934268.
- A. García Hernández, A. Moya, E. Michel, R. Garrido, J. C. Suárez, E. Rodríguez, P. J. Amado, S. Martín-Ruiz, A. Rolland, E. Poretti, R. Samadi, A. Baglin, M. Auvergne, C. Catala, L. Lefevre, and F. Baudin. Asteroseismic analysis of the CoRoT δ Scuti star HD 174936. *A&A*, 506:79–83, October 2009. doi: 10.1051/0004-6361/200911932.
- P. Gaulme, F.-X. Schmider, J. Gay, T. Guillot, and C. Jacob. Detection of jovian seismic waves: a new probe of its interior structure. *A&A*, 531:A104, 2011. doi: 10.1051/0004-6361/201116903.
- M.-J. Giannoni, A. Voros, and J. Zinn-Justin. *Chaos and quantum physics - Les Houches Lectures Session LII*. Les Houches Summer School Proceedings Series. North-Holland, 1991. ISBN 9780444892775.
- J. F. González, S. Hubrig, D. W. Kurtz, V. Elkin, and I. Savanov. Discovery of pulsational line profile variations in the δ Scuti star HD21190 and in the Ap Sr star HD218994. *MNRAS*, 384:1140–1144, March 2008. doi: 10.1111/j.1365-2966.2007.12779.x.
- J. Goodricke and J. Bayer. a Series of Observations on, and a Discovery of, the Period of the Variation of the Light of the Star Marked δ by Bayer, Near the Head of Cepheus. in a Letter from John Goodricke, Esq. to Nevil Maskelyne, D. D. F. R. S. and Astronomer Royal. *Royal Society of London Philosophical Transactions Series I*, 76:48–61, 1786.
- D. O. Gough. EBK Quantization of Stellar Waves. In Y. Osaki, editor, *Hydrodynamic and Magnetodynamic Problems in the Sun and Stars*, page 117, 1986.
- D. O. Gough. Linear adiabatic stellar pulsation. In J.-P. Zahn & J. Zinn-Justin, editor, *Astrophysical Fluid Dynamics - Les Houches 1987*, pages 399–560, 1993.
- D. O. Gough and M. J. Thompson. The effect of rotation and a buried magnetic field on stellar oscillations. *MNRAS*, 242:25–55, January 1990.
- M. J. Goupil. Effects of Rotation on Stellar p-Mode Frequencies. In *The Rotation of Sun and Stars*, volume 765 of *Lecture Notes in Physics*, Berlin Springer Verlag, pages 45–99, 2009. doi: 10.1007/978-3-540-87831-5_3.
- T. Guhr, A. Müller-Groeling, and H. A. Weidenmüller. Random-matrix theories in quantum physics: common concepts. *Phys. Rep.*, 299:189–425, June 1998. doi: 10.1016/S0370-1573(97)00088-4.
- T. Guillot. Probing the Giant Planets. *Physics Today*, 57(4):63–69, 2004. doi: 10.1063/1.1752424.
- M. C. Gutzwiller. *Chaos in classical and quantum mechanics*. Interdisciplinary applied mathematics. Springer-Verlag, 1990. ISBN 9780387971735.

- M. C. Gutzwiller. The semi-classical quantization of chaotic Hamiltonian systems. In M.-J. Giannoni, A. Voros & J. Zinn-Justin, editor, *Chaos and Quantum Physics - Les Houches Lectures Session LII*, pages 201–249, 1991.
- M. C. Gutzwiller. Quantum chaos. *Scientific American*, 266:78–84, January 1992. doi: 10.1038/scientificamerican0192-78.
- F. Haake. *Quantum Signatures of Chaos*. Springer Berlin Heidelberg, 2010. ISBN 9783642102592.
- G. Handler. Asteroseismology. arXiv:1205.6407, May 2012.
- C. J. Hansen, S. D. Kawaler, and V. Trimble. *Stellar interiors : physical principles, structure, and evolution, 2nd ed.* New York: Springer-Verlag, 2004.
- E. J. Heller. Bound-state eigenfunctions of classically chaotic hamiltonian systems: Scars of periodic orbits. *Phys. Rev. Lett.*, 53:1515–1518, Oct 1984. doi: 10.1103/PhysRevLett.53.1515.
- K. Karami. Third Order Effect of Rotation on Stellar Oscillations of a B Star. *Chinese J. Astron. Astrophys.*, 8:285–308, June 2008. doi: 10.1088/1009-9271/8/3/06.
- J. B. Keller and S. I. Rubinow. Asymptotic solution of eigenvalue problems. *Annals of Physics*, 9:24–75, January 1960. doi: 10.1016/0003-4916(60)90061-0.
- R. Kippenhahn and A. Weigert. *Stellar structure and evolution*. Astronomy and astrophysics library. Springer-Verlag, 1994. ISBN 9783540580133.
- H. Kjeldsen, T. R. Bedding, M. Viskum, and S. Frandsen. Solarlike oscillations in eta Boo. *AJ*, 109:1313–1319, March 1995. doi: 10.1086/117363.
- H. Kjeldsen, T. R. Bedding, and J. Christensen-Dalsgaard. Measurements of Stellar Properties through Asteroseismology: A Tool for Planet Transit Studies. *Proceedings of the International Astronomical Union*, 4(Symposium S253):309–317, 2008. doi: 10.1017/S1743921308026537.
- M. Kuś, F. Haake, and D. Delande. Prebifurcation periodic ghost orbits in semiclassical quantization. *Phys. Rev. Lett.*, 71:2167–2171, Oct 1993. doi: 10.1103/PhysRevLett.71.2167.
- L. D. Landau and E. M. Lifshitz. *Fluid mechanics*. Course of theoretical physics, Oxford: Pergamon Press, 1959.
- E. Larose, L. Margerin, B. A. van Tiggelen, and M. Campillo. Weak localization of seismic waves. *Phys. Rev. Lett.*, 93:048501, Jul 2004. doi: 10.1103/PhysRevLett.93.048501.
- P. Ledoux. The Nonradial Oscillations of Gaseous Stars and the Problem of Beta Canis Majoris. *ApJ*, 114:373, November 1951. doi: 10.1086/145477.
- O. Legrand, C. Schmit, and D. Sornette. Quantum chaos methods applied to high-frequency plate vibrations. *EPL (Europhysics Letters)*, 18(2):101, 1992.
- R. B. Leighton, R. W. Noyes, and G. W. Simon. Velocity Fields in the Solar Atmosphere. I. Preliminary Report. *ApJ*, 135:474, March 1962. doi: 10.1086/147285.
- A. J. Lichtenberg and M. A. Lieberman. *Regular and stochastic motion*. Springer-Verlag, 1983.

- F. Lignières and B. Georgeot. Wave chaos in rapidly rotating stars. *Phys. Rev. E*, 78(1): 016215, July 2008. doi: 10.1103/PhysRevE.78.016215.
- F. Lignières and B. Georgeot. Asymptotic analysis of high-frequency acoustic modes in rapidly rotating stars. *A&A*, 500:1173–1192, June 2009. doi: 10.1051/0004-6361/200811165.
- F. Lignières, M. Rieutord, and D. Reese. Acoustic oscillations of rapidly rotating polytropic stars. I. Effects of the centrifugal distortion. *A&A*, 455:607–620, August 2006. doi: 10.1051/0004-6361:20065015.
- F. Lignières, B. Georgeot, and J. Ballot. P-modes in rapidly rotating stars: Looking for regular patterns in synthetic asymptotic spectra. *Astronomische Nachrichten*, 331:1053, December 2010. doi: 10.1002/asna.201011455.
- A. Maeder. *Physics, Formation and Evolution of Rotating Stars*. Springer Berlin Heidelberg, 2009. doi: 10.1007/978-3-540-76949-1.
- A. Maeder and G. Meynet. Rotating massive stars: From first stars to gamma ray bursts. *Rev. Mod. Phys.*, 84:25–63, Jan 2012. doi: 10.1103/RevModPhys.84.25.
- L. Mantegazza, E. Poretti, E. Michel, M. Rainer, F. Baudin, A. García Hernández, T. Seaman, M. Alvarez, P. J. Amado, R. Garrido, P. Mathias, A. Moya, J. C. Suarez, M. Auvergne, A. Baglin, C. Catala, and R. Samadi. Pulsation spectrum of Delta Sct stars: the binary HD 50870 as seen with CoRoT and HARPS. *ArXiv e-print 1203.0221*, March 2012.
- L. Mehta. *Random Matrices*. Number v. 142 in Pure and Applied Mathematics. Elsevier/Academic Press, 2004. ISBN 9780120884094.
- W. H. Miller. Semiclassical quantization of nonseparable systems: A new look at periodic orbit theory. *J. Chem. Phys.*, 63:996–999, July 1975. doi: 10.1063/1.431410.
- J. D. Monnier, M. Zhao, E. Pedretti, N. Thureau, M. Ireland, P. Muirhead, J.-P. Berger, R. Millan-Gabet, G. Van Belle, T. ten Brummelaar, H. McAlister, S. Ridgway, N. Turner, L. Sturmann, J. Sturmann, and D. Berger. Imaging the Surface of Altair. *Science*, 317:342–, July 2007. doi: 10.1126/science.1143205.
- B. Mosser. The pressure mode oscillation spectrum of a rotating gaseous sphere: Application to jupiter. *Icarus*, 87(1):198 – 209, 1990. ISSN 0019-1035. doi: 10.1016/0019-1035(90)90030-D.
- J. U. Nöckel and A. D. Stone. Ray and wave chaos in asymmetric resonant optical cavities. *Nature*, 385:45–47, January 1997. doi: 10.1038/385045a0.
- S. Nonnenmacher. Anatomy of quantum chaotic eigenstates. arXiv:1005.5598, January 2012.
- E. Ott. *Chaos in Dynamical Systems*. Cambridge University Press, 2002. ISBN 9780521010849.
- R.-M. Ouazzani, M.-A. Dupret, and D. R. Reese. Pulsations of rapidly rotating stars. *A&A*, 547:A75, 2012. doi: 10.1051/0004-6361/201219548.
- J. C. Papaloizou and J. E. Pringle. Numerical computations of the oscillations of rapidly rotating white dwarfs. *MNRAS*, 190:43–53, January 1980.

- M. Pasek and B. Georgeot. Regular and irregular pressure modes in rapidly rotating stars. In *Studying Stellar Rotation and Convection*, volume 865 of *Lecture Notes in Physics*, Berlin Springer Verlag, 2013.
- M. Pasek, B. Georgeot, F. Lignières, and D. R. Reese. Regular Modes in Rotating Stars. *Physical Review Letters*, 107(12):121101, September 2011. doi: 10.1103/PhysRevLett.107.121101.
- M. Pasek, F. Lignières, B. Georgeot, and D. R. Reese. Regular oscillation sub-spectrum of rapidly rotating stars. *A&A*, 546:A11, October 2012. doi: 10.1051/0004-6361/201219716.
- I. C. Percival. Regular and irregular spectra. *Journal of Physics B Atomic Molecular Physics*, 6:L229–L232, September 1973. doi: 10.1088/0022-3700/6/9/002.
- J. Perdang. Introductory report : Non-linear Dynamics and Stellar Oscillations. In *Liege International Astrophysical Colloquia*, volume 25 of *Liege International Astrophysical Colloquia*, pages 425–453, 1984.
- J. Perdang. Asymptotics and quantum chaos in stellar oscillations. In D. O. Gough, editor, *NATO ASIC Proc. 169: Seismology of the Sun and the Distant Stars*, pages 141–171, 1986.
- J. Perdang. Stellar Acoustic Ray Patterns. In J. Christensen-Dalsgaard and S. Frandsen, editors, *Advances in Helio- and Asteroseismology*, volume 123 of *IAU Symposium*, page 125, 1988.
- H. Poincaré. Sur le problème des trois corps et les équations de la dynamique. *Acta Mathematica*, 13:A3–A270, 1890. ISSN 0001-5962. 10.1007/BF02392506.
- W. H. Press, S. A. Teukolsky, W. T. Vetterling, and B. P. Flannery. *Numerical recipes in FORTRAN. The art of scientific computing*. Cambridge: University Press, 1992.
- W. H. Press, S. A. Teukolsky, W. T. Vetterling, and B. P. Flannery. *Numerical Recipes 3rd Edition: The Art of Scientific Computing*. Cambridge University Press, 2007. ISBN 9780521880688.
- D. Reese. *La modélisation des oscillations d'étoiles en rotation rapide*. PhD thesis, Université Toulouse III - Paul Sabatier, 2006.
- D. Reese, F. Lignières, and M. Rieutord. Acoustic oscillations of rapidly rotating polytropic stars. II. Effects of the Coriolis and centrifugal accelerations. *A&A*, 455:621–637, August 2006. doi: 10.1051/0004-6361:20065269.
- D. Reese, F. Lignières, and M. Rieutord. Regular patterns in the acoustic spectrum of rapidly rotating stars. *A&A*, 481:449–452, April 2008. doi: 10.1051/0004-6361:20078075.
- D. R. Reese. Oscillations in rapidly rotating stars. *Astronomische Nachrichten*, 331:1038, December 2010. doi: 10.1002/asna.201011452.
- D. R. Reese, K. B. MacGregor, S. Jackson, A. Skumanich, and T. S. Metcalfe. Pulsation modes in rapidly rotating stellar models based on the self-consistent field method. *A&A*, 506:189–201, October 2009. doi: 10.1051/0004-6361/200811510.
- L. E. Reichl. *The Transition to Chaos: Conservative Classical Systems and Quantum Manifestations*. Institute for Nonlinear Science. Springer, 2004. ISBN 9780387987880.

- M. Rieutord. Approaching the Low-Frequency Spectrum of Rotating Stars. In J.-P. Rozelot and C. Neiner, editors, *The Rotation of Sun and Stars*, volume 765 of *Lecture Notes in Physics*, Berlin Springer Verlag, pages 101–121, 2009. doi: 10.1007/978-3-540-87831-5_4.
- M. Rieutord, T. Corbard, B. Pichon, B. Dintrans, and F. Lignières. The ESTER project. In F. Casoli, T. Contini, J. M. Hameury, and L. Pagani, editors, *SF2A-2005: Semaine de l’Astrophysique Francaise*, page 759, December 2005.
- A. L. Rosen, M. R. Krumholz, and E. Ramirez-Ruiz. What Sets the Initial Rotation Rates of Massive Stars? *ApJ*, 748:97, April 2012. doi: 10.1088/0004-637X/748/2/97.
- F. Royer. On the Rotation of A-Type Stars. In *The Rotation of Sun and Stars*, volume 765 of *Lecture Notes in Physics*, Berlin Springer Verlag, pages 207–230, 2009. doi: 10.1007/978-3-540-87831-5_9.
- F. Royer, J. Zorec, and A. E. Gómez. Rotational velocities of A-type stars. III. Velocity distributions. *A&A*, 463:671–682, February 2007. doi: 10.1051/0004-6361:20065224.
- H. Saio. Rotational and tidal perturbations of nonradial oscillations in a polytropic star. *ApJ*, 244:299–315, February 1981. doi: 10.1086/158708.
- R. Schack and C. M. Caves. Hypersensitivity to perturbations in the quantum baker’s map. *Phys. Rev. Lett.*, 71:525–528, Jul 1993. doi: 10.1103/PhysRevLett.71.525.
- E. Schatzman. A theory of the role of magnetic activity during star formation. *Annales d’Astrophysique*, 25:18, February 1962.
- A. I. Schnirelman. Ergodic properties of eigenfunctions. *Usp. Mat. Nauk*, 29(6(180)): 181–182, 1974. ISSN 0042-1316.
- H. Schomerus and M. Sieber. Bifurcations of periodic orbits and uniform approximations. *Journal of Physics A Mathematical General*, 30:4537–4562, July 1997. doi: 10.1088/0305-4470/30/13/010.
- L. S. Schulman. *Techniques and Applications of Path Integration*. Dover Books on Physics Series. Dover Publications, 2005. ISBN 9780486445281.
- H. G. L. Schwefel, H. E. Tureci, A. D. Stone, and R. K. Chang. Progress in asymmetric resonant cavities; using shape as a design parameter in dielectric microcavity lasers. *Optical Microcavities*, pages 415–496, 2004.
- R. Shankar. *Principles of Quantum Mechanics*. Springer, 1994. ISBN 9780306447907.
- A. E. Siegman. *Lasers*. University Science Books, 1986. ISBN 9780935702118.
- R. Simon. Rotational Perturbation of a Radial Oscillation Gaseous Star. *A&A*, 2:390, August 1969.
- P. Smeyers and J. Denis. Second Order Rotational Perturbation of Non-Radial Oscillations of a Star. *A&A*, 14:311, September 1971.
- P. So, S. M. Anlage, E. Ott, and R. N. Oerter. Wave Chaos Experiments with and without Time Reversal Symmetry: GUE and GOE Statistics. *Phys. Rev. Lett.*, 74:2662–2665, Apr 1995. doi: 10.1103/PhysRevLett.74.2662.
- F. Soufi, M. J. Goupil, and W. A. Dziembowski. Effects of moderate rotation on stellar pulsation. I. Third order perturbation formalism. *A&A*, 334:911–924, June 1998.

- A. Steane. Quantum computing. *Reports on Progress in Physics*, 61(2):117, 1998.
- H.-J. Stöckmann and J. Stein. “Quantum” chaos in billiards studied by microwave absorption. *Phys. Rev. Lett.*, 64:2215–2218, May 1990. doi: 10.1103/PhysRevLett.64.2215.
- A. D. Stone. Einstein’s Unknown Insight and the Problem of Quantizing Chaos. *Physics Today*, 58(8):080000–43, August 2005. doi: 10.1063/1.2062917.
- J. C. Suárez, M. J. Goupil, and P. Morel. Effects of moderately fast shellular rotation on adiabatic oscillations. *A&A*, 449:673–685, April 2006. doi: 10.1051/0004-6361:20054181.
- M. Tassoul. Asymptotic approximations for stellar nonradial pulsations. *ApJS*, 43:469–490, August 1980. doi: 10.1086/190678.
- M. J. Thompson, J. Toomre, E. R. Anderson, H. M. Antia, G. Berthomieu, D. Burtonclay, S. M. Chitre, J. Christensen-Dalsgaard, T. Corbard, M. DeRosa, C. R. Genovese, D. O. Gough, D. A. Haber, J. W. Harvey, F. Hill, R. Howe, S. G. Korzennik, A. G. Kosovichev, J. W. Leibacher, F. P. Pijpers, J. Provost, E. J. Rhodes, J. Schou, T. Sekii, P. B. Stark, and P. R. Wilson. Differential rotation and dynamics of the solar interior. *Science*, 272(5266):1300–1305, 1996. doi: 10.1126/science.272.5266.1300.
- S. Tomsovic. Tunneling and chaos. *Physica Scripta*, 2001(T90):162, 2001.
- R. Townsend. A cartoon overview of the fundamentals of stellar seismology. KITP Blackboard Lunch, 2011.
- S. Turck-Chièze, S. Couvidat, L. Piau, J. Ferguson, P. Lambert, J. Ballot, R. A. García, and P. Nghiem. Surprising sun: A new step towards a complete picture? *Phys. Rev. Lett.*, 93:211102, Nov 2004. doi: 10.1103/PhysRevLett.93.211102.
- H. E. Tureci, H. G. L. Schwefel, A. D. Stone, and E. E. Narimanov. Gaussian-optical approach to stable periodic orbit resonances of partially chaotic dielectric micro-cavities. *Optics Express*, 10:752, August 2002.
- H. E. Tureci, H. G. L. Schwefel, Ph. Jacquod, and A. D. Stone. Modes of wave-chaotic dielectric resonators. In Emil Wolf, editor, *Progress in Optics*, volume 47 of *Progress in Optics*, pages 75 – 137. Elsevier, 2005. doi: 10.1016/S0079-6638(05)47002-X.
- D. Ullmo, M. Grinberg, and S. Tomsovic. Near-integrable systems: Resonances and semiclassical trace formulas. *Phys. Rev. E*, 54:136–152, Jul 1996. doi: 10.1103/PhysRevE.54.136.
- W. Unno, Y. Osaki, H. Ando, H. Saio, and H. Shibahashi. *Nonradial oscillations of stars*. Tokyo: University of Tokyo Press, 1989.
- K. Uytterhoeven, A. Moya, A. Grigahcène, J. A. Guzik, J. Gutiérrez-Soto, B. Smalley, G. Handler, L. A. Balona, E. Niemczura, L. Fox Machado, S. Benatti, E. Chapellier, A. Tkachenko, R. Szabó, J. C. Suárez, V. Ripepi, J. Pascual, P. Mathias, S. Martín-Ruiz, H. Lehmann, J. Jackiewicz, S. Hekker, M. Gruberbauer, R. A. García, X. Dumusque, D. Díaz-Fraile, P. Bradley, V. Antoci, M. Roth, B. Leroy, S. J. Murphy, P. De Cat, J. Cuypers, H. Kjeldsen, J. Christensen-Dalsgaard, M. Breger, A. Pigulski, L. L. Kiss, M. Still, S. E. Thompson, and J. Van Cleve. The Kepler characterization of the variability among A- and F-type stars. *A&A*, 534:A125, 2011. doi: 10.1051/0004-6361/201117368.
- A. Vagov, H. Schomerus, and V. V. Zalipaev. Asymptotic-boundary-layer method for unstable trajectories: Semiclassical expansions for individual scar wave functions. *Phys. Rev. E*, 80(5):056202, November 2009. doi: 10.1103/PhysRevE.80.056202.

- Y. V. Vandakurov. The Frequency Distribution of Stellar Oscillations. *AZh*, 44:786, 1967.
- S. V. Vorontsov. Natural oscillations of the giant planets - The influence of differential rotation. *AZh*, 58:1275–1285, December 1981.
- A. Voros. Semi-classical approximations. *Ann. Inst. H. Poincaré Sect. A (N.S.)*, 24(1): 31–90, 1976.
- A. Voros. Semi-classical ergodicity of quantum eigenstates in the Wigner representation. In Giulio Casati and Joseph Ford, editors, *Stochastic Behavior in Classical and Quantum Hamiltonian Systems*, volume 93 of *Lecture Notes in Physics*, pages 326–333. Springer Berlin Heidelberg, 1979. ISBN 978-3-540-09120-2. doi: 10.1007/BFb0021756.
- S. Weigert. The problem of quantum integrability. *Physica D: Nonlinear Phenomena*, 56(1):107 – 119, 1992. ISSN 0167-2789. doi: 10.1016/0167-2789(92)90053-P.
- H. Weyl. Das asymptotische verteilungsgesetz der eigenwerte linearer partieller differentialgleichungen (mit einer anwendung auf die theorie der hohlraumstrahlung). *Mathematische Annalen*, 71:441–479, 1912. ISSN 0025-5831. 10.1007/BF01456804.
- E. P. Wigner. On the Quantum Correction For Thermodynamic Equilibrium. *Physical Review*, 40:749–759, June 1932. doi: 10.1103/PhysRev.40.749.
- E. P. Wigner. On a class of analytic functions from the quantum theory of collisions. *The Annals of Mathematics*, 53(1):pp. 36–67, 1951. ISSN 0003486X.
- V. V. Zalipaev, F. V. Kusmartsev, and M. M. Popov. High-energy localized eigenstates of an electronic resonator in a magnetic field. *Journal of Physics A Mathematical General*, 41(6):065101, February 2008. doi: 10.1088/1751-8113/41/6/065101.
- W. H. Zurek. Decoherence and the transition from quantum to classical – REVISITED. arXiv:quant-ph/0306072, June 2003.
- K. Zwintz, T. Kallinger, D. B. Guenther, M. Gruberbauer, R. Kuschnig, W. W. Weiss, M. Auvergne, L. Jorda, F. Favata, J. Matthews, and M. Fischer. Pulsational Analysis of V 588 Mon and V 589 Mon Observed with the MOST and CoRoT Satellites. *The Astrophysical Journal*, 729(1):20, 2011.
- K. Zwintz, P. Lenz, M. Breger, A. A. Pamyatnykh, T. Zdravkov, R. Kuschnig, J. M. Matthews, D. B. Guenther, A. F. J. Moffat, J. F. Rowe, S. M. Rucinski, D. Sasselov, and W. W. Weiss. Regular frequency patterns in the classical δ Scuti star HD 144277 observed by the MOST satellite. *A&A*, 533:A133, September 2011. doi: 10.1051/0004-6361/201117272.

Application of quantum chaos methods to the oscillations of rapidly rotating stars

Abstract: Asteroseismology aims at inferring internal properties of stars from the analysis of their oscillation mode frequencies. This analysis can be greatly facilitated by an a priori information on the basic structure of the oscillation spectrum given by an asymptotic formula. Up to now, the only existing asymptotic formula for stellar oscillations was derived in the spherically symmetric case. For a rapidly rotating star, spherical symmetry is broken by the centrifugal force, and thus an adequate asymptotic theory was missing. Yet, rapid rotation is common among non-evolved intermediate mass and massive pulsating stars, and many of them are found in the data of asteroseismology space missions CoRoT and Kepler.

The ray limit of pressure waves that causes stellar oscillations can be described by a Hamiltonian dynamical system. It was shown that this system undergoes a transition, as the rotation rate of the star increases, from an integrable to a mixed system where stable and chaotic regions coexist in phase space. In this thesis, it is shown how to obtain semi-analytical formulas for regular frequency spacings in the pressure mode spectrum of rapidly rotating stars by using ray theory and techniques from quantum chaos. These formulas relate regular frequency spacings to physical properties of the star, which provides a new theoretical tool for the asteroseismology of rapidly rotating stars.

Keywords: quantum chaos, semi-classical methods, stellar oscillations, stellar rotation, asteroseismology

Application des méthodes du chaos quantique aux oscillations d'étoiles en rotation rapide

Thèse de physique de la matière soutenue par Michael PASEK le 20 décembre 2012 à l'Université Paul Sabatier, Toulouse. Thèse encadrée par Bertrand GEORGEOT au Laboratoire de Physique Théorique, Université Paul Sabatier, 118 route de Narbonne, 31062 Toulouse Cedex 4, France et co-encadrée par François LIGNIÈRES à l'Institut de Recherche en Astrophysique et Planétologie, 14 avenue Edouard Belin, 31400 Toulouse, France.

Résumé : L'astérosismologie a pour but de déduire les propriétés internes des étoiles à partir de l'analyse de leurs fréquences d'oscillation. Cette analyse peut-être grandement facilitée par des informations a priori sur la structure du spectre d'oscillation, telles que celles que l'on peut obtenir par une formule asymptotique. Jusqu'à maintenant, une telle formule asymptotique n'était disponible que pour les étoiles à symétrie sphérique. Or pour une étoile en rotation rapide, la force centrifuge aplattit l'étoile, et la formule asymptotique n'est plus valable. Pourtant, les étoiles pulsantes en rotation rapide sont communes parmi les étoiles massives et de masse intermédiaire de la séquence principale, et un grand nombre d'entre elles sont observées par les missions spatiales dédiées à l'astérosismologie comme CoRoT et Kepler.

Dans le cas des modes d'oscillation de pression, la limite asymptotique des rayons acoustiques peut-être décrite par un système dynamique Hamiltonien. Ce système passe, lorsque l'on augmente la vitesse de rotation d'un modèle d'étoile, d'un système intégrable à un système mixte, où des régions stables et chaotiques co-existent dans l'espace des phases. Dans cette thèse, nous montrons comment obtenir des formules semi-analytiques prédisant des espacements réguliers de fréquences dans le spectre des modes de pression d'étoiles en rotation rapide, en utilisant la théorie des rayons ainsi que les méthodes du chaos quantique. Ces formules relient les espacements réguliers de fréquences d'oscillations aux quantités physiques internes des étoiles, ce qui fournit un nouvel outil théorique pour l'astérosismologie des étoiles en rotation rapide.

Mots-clés : chaos quantique, méthodes semi-classique, oscillations d'étoiles, rotation stellaire, astérosismologie